GAS FIRED FLUIDIZED BEDS

by

CHRISTOPHER ROGER WESTWOOD

A Thesis Submitted in Fulfilment of
the Requirement for the Degree of
Doctor of Philosophy

THE UNIVERSITY OF ASTON IN BIRMINGHAM

March 1975

S U M M A R Y

Investigations, both experimentally and theoretically, have been made of gas combustion in fluidized beds. A mathematical model has been developed which gives a qualitative estimation of the bed temperature profiles in the axial direction. The concept of Effective Thermal Conductivity is discussed, and bed conductivities are re-defined bearing in mind the contribution of particle recirculation.

Experiments have been performed with particle sizes ranging from 0.6 mm to 1.4 mm diameter. Results are presented for the effect of particle size, bed height and throughput on the bed behaviour. Two distributor plates have been used: mild steel and refractory. Comparisons are made between the two. Stability of combustion has been studied, and two mechanisms have been observed by means of which a bed becomes unstable. Chemical analysis of the combustion products has shown that even with shallow beds (5 cm deep), CO emissions are very small with excess air levels of not less than five percent.

A C K N O W L E D G E M E N T S

I wish to acknowledge my gratitude to my supervisors (Professor D E Elliott and Dr J Broughton) for their help and guidance during this work, and to the Science Research Council who financed me.
I am profoundly grateful to my former colleagues in the Department of Mechanical Engineering for their help and advice - in particular, Mrs Joan Lloyd who typed the manuscript and the late Mr Edward Denchfield and his laboratory staff.

TABLE OF CONTENTS

CHAPTER 1

INTRODUCTION

If a fluid is passed up through a bed of particles it is found that when the flow rate is increased a condition is attained where the bed begins to expand and manifests the behaviour of a fluid - hence the name fluidized bed. A useful property of a fluidized bed is the very high rate of heat transfer that can be obtained at an immersed surface. This property, combined with the high uniformity of temperature and wide ranges of combustion atmospheres, suggests applications in the design of boilers and heat treatment plant.

A major advantage of fluidized combustion is the low range of temperatures at which combustion can occur - this should reduce levels of atmospheric pollution. Figure 1 shows the equilibrium concentrations for NO and CO at different temperatures. Conventional furnace flames would be in the range above 2 000^{o}K, where fluidized furnaces would operate below 1 500^{o}K. These equilibrium concentrations may not represent what is measured at the exit of a combustion system; this is due to rapid cooling of post-combustion products, (Johnson[1]). Nevertheless, the equilibrium concentrations give an indication of the scale on which improvements may be made.

There are three methods of initiating gas combustion in a fluidized bed. One way is to incorporate a burner in the air line before the distributor plate *(Figure 2)*. This method requires a distribution plate and high quality ducting that can withstand the initially high temperatures, and a burner that can operate at the initially high bed pressures. The other two methods involve heating the bed at the surface and allowing particle recirculation

to raise the bed temperature, and this may be achieved by lighting an air-gas mixture above the bed or by firing a burner down into the bed. Since the quantity of fluidizing medium required to fluidize the bed depends upon the temperature *(Figure 3)*, a high initial throughput would be required before steady combustion is achieved. However since this is achieved fairly rapidly, the disadvantage of high initial throughputs should not offset the many advantages to be gained from fluidized combustion.

A recent paper by Pillai and Elliott[2] has already outlined design considerations for shallow bed boilers and proposes a design for a two-stage boiler based upon a system developed at Aston University[3]. The boiler consists of two fluidized beds in series (Fig.4) Combustion occurs in the bottom bed where some fifty per cent of the heat is transferred to the circulating water, and the final heat transfer occurs in a secondary bed placed over the combustion bed. With suitable modifications, this system may be adapted for steam raising.

Up until now there has been very little research work in gas-fired fluidized beds. Important areas requiring further study include:

[1] A study of what air-gas ratios are possible in fluidized combustors

[2] A study of how the bed temperature depends upon the air and gas throughput

[3] A study of how the bed conditions depend upon the particle size

[4] A study of what pollution emissions may be expected from a

fluidized combustor.

The following chapters will attempt to make some contribution in these areas.

CHAPTER 2

APPRAISAL OF FLUIDIZATION TECHNOLOGY

2.1 INTRODUCTION

An inspection of any standard reference on fluidization[4,5] will show the inordinate number of papers published on fluidization over the past twenty years. Only a small number of these report studies in gas-fired fluidized beds. The following chapter will review these papers, and those whose contents have a direct bearing upon fluidized combustion.

2.2 ONSET OF FLUIDIZATION (The Incipient State)

Ergun has shown that for fixed beds the pressure drop (ΔP_B) across the bed is related to the bed voidage (ε), the fluidizing velocity (U) (see *Figure 5*), the viscosity of the fluidizing medium (μ), the density of the fluidizing medium (ρ_f), the particle diameter (d) and the bed height (H) by:

$$\frac{\Delta P_B}{H} = \frac{150(1-\varepsilon)^2}{\varepsilon^3}\frac{\mu U}{d^2} + \frac{1.75}{\varepsilon^3}\frac{\rho_f U^2}{d} \qquad (1)$$

At incipient fluidization, the pressure drop through the bed is just sufficient to balance the weight of the particles:

$$\Delta P_B = (\rho_s - \rho_f)(1-\varepsilon_{mf})H_{mf}\, g \qquad (2)$$

where ρ_s is the density of the solid particles. Substituting equation (2) into equation (1):

$$\frac{\rho_f(\rho_s-\rho_f)}{\mu^2} g d^3 = \frac{150(1-\varepsilon_{mf})}{\varepsilon_{mf}^3}\frac{U_{mf}\, d\, \rho_f}{\mu} + \frac{1.75}{\varepsilon_{mf}^3}\left[\frac{U_{mf}\, d\, \rho_f}{\mu}\right] \qquad (3)$$

In these equations the particle diameter (d) is given by:

$$d = d_p \times \phi_s$$

where d_p is the diameter of a sphere having the same volume as the particles, and ϕ_s is the ratio of the surface area of a sphere (of same volume as the particles) to the surface area of the particles.

With larger particles (above 1 mm diameter), Cranfield[7,8] has suggested that a factor of 180 in place of 150 in equation (3) is preferable. Equation (3) is for particles within a very close size range. With a mixture from a wide range of diameters, the value of particle size will have to be modified to suit the size distribution.

2.3 FORMATION OF BUBBLES

Two important contributions on bubble formation have been made by Davidson and Harrison[9], and by Cranfield[7], the latter being for particles over 1 mm diameter. Davidson and Harrison have shown that the volume of a bubble formed in a bed of fine particles will correlate well to a bubble formed in a liquid given the same orifice and flow rate. The actual bubble formation is as shown in *Figure 6*. A void is formed at the orifice which grows, resembling a paraboloid. Upon reaching a critical size, the interface with the surrounding bed becomes unstable and collapses. The result is a kidney-shaped bubble with a spherical cap.

Cranfield[7] worked with large light particles and found that bubbles were not formed at the distributor plate, but in the bed itself. The point of bubble formation depended upon the level of excess air; for a "steady bubbling state" his bubbles were formed at about 2 cm above the distributor, and at lower levels of excess

air the bubbles were formed nearer the plate. The mechanism of bubble formation is shown in *Figure 7*. A lenticular cavity is first formed above the distributor plate. Additional gas, which is pushed in, forces the bubble into a dumb-bell shape which eventually splits into two separate spherical bubbles.

Both of these bubble formation mechanisms have been for pierced plate distributors; little or no information is available for a wide range of particle sizes and densities and none is available for bubble formation in combustion beds.

2.4 AXIAL TRANSPORTATION OF PARTICLES

One of the early works on the transportation of solids was that of Talmor and Benenati[10]. They worked with various sizes of bed diameter and particle diameters, and with varying gas densities, finding that their results could be correlated by:

$$\dot{M} = 0.785(\dot{V} - \dot{V}_{mf}) \exp(-66.3\, d) \qquad (4)$$

where $\dot{M}$ = mas flow rate across a section (gm/s)

$\dot{V}$ = volume rate fluidizing medium (cm^3/s)

$\dot{V}_{mf}$ = that required for the incipient state

d = particle diameter (cm)

An explanation of the mechanism of particle movement was proposed by Rowe and Partridge[11] from visual experiments they had performed with single bubbles. According to Rowe and Partridge there were two distinct mechanisms involved in particle transporation (see *Figure 8*). The first mechanism is due to the inherent viscous nature of the bed: one effect of a bubble rising through a fluidized

bed is the inducement of a drift in a similar manner to that produced when a solid sphere is dragged through a viscous liquid. The second mechanism consists of particles forming part of the bottom half of the bubble which either all find their way to the top of the bed or, in the case of deep beds, will be deposited in the bed at intervals and replaced each time by another batch of particles. *Figure 8* shows the effect of a bubble rising through a fluidized bed, the bottom half having been dyed - both mechanisms are seen to occur.

In a more recent paper, Rowe and Partridge[12] have published the results of X-ray studies showing how the quantity of particles within the bubble varies with particle size. These results show that the bubble quantity increases as the particle size is increased. Although this may appear to conflict with the findings of Talmor and Benenati (see equation (4)), it should be noted that Rowe and Partridge studied one mechanism in isolation where Talmor and Benenati studied the two combined. This point has been highlighted in a more recent paper by Woollard and Potter[13] who have produced more data to support equation (4) and have discussed the relative effects of both mechanisms.

For larger particles it appears that there is no transportation by particles forming part of the bubble. Cranfield[7] has shown that with these particles there are spherical bubbles (as opposed to the kidney-shaped bubbles with small particles) and only the viscous transportation exists. Cranfield also found that the rate of transportation depended upon which section it was being measured; it increases for longer distances from the distributor plate.

Transportation rates were found to be many times greater than those predicted by equation (4).

The works reviewed so far have been for isothermal beds with no steep temperature gradients, and the solid transportation has been conveniently related to the volume of fluidizing medium in excess of that required for the incipient state. In a combustion bed, there are very steep gradients along the temperature profile of the fluidizing medium. The air enters at a temperature of approximately 300°C to be heated up to over 1 000°C. Under these conditions there is no information about solid transportation in the first few centimetres of bed depth.

2.5 INTERACTION BETWEEN GAS IN BUBBLE AND DENSE PHASES

The majority of studies relating to the interaction between dense and bubble phases rest upon foundations established by Davidson[15]. Davidson developed a model to account for the flow of solids around a bubble, a model that can then be adapted to explain the interaction between the gas in a bubble and that in the surrounding dense phase. The model is built around three postulates:

[1] The bubble is treated as solid and spherical

[2] The dense phase behaves as a liquid of density $\rho_s(1 - \varepsilon_{mf})$

[3] The gas flow in the dense phase is uncompressible and is governed by Darcy's Law:

$$(U_{gas} - U_{solid})_x = K.\frac{\partial P}{\partial x}$$

The following boundary conditions are assumed:

[1] Far from the bubble, the undisturbed pressure gradient exists

[2] The pressure in the bubble is constant

From these considerations it is found that the stream function (ψ) of the gas outside of the bubble at co-ordinates (r, θ) is given by:

$$\psi = (U_b - U_i) \frac{r^2 \sin^2\theta}{2} \left[1 - \frac{A^3}{r^3}\right] \qquad (5)$$

where U_b = bubble velocity

U_i = interstitial gas velocity

$A^3 = a^3 \left[\frac{U_b + 2U_i}{U_b - U_i}\right]$

a = bubble radius

To allow for the gas motion within the bubble, Pyle and Rose[14] have extended the model to show that:

$$\psi = \tfrac{3}{4} U_{mf} \left[\left(2 + \frac{U_b}{U_{mf}}\right) \frac{r^2}{a^2} - \left(4 + \frac{U_b}{U_{mf}}\right) \right] r^2 \sin^2 O \qquad (6)$$

Predicted fluid streamlines are shown in *Figure 9*. They indicate that for very high ratios of U_b/U_i the bubble gas only penetrates a small cloud outside of the bubble and only a little contact between the gas in the two phases occurs. The cloud diameter approaches the bubble diameter as the velocity ratio is increased. As the ratio becomes less than one, the gas in the emulsion phase uses the bubble as a short cut. Clearly, high ratios are not good if interaction between the two phases is required. Experimental evidence of this cloud formation has been published by Rowe and Partridge[11,16].

The obvious extension of this work is to study how the bubbles affect chemical reactions within the bed. Such a study has been made by Rowe and Partridge[17]. No similar study has been made with

high temperature combustion beds.

2.6 AXIAL THERMAL CONDUCTIVITY

Several papers have reported very high thermal conductivities in the axial direction. They all agree on what is defined as the 'effective thermal conductivity' of a fluidized bed.

One of the earlier papers on fluidized bed conductivities was that of Shrikhande[18]. Shrikhande worked with very tall columns and obtained thermal conductivities by measuring the bed temperature, at approximately 12 cm intervals, for different rates of heat transfer through the bed. Linear temperature profiles were found and from this it was possible to define an 'effective Thermal Conductivity' as that which enabled the heat transfer to be described by Fourier's Law. This conductivity had the same value for heat conducted both up and down the bed. It was found that the effective thermal conductivity increased linearly for an increase in fluidizing velocity. Conductivities ranging from 15 to 107 cal/cm.s^{o}C (63 to 450 kW/M^{o}C) were reported for glass beads of varying diameters.

Similar results were published by Lewis, Gilliand and Girovard[19]. Conductivities ranging from 0.4 to 103 cal/cm.s^{o}C (2 to 430 kW/M^{o}C) were noted. Measurements of conductivities in the radial direction produced values of only about two per cent of those in the axial direction. In this work a honeycomb baffle was placed half-way down the bed and although this did not affect the conductivities above and below the baffle, it did produce a sharp temperature discontinuity in the bed. This baffle would have stopped

the vertical solids movement inside it, and probably reduced the bed conductivity.

In a later paper by Jain and Chen[20], an attempt was made to relate the effective thermal conductivity to the solid movement within the bed. With the thermal diffusivity defined by:

$$\alpha = \frac{K_e}{\rho_b C}$$

where ρ_b = bed density

C = particle specific heat

K_e = effective thermal conductivity

α = thermal diffusivity

and starting from the work of Gabor[21] it was argued that:

$$\alpha = K\left[\frac{\dot{V} - \dot{V}_{mf}}{\dot{V}_{mf}}\right]^{\frac{5}{3}}$$

where K is a constant, and therefore

$$K_e = \rho_b \, C \, K\left[\frac{\dot{V} - \dot{V}_{mf}}{\dot{V}_{mf}}\right]^{\frac{5}{3}}$$

Their experimental evidence tended to support this equation.

The results of several Russian workers have been published by Zabrodsky[22]. These tend to agree with the work previously mentioned, but one interesting point arises: the Russian workers recorded bed temperatures at very close intervals and found that there was not a linear temperature gradient near the bottom of the bed. From this they concluded that the effective thermal conductivity was much less in the bottom regions.

The most noticeable aspects of these works is the very high range of conductivities. Contributions from the heat capacity of the fluidizing medium are small in comparison. As will be demonstrated in the following chapter, problems arise from the concept of the effective thermal conductivity when attempts are made to model fluidized combustors.

2.7 GAS COMBUSTION IN FLUIDIZED BEDS

Although a considerable amount of work has been reported on chemical reactions in fluidized beds, very little has been published on fuel-gas combustion.

A Russian paper by Baskakov, Kunos and Svetlakov[23] has reported several fluidized bed combustors that have been built as heat treatment furnaces. This paper points out the wide range of chemical atmospheres, and the uniformity of temperatures, that are obtained in a gas-fired fluidized bed. In particular, this paper mentions a two-stage combustor where a rich air-gas mixture is injected in the bottom of the bed, and the air required for complete combustion is injected near the top of the bed. The backflow of particles *(Figure 10)* ensures an even temperature distribution, and initiates the reaction in the rich mixture at the bottom of the bed. Comparing heat transfer rates with fluidized beds and conventional combustion furnaces, Baskakov quotes a five-fold increase in one particular wire heating process as a result of fluidization.

Another Russian paper by Baskakov and Antifeev[24] reviews several reports of tests performed on small gas-fired beds. On one small bed reported, combustion was initiated by igniting an air-gas

mixture above the surface of the bed and allowing it to slowly warm up. It was found that combustion, when it occurred, was accompanied by violent explosions within the bed, but these explosions ceased at temperatures above 1 000°C. An unsuccessful attempt to obtain combustion within the bed with separate air-gas injection was reported. It was found that combustion would only occur above the bed - probably due to bad mixing within fluidized beds. Baskakov argued that heat losses were very high from laboratory beds and because of this, high temperatures could only be obtained with particles over 1 mm diameter. Baskakov's high heat losses were probably the result of using very deep beds.

Tamalat[25] has reported an interesting study of fluidized gas combustion but with separate air and gas injection. Initial studies were performed by splitting an air box in two, injecting different gases into the bed and noting the degree of mixing. Tamalat found that mixing was only noticeable at the interface of the two gas streams. Using data from his experiments, Tamalat was able to space his jets in such a way as to operate a bed (70 cm deep) with separate air and gas injection, giving complete combustion at temperatures above 800°C.

In Chapter 1, the possibility of reducing NO_x emissions with fluidization was mentioned. What little work published so far tends to support this. In a very important paper (in this field) by Jarry, Anastasia, Carls, Jonke and Vogel[26], the results from NO_x measurements are discussed. These workers measured NO_x emissions from both the combustion of coal and natural gas in fluidized beds. Their results indicated that NO_x emissions from gas combustion are

in accordance with those calculated from equilibrium considerations. Emission levels from coal were found to be above the equilibrium concentrations. They suggested that this could be due to coal particles being at a temperature much higher than the bed. It could also have been caused by nitrogen within the coal particles. From this work, it can be assumed that the equilibrium concentrations given in *Figure 1* are a useful guide.

A comprehensive study of gas combustion within fluidized beds has been made by Broughton[27]. Another unsuccessful attempt to obtain combustion with separate air-gas injection is reported and combustion is only obtained above the bed surface. With pre-mixed combustion, Broughton studies the temperature variation down the axial length of the bed. It was found that the temperature was constant for the greater length of the bed, but near the distributor plate the temperature increased to a maximum and then decreased towards the plate. Temperatures inbetween the distributor plate and the point of maximum temperature were found to fluctuate considerably. Subsequent temperature measurements in the radial direction detected only a variation near the wall in the top (isothermal) section of the bed, but found considerable variation of temperature as the probe traversed the region near the distributor plate. Broughton obtained successful pre-mixed combustion with all of his particles (below 1 mm diameter) until he worked with particles as small as 0.3 mm diameter. To explain this, Broughton invoked Davidson's model to show that with very small particles a high proportion of the feed gas passes rapidly through the bed in the bubble phase and does not mix within the bed. This by-pass would

also remove some heat from the bed. By assuming that the rate of chemical reaction in the bed is high, then it can be argued that the 'effective rate of reaction' depends upon the rate of interaction between the bed and bubble phases. Broughton has shown that for any height above the distributor (H), the ratio of the concentration of initial feed at that height to that at the entry is given by:

$$\frac{C_e}{C_o} = \frac{\left[1 - \frac{U_{mf}}{U}\right]}{\sqrt{g\ d^3}} \exp(-6.34\ U_{mf}\ H) \qquad (7)$$

Broughton calculated that for:

U_{mf} = 4 cm/s

U = 8 cm/s

d = 0.4 cm

H = 15 cm

then 20% has by-passed the bed. It was found that with the larger particles, chemical equilibrium was attained for both rich and lean mixtures.

Another recent, and more extensive, study of gas combustion in fluidized beds has been published by Cole and Essenhigh[28]. Here again, an attempt to obtain bed combustion with separate air-gas injection was unsuccessful. However, this work is interesting in that rather than revert to a pre-mixed feed, the authors placed a layer (approximately 11 cm deep) of coarse limestone over the distributor plate and fed the separate air and gas streams in beneath this layer. The gas was found to mix within this coarse bed and could burn in a layer of smaller fluidized particles above.

Considerable importance must be attached to this since it allows the good combustion characteristics of a pre-mixed system to be combined with the major advantage of separate air-gas injection - no possibility of combustion 'flash-back' into the air box. There is still the possibility, however, of combustion occurring in the limestone at the bottom with the chance of damage to the bed.

Studies of light up were made and explosions similar to those reported by Baskakov were observed. Cole and Essenhigh found that this could be alleviated by a systematic method of initiating combustion; a gas-air mixture at one-tenth of the minimum fluidizing velocity was initially ignited above the surface followed by an increase to half of the minimum fluidizing velocity and control adjustments as combustion proceeds down the bed. This method could cause complications for industrial plant with an automatic start-up.

Tests were also performed to evaluate at what bed temperatures could a fresh air-gas mixture be injected with an initiation of combustion. It was found that this would occur at bed temperatures even as low as 400°C. This temperature is remarkably low. It is probable that there were hot spots within the bed or high temperature zones on the bed casing and these were sufficient to initiate combustion.

Studies of temperature and chemical concentration curves for beds above 1 000°C showed combustion to be complete at about 2.5 cm above the distributor and, as with previous works, an elevated temperature zone was observed in the first 2 cm above the distributor. Cole and Essenhigh suggested that this elevated temperature region may be due to hot particles recirculating and preheating the feed gas.

An interesting paper presented by Elliott and Virr[29] at the Third International Conference on Fluidized Bed Combustion outlines initial studies at Aston University. They argued that shallow beds are preferable to deep beds since this would reduce the heat loss from the bed container. Because of this, their work was involved in studying how shallow a bed could be used without combustion occurring above the bed surface. All of this work was with pre-mixed air-gas supplies, separate gas injection being rejected because deep beds would be required for complete combustion. Initiation of bed combustion was obtained by igniting an air-gas mixture just above the surface and allowing particle recirculation to warm up the bed.

This paper presented data on noise emissions from combustion beds over a wide range of operating conditions. Decibel readings over a range of frequencies (125-6 000 Hz) show very high noise levels at temperatures of about 700°C, but with very much reduced levels at temperatures above 1 000°C. Elliott attributed the high noise levels at low temperatures to the delayed combustion, or pre-heated explosion, of the bubbles. Although high temperatures favour low noise levels, Elliott stressed the need for particles with very high fusion temperatures if beds were to be operated in these conditions.

Exploratory studies into the possibility of reducing atmospheric pollution by fluidization have shown the advantages to be gained. NO_x levels were of the same order as those reported by Jarry *et al*[26], and near stoichiometric conditions CO/CO_2 ratios of less than .002 were observed. These represent a considerable

improvement on the conventional gas burner as would be expected from the data in *Figure 1*.

An interesting part of Elliott's paper is the work on surface radiation. With the radiation efficiency of the bed defined as:

$$1 - \frac{\text{heat lost in gas exhaust}}{\text{heat supplied by fuel}}$$

it was found that by reducing the bed temperature below 1 100°C it was possible to obtain radiation efficiencies in excess of fifty per cent. This compares with a normal domestic radiant gas heater that only has efficiencies in the region of twenty-five to thirty-five per cent. Elliott found that the emissivity of a gently bubbling bed was very near to that of the solid material from which the particles are ground. However, when the bed was violently bubbling and there was a cloud of ejected particles above the bed, Elliott observed that these particles appeared a duller colour than what should be expected for the bed temperature. Elliott concluded that the particles in the cloud had been ejected at the bed temperature, and were cooling down as they fell back towards the bed by radiating heat. Elliott indicated that this process could increase the effective surface emissivity.

There are some doubts as to the parameters used in the Stefan-Boltzmann radiation equation when applied to a fluidized bed. Because of the temperature gradients near the surface, there are problems as to which value of temperature must be used in the equation, and because of the particle cloud above the bed surface, it is difficult to think of an emissivity in the same way as for a solid radiating

surface. To avoid any confusion, a bed will be assumed to radiate at the temperature in the isothermal region and the emissivity will then be taken to satisfy the radiation equation. This point was not made in Elliott's paper. It will be helpful to think in these terms when discussing the experimental work of Chapter 4.

CHAPTER 3

A THEORETICAL STUDY OF GAS COMBUSTION IN FLUIDIZED BEDS

3.1 INTRODUCTION

An understanding of the mechanism of gas combustion in a fluidized bed requires a knowledge of the nature of the chemical reactions proceeding within the bed, and a knowledge of the transportation mechanisms within the bed. In this respect the transportation mechanisms will include convective terms that are due to the mass movement of matter on a macroscopic scale, diffusion terms that are due to the movement of gases on a microscopic scale, and conductive terms that are due to the transportation of heat along a temperature gradient. An attempt to model a process with these terms usually produces a differential equation, and a complete knowledge of all of the influencing factors is required before accurate solutions can be made giving the temperature and chemical concentration profiles within the bed.

Unfortunately, such detailed information is not available; our knowledge of simple hydro-carbon reactions is incomplete and there is little data on particle transportation that can be readily adapted to the study of combustion systems. Nevertheless, a considerable amount of work has been done in these separate fields and it is the purpose of this chapter to bring together as much of it as is possible and gain an insight into the phenomenon of fluidized combustion.

3.2 THE PROBLEM

A temperature probe traversed through a combustion bed in the

axial direction will produce one of two temperature profiles shown in *Figure 11*. They differ in the amount of temperature variation along the axis, and how close this variation is to the distributor plate. This point will be explained in the experimental study of Chapter 4. There are three interesting regions along the temperature profile: zone A where the temperature is increasing to a maximum, zone B where it reduces until a steady value is attained, and zone C (just beneath the surface) where the temperature begins to decrease when a probe is traversed upwards. The problem is to interpret these profiles in the light of existing work on bed transportation.

Baskakov and Antifeev's argument[24] that the bed temperature is governed by the heat loss is a reasonable starting point from which to analyse combustion bed behaviour. For a well-lagged bed it is possible to considerably reduce the losses from the bed casing and assume the only loss occurring is due to surface radiation. The steady flow analysis for the bed *(Figure 12)* is:

$$\dot{N}_{gas}(\Delta H) = \dot{Q}_{rad} + \sum_i \dot{N}_i (h_T - h_o)_i \qquad (8)$$

where $\dot{N}_{gas}$ = molar flow of fuel gas

ΔH = heat release per mole of gas

$\dot{Q}_{rad}$ = surface radiation

$\dot{N}_i$ = flow of species i in the combustion products

h_T = molar enthalpy at bed temperature T

h_o = molar enthalpy at feed temperature

$\dot{Q}_{rad}$ is given by:

$$\dot{Q}_{rad} = A \varepsilon_r \sigma T^4$$

where A = bed surface area

ε_r = effective surface emissivity

σ = Stefan Boltzmann constant

With the combustion products assumed to be at the same temperature as the bed, and with reasonable values inserted in the above equations, it should be possible to calculate the bed temperature under given conditions. *Figure 13* shows how the bed temperature will vary for any gas throughput. It is calculated for the following conditions:

[1] ε_r assumed to be unity and not to vary with the throughput

[2] Air-gas ratio 1.6 times stoichiometric (methane)

[3] Bed diameter 13 cm (based on bed used for experimental study.

With this approach it is possible to evaluate the bed temperature in the isothermal region in terms of the bed throughput.

Given the isothermal region bed temperatures in terms of the gas throughput, the next step would be to formulate and solve the differential flame equation for the temperature variation along the axis of the bed. The one-dimensional flame equation for conditions where diffusion may be neglected is:

$$\frac{d}{dx}\left[K_e A . \frac{dT}{dx}\right] - \frac{A\varepsilon d}{dx}\left[C_p T \rho U_i\right] + \sum_j (h_f^T)_j \frac{d\dot{N}_j}{dx} = 0 \qquad (9)$$

where ε = bed voidage

K_e = effective thermal conductivity

C_p = specific heat of gas mixture

T = bed temperature at x

ρ = density of gas mixture

U_i = interstitial gas velocity

$(h_f^T)_j$ = heat of formation of species j at temperature T

$\dot{N}_j$ = rate at which species j crosses a section

A = bed area

In using this form of the one-dimensional flame equation, the gas has been assumed to be at the same temperature as the solids. If the concept of effective thermal conductivity is taken verbatum, then this assumption should only introduce a negligible error; in Lewis's paper[19] it is argued that the convective contribution of the gases is negligible compared with that due to the bed's conductivity. With this in mind, it should be possible to solve equation (9) subject to the temperature in the isothermal region obeying equation (8). Typical solutions would be as shown in *Figure 14*. For very high gas throughputs, the temperature profile could approach the top curve where the final temperature is near to the adiabatic flame temperature. For low flow rates, the temperature profile is similar to that shown in the bottom curve. The amount of temperature variation along the axis would depend upon the value of thermal conductivity used in the differential equation; with those values reported in Chapter 2, the variation along the axis would be no greater than about $2^{\circ}C$. None of these solutions correspond to the temperature profiles observed in actual

fluidized combustors. In an attempt to resolve this disagreement between the experimental results and theoretical predictions, it can be argued that the temperature profile must be affected by the variations of thermal conductivity near the distributor plate. This approach is not without merit for it can be argued that there must be high conductivities in the upper parts of the bed because of the uniformity of temperature, and low conductivities near the plate explaining the large temperature variations in that region. The only problem is that this would require conductivity variations of over one thousand-fold along the axis. At this point the concept of effective thermal conductivity (as discussed in Chapter 2) will be rejected. By a different interpretation of the previous work on bed conductivity, it will be shown possible to alleviate many of these difficulties.

The work of Jain and Chen[20] provides a starting point to the re-interpretation of fluidized bed thermal conductivities. Their work reports that a baffle half-way down the bed produced sharp temperature discontinuities. By reducing the particle movement in the baffle it was possible to reduce the conductivity there. If reducing the particle movement reduces the conductivity, the question must be asked "how does the particle movement contribute to the heat transfer and temperature profiles?" The following sections will answer this and redefine the thermal conductivity in such a way that not only are the temperature profiles explained, but the disparity between conductivities in the radial and axial directions is reduced.

3.3 TRANSPORATION MECHANISMS

(a) Conductive Transportation

From hereafter the thermal conductivity of the bed will be defined as the thermal conductivity of a stationary sample of the emulsion phase with zero gas flow, and with a voidage corresponding to that in the incipient state. This corresponds to the conductivity of a packed bed. For analysis it will be assumed that there exists a continuous function describing both the particle and gas temperature fields within the bed. Any effect due to the finite size of the particles will be assumed negligible. Fourier's law of heat conduction will be taken to apply for all points within the bed.

Having defined what, in this work, will be taken as the thermal conductivity of a fluidized bed, there is the problem of obtaining suitable values. Existing work on packed beds has shown the conductivity to consist of two components. There is a component due to the conductivity of the particles and the stagnant fluid which is given by the Deissier Elan correlation[30] (graphs are given in the quoted reference for solution), and a radiative component which has been shown by Schotte[31] to be given by:

$$0.547 \times 10^{-8}\ \varepsilon_r\ d\ T^3\ \frac{\text{cal}}{s\ ^oC\ cm}$$

or

$$2.29 \times 10^{-8}\ \varepsilon_r\ d\ T^3\ \frac{W}{^oC\ cm}$$

The work referred to for calculating thermal conductivities[30,31] are for beds with very small temperature gradients. These conditions do not apply with fluidized combustors, and it will be shown in the

following sections of this chapter that conductivities one order of magnitude higher are required to produce reasonable calculated temperature profiles. Even so, fixed bed conductivities from these references give better estimates than the works reviewed in Chapter 2.

(b) Convective Transportation

In equation (9) there is a convection term due to the air-gas mixture flowing along a temperature gradient, i.e.

$$\left[A \varepsilon \frac{d}{dx}(\rho_f c_f T U_i) \right]$$

It will now be shown that there is a similar convective effect caused by the movement of particles.

In Chapter 2 it was mentioned that bubbles rising up through a bed will carry particles with them. This upwards flow will be balanced by an equal downwards flow of solids in the surrounding bed. With this in mind, it will now be possible to see how particle transportation aids the axial heat transfer. Consider a section normal to the bed's axis. Across the section solids in the emulsion phase will be flowing downwards with a temperature T_s. The solids transported up through this section need not be at this temperature because they have been carried up from the bottom of the bed where the emulsion phase is at a different temperature. If these particles are at a temperature T_b, then there is a convective term in the direction of gas flow given by:

Fig. 15

$$\dot{M} C(T_b - T_s)$$

where $\dot{M}$ = particle transportation rate

C = particle specific heat

If $T_s > T_b$ then the direction of heat flow due to particle movement is against the direction of gas flow. It is this convection that aids the conductivity of the bed.

Now it is possible to see what part particle transportation plays. For if one considers a bed where the temperature in the isothermal region is below the adiabatic flame temperature, then a considerable amount of heat must be radiated from the bed surface. Particle transportation must be the mechanism by which this heat is transported through the isothermal zone.

3.4 THE DIFFERENTIAL EQUATION

(a) Transportation Terms

Consider two parallel planes cutting the axis at $x - \frac{\delta x}{2}$ and $x + \frac{\delta x}{2}$. The rate of heat transfer due to conduction across $x - \frac{\delta x}{2}$ in the x direction is:

$$- K A \left[\frac{dT_s}{dx} - \frac{d^2T_s}{dx^2} \cdot \frac{\delta x}{2} \right]$$

Similarly, the rate across $x + \frac{\delta x}{2}$ is:

$$- K A \left[\frac{dT_s}{dx} + \frac{d^2T_s}{dx^2} \cdot \frac{\delta x}{2} \right]$$

The difference between heat being conducted across $x + \frac{\delta x}{2}$ and that normal to $x - \frac{\delta x}{2}$ is:

$$- K.A. \frac{d^2T_s}{dx^2} \cdot \delta x$$

where K is assumed not to vary with temperature, and this is the rate at which energy must be released within these two planes to produce such changes of temperature gradient.

The rate at which heat is transported across $x - \frac{\delta x}{2}$ by gas motion is:

$$\dot{m} C_p \left[T_g - \frac{dT_g}{dx} \cdot \frac{\delta x}{2} \right]$$

where $\dot{m}$ = mass rate of gas flow, and the rate across $x + \frac{\delta x}{2}$ is:

$$\dot{m} C_p \left[T_g + \frac{dT_g}{dx} \cdot \frac{\delta x}{2} \right]$$

The rate of energy release required within the two planes to produce such changes in gas temperature is given by:

$$\dot{m} C_p \frac{dT_g}{dx} \cdot \delta x$$

The rate of heat transfer across $x - \frac{x}{2}$ by particle movement is given by:

$$\dot{M} C(T_b - T_s) - C \frac{d}{dx} \left[\dot{M}(T_b - T_s) \right] \frac{\delta x}{2}$$

and across $x + \frac{\delta x}{2}$ by:

$$\dot{M} C(T_b - T_s) + C \frac{d}{dx} \left[\dot{M}(T_b - T_s) \right] \frac{\delta x}{2}$$

The required rate of energy liberation is:

$$C \cdot \frac{d}{dx} \left[\dot{M}(T_b - T_s) \right] \delta x$$

Both gas and solid specific heats have been assumed not to vary with temperature.

The total rate of energy liberation between the two planes to produce all of these effects is given by:

$$C \frac{d}{dx}\left[\dot{M}(T_b - T_s)\right]\delta x + \dot{m} C_p \frac{dT_g}{dx} \cdot \delta x - K.A. \frac{d^2T_s}{dx^2} \cdot \delta x$$

and this energy is released by chemical reaction.

(b) Thermo-chemical Aspects

If $\dot{N}_j$ is the molar rate at which species j crosses the plane at $x - \frac{\delta x}{2}$, and $\dot{N}_j + \delta\dot{N}_j$ is the rate at which species j crosses the plane at $x + \frac{\delta x}{2}$, then the rate of heat release from the change in chemical composition within the two planes is:

$$- \sum_{j=1}^{N} (h_f^T)_j \, \delta\dot{N}_j$$

where N = number of chemical species considered. However

$$\delta\dot{N}_j = \frac{d\dot{N}_j}{dx} \delta x \qquad (10)$$

and the rate of heat release becomes:

$$- \sum_{j=1}^{N} (h_f^T)_j \frac{d\dot{N}_j}{dx} \delta x$$

Combining this with the equation for the transportation terms

$$C \frac{d}{dx}\left[\dot{M}(T_b - T_s)\right] + \dot{m}c_p \frac{dT_g}{dx} - KA \frac{d^2T_s}{dx^2} + \sum_{j=1}^{N} (h_f^T)_j \frac{d\dot{N}_j}{dx} = 0 \qquad (11)$$

Not all of the $\dot{N}_j$ can vary arbitrarily. If there are M atomic species

from which the N chemical components are derived, then at all stages during the combustion process the N chemical components must satisfy a conservation equation of the form:

$$\sum_{j=1}^{N} a_{ij} \dot{N}_j = b_i \quad (i = 1, M) \tag{12}$$

and for any change in composition

$$\sum_{j=1}^{N} a_{ij} (\dot{N}_j + \delta N_j) = b_i \quad (i = 1, M) \tag{13}$$

Subtracting equation (12) from equation (13)

$$\sum_{j=1}^{N} a_{ij} \delta\dot{N}_j = 0$$

If R is the rank of a_{ij} (where $R < M$) then only (N-R) of the $\dot{N}_j$ can vary independently. Denote these by $\dot{N}_R$, then

$$\sum_{j=1}^{R} a_{ij} \delta\dot{N}_j = - \sum_{j=1}^{N} a_{iR} \delta\dot{N}_R \tag{14}$$

and the $\delta\dot{N}_j$ can only vary in accordance with equation (14). This imposes a constraint on equation (11).

3.5 KINETICS OF REACTION

In this work it will be assumed that the ratio of the bubble velocity to the interstitial gas velocity is less than one. If this is the case, then the gases in the two phases will mix. This is valid with large particles, but fails for small particles where

Broughton[26] has shown that phase interaction dominates the reaction. The problem here is to relate the rates of chemical reaction to the derivatives

$$\frac{d\dot{N}_j}{dx}$$

A simple approximation would be to assume that the bed expansion is such that the gas in each phase is, on average, rising at the bed interstitial velocity - which corresponds to

$$\frac{U_{mf}}{\varepsilon_{mf}}$$

At any instant

$$\dot{N}_j = \dot{N} c_j$$

where C_j is the concentration of species j at that instant, and $\dot{N}$ is the total molar flow rate at that instant. From this:

$$\frac{d\dot{N}_j}{dt} = \frac{d}{dt}(\dot{N} c_j)$$

If $C_j \, d\dot{N}/dt$ is small in comparison with $\dot{N} \, dc_j/dt$, then a good approximation is:

$$\frac{d\dot{N}_j}{dt} = \dot{N} \frac{dc_j}{dt} \qquad (15)$$

The problem is to evaluate dc_j/dt.

Simple hydrocarbon reactions tend to be very complicated. The reaction mechanisms have been shown by Semenoff[32] to depend upon small concentrations of activated particles; these may be free radicals or free atoms. Any one of these activated particles may

combine with one of the reactant molecules to produce even further numbers of activated particles. These activated particles are, themselves, reduced in number by surface reactants. An idea of how complex the situation is, is given in a proposed methane combustion mechanism by Karmilova, Enikolopyan and Nalbandyan[33]. The mechanism is as follows:

$$CH_4 + O_2 \rightarrow \cdot CH_3 + \dot{H}O_2$$

$$\dot{C}H_3 + O_2 \rightarrow CH_2O + \dot{O}H$$

$$\dot{O}H + CH_4 \rightarrow H_2O + \dot{C}H_3$$

$$\dot{O}H + CH_2O \rightarrow H_2O + \dot{H}CO$$

$$CH_2O + O_2 \rightarrow \dot{H}CO + \dot{H}O_2$$

$$\dot{H}CO + O_2 \rightarrow CO + \dot{H}O_2$$

$$\dot{H}O_2 + CH_4 \rightarrow H_2O_2 + \dot{C}H_3$$

$$\dot{H}O_2 + CH_2O \rightarrow H_2O_2 + \dot{H}CO$$

$$\dot{O}H \rightarrow \text{wall reaction}$$

It may be worth noting that before any reproducible results were obtained, the reaction vessel had to be washed and conditioned by the reaction for twelve months.

To enable any theoretical study of the bed combustion, a simple reaction will have to be assumed:

$$\frac{d}{dt}[CH_4] = -[O_2]^P[CH_4]^Q K_r \exp\left[\frac{-\Delta E}{RT}\right] \qquad (16)$$

where the figures in parenthesis represent the concentrations. Following the work of Karmilova *et al*, it will be accepted that:

$P = 1.0$

$Q = 2.0$

$\Delta E = 46$ k.cal/mole

and it will be assumed that only CH_4, N_2, CO_2, O_2 and H_2O occur in the reacting mixture ~~with~~ in appreciable quantities.

3.6 SIMPLE SOLUTIONS FROM THE MODEL

An introductory illustration of how the model allows for solids transport and describes a combustion system can be made after a few assumptions. A more complex study will be made in Section 3.7. These assumptions are:

[1] The gas temperature is equal to the particle temperature in the dense phase

[2] The particles transported by the bubbles are from the very bottom of the bed and are at the same temperature as the distributor plate

[3] The reaction commences at the exit from the distributor plate.

None of these assumptions truly describe the system, but they enable an illustrative solution of the equations.

Certain boundary conditions must be specified before a solution may be yielded. The most obvious boundary condition would be the temperature in the isothermal region. This temperature depends upon the gas throughput and the heat radiated from the surface. Another boundary condition could be the temperature at the distributor plate. The work in Chapter 4 will show that these two temperatures are related; this point will also be highlighted in the following

paragraphs. In the absence of radiation data, an assumed value of bed temperature will have to be used. In this chapter it is convenient to use the plate temperature as the boundary condition and assume that the resulting temperature in the isothermal region will be in accordance with radiation considerations. The boundary conditions will be specified and discussed below.

[1] The temperature at the plate will be assumed. It will also be assumed that it will meet the above requirements.

[2] At x = 0, the temperature of the gas mixture will be given in terms of the solids temperature derivative by:

$$\dot{m}(h - h_o) = K.A. \frac{dT_s}{dx}$$

where h_o is this instance is the specific enthalpy of the feed gas mixture (approximately ambient conditions). This also adds another requirement upon the plate temperature: not only must the assumed value yield the correct temperature in the isothermal region, but it must be sufficient for the heat transfer to the distributor plate that is required to transfer the above-mentioned heat (i.e. that conducted back down the bed) to the oncoming gas mixture.

[3] As mentioned in the simplification of the model, the chemical concentrations at x = 0 are for an unreacted mixture. This is not realistic (i.e. mixtures above 1 000^{o}C without reaction) but at the moment is a useful boundary condition. A more realistic solution will be made later.

These three boundary conditions are sufficient to solve equation (11) for the simplified conditions under consideration. With $T_s = T_g = T$, equation (11) becomes:

$$K.A.\frac{d^2T}{dx^2} + (\dot{M}C - \dot{m}c_p)\frac{dT}{dx} - \sum_{j=1}^{N} (h_f^T)_j \frac{d\dot{N}_j}{dx} = 0 \qquad (17)$$

subject to chemical kinetics (equation (16)) and atomic balances (equation (14)). Equation (17) can be integrated once to yield:

$$K.A.\frac{dT}{dx} + (\dot{M}C - mc_p)T - \sum_{j=1}^{N} \int_{\phi=\dot{N}_j^o}^{\phi=\dot{N}_j} (h_f^T)_j \, d\phi = \text{constant} \qquad (18)$$

Substitute boundary condition (2) and the restriction that at $x = 0$, $T = T_b$ = plate temperature and temperature of the upwards transported solids, then:

$$-\sum_{j=1}^{N} \int_{\phi=\dot{N}_j^o}^{\phi=\dot{N}_j} (h_f^T)_j \, d\phi = \dot{m}(h - h_o) + MC(T - T_b) - KA\frac{dT}{dx} \qquad (19)$$

Solving equation (19) is simply a case of supplying the data and performing the numerical integration. The following will be assumed:

T_b = 1 200°C

K = 0.04 cal/cm.s.°C (.167 W/cm.°C)

c_p = .265 cal/gm.°C (1.1 J/gm °C)

A = 132.75 cm^2

C = .2 cal/gm °C (.84 J/gm °C)

$\dot{V}_{air}$ = 200 L/m

$\dot{V}_{gas}$ = 13 L/m

ρ_s = 5.18 gm/cm^3

d_p = (1.0 - 1.4) mm

ϕ_s = 0.81

Values of $(h_f^T)_j$ and $(h - h_o)$ will be taken from reference 33.

To evaluate $\dot{M}$ it is necessary to know the amount of excess volume of the gas mixture above that required for the incipient state, and the amount of solids per unit volume of this excess. If the incipient volume is calculated from equation (3) then it will be found later in this chapter that solids circulations of at least one hundred times those predicted by equation (4) will be required to yield reasonable results. This will be shown in Chapter 4 to be partly due to the errors in equation (3) at high temperatures. Therefore $\dot{M}$ will be given by:

$$\dot{M} = (\lambda)\ 0.785(\dot{V} - V_{mf})\ \exp(-66.3\ d)$$

where λ is a factor to correct equation (4) and will vary from 100 to 500.

Figure 16 shows typical computed temperature profiles with different values of the chemical rate constant (K_r) - λ has been taken as 500. The degree of reaction (λ_r) shown in *Figure 16* is defined as the ratio of the molar flow rate of methane at any point to that at inlet. Since all of these profiles have been computed with the same value for the plate temperature then the final temperature in the isothermal region is the same. For the lower values of K_r, this final temperature is approached at very long distances from the distributor plate. From this, it is possible to define the 'Isothermal

Bed Temperature' as the limit of T(x) as x approaches infinity. How near the bed temperature is to this at any point is shown in *Figure 16* to depend upon the assumed rate of chemical reaction.

These profiles have reproduced temperature variations along the bed axis similar to those obtained in a combustion bed - the only fault with the results so far is that the temperature variations are too small and this will be remedied in the following section. However, what is important with the model so far is that it reproduces the isothermal region in the combustion bed, and it is possible to see how heat is being transported through this region. Equation (19) can be re-arranged to give:

$$\delta T = \frac{\left[- \sum_{j=1}^{N} \int_{\phi=\dot{N}_j^o}^{\phi=\dot{N}_j} (h_f^T)_j \, d\phi - \dot{m}(h - h_o) \right]}{\dot{M}C} \qquad (20)$$

where δT is the temperature difference between the particles transported by the bubbles and those in the dense phase at any section across the bed. When the reaction is complete then the integral term in equation (20) represents the total energy release from the chemical reaction. Some of this is transported in terms of the enthalpy of the combustion gas (i.e. $\dot{m}(h - h_o)$) and the remainder is transported by particle convection and radiated from the bed surface.

If one assumes different particle transportation rates then other temperature differences (i.e. δT) will be required to transport the radiative component through the isothermal region. *Figure 17*

shows temperature profiles when the mass transportation rate is varied from one hundred to five hundred times that predicted by equation (4) - a value of $10^{14} s^{-1}$ has been used for K_r. These profiles show an increase in δT as the transportation rate is reduced. Since the same plate temperature has been used in *Figure 17*, then the isothermal bed temperatures are seen to be different. This is a hypothetical case only: any change of bed transportation rates would undoubtedly change the plate temperature and the isothermal bed temperature is, strictly speaking, only dependent upon surface radiation.

The following sections will now make a more realistic application of equation (11). By allowing for temperature differences between the particles and gas mixture at entry, it will be possible to obtain calculated profiles with the same magnitude of temperature variation one observes with a fluidized combustor.

3.7 MORE DETAILED APPLICATION OF MODEL

(a) Equations and Boundary Conditions

The previous section has given a few results from a much simplified application of the model. With these few results in mind, a more realistic study will now be made. Equation (11) will be adapted to the condition where the gas temperature at inlet is below the solids temperature. In the previous section it was assumed, for simplicity, that the drift particles were at the plate temperature. A more realistic approach will now be made where it is assumed that the bubble drags particles, upon formation, from a region just above the plate. The mean temperature of these particles will correspond

to the emulsion phase temperature at some hypothetical point just above the distributor plate. With the short distances involved with shallow beds, it will be assumed that there is little mixing between the particles in the two phases and hence this mean temperature is constant as the particles are dragged up through the bed.

Two forms of equation (11) will be used: above the hypothetical point in the emulsion phase (as mentioned above) it will be assumed that $\dot{M}$ has a definite positive value, and below this point it will be assumed that $\dot{M}$ is zero. As in section (3.6) it will be assumed that there is perfect mixing of the gases in the two phases. To allow for heat transfer between gas and particles, a further restriction must be imposed upon equation (11). This is obtained by equating the rise in enthalpy of the gas mixture as it flows in between two planes to the heat transferred to the gas by particles within the two planes and the energy liberated by combustion within the two planes. The result is:

$$\dot{m}c_p \frac{dT_g}{dx} = h_a a(T_s - T_g) - \sum_{j=1}^{N} (h_f^T)_j \frac{d\dot{N}_j}{dx} \qquad (21)$$

where a = total particle surface area per unit length of bed

h_a = gas-particle heat exchange coefficient.

This will be used in the form:

$$\frac{dT_g}{dx} = H(T_s - T_g) - \frac{1}{\dot{m}c_p} \sum_{j=1}^{N} (h_f^T)_j \frac{d\dot{N}_j}{dx}$$

where $H = h_a a/\dot{m}c_p$. H will be assumed not to vary for different points within the bed.

First consider the region just above the distributor plate where $\dot{M}$ is zero. Equation (11) integrates to:

$$K.A.\frac{dT_s}{dx} - \dot{m}c_p T_g - \sum_{j=1}^{N} \int_{\phi=N_j^o}^{\phi=\dot{N}_j} (h_f^T)_j \, d\phi = \text{constant} \qquad (22)$$

There are two boundary conditions:

(1) $$KA\left[\frac{dT_s}{dx}\right]_{x=0} = \left[\dot{m}(h_T - h_o)\right]_{x=0}$$

(2) Inlet chemical composition is that for an unreacted mixture.

Substituting these into equation (22) yields:

$$\text{constant} = KA\left[\frac{dT_s}{dx}\right]_{x=0} - \left[\dot{m}c_p T_g\right]_{x=0}$$

With equation (21) it is possible to obtain a solution.

Now consider the region where $\dot{M}$ has a definite non-zero value. Let X be the distance from the plate where the emulsion temperature is the same as the drift particle temperature. Equation (11) integrates to:

$$K.A.\frac{dT_s}{dx} - \dot{M}C(T_b - T_s) - \dot{m}c_p T_g - \sum_{j=1}^{N} \int_{\phi=N_j^o}^{\phi=\dot{N}_j} (h_f^T)_j \, d\phi = \text{constant} \qquad (23)$$

The boundary conditions for this equation follow from the solution of equation (22) at $x = X$. When $x = X$, equation (23) becomes:

$$K.A\left[\frac{dT_s}{dx}\right]_{x=X} - \left[\dot{m}c_p T_g\right]_{x=X} = \text{constant}$$

For a continuous temperature function it is required that at x = X the temperature and their derivatives are the same in equation (23) as in equation (22). Similarly, in the integral term in equation (23) the lower limit of the integral corresponds to that for values of $\dot{N}_j$ at x = X.

The only major assumption to be made before solutions are possible is how the amount of gas in the bubble phase is determined. In this more detailed study, it is being accepted that the gas and solids are at different temperatures. A problem arises in determining at what point bubbles are formed, and what is their total volume. There is no data available to solve this. To circumvent this problem it will be assumed that the plate temperature may be taken as a reference and the bubble volume calculated by assuming the gases to be at this temperature. There is no justification for this other than it allows calculations to proceed. A full discussion of this problem will be given later in this chapter.

(b) Similarity Between This Work and That of ~~Essenhigh~~ COLE & ESSENHIGH[24] & ~~Cole~~[24]

Figure 18 shows a typical computed temperature profile. Superimposed are calculated values of the degree of reaction. A gas inlet temperature of 500°C has been assumed, and the particle temperature at the distributor plate has been taken as 1 100°C. A value of X = 0.5 cm has been used - the experimental results of Chapter 4 suggest this to be a reasonable value. Other parameters are:

$$K = 0.04 \frac{\text{cal}}{\text{s.cm.}^{\circ}\text{C}} \quad \left[\text{or } 0.167 \frac{\text{W}}{\text{cm}^{\circ}\text{C}}\right]$$

$\dot{M}$ = 500 x (equation 4)

$H = 25\ cm^{-1}$

$K_r = 10^{11}\ s^{-1}$

All other parameters are as used in Section 3.6.

In this temperature profile the isothermal bed temperature is produced for large distances from the distributor plate, and the variations in solids temperature along the axis are similar in magnitude to those reported in Chapter 4. *Figure 18* shows that at the point of maximum gas temperature the gas mixture is in the initial stages of reaction. This falls very much into line with the Cole and Essenhigh's suggestion that temperature profiles near the distributor plate are due to solids recirculating and heating the oncoming gas stream. If a steady flow energy balance is taken at the point of maximum solids temperature, there are no conductivity terms giving

$$\dot{m}(h - h_o) = \dot{M}C(T_S - T_B) - \sum_{j=1}^{N} \int_{\dot{\phi}=\dot{N}_j^c}^{\dot{\phi}=\dot{N}_j} (h_f^T)_j \, d\dot{\phi} \qquad (24)$$

Figure 18 shows that at the point of maximum solids temperature the reaction has only just begun and the last term in equation (24) must be very small. Since the points of maximum solids temperature and maximum gas temperature very nearly coincide it may be argued, from equation (24), that the oncoming gas mixture gains its maximum increase in enthalpy (during the first 0.5 cm or so), mainly due to particle recirculation. Also, the mechanism

by which the gas mixture is heated is by gas-particle heat exchange. This is in agreement with Cole & Essenhigh.

To explain how the temperature profile in *Figure 18* is produced, it is necessary to examine the terms in equation (11). The moduli of these terms are given in *Figure 19*. For distances less than 0.5 cm from the distributor plate there are only two terms which dictate the value of d^2T_s/dx^2. They are a term due to the motion of the fluidizing medium given by:

$$\dot{m} C_p \frac{dT_g}{dx}$$

and a term due to the rate of heat release from the chemical reaction which is given by:

$$\sum_{j=1}^{N} (h_f^T)_j \frac{\dot{dN}_j}{dx}$$

Just above the distributor plate the former term tends to make d^2T_s/dx^2 positive, the latter tends to make it more negative, and since the former is dominant then dT_g/dx very slowly increases. Since the chemical term is increasing very rapidly, *Figure 18* shows that the rise in dT_s/dx is very small in this region - nearly constant in fact. At A the chemical term has become dominant and now dT_g/dx is reducing. Again this gives only slight changes in the profile and the temperature profile approximates to a straight line. At B the gas temperature has reached its maximum value and the values of dT_g/dx are becoming negative. Now both terms are reducing dT_s/dx. This again gives only moderate decreases. At C the particle transportation term:

$$\dot{M}C \frac{dT_s}{dx}$$

comes into effect and the solids temperature profile is seen to reach a maximum where the temperature reduces for increase in distance. This is at D. Now inbetween C and D the particle term was making d^2T_s/dx^2 negative but after D it reverses sign to force it positive. It is the combination of these three terms that now produce the exponential solids temperature profile after D. When all of these terms very nearly cancel each other the bed temperature is very nearly constant, and for very large (one should say infinite) distances from the distributor plate all terms are zero - which defines the isothermal bed temperature.

In conclusion, it can be stated that the results of this model are, from what has been discussed so far, in complete accordance with the explanation of Cole & Essenhigh. There are, however, conditions where the proposition presented by Cole and Essenhigh may not fully explain the temperature profiles. In this work two types of temperature profile have been observed - as shown in *Figure 11*. They differ with regard to the magnitude of the plate temperature compared with the isothermal bed temperature. Previous workers have only observed profiles as shown in the top of *Figure 11* and these can be explained by Cole & Essenhigh. In the case of the bottom profile in *Figure 11*, the particle movement does not play any part at the point where the solids temperature is a maximum, and this will be explained in section 3.7(h).

(c) Practical Aspects of the Calculated Profiles

Before discussing the relative effects of the parameters in equation (11) it is worthwhile examining the consequences of those results portrayed in *Figure 18*. As the reaction proceeds, the gas temperature is seen to overshoot the solids temperature, reach a maximum value, and then fall rapidly. From a pollution point of view this is disturbing since one of the advantages assumed for a fluidized combustor has been its low gas temperature and hence its low pollution level. Since the literature has not reported any gas temperature measurements it has always been assumed that the temperature of the solids would give an indication of CO and NO_x emissions as indicated by the work of Jarry *et al*[26]. *Figure 18* indicates that this need not be the case.

The following sections will now examine how the parameters in equation (11) affect the temperature profiles. In particular, section 3.7(f) will show how much the gas temperature depends upon the gas throughput and particle-gas heat transfer.

(d) Effect of Thermal Conductivity

The values of thermal conductivity used so far in this chapter are one order of magnitude higher than those calculated for a packed bed. In view of the comments in 3.3(a) this demands an explanation.

The problem arises in how the thermal conductivity should be estimated. In section 3.3(a) it was argued that the most reasonable conductivity to use would be that of a packed bed, and this could be estimated from the Deissler-Elan correlation with an added

radiation component calculated from Schotte's formula. A conductivity based upon this method was found to give axial temperature variations of about five times too high. It may be that the fixed bed correlations do not apply under these conditions. Most of the work on fixed beds at these temperatures has been with very small temperature gradients - clearly this is not the case in a fluidized combustor where temperature gradients are considerable. Work on packed beds has been under conditions where the gas temperature has been very nearly equal to the solids temperature and under these conditions the temperature gradients of both solid and gas are almost identical. In the case of the entry region of a fluidized combustor the gas temperature gradient can be as much as five times more than the solids temperature gradient. The latter may present a major deviation from normal fixed bed conditions but calculations allowing for two conductivity terms (both gas and bed conductivities) have produced no appreciable difference.

Figure 20 shows how the temperature profile behaves for variations in magnitude of ten times the calculated fixed bed conductivities. The profiles are similar to what one obtains with a fluidized combustor and show that large fluctuations in temperature are favoured with low conductivities. This is to be expected since in equation (11) d^2T_s/dx^2 is inversely proportional to the thermal conductivity. Therefore a decrease in conductivity will favour a higher rate of increase of temperature gradient in the bed entry region.

The profile for K = 0.01 cal/cm.s^{o}C is of special interest because the maximum solids temperature is reached before the point at which

particle circulation is included. This is different to the type of curve examined in section 3.7(b) and will be discussed in section 3.7(f).

(e) Effect of Particle Transportation Rate

The particle transportation rate controls the difference between the maximum solids temperature and the isothermal bed temperature. *Figure 21* shows that high transportation rates favour low temperature differences, and low rates favour high differences. Multiples of inbetween one hundred and five hundred times those transportation rates estimated from equation (4) have been used. These correspond to mass flow rates of up to 7 kg/s.

It should be pointed out that although the particles in the bubble wake have been assumed to have a constant temperature, the temperature will in fact vary as the bubble rises. This variation will be due to a constant interchange between these particles and those in the emulsion phase which will be at a different temperature. However, for the short distances involved this will be very small and the assumption should be valid.

Similarly, it has been assumed that the transportation rate is the same for all sections above x = 0.5 cm. In fact, the rate of transportation will be very low near the bottom of the bed and increasing in the vertical direction. This would widen the difference between the maximum solids and the isothermal bed temperature.

(f) Effect of Chemical Kinetics and Gas-Particle Heat Exchange

These two parameters more than any others dictate the shape

of both gas and solids temperature profile. Since they have a similar effect in equation (11), it is difficult to discuss either one in isolation. This section will show what combined effect the two can have on the calculated temperature profiles.

For convenience, a heat transfer factor H has been used, and this is defined as

$$H = \frac{h_a a}{\dot{m} C_p}$$

With the particles and gas flow rates used in these calculations, this becomes

$$H = h_a \times 66 \times 10^2 \frac{cm\ ^\circ C\ s}{cal}$$

$$\text{or} \quad h_a \times 15.7 \times 10^2 \frac{cm\ ^\circ C}{W}$$

and a value of $H = 100\ cm^{-1}$ corresponds to $h_a = 1.5 \times 10^{-2}$ cal/cm^2 $^\circ$C s (6.3×10^{-2} W/cm^2 $^\circ$C).

Considerable doubt arises as to the evaluation of h (see Kunii & Levenspeil[5]), so the values used have been those which have produced reasonable results. Kunii & Levenspeil recommend that h is derived from:

$$N_u = 0.03\ R_e^{1.3}$$

which for the bed conditions used gives a value for h_a of

$$.73 \times 10^{-3} \frac{cal}{cm^2\ ^\circ C\ s} \left[3.06 \times 10^{-1} \frac{W}{cm^2\ ^\circ C}\right]$$

No experimental data is available for a comparison, but the results of this correlation compare well with the values of h_o used:

$$(.15 \times 10^{-2} \text{ to } 1.5 \times 10^{-2}) \quad \frac{\text{cal}}{\text{cm}^2\ {}^{o}\text{C s}}$$

$$(.63 \text{ to } 6.3) \times 10^{-2} \quad \frac{\text{W}}{\text{cm}^2\ {}^{o}\text{C}}$$

Figure 22 shows the effect of varying H on the solids temperature. All of the other parameters are the same as those used in *Figure 18*. There is very little change in the temperature profile shape. The isothermal bed temperatures are different because the same distributor plate temperatures have been used.

The values used for H do, however, have a profound effect upon the gas temperatures. *Figure 23* shows how the gas temperature profile is influenced for those conditions given in *Figure 22*. Clearly, for low values of H the gas temperature can rise considerably above the solids temperature, and this is not desirable when considering possible CO and NO_x emissions.

Figure 24 shows how the assumed rate of chemical reaction affects the solids temperature profile. Calculations have shown that with sufficiently high or very low values of H it is possible, with suitable values of K_r, to obtain profiles that are not explained by the work of Cole and Essenhigh. One example was shown in *Figure 20*, other examples are shown for the higher values of K_r in *Figure 24*. If the conditions are suitable, then the reaction may proceed in such a manner that the point of maximum solids temperature is reached before particle recirculation begins.

This occurs either for very high values of H where the gas-air mixture is preheated very rapidly, or for a very low value of H where the gas temperature overshoots the solids temperature considerably, resulting in very high rates of reaction. Therefore there will be an upper and lower limit of throughput, and outside of these limits this class of profile will occur. This will be seen to apply in Chapter 4. What has just been described is the second class of profile depicted in *Figure 11*. It is conspicuous by the very short distances in which the maximum solids temperature variation occurs and, in some instances, by the isothermal bed temperature being below the distributor plate temperature.

Calculations for the gas temperature profile show that high values of K_r increase the rate of temperature rise as do high values of H.

3.8 PROBLEMS WITH THE MODEL, AND AREAS REQUIRING MORE DETAILED STUDY

There are three areas of importance in studying a fluidized combustor. They are the final .5 cm or so at the bed surface where the surface radiation occurs, the section comprising of the inlet to the air box and entry to the bed, and the remaining portion of the bed which is inbetween these other two sections. All of these three areas are interdependent, and so far only the latter has been discussed.

In the calculations so far it has been assumed that the bed surface will radiate at whatever the calculated bed temperature turns out to be: no effort was made to think in terms of matching the initial boundary conditions in such a way as to ensure complete

harmony in this respect. Similarly, no attempt was made to match the surface heat transfer between the bed and the distributor plate in such a manner that the bed temperature at the plate was sufficient for the surface heat flux to equal the enthalpy gain of the fluidizing medium as it made its exit from the distributor plate. Instead, an arbitrary temperature was chosen which was assumed to allow for this. As this elementary discussion shows, all three regions of the bed are important and each must be fully understood before a proper insight into the behaviour of fluidized combustion can be made.

In developing a mathematical model for a fluidized combustor it should be clear how the mathematical results should be interpreted with respect to the results obtained from an experimental study. In this model problems may arise when comparing calculated and observed temperature profiles - as will now be explained. In the model a clear distinction is made between the temperature of the solids transported by the bubbles and the temperature of those particles in the emulsion phase. The model assumes there to be two distinct phases that can be studied separately. In an experimental study (as will be seen in Chapter 4), the distinction between the two phases is not so clear. This problem is highlighted by considering the case of a vigorously bubbling fluidizing bed with very high rates of particle transportation. For high solid transportation rates an instantaneous picture of the particle drift would be as shown in *Figure 25*. The shaded zones will be at a different temperature to those that are unshaded. There is little difficulty in envisaging a mathematical solution for a bed with a

high mass transportation rate, but the problem arises as to how an actual thermocouple temperature reading should be interpreted when measured in a condition such as that shown in *Figure 25*. For even higher mass recirculation rates the distinction between the two phases will disappear and the bed will be completely mixed - under these conditions the model will be of little use. That the zones in *Figure 25* correspond to different temperatures has already been shown by Lewis, Gilliand and Girouard[19]; the whole of the work in this chapter rests firmly upon that fact.

Although the simple chemical kinetic equations used have been helpful in explaining the temperature profiles, they represent a gross distortion of the truth. In this simple model it was assumed that only one reaction occurred, and that this was allowed to proceed towards completion without any regard for equilibrium conditions. It was further assumed that the same kinetic considerations applied between the two extremes of gas temperature (at the bed inlet and exit) and that these extremes could be bridged by an Arrhenius factor. The reaction was assumed to take place in the gas phase and no attempt was made to consider any other mechanism such as including for particle surface effects. A complete specification of the reaction mechanism presents a formidable task, and this is the only excuse for such a gross oversimplification. A complete specification of the reaction mechanism would require a knowledge of all of the important chemical reactions that are taking place within the bed, and these should allow for the formation and destruction of such species as oxygen atoms, hydrogen atoms and hydroxyl radicals. This in

turn would require a knowledge of how the particle surface affects the destruction of radicals. With all of this information available it might be possible to write a number of independent chemical equations, complete with forward and reverse rates, and specify the state of the reaction in all of the stages. At present, this is beyond our reach and the simple model, notwithstanding its faults, does give a reasonable picture of the combustion process.

To enable calculations to take place, a few assumptions had to be made about the growth of bubbles in the bed. Since the gas temperature and volume is increasing as it rises through the bed, it is difficult to state at which point bubbles will form, and at what point particle recirculation will begin and what will be its rate of transportation. When the gas temperature is constant, then one can estimate a reasonable depth at which bubbles begin to form by reference to such works as Cranfield [8] Geldart[8]. To estimate the mass transport rate at some point higher up in the bed is a matter of consulting the many papers published on this topic. The only major obstacle is not knowing at what point the particles begin to circulate in appreciable numbers. This difficulty is enhanced by not knowing where the bubbles are formed when studying combustion systems. The following assumptions had to be made:

(1) The particles are transported from, and at a temperature of, .5 cm above the distributor plate

(2) The volume of gas in the bubble is calculated by assuming the gas is at the same temperature as the particles at the bed entry.

The former is based upon experimental grounds, but the latter is

an assumption of convenience.

3.9 BRIEF SUMMARY AND CONCLUSIONS OF THE MATHEMATICAL STUDY

The simple model proposed in this chapter has attempted to explain the mechanisms of a fluidized gas combustor. By allowing for particle movement due to bed bubbling, it has been possible to reproduce temperature profiles which bear a strong resemblance to those obtained in a fluidized combustor. All through the development of the model, an attempt was made to use as much existing knowledge about fluidization technology as was possible, and in doing so a high degree of concordance was found between these calculated results and the work of Cole & Essenhigh in explaining their experimental results. One thing that this work has highlighted is the problem of interpreting fluidized bed thermal conductivities. This work suggests that the true thermal conductivity of a fluidized bed is the conductivity of a packed bed at the same voidage. The very high values of 'effective thermal conductivity' reported have been due to particle movement and when it is considered how much this depends upon particle temperature differences, then all such thermal conductivities should be treated with caution.

The mathematical results suggest that low conductivities and low particle-gas heat transfer coefficients will result in large temperature gradients in the lower parts of the bed, and that low particle transportation rates will result in large temperature differences between the final (isothermal) bed temperature and the maximum bed temperature.

CHAPTER 4

EXPERIMENTAL STUDY OF METHANE COMBUSTION IN FLUIDIZED BEDS

4.1 INTRODUCTION

The work reported in this chapter is for large dense particles and with higher fluidizing velocities than those reported by previous workers in this field. These results, together with those of Broughton *et al*, have influenced the mathematical study of Chapter 3 and wherever possible, they will be discussed in the light of that study.

4.2 DESCRIPTION OF EQUIPMENT AND EXPERIMENTAL TECHNIQUE

(a) Bed Construction and Operation

Two bed constructions were used, *(Figures 26 & 27)*: for smaller particles (below 1.0 mm diameter) a bed with a porous refractory distributor plate was used, and for larger particles a bed with a mild steel distributor plate was used. The bed was made such that changing the distributor plate only amounted to unbolting the top of the bed and replacing it with a top piece suitable for that distributor plate. All bolted joints were sealed by 0.8 mm thick gaskets. The bed was fabricated from ordinary mild steel tube. Although this had the disadvantage that the combustion tube rapidly oxidised and periodically had to be replaced, this was offset by the small capital cost involved.

The mild steel distributor plate was fabricated from 9.525 mm thick plate. Rows of 1.5875 mm (1/16 in drill) diameter holes at 6.35 mm centres were found to give good fluidization.

The refractory plate was made from a 2.5 cm thick refractory block (supplied by Daltons Ltd, reference 3E 314). A gap of approximately 0.75 mm was allowed inbetween the refractory block and the mild steel combustion tube, and this gap was packed with asbestos fibre and sealed at the top and bottom with FORTAFIX cement (supplied by Fortafix Ltd).

The bed was insulated by a 3 cm thick layer of KAOWOOL (supplied by Morgan Refractories Ltd) and this was covered by a layer of Aluminium Foil (supplied by Aluminium Foils Ltd). The presence of the reflecting foil was found to increase the outer temperature of the lagging. Without the foil, one could place ones hands upon the lagging without any danger, and by placing ones hands a short distance away from the lagging one could sense heat being radiated away from the bed. However, with the reflecting foil in position one could not place ones hands upon the foil due to the high temperatures, and one could not sense any radiation away from the bed. Notwithstanding the reduction in radiation loss gained by introducing the foil, it was found that bed temperatures were the same both with and without the foil, and it was concluded that the losses from the sides of the bed were negligible.

To ensure that no particles were ejected from the bed at high velocities, a gauze plate was fitted over the top of the bed. This was made from 0.6 mm stainless steel mesh sandwiched inbetween two mild steel plates *(Figure 28)*. The gauze plate was found to increase the temperature of the upper sections of the combustion tube which glowed red whenever the gauze was fitted. Without the gauze plate those same upper sections appeared a dull-black colour,

but no difference in bed temperature was noticed due to the presence or absence of the gauze.

Combustion could be initiated by passing a stoichiometric (or near stoichiometric) mixture through the bed at about one and a half times the minimum fluidizing velocity and igniting it above the bed surface. The temperature of the bed would increase slowly in the temperature range up to 400°C, but after this the temperature would increase rapidly and would be accompanied by violent explosions within the bed. These explosions were capable of shaking the bed. Comparatively silent combustion was obtained with temperatures above 1 000°C. The time for the bed temperature to reach 1 000°C was about forty minutes; another thirty minutes were required for the bed to attain thermal equilibrium with its environment.

During the 'light-up' sequence it was found that a flame could be held on the bed surface even when the fluidizing velocity was in excess of the normal flame velocity. This may have been due to each particle at the surface acting as a bluff body flame holder.

To ensure that no particles were ejected during 'light-up', a funnel and a large gauze plate were fitted over the bed (see *Figures 29 & 30*). The funnel ensured that the gauze was well away from the flame that had been established on the bed surface; otherwise the gauze would have disintegrated due to the high temperatures. With smaller particles it was possible to 'light-up' with the smaller gauze plate.

BED CASING AND THERMOCOUPLE POSITIONER

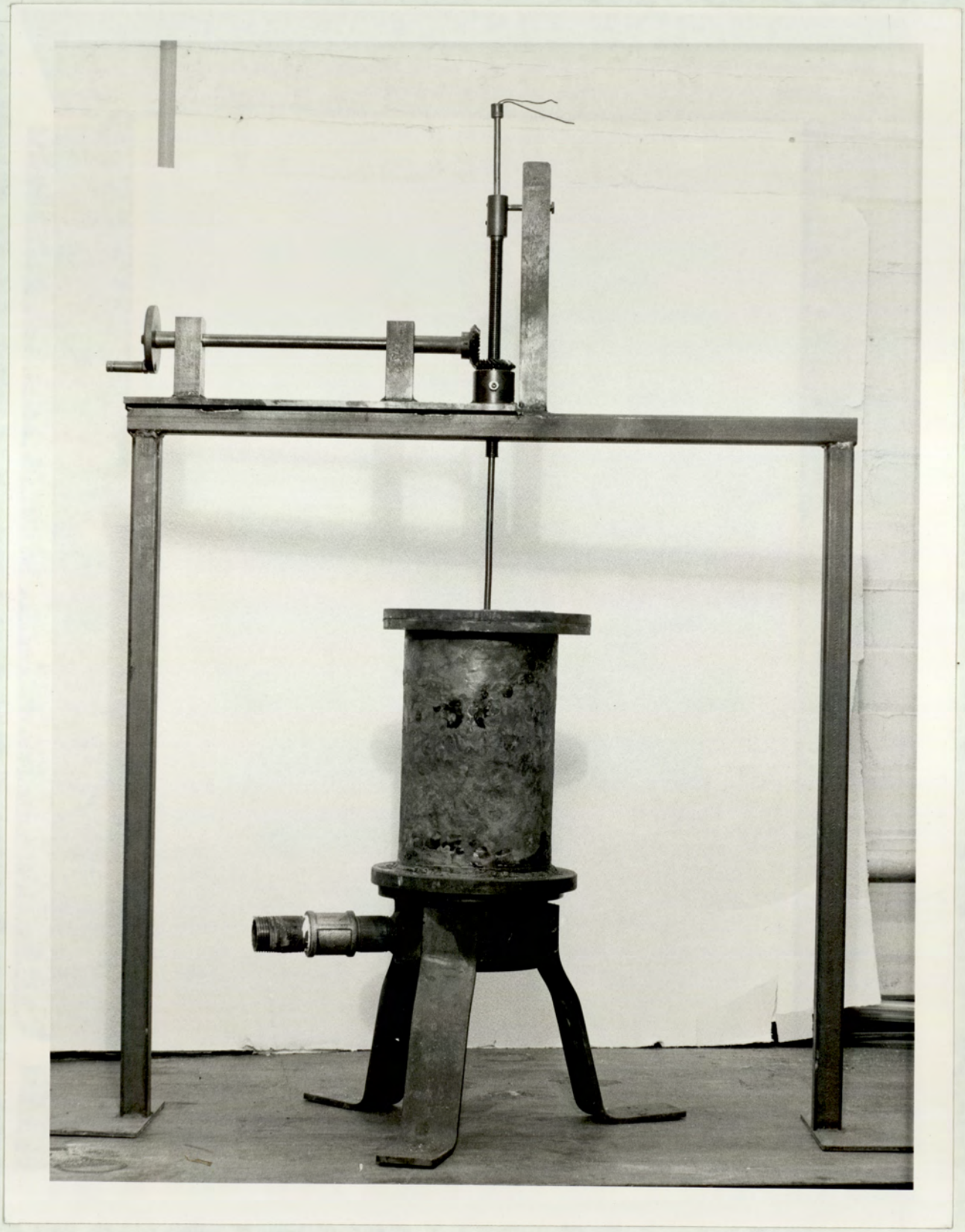

(b) Temperature Measurement

Temperatures were either recorded by a digital pyrometer (type Veritell-D, supplied by D A Pitman Ltd) or, when a time-temperature trace was required, a Leeds and Northrup type W Speedomax recorder was used. Two digital pyrometers were used: one recorded the gas inlet temperatures, the other recorded the bed temperature. Both were calibrated for their own range of working temperatures. Chrome-alumel thermocouples were used to sense the temperatures and these were fed via a selector switch (CROPCO type SQ2 supplied by the Croydon Precission Instrument Company) to the appropriate temperature recorder. Two types of thermocouple were used to sense bed temperatures: a 6.35 mm diameter sheathed thermocouple (supplied by Pyrotenax Ltd) and a 3.63 mm diameter sheathed thermocouple (supplied by Spembly Ltd). There was no great difference in the readings from either of these thermocouples - the larger diameter thermocouple had the advantage of greater rigidity. For sensing gas supply temperatures, simple thermocouples were made in the laboratory from chrome-alumel and these were adequate.

The sheathed thermocouples were accurately positioned in the bed by using a screw-thread device. One revolution of the screw would displace the thermocouple 1.5875 mm (ie 1/16 in pitch). The thermocouple positioner, bed and gauze plate are shown in plate (1).

(c) Flow Measurements

All flow rates were measured by rotameters (supplied by The

Rotameter Manufacturing Company Ltd). For our flow measurements, tube sizes ranging from a 25 tube to a 65 tube were used. A size 7 tube was used for measuring the methane flow rate. This methane rotameter was calibrated with Boy's Bell type gas meter (supplied by Alex Wright and Company Ltd), and it was found that the rotameter manufacturer's calibration chart was accurate when corrected from air to methane. The gas meter itself was checked by passing a known quantity of air by means of a large vacuum tank and the gas meter error was found to be negligible. All other rotameters were checked by comparison with one and another. The flow metering was arranged as shown in *Figure 31*. Given the temperature and pressure of the gases, it was possible to convert all flow rates to standard values at a temperature of 15^{o}C and a pressure of 760 mm Hg. The air was supplied by a blower (supplied by Service Electrical Company Ltd, type 428).

(d) Particles and Minimum Fluidization Velocities

Two particle materials were used, one was silica dioxide and the other was a zirconium silicate compound. These were supplied by the Associated Lead Company Ltd. Silica dioxide was chosen as a common fluidized solid, and zirconium silicate was chosen because of its very high density and hence it very high minimum fluidization velocities. Diameters ranging from 0.6 to 1.4 mm were used. To determine the minimum fluidization velocity a probe was used to measure the pressure drop between any two planes in the bed, and from the variation of pressure drop with gas flow the minimum fluidization velocity could be determined.

The probe consisted of two stainless steel tubes immersed in the bed (as shown in *Figure 32*) and connected to a manometer.

Two types of pressure drop - flow rate curves appear to be published by investigators in this field. Some results give a linear relationship between pressure drop and flow rate, and others give a polynomial relationship. In this work linear relationships were obtained, but with some deviation at low flow rates (see *Figure 33*). With these probes it was found that when the point of minimum fluidization had been reached, then for slight increases in throughput the pressure drop would be constant, but for further increases the pressure drop would begin to oscillate as bubbles were passing inbetween the two planes. This oscillation was more pronounced with the very large zirconium silicate particles. The most common method of determining the point of minimum fluidization has been to measure the total pressure drop through the bed. As will be seen later, the method used in this work has the advantage that it can be easily adapted for measurements in high temperature beds.

Before the experimental values of U_{mf} could be compared with those calculated from equation (3) it was necessary to determine ε_{mf} and ϕ_s since they are required in this equation. To evaluate ε_{mf}, a special column was made from perspex with a calibrated height scale. By measuring the height for different quantities of particles, with the column in the incipient state, it was possible to evaluate ε_{mf} from the graph of mass-height as follows:

We have $\rho_s A (1-\varepsilon_{mf}) H_{mf} = M$

where A = bed area

M = mass of particles

$$\therefore (1-\varepsilon_{mf})\ \rho_s\ A = \frac{M}{H_{mf}} = \text{(M-H gradient)}$$

and from this, ε_{mf} is evaluated.

To determine values for ϕ_s, the particles were viewed under a microscope and their shape compared with those compiled by Rittenhouse[35]. The advantage of the Rittenhouse two-dimensional chart is its simplicity, and there appears to be very little error when comparing results with the more difficult statistical sampling techniques (errors of less than two per cent quoted in Rittenhouse's paper).

The diameter of the particles was taken as the geometric mean of the sieve sizes. In this work the particles used were sieved inbetween very fine limits. Table 1 gives information about the particles, both calculated and measured. With the silica dioxide particles there seems very little to suggest that of the two equations for determining U_{mf} (equation 3 and Cranfield[7,8]), one is better than the other. However, with the very dense particles, equation 3 gives the better results.

The method described for measuring U_{mf} can readily be adapted for measuring under conditions of high temperature as follows. The bed is first heated above the required temperature range by combustion. When the air and gas supply are stopped, the rate of fall of bed temperature is very small. This is so even when air is passed through the bed at velocities not much

higher than U_{mf}. Therefore, it is simply a case of placing the probe in the uppermost regions of the bed, slowly increasing the air flow and noting the pressure drop. To ensure that the bed temperature does not vary too much during the measuring process, U_{mf} can be estimated by slowly increasing the flow rate and only noting at what point the pressure drop becomes constant. This method was tested with the bed at ambient conditions and differences of no more than five per cent were found when comparing with graphical estimates such as in *Figure 33*. With this method it was possible to reduce the time consumed in taking data from a wide range of conditions and, as a result, there was very little fluctuation in bed temperature during the process. For measurements at a lower temperature it is simply a case of passing a large quantity of air through the bed until the desired temperature is obtained, and then repeating the process over again. This method does not require the expense of an air pre-heater.

The probe is placed at the top of the bed to ensure that the air has reached the same temperature as the particles. With bed heights of 8 to 10 cm and the low flow rates involved, this should present no problem.

Experiments at high temperatures have found that equation (3) is no longer valid. Results are presented in *Figure 38* for the large zirconium silicate particles and show a considerable deviation from the predictions of equation (3). Observations of the bed surface support the experimental values of U_{mf}: when the bed was seen by pressure readings to be in the incipient state it could easily be stirred, and for slight increases in flow rate

bubbles could be seen even though equation (3) would predict that the bed should not be in the fluidized state.

The discrepancy between measured and calculated minimum fluidization at high temperatures is interesting. Since Erguns' equation has been tested for many different gas densities and viscosities, then one would expect the equation for U_{mf} to apply when high temperatures are used. It appears as though a bed has a higher fluidity at high temperatures. A recent paper published by Mii, Yoshida and Kunii[36] has reported a similar behaviour at high temperatures. This is an area that requires further study.

(e) Gas Sampling Equipment

A gas chromatograph was used to separate and measure the concentrations of the components within the post-combustion gas mixture. This was supplied by Pye-Unicam Ltd, being a type 104 A. A katharometer detector was used with helium as the carrier gas. Two columns were required to separate the products in the combustion products: a silica gel column that separated H_2, CO, CH_4, CO_2 and air (O_2 & N_2), and a molecular sieve column that separated O_2, H_2, N_2, CH_4 and CO. Each column was calibrated by passing known samples of gas through at the working temperature (50°C). To detect very small concentrations a large sampling tube was required and it was found that a 10 m.l capacity was adequate. With this arrangement it was possible to detect concentrations of order 10^{-5} and measure those of order 10^{-4}. Before the gas sample could be analysed it had to be quenched. Two types of cooling probe were tried: one based upon a design reported by Fristrom

and Westenberg[37] made from quartz, and one manufactured from copper tube and water cooled. It had been hoped that the quartz tube would have sufficed since this could be immersed in the bed without causing too much disturbance. Although this probe is suitable for flame studies and the rapid cooling at the orifice will quench the combustion products, when it was immersed within the bed, or even placed above the bed surface, it was found that the combustion products reheated due to the extremes of temperature in the surroundings and the reaction would proceed to completion. Even when this probe was placed just above the distributor plate and sampling an unreacted mixture, by the time the sample had passed through the very high temperature zones and reached the chromatograph, the reaction had reached completion. With the water cooled proble, however, there was no such problem. It had the disadvantage that it could be immersed in the bed without causing considerable disturbance, but it could quench the sample and the water cooled jacket prevented any reheating. The water cooled probe is shown in *Figure 39*. It was possible to take exit samples by placing the probe a short distance above the bed surface, and this did not in any way disturb the bed. Water condensation was found to be a problem in the supply line and this was alleviated by the incorporation of a silica gel filter.

To suck the sample gas through the chromatograph, a high vacuum pump was used. This was supplied by The Edward Hughs Vacuum Company Ltd, being their Speedwac type ES 150. To record the chromatograph output peaks, a Bryants type 2800 pen recorder (supplied by Bryant Instruments Ltd) was used. The peak areas

were measured by a planimeter (manufactured by A.Ott Kempten, Bayern). All joints in the gas line were either special vacuum joints supplied with the chromatograph, or those joints manufactured in the laboratory which were sealed with ARALDITE (supplied by CIBA-GEIGY (UK) Ltd).

4.3 QUALITY OF FLUIDIZATION AND INITIAL COMBUSTION STUDIES

With both types of distributor plate described in Section 4.2(a), it was possible to obtain good fluidization within the bed. There was, however, a clear distinction between the behaviour of silica dioxide particles and the very dense zirconium silicate particles. For shallow beds of about 8 cm depth, there were numerous small bubbles being formed within the silica dioxide bed and breaking randomly on the surface. This resulted in a very slight fluctuation of the smooth bed surface. With the zirconium silicate particles there were few bubbles in the bed but they were large in size. This resulted in a far greater part of the surface area remaining smooth, but the fluctuations in height of this smooth surface were considerable. With these particles the smooth surface of the bed would rise, release its bubble and then fall, almost intact. This pulsating of the bed surface caused a small amount of rotameter fluctuation. The bubbles appeared to favour no particular path.

The bed height had a considerable effect on the quality of fluidization. For increases in bed height above 8 cm (bed diameter = 13 cm), it was observed that bubbles arriving at the bed surface would eject particles up above the bed, and the height to which they

BUBBLES EXPLODING AT THE SURFACE

Photograph taken through side of glass bed

would be ejected was greater for deeper beds. This is to be expected since as a bubble rises in a combustion bed it will grow rapidly. The rapid growth is due to the heating of the gas rising within the emulsion phase, and any gas in excess of that required to maintain the incipient state in the emulsion phase will be forced into the bubbles. Any increase in bubble diameter will increase the bubble velocity, and it is this velocity that determines the height to which the particles are ejected. For as the bubble is just about to break the bed surface, all of those particles situated above the bubble are moving at very nearly the same velocity as the bubble. From this it is to be expected that deeper beds will eject particles to a greater height. Aspect ratios of no greater than .6 were used in this study, and from the wide ranges of conditions examined it was concluded that the the 13 cm diameter bed used, a bed height of about 5 cm or less gave the best quality of fluidization in a combustion bed. With very smallow beds (down to less than 2 cm) it was possible to have combustion beds with very high throughputs and without too much particle ejection.

With deep beds there was observed a considerable difference between the behaviour of the two types of particle. With silica dioxide particles the bed surface would rise on one side of the bed as the bubble was about to be ejected. The next bubble would then rise through the shallow side and cause that to rise as the other would fall. So would go the cycle. The bubbles with deep silica dioxide beds were fewer in number compared with those in the shallow beds and this is probably due to bubble coalescence.

With the dense zirconium silicate particles the effect of a deep bed would be that whole of the smooth bed surface would rise rapidly to a considerable height, eject a bubble and the particles above it, and then fall rapidly. What was noticeable about these dense particles was that the surface remained intact until the final moment of bubble release.

Wherever practicable, both types of distributor plate were compared. There was nothing observed to suggest that the type of plate affected the behaviour discussed in the preceeding paragraphs.

The bed temperature had a significant effect upon the combustion behaviour. With the bed operating below 1 000°C there was a considerable noise emission. For beds operating at temperatures as low as 700°C (whether cooled or in the lighting-up stage) it was possible to observe bright blue bubbles bursting within the bed. At this temperature range these bubbles would stand out against the cherry-red emulsion phase (see plate 2); at temperatures of about 1 000°C it was difficult to observe them against the bright yellow emulsion phase. It is probable that with temperatures in the region of 1 000°C the gas, which eventually forms the bubble, has reached a state of reaction such that combustion occurs smoothly within the bubble phase. This would account for the silent combustion above 1 000°C. If this is the case then with bed temperatures as low as 700°C the gas forming the bubble may not have begun to react: it would pre-heat as it rose through the bed, probably to explode as the hot combustion gas came into contact with activated chemical species from the

emulsion phase. Irrespective of what the mechanism is, these explosive bubbles can be observed with low temperature beds, and the blue flashes correspond to the intermittent noise emission from the bed.

It was interesting to observe at which height the bubble would explode. As the bed temperature was increased, it appeared as though the bubbles were exploding further down beneath the bed surface. When the bubble exploded near the surface there was considerable particle agitation. With very deep beds a bubble explosion near the surface was quite spectacular; the whole of the bed surface would be covered by the blue flash from the explosion, and a considerable number of hot particles would be ejected from the bed.

From this prelimary investigation it was concluded that the most worthwhile studies were to be made in shallow beds at temperatures of not less than 1 000^{o}C.

4.4 VARIATION OF BED TEMPERATURE WITH THROUGHPUT

For all of the particles tabulated in Table 1, data is given in *Figures 41-68*, and Tables 2-29 for the effect that the throughput has upon bed temperature. With silica dioxide particles the results given are for a bed packed with 1 kg of particles, and with the zirconium silicate particles the results are for a bed packed with 2 kg of particles. This substantial difference in mass between the two materials is because of the differences in density. With the exception of the (1.0 - 1.4)mm zirconium silicate particles, all of the results presented for this study

have been noted for a bed with a refractory distributor. A mild steel plate was used with these large particles because of the high temperatures involved. Two particular regions in the bed were chosen for study: the isothermal section was studied, and the temperature of a thermocouple placed just upon the distributor plate was studied. As will be shown in a later section, the latter is of interest in studying the combustion stability within the bed.

If one assumes that the only heat losses from the bed are those attributable to surface radiation, then for a fixed air-gas ratio, the variation of isothermal bed temperature with throughput will be as given in *Figure 13*. For very high throughputs the isothermal bed temperature should approach the adiabatic combustion temperature. *Figure 40* gives the variation of the adiabatic temperature with air-gas ratio. It is worthwhile examining if and how such an approach can explain the given experimental data.

An examination of the data for the very large zirconium silicate particles (Figs 41-45) shows that the isothermal bed temperature varied very little for any increase of throughput at a constant air-gas ratio. The only exception are the results for an air-gas ratio of 1.6 times stoichiometric: (Fig 42) these show a considerable variation with changes of throughput. Comparison with *Figure 40* shows that all of these temperatures are well below the adiabatic combustion temperature. Irrespective of the nature of the heat loss, one would only expect a situation where the temperature is nearly constant for changes in throughput when the temperature is near the adiabatic combustion temperature: when the throughput is

so large that bed losses at the adiabatic combustion temperature are small in comparison. Clearly, this is not the case.

An interesting point arises from these results for the large zirconium silicate particles. If the bed temperature is constant when the throughput is increased (for a constant air-gas ratio) and the bed temperature is below the adiabatic combustion temperature, then energy considerations dictate that the amount of heat lost from the bed must vary linearly with the throughput. If the heat loss from the bed is only due to surface radiation, then a situation is arrived at where an increase in throughput increases the surface radiation even though the bed temperature does not vary. This suggests that the emissivity is increasing with bed throughput. This agrees with the suggestion by Elliott and Virr[29] that the emissivity could increase as the bubbling becomes more vigorous.

With these very large zirconium silicate particles the plate temperature decreases with a decrease in flow with gas-lean mixtures. However, when the air supply becomes less than eighty-per-cent in excess of that required for combustion, a condition is attained where a further reduction in flow rate will result in an increase in plate temperature as the throughput is reduced. For very large decreases it is possible for the plate temperature to become unstable and rise rapidly. This rapid rise in temperature is followed at a much later stage by an increase in the isothermal bed temperature.

Results for the (.71 - .85)mm zirconium silicate particles are different. Temperature variations are given in *Figures 46-48*

and Tables 7-9. Since very high temperatures were obtained with these particles it was not possible to work with air-gas ratios less than 1.6 times stoichiometric. At 1.6 times stoichiometric the bed temperature increases with flow rate up to a maximum and then decreases. The variation in temperature, however, is less than 15°C over the range of throughputs studied. Temperature measurements for conditions at the plate show the behaviour of the plate temperature to be similar to that of the bed temperature: however, with larger magnitudes of variation. The results obtained for higher air-gas ratios show that the bed temperature increases with an increase in throughput.

Results for the (0.6 - 0.71)mm zirconium silicate particles are given in *Figures 49-52* and Tables 10-13. With these particles it was possible to work with air-gas ratios as low as 1.4 times stoichiometric. At 1.4 times stoichiometric, there was very little change in bed temperature as the throughput was increased. At 1.6 times stoichiometric the bed temperature increased with an increase in throughput until a maximum bed temperature was reached and then for further increases in throughput the bed temperature decreased. The maximum variation of temperature, however, was only 20°C. For higher air-gas ratios the bed temperature was very sensitive to any change of conditions and increases rapidly with the throughput. The temperature results for 1.8 times stoichiometric are worth of attention. *Figure 51* shows that under these conditions the bed temperature is a convex function of the throughput. However, the simple considerations of Section 3.2 would suggest a concave function of temperature as shown in *Figure 13*.

The data for the silica dioxide particles will show that this is not an isolated case. This further indicates the complexity of bed surface radiation.

Data for the lighter silica dioxide particles is given in *Figures 53-66* and Tables 14-27. For these particles the bed temperature increases with flow rate. All of the temperature profiles give a concave function of throughput with the exception of *Figure 66* where the function is clearly convex.

In Section 3.2 it was stated that two types of axial temperature profile have been observed in this work, and they are shown in *Figure 11*. All previous workers have observed a profile where the isothermal bed temperature is greater than that at the distributor. In this work profiles have also been noticed where the isothermal bed temperature is less than the distributor temperature. The data presented in this section gives an indication of what condition favours which type of profile. In the theoretical discussion on this topic in Chapter 3 it was argued that with very low flow rates the gas could rapidly heat up and produce a situation where the isothermal bed temperature is below the distributor temperature. Experimental results given in this section show that under some conditions a reduction in throughput can increase the plate temperature , and a stable temperature profile is obtained where the plate temperature is greater than the bed temperature. With other conditions, however, the bed will extinguish before this condition is attained - this will be discussed in the next section.

Although the isothermal bed temperature tends to increase

with throughput, it appears that there is no such simple variation in bed temperature when the flow rate is fixed and the particle size varied. With the silica dioxide the bed temperature of the (0.6 - 0.71)mm particles are below those of the (0.71 - 0.85)mm particles for air-gas ratios of less than 1.4 times stoichiometric. With higher air-gas ratios the smaller particles have the higher bed temperatures. The differences in temperature are in general about 10°C, the major exception being the results for twice the stoichiometric air-gas ratio where there are differences of as much as 40°C. With the zirconium silicate particles the results for all of the (0.71 - 0.85)mm tests give greater bed temperatures for a common throughput and air-gas ratio-temperature differences of as much as 80°C being common.

The height of the bed appears to have very little effect upon the plate and isothermal bed temperatures provided that the height is greater than the immediate post-combustion region. If the bed is very deep, however, violent bubbling occurs and then the temperatures vary a little. *Figure 67* and Table 28 give the variations in bed temperature for two different quantities of particles within the bed. With 2 kg of particles the bed is bubbling smoothly, but with 3 kg of particles it is bubbling violently and the bed temperatures for the two conditions in *Figure 67* show that the bed temperatures are about 10°C less with the deeper bed. There are several factors that could explain these differences. As will be explained in a later section, it has been difficult to reproduce results in these tests - 10°C being the normal amount of variation found. As was explained in

Section 4.3, violent bubbling causes possible rotameter errors and this could affect the bed temperature. As was explained in Section 4.3, violent bubbling causes greater particle ejection - and this, by increasing the emissivity, could account for the slight differences. Any one of these factors, or any of them combined, could explain these temperature differences. All that can be stated at the present is that the effect of bed height is very small.

It would appear that the type of distributor plate used can have a considerable effect upon the bed temperature. A series of measurements were made combining the very large zirconium silicate particles with a refractory distributor plate. It was only possible to operate the bed with very high air-gas ratios for fear of damaging the plate, but what observations were made have shown that the temperatures can be as much as 30°C higher with a refractory plate, and this is shown in *Figure 68*. Although visual observations have failed to notice any difference that the type of distributor has upon the bed behaviour, it might be possible that the way the bed is bubbling could be affecting the emissivity. Whatever the reason, this is an important fact to be considered in bed design.

4.5 COMBUSTION LIMITS (LEAN MIXTURES)

There is a very wide range of air-gas mixtures with which stable combustion can be obtained in a fluidized bed. Outside of the stable range of conditions it is not possible to obtain steady state conditions within the bed. This work was concerned with

studying what effect air-gas ratio and throughput have upon bed stability.

In this work, two distinct mechanisms by which the bed could become unstable were observed. The first mechanism occurs when the flow rate is reduced below a critical value and a combustion wave slowly rises up through the bed until all of the combustion takes place upon the bed surface. The second mechanism occurs when the flow rate is reduced and the temperature at the plate begins to rapidly rise. In both cases, the temperature at the distributor plate is the most useful indicator that the bed is unstable.

In the case of instability due to a rising combustion wave, the bed begins to cool at the plate whenever the flow rate is reduced below a critical value, and any temperature measurements made in the uppermost regions of the bed show no indication that the bed is malfunctioning. This is indicated by the time-temperature curve recorded in *Figure 69*. *Figure 69* shows the time-temperature curve recorded by two thermocouples (one placed upon the distributor plate and one placed 2.5 cm above) when the throughput is reduced from a mixture of 200 L/m of air and 11.7 L/m of methane to a mixture of 150 L/m of air and 8.75 L/m of methane. The initial throughput was sufficient to obtain stable combustion, the final throughput was not - in both cases the air-gas ratio was the same. *Figure 69* shows that although the plate temperature is falling rapidly, there is very little variation in the bed temperature 2.5 cm above the plate. At 2.5 cm above the plate there is just a slight temperature change as the combustion wave rises past

the thermocouple, but after this the temperature begins to decrease. The behaviour of the time-temperature profile at the distributor plate is greatly influenced by how far into the unstable region the flow rate is reduced to. If there is a drastic reduction in throughput the drop in plate temperature can become very rapid for a moderate decrease in throughput the plate temperature drops very slowly and at intervals the plate temperature appears to have stabilized - only to fall again. This haphazard variation in plate temperature for moderate decreases is shown, to a small extent, in *Figure 69*. This makes difficult the determination of what the critical throughput is before the bed becomes unstable. Very close to this critical limit, even with a continuous bed operation of an hour, it is difficult to state whether the bed is in a state of stable or metastable equilibrium. The critical flow rate was observed by reducing the flow rate, with a fixed air-gas ratio, and noting the plate temperature. To obtain an accurate estimate, a stable flow rate was noted that was near the critical point along with an unstable flow rate. Knowing the critical point to be somewhere inbetween these two limits, it was a matter of trial and error until a reasonable flow rate could be seen as being, or very nearly being, the critical flow rate.

Figures 70 & 71 give the critical flow rates for the silica dioxide particles. The region to the right of the curve represents the stable combustion zone and that to the left the unstable zone. These two curves show how much the air-gas ratio influences the critical flow rate. Both graphs show that as the air-gas ratio increases, the critical flow rate increases rapidly. These curves

suggest that stable combustion is not possible with an air-gas ratio of much more than 2.1 times stoichiometric. In fact, subsequent attempts to obtain stable combustion above this condition were a failure. It was difficult to obtain the critical flow rate for the zirconium silicate particles (as will be explained in the following paragraphs) but what few results that could be obtained are given in *Figure 72*.

The other mechanism of instability is, perhaps, the most serious. It appears to be predominant with large-heavy particles, but with the small silica dioxide particles it only occurs near to stoichiometric air-gas ratios. Whether or not this mechanism is related to any form of combustion "flash back" has yet to be determined, but the combustion was not observed to flash back into the air box in any of the experiments performed here.

It may be worth mentioning that during preliminary studies a test was performed where the throughput was reduced, inadvertently, below this critical limit and the bed left for thirty minutes to reach steady state conditions. Only one thermocouple had been placed in the bed, and this was recording the temperature in the isothermal region. During the first few minutes there was nothing from the thermocouple readings to suggest that the bed was malfunctioning. Thirty minutes later the bed temperature had risen such that the thermocouple had been irreparably damaged, the particles fused and the combustion tube reduced to a state of partial disintegration. During this experiment, a mild steel plate had been used. Had a refractory plate been used this would probably have cracked. Although the upper parts of the bed had been

destroyed there was no evidence of combustion occurring beneath the distributor plate. Whether or not the bed would have flashed back if left for a longer time was not established: at the time it was not considered prudent to try. This example gives an indication of the risks involved when operating a bed near these conditions.

To understand the conditions that result in this form of instability, it is necessary to refer back to the work of Section 4.4. Here a condition at the distributor plate was observed where a reduction in throughput could result in an increase in plate temperature. Although the plate temperatures would increase for moderate reductions in flow, a stable temperature profile could be obtained within the bed, provided the reduction in throughput was not too great. If reduced too far, lowering the throughput results in an uncontrolled rise in plate temperature which is followed, at a later stage, by a rapid rise in the isothermal bed temperature.

Since it is difficult to establish at what throughput the temperature begins to rapidly rise, the critical throughput will be defined as that where the plate temperature is a minimum: at the point where further reductions result in an increase of plate temperature. The results for the large zirconium silicate particles show that this critical flow rate is the same for a wide range of air gas ratios, and corresponds (with this bed) to an air flow rate of 175 L/m. It is not possible to obtain sufficient information for the other particles: the other mechanism of instability is predominant.

Since no detailed information of the gas temperatures within fluidized combustors is available, it is difficult to establish why a bed becomes unstable. The probable reason is that near the critical limits the bottom of the bed is not fluidized and is behaving as a porous combustor. This is an area requiring further study.

4.6 AXIAL TEMPERATURE PROFILES

Temperature profile measurements in the axial direction resulted with two distinct types of profile as depicted in *Figure 11*. When placing the temperature probe at any position below the isothermal region, considerable fluctuations in temperature were noted. These fluctuations consisted of a random vacillation of the pyrometer reading inbetween two temperature limits when a thermocouple had been positioned within the bed - the time of one complete cycle being about thirty seconds. The magnitude of this fluctuation depended upon the position of the probe within the bed: in the isothermal region it was only about $2^{\circ}C$, near the distributor plate the variation could be as much as $30^{\circ}C$. These fluctuations may be attributable to two things:

[1] particles being transported by the bubbles brushing past the thermocouple and changing the local temperature field

[2] the continual removal and replacement of particles near the distributor plate. In Chapter 3, for the sake of an analysis, it was assumed that there is a continuous flow of solids. Clearly this is not so with a finite number of bubbles; and there must be a continual flow of emulsion

phase particles down past the thermocouple. This would cause a vacillation in the temperature field near the thermocouple.

When the thermocouple was moved in the radial direction, it was found that the mean value of the temperature varied. Again, the variation was greatest just above the distributor plate, but in the isothermal region it was difficult to notice. These radial variations resembled those reported by Broughton[27].

The initial studies raised some doubt as to what the true interpretation is of a thermocouple reading from a fluidized bed. As mentioned in Section 3.8 there is the problem of distinguishing between the emulsion temperature and the temperature of the particles in the bubble wake. Also there can be another problem in evaluating what effect the difference in temperatures between the fluidizing gas and the particles will have on the pyrometer readings. In this work large sheathed thermocouples have been used. Since there is a high degree of contact between the particle and thermocouple surfaces and high rates of thermal radiation between the particles and thermocouple, then the recorded temperature should approximate to the particle temperature.

With all of this in mind, it was decided that for a detailed study of the axial temperature profiles, the best conditions to work with are those close to the incipient state. This had the advantage that the particle recirculation would be low, and on average the recorded temperature would be very close to the emulsion temperature. It would then be possible to make some test of the assumptions made developing the mathematical model in

the last Chapter. The only particles with which it was possible to work very near to the incipient state were the (1.0 - 1.4)mm zirconium silicate: with these it was possible to work as low as 1.5 times the minimum fluidization velocity (based on conditions in the isothermal region). Temperature profiles are given for these particles in *Figures 73-81*. Tables 30-39 give the average temperatures and the amount of fluctuation. All results are for a thermocouple traversed along the centre line of the bed. The temperatures plotted in *Figures 73-81* are the mean values at any point.

In Chapter 3 a particular class of temperature profile was discussed where the maximum solids temperature occurs very near to the distributor plate and the temperature profile (in that region) is not governed by particle transportation. *Figure 81* shows the two types of temperature profile that belong to this class. In one profile the isothermal bed temperature is below the distributor temperature, and in the other it is just above. As indicated by the theoretical study of Chapter 3, these profiles occur at very low throughputs.

By making a few simple assumptions, it is possible to make an estimate of the solid transportation within the bed from these temperature profiles. If in equation(11) it can be assumed that after the point of maximum solids temperature the convective and chemical kinetic terms are small in comparison, then

$$K.A.\frac{d^2T_s}{dx^2} + MC\frac{dT_s}{dx} = 0$$

$$\text{or} \quad \frac{d^2T_s}{dx^2} + \lambda \frac{dT_s}{dx} = 0$$

where $\lambda = \dot{M}C/KA$

This can be integrated to give:

$$T_s = A + B.\exp(-\lambda x) \qquad (24)$$

where A and B are constants.

In *Figures 73-80* the values of log $(T_s - T_{BED})$ are plotted against x and give a value of λ for each curve. The exponential formula of equation (24) is seen to fit the results well. Large deviations from this are only found near the point of maximum solids temperature where the chemical kinetic term has a strong influence, and near the isothermal bed temperature where errors are to be made in detecting small differences in temperature. In this respect, the theory enables a study of this region in terms of the particle recirculation. The values of λ quoted in *Figures 73-80* range from 1.68 to 3.307 cm^{-1}. Since $\dot{M}$ will have varied over the range of distances from which λ was measured, it will be possible to obtain an approximate value of $\dot{M}$ by assuming values for K and C. We have:

$$\dot{M} = \frac{KA\lambda}{C}$$

and using

$$K = 0.04 \frac{cal}{cm\,^oC.s} \left[.167 \frac{W}{cm\,^oC}\right]$$

$$\text{and} \quad C = 0.2 \frac{cal}{gm\,^oC} \left[.84 \frac{J}{gm\,^oC}\right]$$

this gives $\dot{M}$ ranging from .0435 to .086 kg/s. The values used in Chapter 3 were from .4 to 2 kg/s. These two sets of values differ by a factor of ten. Values of $\dot{M}$ obtained from the experimental results are an average since $\dot{M}$ will have higher values for points further up the bed. Since the high values of $\dot{M}$ used in Chapter 3 were only to produce the small temperature difference between emulsion phase and bubble phase particles in the isothermal region, these small measured approximations represent the small order of magnitude for $\dot{M}$ near the points of maximum solids temperature variation.

In this work no attempt was made to study the temperature profiles near the bed surface. Initial exploratory studies in this region produced profiles as shown in *Figure 11* with the temperature rapidly decreasing near the surface. These profiles were similar to those reported by Broughton[27]. With Elliott's work on surface radiation[29] in mind, it was concluded that the temperature profiles in this region were probably due to the changes in temperature of the ejected particles, and this phenomenon is worthy of a study of its own.

4.7 CHROMOTOGRAPHY STUDIES

The purpose of these studies was two-fold: the studies of the combustion gases enabled a check on the rotameter readings, and at the same time provided an indication to the reaction's state of completion within the bed. Comparing air-gas ratios from rotameter and chromatograph readings produced a difference of less than five per cent.

Before an assessment could be made of how near to equilibrium the combustion products were, the equilibrium concentrations were needed. These are given in Appendix 2. A few of these equilibrium concentrations are given in *Figures 82 & 83*. *Figure 82* gives the equilibrium concentrations for stoichiometric mixtures. This shows the possible order of magnitudes to be obtained in an equilibrium mixture. *Figure 83* shows how the CO concentration varies in an equilibrium mixture for changes in the air-gas ratio. If equilibrium conditions are obtained, then *Figure 83* indicates that only with stoichiometric conditions should any CO be recorded, and this should only be a slight trace.

When measurements were taken for the conditions described in Section 4.4, no traces of CO or H_2 were observed for air-gas ratios above 1.1 times stoichiometric. Below five per cent excess air, large CO peaks were produced from the chromatograph, with considerable traces of H_2.

Difficulties were encountered in establishing stoichiometric conditions: the rotameters were not sufficiently precise for a very accurate determination. To circumvent this problem the air flow was set to a steady value and the gas flow very slightly adjusted until the chromatograph produced stoichiometric peaks. *Figure 84* shows a typical set of CO concentrations as the gas flow is varied - although higher than the equilibrium concentrations they vary similarly with air-gas ratio. CO/CO_2 ratios of about .24 were observed at stoichiometric. These ratios are very high and represent large concentrations of CO in the combustion gas. With five per cent excess air chromatograph readings were obtained

giving one-fifth of this ratio. Doubts arise as to whether these chromatograph readings are the concentrations for a pure sample of the combustion gas: air may have infiltrated the line giving a stoichiometric reading on the chromatograph when the combustion sample may have been for less than stoichiometric air. Since the possible errors in the rotameter readings (see the next section) and the differences between chromatograph and rotameter air-gas ratios overlap, it is difficult to assess the situation. Every effort was made to ensure that no leaks could occur in the sample line.

One factor that helps to clarify this condition is the hydrogen concentration of the combustion mixture. *Figure 85* shows how sensitive the equilibrium hydrogen concentration is to any slight change in the air-gas ratio at the stoichiometric point. When the chromatograph indicated a stoichiometric mixture the hydrogen concentrations were as high as 0.002. This is high compared with the stoichiometric equilibrium concentration of 0.0000204. If a concentration of 0.002 for hydrogen is an equilibrium concentration, then the air-gas ratio corresponding to this value is 0.95 times stoichiometric. There are two possibilities to be considered: the first is that the measured concentrations of hydrogen are equilibrium values, the second is that they are not. If they are equilibrium values then the gas sample probably includes air from a leak in the sample line and whatever the conditions, gives an air-gas ratio from the chromatograph of stoichiometric conditions when the air-gas ratio is 0.95 times stoichiometric. If the hydrogen concentrations are not equilibrium

values then the corresponding equilibrium concentration will be smaller and this corresponds to an air-gas ratio greater than 0.95 times stoichiometric and nearer to stoichiometric conditions. From this it must be concluded that the actual stoichiometric conditions are found somewhere inbetween the chromatograph readings of stoichiometric and 1.05 times stoichiometric air-gas ratios as shown by the CO readings given in *Figure 84*. Therefore the probability is that the CO concentrations at stoichiometric conditions are quite high.

It was only possible to measure stoichiometric concentrations with the (0.6 - 0.71)mm silica dioxide particles because of the high bed temperatures. The results given in *Figure 84* are for the bed at 1 400^{o}K and are typical of the results obtained at slightly lower temperatures.

An important aspect of this work was a chromatograph study of the combustion gas for beds operating in the unstable zones discussed in Section 4.5. Studies revealed that even with an unstable bed, the combustion reaches the same degree of completion as does a stable bed operating with the same temperature and air-gas ratio. Even when the condition occurs where the combustion wave is rising through the bed, the reaction is still approaching completion.

4.8 DISCUSSION OF RESULTS

Before discussing the experimental results, a few brief comments need to be made regarding the accuracy of the experimental work and what magnitude of errors should be allowed for when

comparing these with any other similar results.

Bed temperature comparisons present a formidable problem. In this work the pyrometers were recalibrated for every temperature range being used. They were calibrated by supplying a given voltage from a potential source and comparing the reading with the thermocouple calibration chart. Over a typical temperature range of 200°C (at 1 000°C) the maximum error from the pyrometer was about 1.5°C. There are no problems as to the accuracy of the measuring equipment, only to the interpretation of results. The interpretation problems have been discussed in Sections 3.8 and 4.4, and in addition to this there is a problem of reproducibility of results; even with the pyrometer carefully calibrated, attempts to reproduce experiments under exactly the same conditions produce differences in the isothermal bed temperature of as much as 10°C. This may be a small factor when considering bed temperatures as high as 1 200°C, but in some experiments this reproducibility factor could mask any experimental variables. A good example is the study of what effect bed height has upon isothermal bed temperature: in these experiments all differences were found to be within this reproducibility margin.

In the case of flow measurement there are problems in allowing for pressure and temperature variations when measurements are being taken. The rotameter flow equations only give an approximate guide for conditions other than those for which the rotameters were calibrated. The possibility of errors of as much as five per cent cannot be discounted.

Chromatography results, however, have shown that the air-gas

ratios were all within five per cent. The error in a chromatograph concentration being in the region of three to five per cent. Two grades of methane were used: sewage and pure methane. The sewage methane was supplied by Air Products Ltd with a guaranteed methane concentration of not less than 98.5 per cent. Chromatograph checks showed this, in fact, to be never less than 99.0 per cent. The remainder was made up of higher hydrocarbons, nitrogen, oxygen and carbon dioxide. The pure methane was 99.9 per cent pure. This pure grade was used only in the preliminary chromatography work. Any errors due to gas impurity may be considered negligible.

The only measurements subject to any appreciable errors would be those for the critical throughputs of Section 4.5. Due to the difficulty in establishing the critical point, all measurements may be in error to as much as ten per cent.

The important aspects of the experimental work are summarized below:

(a) Experimental results of Section 4.4 suggest that the bed emissivity may increase with fluidizing velocity, as proposed by Elliott and Virr[29]

(b) Experimental work has shown that the bed temperatures depend upon the type of distributor plate used.

(c) Experimental work has suggested that bed height has little or no effect upon bed temperature

(d) Experimental work has shown that under some conditions the bed temperatures will be increased by reducing the throughput

(e) Experimental work has identified two distinct mechanisms by which a bed will become unstable

(f) Experimental work has shown that above ten per cent excess air the carbon monoxide emissions for shallow beds are negligible, but below five per cent excess air they can be high.

In formulating the mathematical model of Chapter 3, the following features of this experimental work had to be accounted for:

(a) The isothermal region above the distributor plate

(b) The large variations in the axial temperature profile near the distributor plate.

In providing these features the model must explain how all of the heat is transported through the isothermal region. Since the combustion gases leave the bed at a temperature close to the isothermal bed temperature then there must be a mechanism by which the radiative component is transported to the bed surface. Chapter 3 has proposed that this is due to particle transportation.

CHAPTER 5

CONCLUSIONS

The object of this Chapter will be to briefly outline what this work suggests to be the mechanism of gas combustion within fluidized beds, and suggest areas for further study.

5.1 MECHANISM OF COMBUSTION

From the experimental and theoretical studies of Chapters 3 and 4, the following mechanism is proposed.

The gas mixture enters the bed from the distributor plate with a temperature less than the particles immediately above the distributor plate. Coming into contact with these particles, the temperature of the gas mixture begins to increase and the chemical reaction between the fuel gas and the oxygen in the air proceeds slowly. Depending upon the temperature of the gas mixture and the amount of gas passing through the bed the solids just above the plate may, or may not, be fluidized. At some distance above the plate, however, the temperature and throughput of the gas mixture will be such that there is more gas flowing through the bed than is required to maintain the incipient state, and bubbles will be formed. At the instance of bubble formation, that gas which forms the bubble phase and that gas which continues in the emulsion phase will be identical with respect to temperature, pressure and chemical composition. However, once the bubbles are formed the reactions in the two phases proceed at different rates, and how close in temperature and chemical concentration the gases in the two phases are will depend upon the interaction

between the two phases.

Once the bubbles have been formed, the behaviour of the bed changes. As the bubbles begin to rise they drag particles up from beneath them. Although there is a continuous exchange between these particles and the particles in the dense phase, it can be assumed that for shallow beds the temperature of the particles in this bubble induced drift is constant. As these particles are rising, so particles in the emulsion phase are travelling downwards in the bed.

As the gas mixture rises through the bed then its temperature increases and any increase in temperature will increase the rate of chemical reaction. When the reaction has reached chemical equilibrium (both in bubble and emulsion phases) the energy liberated from the reaction has to be transported up through the bed. Three processes transport this energy: they are the convective effect of the hot combustion products, the convective effect of the bubble induced drift and the bed conductivity. The combined effect of these three processes is that in the post-combustion region the bed temperature is constant for a considerable distance.

Near the bed surface the temperature of the combustion products are now very close to the temperature of the solids in the emulsion phase. At the bed surface the energy liberated by the chemical reaction is transported from the bed either by the flow of combustion gases, or by surface radiation.

5.2 AREAS REQUIRING FURTHER STUDY

Some points requiring further study have been mentioned in Chapters 3 and 4. A brief list is given below:

(a) A study of the effect the distributor plate has upon the entry gas temperature, and hence the final temperature of the bed

(b) A complete study of the surface emissivity: how does it vary with temperature, bed height and bed bubbling characteristics

(c) A study of particle transportation near the point of bubble formation and a study of how bubbles are formed in combustion beds

(d) A study of fixed and fluidized bed thermal conductivities at high temperatures and with large temperature gradients

(e) A detailed study of bed instability, possibly with a study of combustion in fixed beds to see if the two are related

(f) A study of combustion with fuel rich mixtures

(g) A study of chemical kinetics within fluidized combustion beds.

NOMENCLATURE

NOMENCLATURE

A	Area
a_{ij}	Constants in mass balance equation
b_i	" " " " "
C	Solids specific heat
c_p	Gas mixture specific heat
c	Concentration (also c_j)
d	Particle diameter
d_p	Equivalent particle diameter
ΔE	Activation energy
H	Bed height, also gas-particle heat transfer factor
H_{mf}	Bed height in incipient state
ΔH	Heat of reaction
h_T	Enthalpy of gas mixture at temperature T
h_o	Enthalpy of gas mixture at ambient
h_a	Gas-particle heat transfer coefficient
$(h_f^T)_j$	Enthalpy of formation of species j at temperature T
K_e	Effective thermal conductivity
K	Thermal conductivity, also used for constants
K_r	Reaction rate factor
$\dot{M}$	Particle recirculation, or transportation, rate
$\dot{m}$	Mass flow of gas mixture
$\dot{N}$	Molar flow rate (also $\dot{N}_i$ and $\dot{N}_{gas}$)
N_u	Nusselt number
ΔP_B	Bed pressure drop
$\dot{Q}_{rad}$	Bed surface radiation rate

Nomenclature (contd)

r	Radius
R	Gas constant
Re	Reynold's number
T	Temperature (also T_g and T_s)
δT	Temperature difference between particles in dense and bubble phases
U_{mf}	Minimum fluidizing velocity
U_b	Bubble velocity
U_i	Interstitial gas velocity
$\dot{V}$	Volume rate of gas mixture
$\dot{V}_{mf}$	Volume rate of gas mixture in incipient state (also $\dot{V}_{gas}$ and $\dot{V}_{air}$)
α	Thermal diffusivity
ε	Voidage
ε_{mf}	Voidage in the incipient state
ε_r	Emissivity
λ	$\dot{M}C/KA$, also used as a multiplying factor in the particle transportation equation
μ	Viscosity
ρ	Density
ρ_f	Density of a gas mixture (also ρ)
ρ_b	Bed density
σ	Stefan Boltzmann constant
ϕ_s	Particle shape factor
ψ	Stream function

TABLES OF RESULTS

TABLE 1

PARTICLE DATA

MATERIAL	DIAMETER mm	DENSITY gm/cm^3	ε_{mf}	Φ_s	U_{mf} cm/s	U_{mf} CALCULATED	
						A cm/s	B cm/s
Silica Dioxide	0.6 -0.71	2.608	0.4033	0.85	27.75	26.2	22.8
"	0.71 -0.85	"	0.4151	0.79	27.2	33.4	29.5
Zirconium Silicate	1.0 -1.4	5.18	0.435	0.81	113	103	97.9
"	0.71 -0.85	"	0.388	0.85	67.5	52.8	47.7
"	0.6 -0.71	"	0.396	"	54.5	44	39.1

A ~ Calculated from Equation 3

B ~ Calculated from Reference 7

Pressure drop data given in *Figures 33-37*

TABLE 2

BED TEMPERATURES
1.5 x STOICHIOMETRIC
PARTICLES: (1.0-1.4) mm DIAMETER
ZIRCONIUM SILICATE

$\dot{V}_A$ (L/M)	$\dot{V}_G$ (L/M)	T_{PLATE} (^{o}C)	T_{BED} (^{o}C)
262	18.3	1185.5	1183.5
242	16.9	1181.5	1184.5
225	15.7	1183.5	1185.5
208	14.6	1173.5	1183.5
187	13.1	1159.5	1180.5
175	12.3	1158.5	1182.5
160	11.2	1163.0	1182.5

TABLE 3

BED TEMPERATURES
1.6 x STOICHIOMETRIC
PARTICLES: (1.0-1.4) mm DIAMETER
ZIRCONIUM SILICATE

$\dot{V}_A$ (L/M)	$\dot{V}_G$ (L/M)	T_{PLATE} (^{o}C)	T_{BED} (^{o}C)
262	17.2	1163	1163.5
242	15.9	1163	1167.5
225	14.8	1167	1163.5
208	13.7	1133.5	1150.5
186	12.2	1072	1141.5
175	11.5	1042	1144.5
160	10.5	1060	1134.5

TABLE 4

BED TEMPERATURES
1.7 x STOICHIOMETRIC
PARTICLES: (1.0-1.4)mm DIAMETER
ZIRCONIUM SILICATE

$\dot{V}_A$ (L/M)	$\dot{V}_G$ (L/M)	T_{PLATE} (^{o}C)	T_{BED} (^{o}C)
277	17.1	1110	1121.5
262	16.2	1107.5	1127.5
242	15.0	1109.5	1131.5
225	13.9	1110	1133.5
208	12.9	1081	1133.5
191	11.8	1069.5	1127.5
175	10.8	1029.5	1122.5
160	9.9	1075	1126.5

TABLE 5

BED TEMPERATURES
1.8 x STOICHIOMETRIC
PARTICLES: (1.0-1.4)mm DIAMETER
ZIRCONIUM SILICATE

$\dot{V}_A$ (L/M)	$\dot{V}_G$ (L/M)	T_{PLATE} (^{o}C)	T_{BED} (^{o}C)
277	16.2	1105.5	1106
262	15.3	1104.5	1113.5
242	14.1	1069.5	1113.5
225	13.1	1064	1105.5
208	12.1	969.5	1107.5
200	11.7	940	1113

TABLE 6

BED TEMPERATURES
2.0 x STOICHIOMETRIC
PARTICLES: (1.0-1.4) mm DIAMETER
ZIRCONIUM SILICATE

$\dot{V}_A$ (L/M)	$\dot{V}_G$ (L/M)	T_{PLATE} (^{o}C)	T_{BED} (^{o}C)
297	15.6	1036	1082
277	14.5	1037	1080.5
262	13.8	1017.5	1073.5
242	12.7	967.5	1072.5
225	11.8	983	1076.5

TABLE 7

BED TEMPERATURES
1.6 x STOICHIOMETRIC
PARTICLES: (0.71-0.85) mm DIAMETER
ZIRCONIUM SILICATE

$\dot{V}_A$ (L/M)	$\dot{V}_G$ (L/M)	T_{PLATE} (^{o}C)	T_{BED} (^{o}C)
195	12.8	1186.5	1193.5
175	11.5	1194.5	1195.5
160	10.5	1206.5	1204.5
144	9.5	1191	1200.5
135	8,9	1173	1197.5

TABLE 8

BED TEMPERATURES
1.8 x STOICHIOMETRIC
PARTICLES: (0.71-0.85) mm DIAMETER
ZIRCONIUM SILICATE

$\dot{V}_A$ (L/M)	$\dot{V}_G$ (L/M)	T_{PLATE} (^{o}C)	T_{BED} (^{o}C)
215	12.5	1125	1151.5
195	11.4	1065	1134.5
175	10.2	1053.5	1123.5
160	9.3	1025.5	1114.5

TABLE 9

BED TEMPERATURES
2.0 x STOICHIOMETRIC
PARTICLES: (0.71-0.85) mm DIAMETER
ZIRCONIUM SILICATE

$\dot{V}_A$ (L/M)	$\dot{V}_G$ (L/M)	T_{PLATE} (^{o}C)	T_{BED} (^{o}C)
235	12.3	1069.5	1126.5
215	11.3	1056	1115.5
195	10.2	1051.5	1107.5
175	9.2	1029	1085.5

TABLE 10

BED TEMPERATURES
1.4 x STOICHIOMETRIC
PARTICLES: (0.6-0.71)mm DIAMETER
ZIRCONIUM SILICATE

$\dot{V}_A$ (L/M)	$\dot{V}_G$ (L/M)	T_{PLATE} (^{o}C)	T_{BED} (^{o}C)
114	10.8	1126	1144.5
129	9.7	1125	1144.5
112	8.4	1107	1142.5
109	8.2	1155	1148.5

TABLE 11

BED TEMPERATURES
1.6 x STOICHIOMETRIC
PARTICLES: (0.6-0.71)mm DIAMETER
ZIRCONIUM SILICATE

$\dot{V}_A$ (L/M)	$\dot{V}_G$ (L/M)	T_{PLATE} (^{o}C)	T_{BED} (^{o}C)
175	11.5	1125	1117.5
160	10.5	1126.5	1118.5
144	9.5	1102	1122.5
129	8.5	1074	1117.5
112	7.4	986.5	1108.5
99	6.5	962	1102.5
90	5.9	1062	1100.5

TABLE 12

BED TEMPERATURES
1.8 x STOICHIOMETRIC
PARTICLES: (0.6-0.71)mm DIAMETER
ZIRCONIUM SILICATE

$\dot{V}_A$ (L/M)	$\dot{V}_G$ (L/M)	T_{PLATE} (^oC)	T_{BED} (^oC)
195	11.4	1079.5	1097.5
175	10.2	1072	1084.5
160	9.3	1058	1079.5
144	8.4	1044	1071.5
129	7.5	1024	1072.5

TABLE 13

BED TEMPERATURES
2.0 x STOICHIOMETRIC
PARTICLES: (0.6-0.71)mm DIAMETER
ZIRCONIUM SILICATE

$\dot{V}_A$ (L/M)	$\dot{V}_G$ (L/M)	T_{PLATE} (^oC)	T_{BED} (^oC)
215	11.3	1066	1077.5
195	10.2	1049.5	1070.5
175	9.2	1035	1051.5
160	8.4	1011	1037.5

TABLE 14

BED TEMPERATURES
STOICHIOMETRIC
PARTICLES: (0.71-0.85) mm DIAMETER
SILICA DIOXIDE

$\dot{V}_A$ (L/M)	$\dot{V}_G$ (L/M)	T_{PLATE} (^oC)	T_{BED} (^oC)
92	9.5	1153	1150.5
82	8.6	1112	1121.5
66	6.9	1140	1086.5

TABLE 15

BED TEMPERATURES
1.2 x STOICHIOMETRIC
PARTICLES: (0.71-0.85) mm DIAMETER
SILICA DIOXIDE

$\dot{V}_A$ (L/M)	$\dot{V}_G$ (L/M)	T_{PLATE} (^oC)	T_{BED} (^oC)
112	9.8	1106	1113.5
98	8.6	1105	1110
82	7.2	1070	1081
75	6.6	1053.5	1067
66	5.8	1071	1045

TABLE 16

BED TEMPERATURES
1.4 x STOICHIOMETRIC
PARTICLES: (0.71-0.85) mm DIAMETER
SILICA DIOXIDE

$\dot{V}_A$ (L/M)	$\dot{V}_G$ (L/M)	T_{PLATE} (^{o}C)	T_{BED} (^{o}C)
144	10.8	1073.5	1075.5
129	9.7	1072.5	1079.5
112	8.4	1062	1072.5
98	7.4	1047	1064.5
82	6.2	1023.5	1045.5
75	5.6	983	1021.5

TABLE 17

BED TEMPERATURES
1.6 x STOICHIOMETRIC
PARTICLES: (0.71-0.85) mm DIAMETER
SILICA DIOXIDE

$\dot{V}_A$ (L/M)	$\dot{V}_G$ (L/M)	T_{PLATE} (^{o}C)	T_{BED} (^{o}C)
144	10.8	1058.5	1059.5
129	9.7	1048	1057.5
112	8.4	1028	1041.5
98	7.35	1018.5	1037.5
82	6.15	983.5	1019.5

TABLE 18

BED TEMPERATURES
1.8 x STOICHIOMETRIC
PARTICLES: (0.71-0.85) mm DIAMETER
SILICA DIOXIDE

$\dot{V}_A$ (L/M)	$\dot{V}_G$ (L/M)	T_{PLATE} (^{o}C)	T_{BED} (^{o}C)
160	9.3	1012.5	1030.5
144	8.4	986.5	1002.5
129	7.5	980.5	1002.5
112	6.5	970	986.5
98	5.7	948.5	966.5

TABLE 19

BED TEMPERATURES
2.0 x STOICHIOMETRIC
PARTICLES: (0.71-0.85) mm DIAMETER
SILICA DIOXIDE

$\dot{V}_A$ (L/M)	$\dot{V}_G$ (L/M)	T_{PLATE} (^{o}C)	T_{BED} (^{o}C)
195	10.2	966	992.5
175	9.2	956	981.5
160	8.4	946.5	966.5
144	7.6	928.5	939.5
129	6.8	910	923.5
120	6.3	906.5	920.5

TABLE 20

BED TEMPERATURES
2.1 x STOICHIOMETRIC
PARTICLES: (0.71-0.85)mm DIAMETER
SILICA DIOXIDE

$\dot{V}_A$ (L/M)	$\dot{V}_G$ (L/M)	T_{PLATE} (^{o}C)	T_{BED} (^{o}C)
195	9.8	923.5	939.5
175	8.8	916.5	930.5
167	8.4	913	923.5
160	8.0	903.5	918.5

TABLE 21

BED TEMPERATURES
1.0 x STOICHIOMETRIC
PARTICLES: (0.6-0.71)mm DIAMETER
SILICA DIOXIDE

$\dot{V}_A$ (L/M)	$\dot{V}_G$ (L/M)	T_{PLATE} (^{o}C)	T_{BED} (^{o}C)
74	7.8	1109	1124.5
67	7.0	1092	1114
60	6.3	1083	1102
55	5.8	1065	1089
48	5.0	1082	1062

TABLE 22

BED TEMPERATURES
1.2 x STOICHIOMETRIC
PARTICLES: (0.6-0.71) mm DIAMETER
SILICA DIOXIDE

$\dot{V}_A$ (L/M)	$\dot{V}_G$ (L/M)	T_{PLATE} (^{o}C)	T_{BED} (^{o}C)
100	8.8	1101	1106.5
93	8.1	1094	1098
86	7.5	1082.5	1086
80	7.0	1063	1075
74	6.5	1057	1077
67	5.9	1044	1068
60	5.3	1014	1049
55	4.8	981	1029

TABLE 23

BED TEMPERATURES
1.4 x STOICHIOMETRIC
PARTICLES: (0.6-0.71) mm DIAMETER
SILICA DIOXIDE

$\dot{V}_A$ (L/M)	$\dot{V}_G$ (L/M)	T_{PLATE} (^{o}C)	T_{BED} (^{o}C)
129	9.7	1083.5	1076.5
112	8.4	1077.5	1078.5
98	7.4	1068	1073.5
82	6.2	1020.5	1044.5
65	4.9	969	1023.5

TABLE 24

BED TEMPERATURES
1.6 x STOICHIOMETRIC
PARTICLES: (0.6-0.71) mm DIAMETER
SILICA DIOXIDE

$\dot{V}_A$ (L/M)	$\dot{V}_G$ (L/M)	T_{PLATE} (^{o}C)	T_{BED} (^{o}C)
129	8.5	1042.5	1050.5
112	7.4	1026.5	1039.5
98	6.4	1014	1034.5
82	5.4	991.5	1018.5
65	4.3	937.5	993.5

TABLE 25

BED TEMPERATURES
1.8 x STOICHIOMETRIC
PARTICLES: (0.6-0.71) mm DIAMETER
SILICA DIOXIDE

$\dot{V}_A$ (L/M)	$\dot{V}_G$ (L/M)	T_{PLATE} (^{o}C)	T_{BED} (^{o}C)
144	8.4	1006.5	1023.5
129	7.5	992.5	1013.5
112	6.5	972.5	991.5
98	5.7	953.5	973.5
90	5.3	934.5	962.5

TABLE 26

BED TEMPERATURES
2.0 x STOICHIOMETRIC
PARTICLES: (0.6-0.71)mm DIAMETER
SILICA DIOXIDE

$\dot{V}_A$ (L/M)	$\dot{V}_G$ (L/M)	T_{PLATE} (^{o}C)	T_{BED} (^{o}C)
175	9.2	988	1010.5
160	8.4	976	1001.5
144	7.6	961	986.5
129	6.8	952.5	973.5
112	5.9	932.5	950.5
105	5.5	918.5	936.5
98	5.1	903.5	926.5

TABLE 27

BED TEMPERATURES
2.1 x STOICHIOMETRIC
PARTICLES: (0.6-0.71)mm DIAMETER
SILICA DIOXIDE

$\dot{V}_A$ (L/M)	$\dot{V}_G$ (L/M)	T_{PLATE} (^{o}C)	T_{BED} (^{o}C)
175	8.8	940	970.5
160	8.0	922	944.5
144	7.2	906.5	922.5
135	6.8	900	921.5
129	6.5	902.5	923.5

TABLE 28

COMPARISON OF BED HEIGHTS
1.8 x STOICHIOMETRIC
PARTICLES: (0.6-0.71)mm DIAMETER
ZIRCONIUM SILICATE

	$\dot{V}_A$ (L/M)	$\dot{V}_G$ (L/M)	T_{PLATE} (^{o}C)	T_{BED} (^{o}C)
200 gm	195	11.4	1079.5	1097.5
	175	10.2	1072	1084.5
	160	9.3	1058	1079.5
	144	8.4	1044	1071.5
	129	7.5	1024	1072.5
3000 gm	195	11.4	1075	1090.5
	175	10.2	1060	1077.5
	160	9.3	1051	1070.5
	144	8.4	1032	1068.5

TABLE 29

COMPARISON OF DISTRIBUTOR
1.8 x STOICHIOMETRIC
PARTICLES: (1.0-1.4)mm DIAMETER
ZIRCONIUM SILICATE

	$\dot{V}_A$ (L/M)	$\dot{V}_G$ (L/M)	T_{PLATE} (^{o}C)	T_{BED} (^{o}C)
REFRACTORY PLATE	275	16.0	1119	1132.5
	255	14.9	1120	1141.5
	235	13.7	1117	1144.5
	215	12.5	1095.5	1146.5
	205	12.0	1072	1144.5
M.S. PLATE	277	16.2	1105.5	1106
	262	15.3	1104.5	1113.5
	242	14.1	1069.5	1113.5
	225	13.1	1064	1105.5
	208	12.1	969.5	1107.5
	200	11.7	940	1113

TABLE 30

TEMPERATURE PROFILE
PARTICLES:ZIRCONIUM SILICATE, (1.0-1.4)mm DIAMETER

AIR = 150 L/M
GAS = 12 L/M

ROTATIONS OF SCREW 1 Rev = 0.15875 cm	T ^{o}C	ΔT $\pm^{o}C$
0	1236.5	0.5
1.0	1248.5	0.5
2.0	1253.0	2.0
3.0	1251.5	0.5
3.5	1247.5	0.5
4.0	1245.5	0.5
4.5	1243.0	1.0
5.0	1241.5	0.5
5.5	1241.5	0.5
6.0	1240.5	0.5
7.0	1239.5	0.5
10.0	1237.5	0.5
15.0	1237.5	0.5
20.0	1237.5	0.5

TABLE 31

TEMPERATURE PROFILE
PARTICLES: ZIRCONIUM SILICATE, (1.0-1.4) mm DIAMETER

AIR = 185 L/M
GAS = 11.25 L/M

ROTATIONS OF SCREW 1 Rev = 0.15875 cm	T ^{o}C	ΔT $\pm ^{o}C$
0	973.0	30.0
0.5	1017.5	16.5
1.0	1060.5	7.5
1.5	1038.5	24.5
2.0	1111.5	18.5
2.5	1111.5	22.5
3.0	1127.0	5.0
3.5	1129.0	8.0
4.0	1140.5	13.5
4.5	1157.0	5.0
5.0	1164.5	4.5
5.5	1170.5	6.5
6.0	1166.5	2.5
6.5	1167.5	1.5
7.0	1159.5	3.5
7.5	1156.0	2.0
8.0	1152.0	1.0
8.5	1150.0	2.0
9.0	1149.5	0.5
9.5	1148.0	1.0
10.0	1146.5	0.5
10.5	1145.5	0.5
12.0	1144.5	0.5
13.0	1143.5	0.5
20.0	1143.5	0.5

TABLE 32

TEMPERATURE PROFILE
PARTICLES:ZIRCONIUM SILICATE, (1.0-1.4)mm DIAMETER

AIR = 193 L/M
GAS = 12.5 L/M

ROTATIONS OF SCREW 1 Rev = 0.15875 cm	T ^{o}C	ΔT $\pm^{o}C$
0	1068.5	4.5
2.0	1133.5	3.5
4.0	1157.5	0.5
5.0	1156.0	1.0
5.5	1155.5	0.5
6.0	1154.5	0.5
6.5	1152.0	1.0
7.0	1149.0	1.0
7.5	1146.5	0.5
8.0	1142.5	0.5
8.5	1143.0	0.0
9.0	1143.5	0.5
9.5	1141.0	0.0
15.0	1138.5	0.5
20.0	1138.5	0.5

TABLE 33

TEMPERATURE PROFILE
PARTICLES: ZIRCONIUM SILICATE, (1.0-1.4)mm DIAMETER

AIR = 193 L/M
GAS = 11.7 L/M

ROTATIONS OF SCREW 1 Rev = 0.15875 cm	T ^{o}C	ΔT $\pm^{o}C$
0	964.0	14.0
2.0	1029.0	8.0
4.0	1097.5	2.5
5.0	1125.0	2.0
6.0	1132.0	1.0
7.0	1137.5	0.5
8.0	1142.0	2.0
9.0	1136.5	1.5
9.5	1137.0	1.0
10.0	1136.0	1.0
10.5	1135.0	1.0
11.0	1131.0	1.0
11.5	1128.5	1.5
12.0	1127.5	0.5
12.5	1124.5	0.5
13.0	1122.5	0.5
14.0	1120.5	0.5
16.0	1115.5	0.5
20.0	1114.5	0.5
25.0	1114.5	0.5

TABLE 34

TEMPERATURE PROFILE
PARTICLES: ZIRCONIUM SILICATE, (1.0-1.4) mm DIAMETER

AIR = 168 L/M
GAS = 9.75 L/M

ROTATIONS OF SCREW 1 Rev = 0.15875 cm	T ^{o}C	ΔT $\pm ^{o}C$
0	1072.5	3.5
0.5	1068.0	3.0
1.0	1122.0	9.0
1.5	1134.0	7.0
2.0	1156.0	4.0
2.5	1177.0	2.0
3.0	1188.5	4.5
3.5	1188.5	2.5
4.0	1190.0	1.0
4.5	1188.0	1.0
5.0	1185.5	2.5
5.5	1180.5	3.5
6.0	1176.5	1.5
6.5	1171.5	1.5
7.0	1169.5	0.5
7.5	1164.5	0.5
8.0	1159.5	0.5
8.5	1158.5	1.5
9.0	1156.5	0.5
10.0	1156.5	0.5
11.0	1154.5	0.5
12.0	1154.5	0.5
13.0	1153.5	0.5
14.0	1153.5	0.5
15.0	1152.5	0.5
30.0	1152.5	0.5

TABLE 35

TEMPERATURE PROFILE
PARTICLES:ZIRCONIUM SILICATE, (1.0-1.4)mm DIAMETER

AIR = 181 L/M
GAS = 11.1 L/M

ROTATIONS OF SCREW 1 Rev = 0.15875 cm	T ^{o}C	ΔT $\pm^{o}C$
0	1081.5	3.5
1.0	1088.0	4.0
2.0	1117.5	4.5
3.0	1138.5	0.5
4.0	1155.5	3.5
5.0	1163.5	0.5
6.0	1163.5	0.5
7.0	1161.5	0.5
7.5	1160.5	0.5
8.0	1159.5	0.5
8.5	1157.5	0.5
9.0	1156.5	0.5
9.5	1155.0	1.0
10.0	1154.5	0.5
10.5	1152.5	0.5
11.0	1152.5	0.5
11.5	1151.5	0.5
12.5	1152.0	1.0
16.0	1151.5	0.5
20.0	1151.5	0.5

TABLE 36

TEMPERATURE PROFILE
PARTICLES: ZIRCONIUM SILICATE, (1.0-1.4)mm DIAMETER

AIR = 185 L/M
GAS = 11.1 L/M

ROTATIONS OF SCREW 1 Rev = 0.15875 cm	T ^{o}C	ΔT $\pm^{o}C$
0	1083.5	17.5
1.0	1092.0	4.0
2.0	1132.0	1.0
3.0	1154.0	1.0
4.0	1164.5	0.5
5.0	1167.5	0.5
6.0	1165.5	0.5
6.5	1162.5	0.5
7.0	1160.0	1.0
7.5	1158.0	1.0
8.0	1157.0	1.0
8.5	1155.0	1.0
9.0	1154.0	1.0
9.5	1154.0	1.0
10.0	1152.0	1.0
10.5	1151.0	1.0
11.0	1151.5	0.5
12.0	1149.0	0.0
13.0	1148.5	0.5
15.0	1148.5	0.5
20.0	1148.0	1.0
25.0	1148.5	0.5

TABLE 37

TEMPERATURE PROFILES
PARTICLES:ZIRCONIUM SILICATE, (1.0-1.4)mm DIAMETER

AIR = 235 L/M
GAS = 14.25 L/M

ROTATIONS OF SCREW 1 Rev = 0.15875 cm	T ^{o}C	ΔT $\pm^{o}C$
0	1100.5	5.5
1.0	1109.0	1.0
2.0	1120.0	2.0
3.0	1141.5	2.5
4.0	1154.5	1.5
5.0	1157.0	1.0
6.0	1154.0	1.0
7.0	1150.5	0.5
8.0	1146.5	0.5
9.0	1143.5	0.5
10.0	1140.5	0.5
11.0	1138.5	0.5
12.0	1137.5	0.5
13.0	1135.5	0.5
14.0	1134.5	0.5
15.0	1133.5	0.5
20.0	1133.5	0.5
30.0	1133.5	0.5

TABLE 38

TEMPERATURE PROFILES
PARTICLES: ZIRCONIUM SILICATE, (1.0-1.4)mm DIAMETER

AIR = 144 L/M
GAS = 10.5 L/M

ROTATIONS OF SCREW 1 Rev = 0.15875 cm	T ^{o}C	ΔT $\pm^{o}C$
0	1210.5	2.5
1.0	1217.5	2.5
2.0	1230.5	2.5
3.0	1228.0	4.0
3.5	1226.0	1.0
4.0	1222.0	1.0
4.5	1220.0	1.0
5.0	1219.0	1.0
5.5	1218.0	1.0
6.0	1216.0	1.0
6.5	1216.0	1.0
7.0	1215.0	1.0
8.0	1216.5	0.5
9.0	1216.5	0.5
20	1216.5	0.5

TABLE 39

TEMPERATURE PROFILE
PARTICLES: ZIRCONIUM SILICATE, (1.0-1.4) mm DIAMETER

AIR = 150 L/M
GAS = 9.75 L/M

ROTATIONS OF SCREW 1 Rev = 0.15875 cm	T ^{o}C	ΔT $\pm ^{o}C$
0	1221.0	7.0
0.5	1218.0	4.0
1.0	1228.0	4.0
1.5	1229.5	3.5
2.0	1244.0	7.0
2.5	1217.0	5.0
3.0	1198.5	2.5
3.5	1186.5	1.5
4.0	1178.5	2.5
4.5	1172.5	3.5
5.0	1176.0	3.0
5.5	1169.0	5.0
6.0	1169.5	1.5
6.5	1163.5	1.5
7.0	1163.5	1.5
7.5	1163.5	0.5
8.0	1162.5	0.5
9.0	1161.5	0.5
25	1161.5	0.5

FIG. 1

VARIATION OF CO & NO EQUILIBRIUM CONCENTRATIONS WITH TEMPERATURE

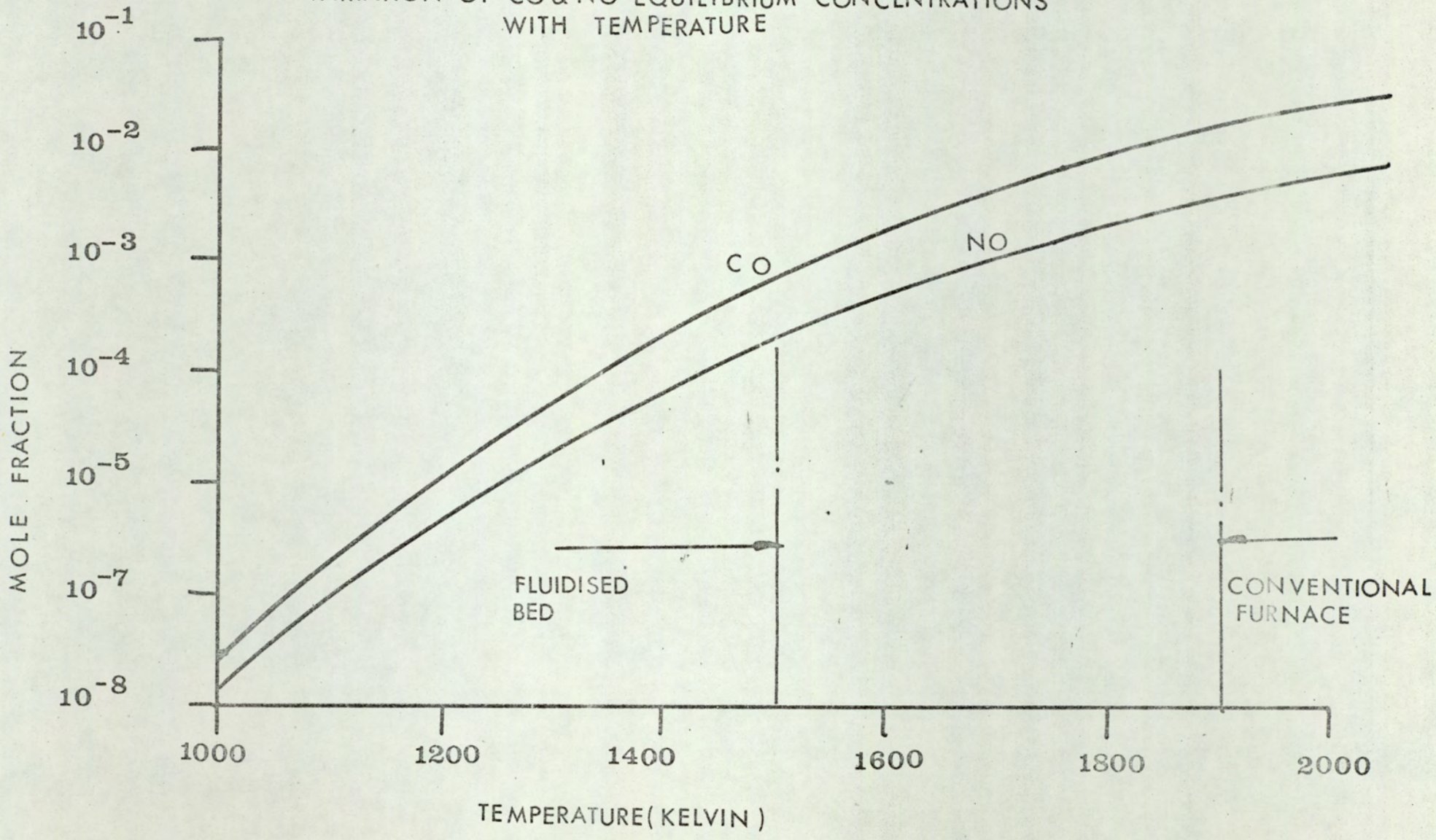

FIG. 2

FLUIDISED COMBUSTOR WITH POST BED BURNER

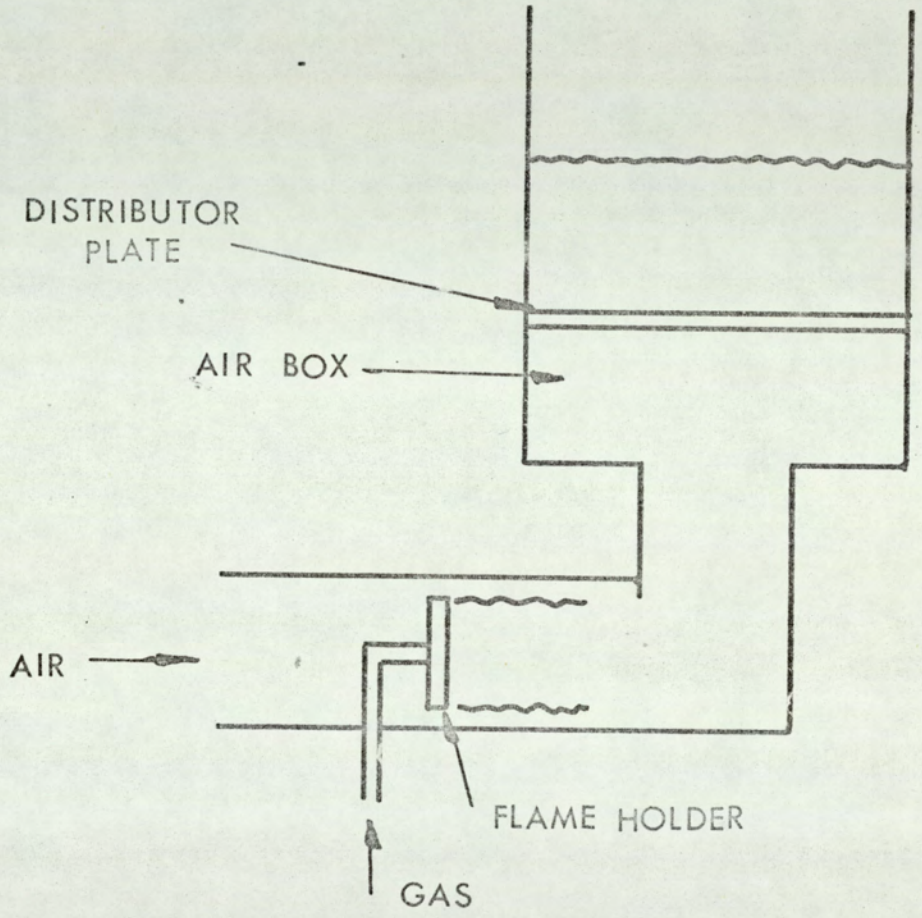

FIG. 3

TEMPERATURE VARIATION OF THE AMOUNT OF AIR REQUIRED TO FLUIDISE 1 C.M.^{2} OF BED AREA WITH PARTICLES AS SPECIFIED BELOW:

DENSITY = 5·18 g.m./ c.m.^{2}

DIAMETER = (1·0 – 1·4) m.m.

VOIDAGE = 0·435

ϕ = 0·81

CALCULATED FROM EQN. 3 CHAPTER 2

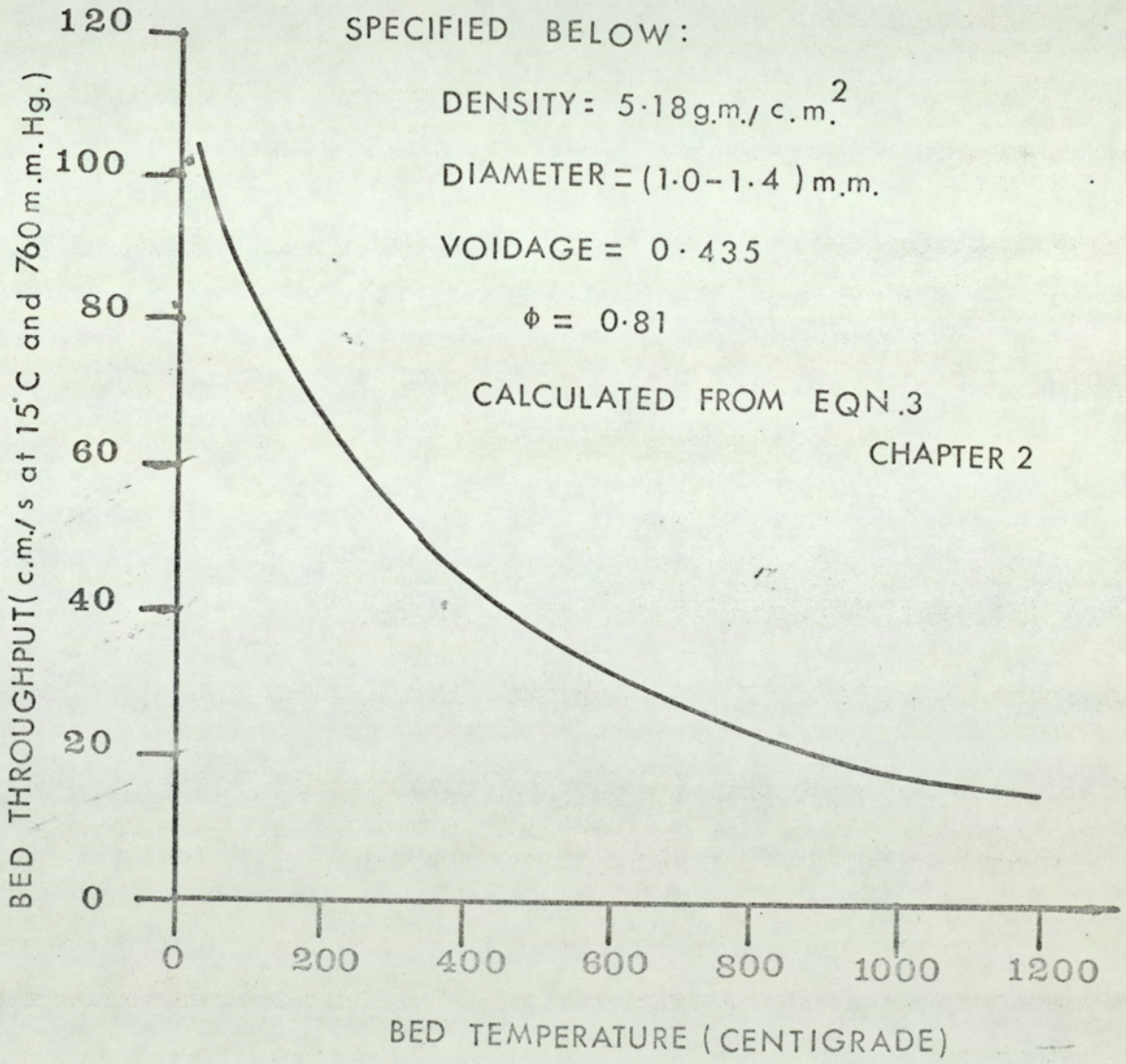

FIG. 4

A TWO STAGE WATER HEATER

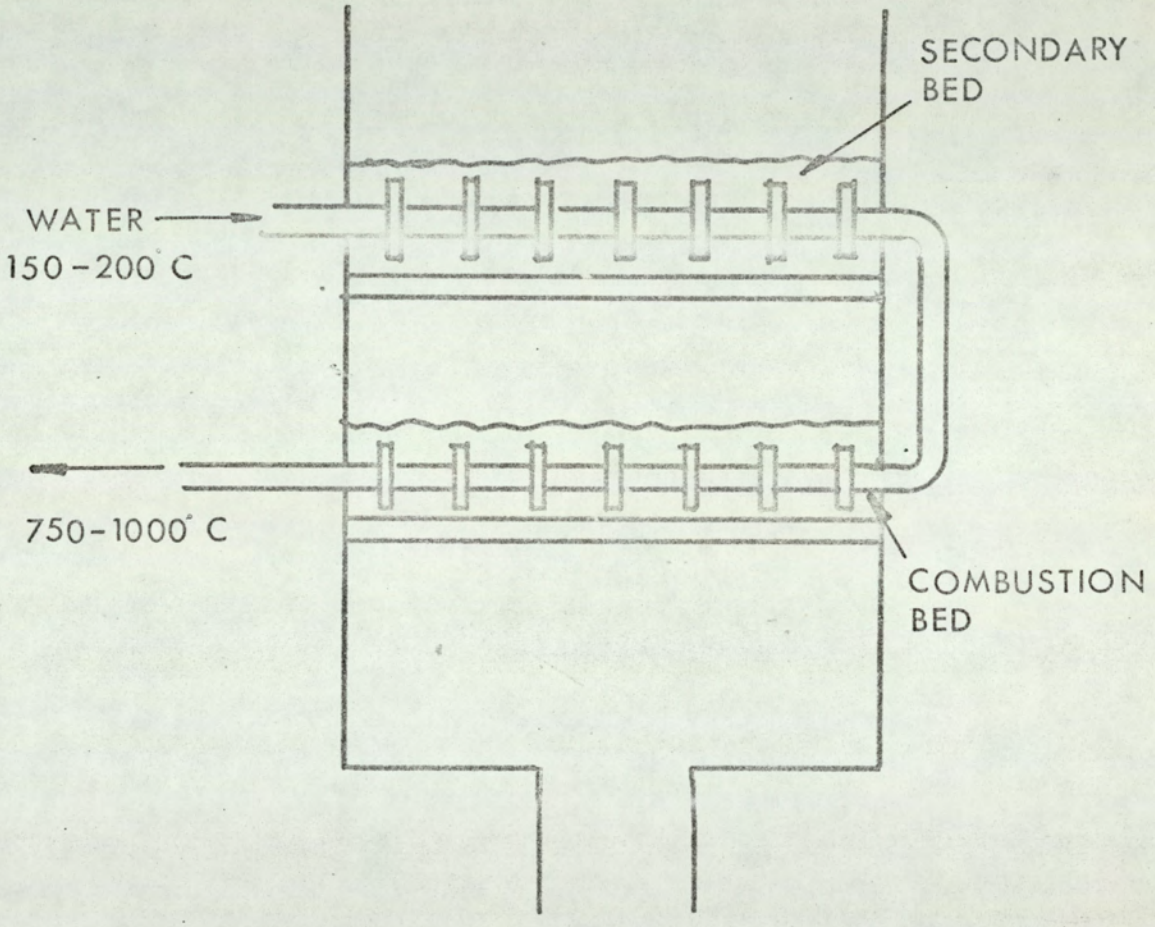

FIG. 5

FLUIDISING VELOCITIES

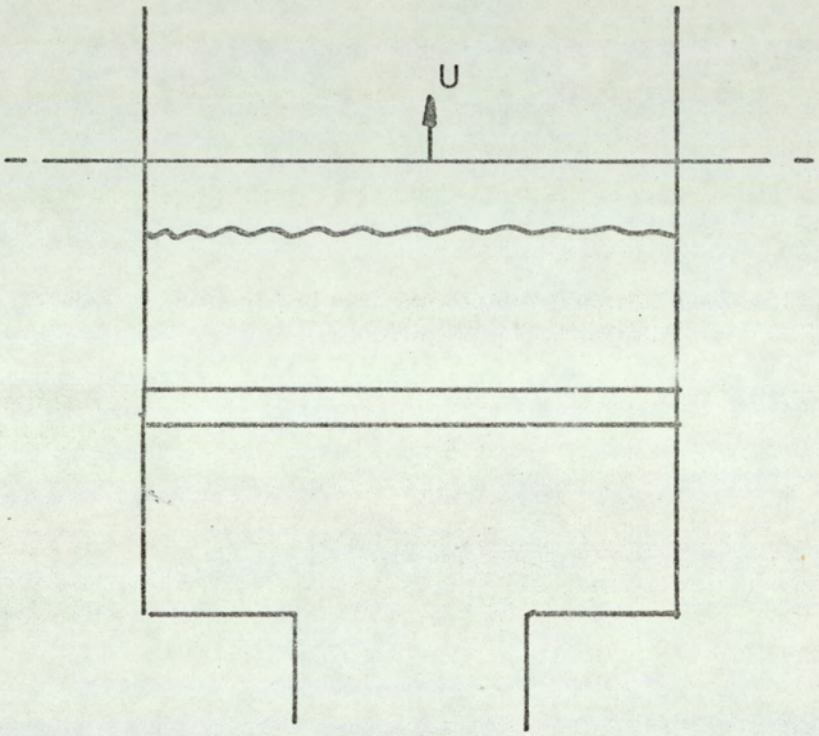

Fluidising Velocity is defined as the velocity in the free bed area as shown above.

At the incipient state $U = U_{mf}$

FIG.6

BUBBLE FORMATION WITH FINE PARTICLES

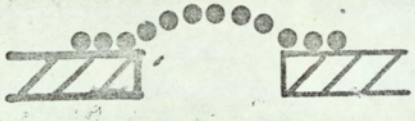

VOID FORMING AT ORIFICE

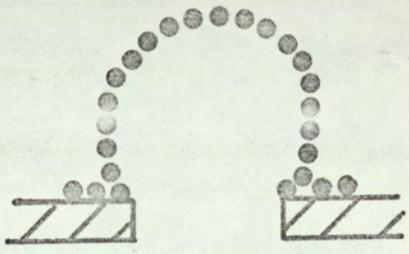

FORMATION OF PARABOLOID

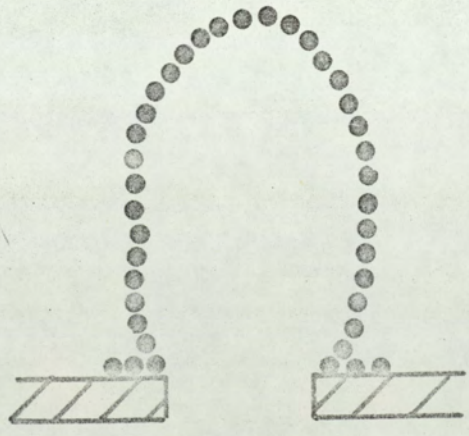

CRITICAL SIZE

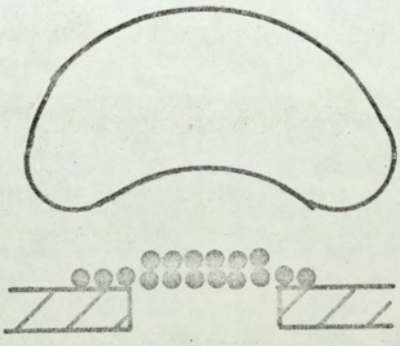

BUBBLE FORMED

FIG.7

BUBBLE FORMATION WITH LARGE PARTICLES

FORMATION OF LENTICULAR CAVITY

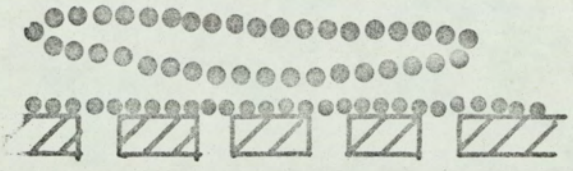

SEPARATION OF DUMB-BELL

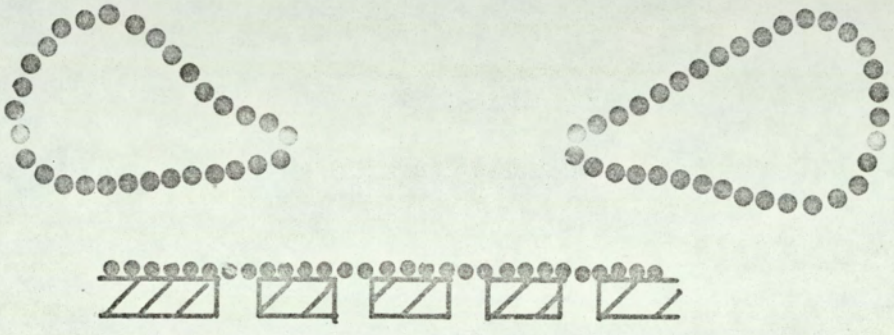

TWO BUBBLES FORMED

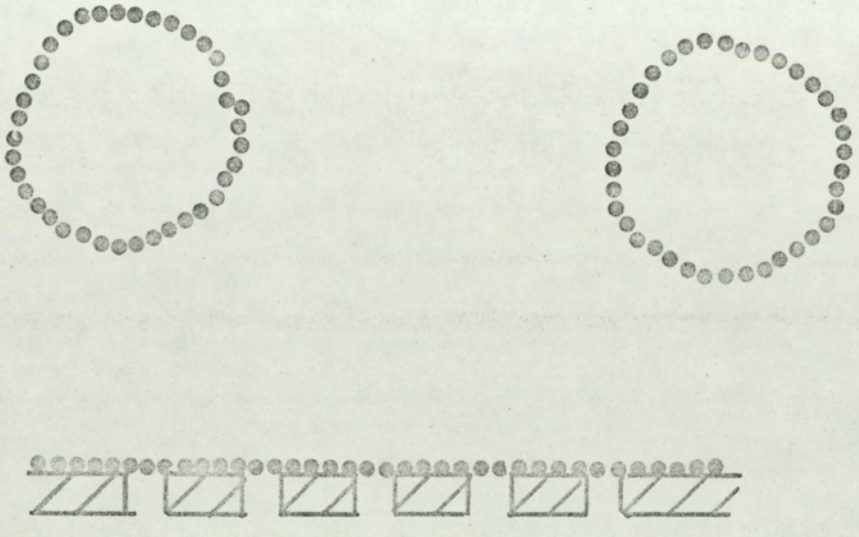

FIG. 8

MECHANISMS OF SOLID TRANSPORTATION

INCIPIENT BED

lower level particles dyed

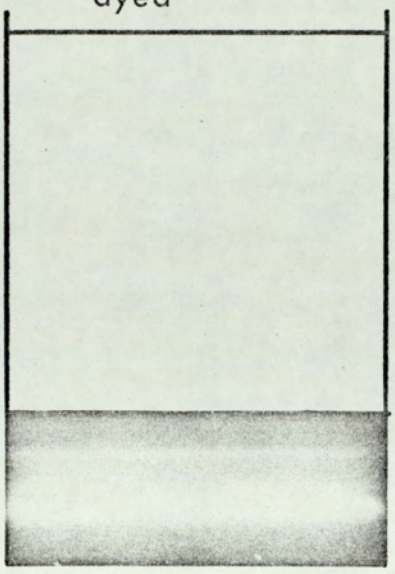

BUBBLE INJECTION

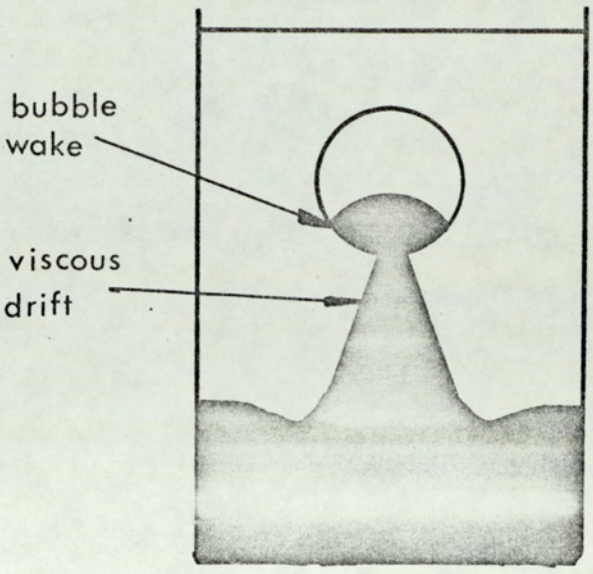

SHALLOW BED

wake deposited on bed surface

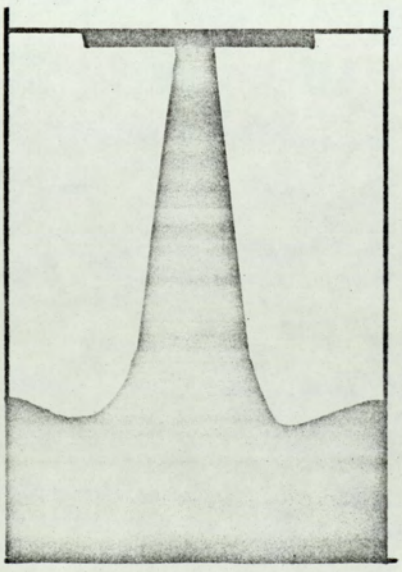

DEEP BED

wake deposited below surface

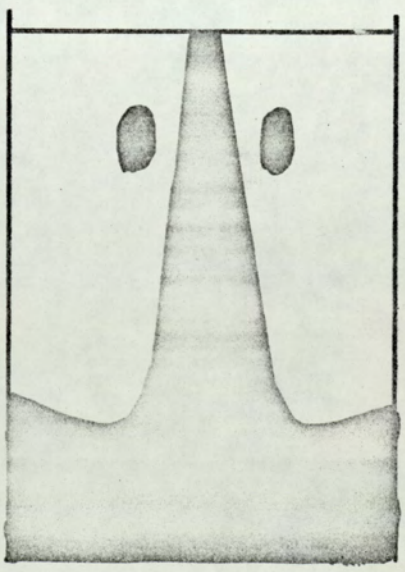

FIG. 9

EFFECT OF BUBBLES ON GAS MIXING

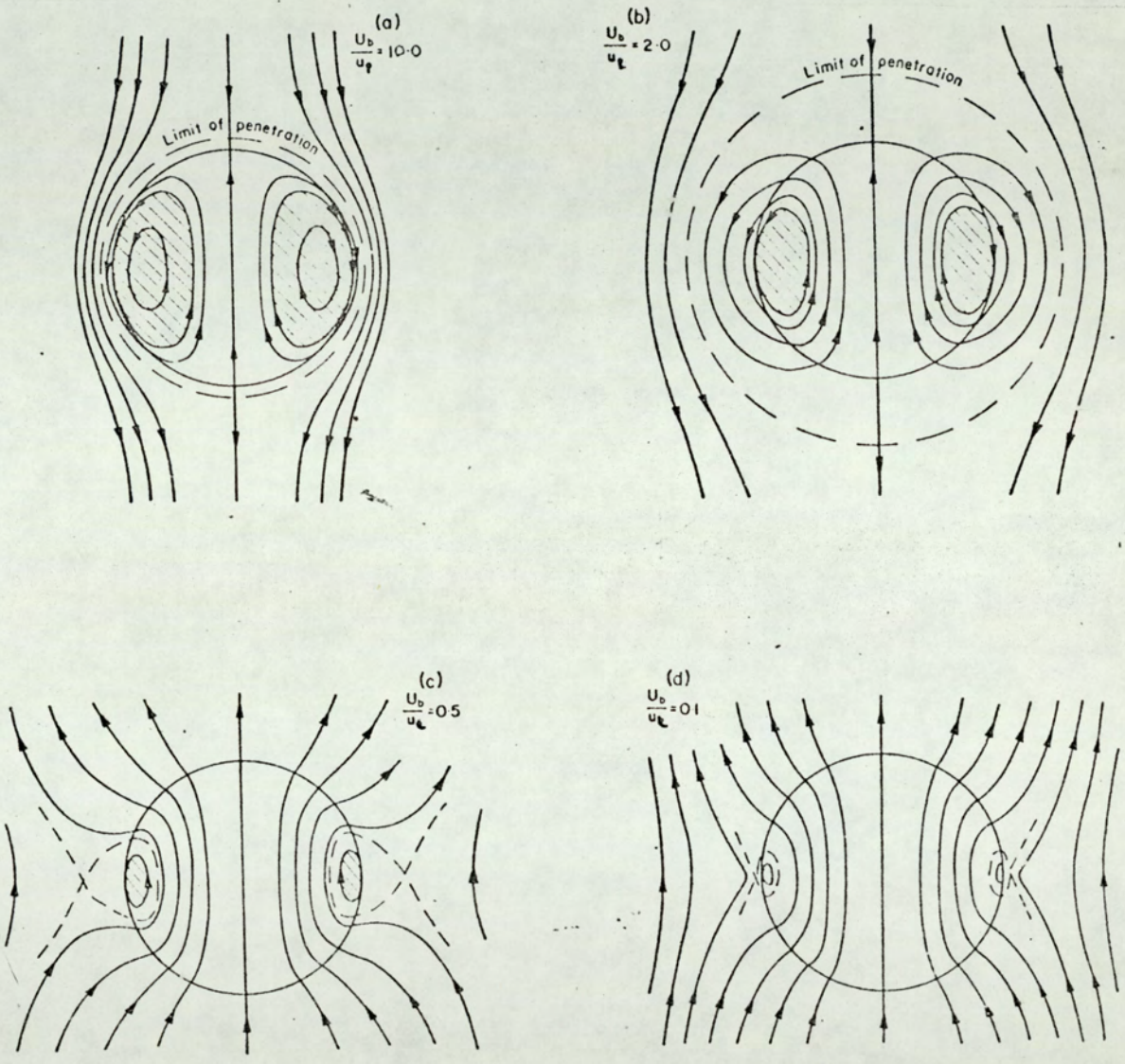

FROM REF. 14

FIG.10

TWO STAGE COMBUSTOR FOR GAS-RICH MIXTURES

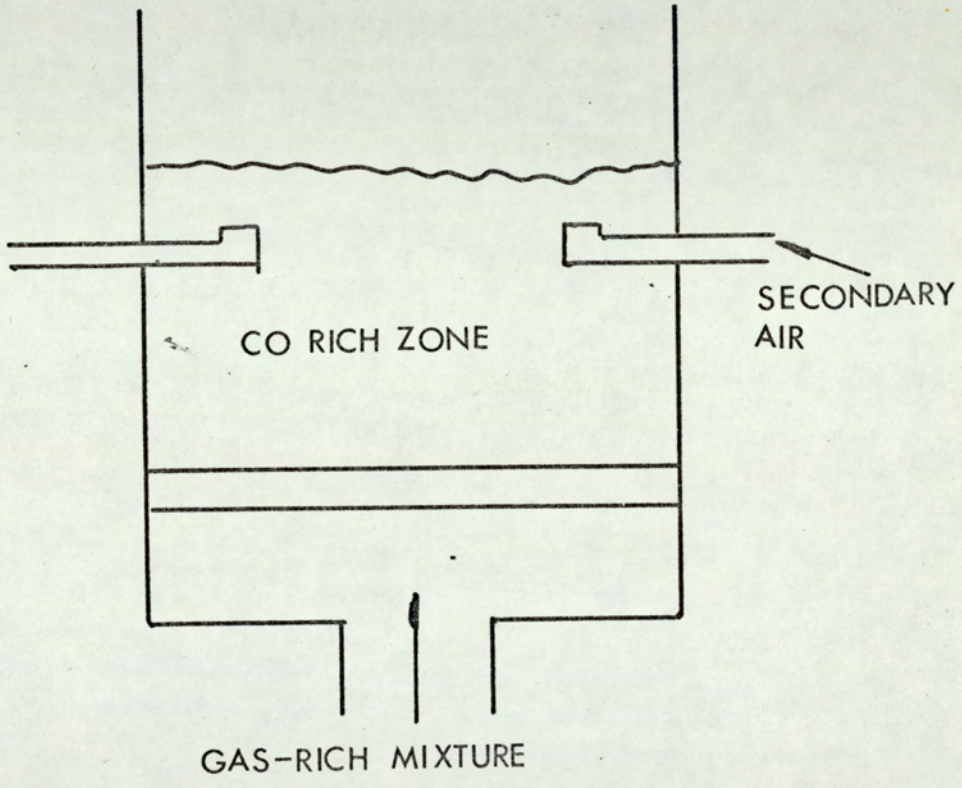

FIG.11

TEMPERATURE PROFILES

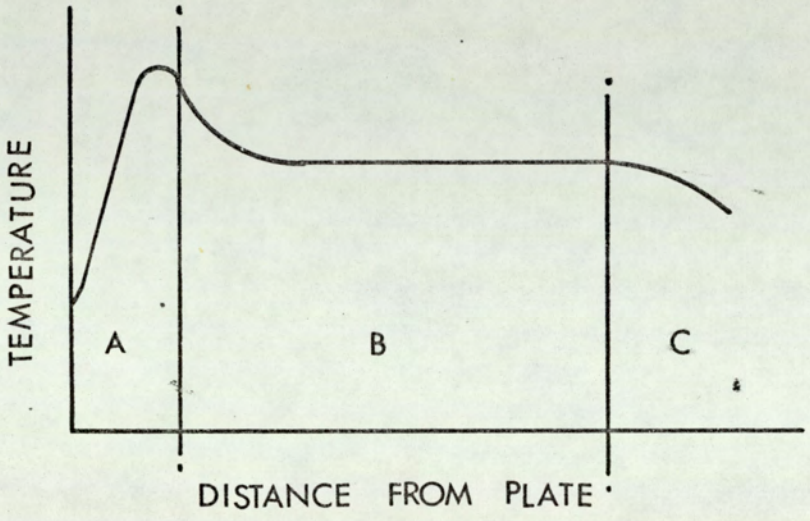

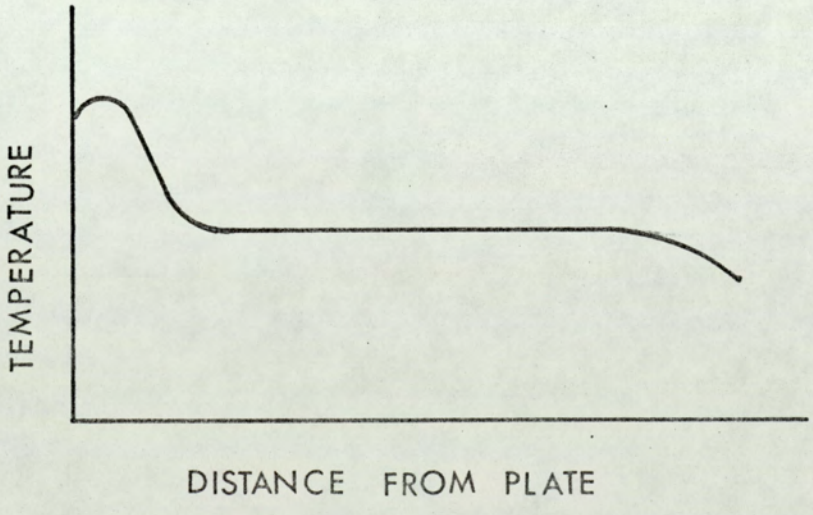

FIG.12

ENERGY BALANCE CONTROL VOLUME

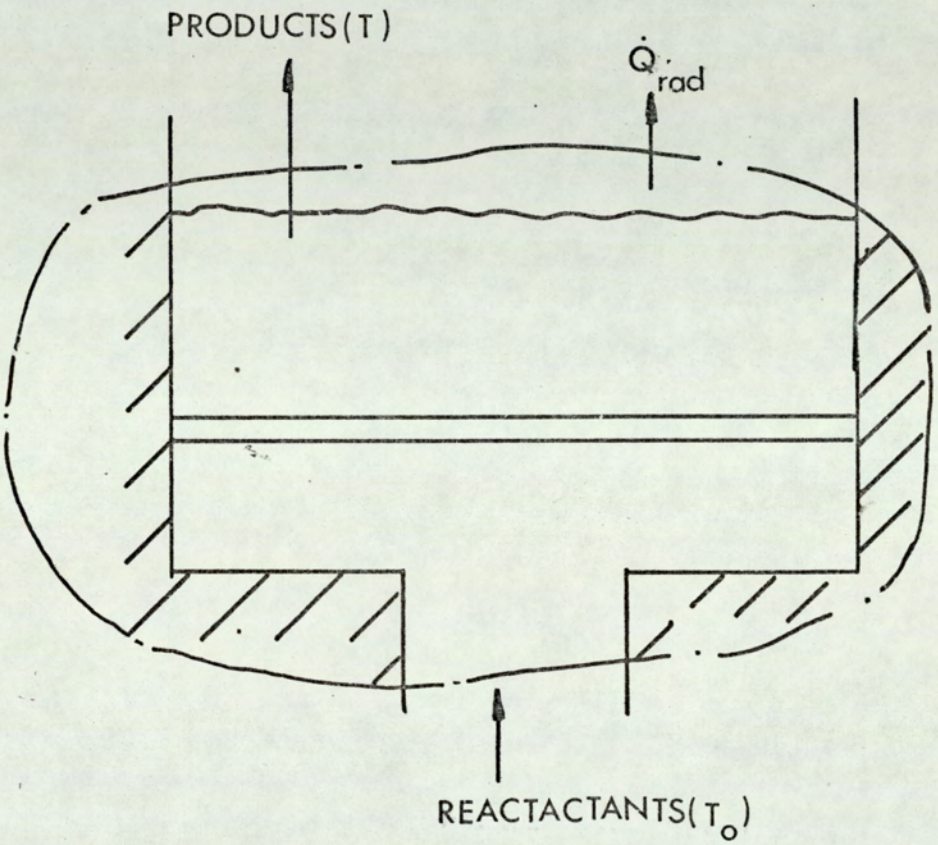

FIG.13

VARIATION OF BED TEMPERATURE WITH THROUGHPUT

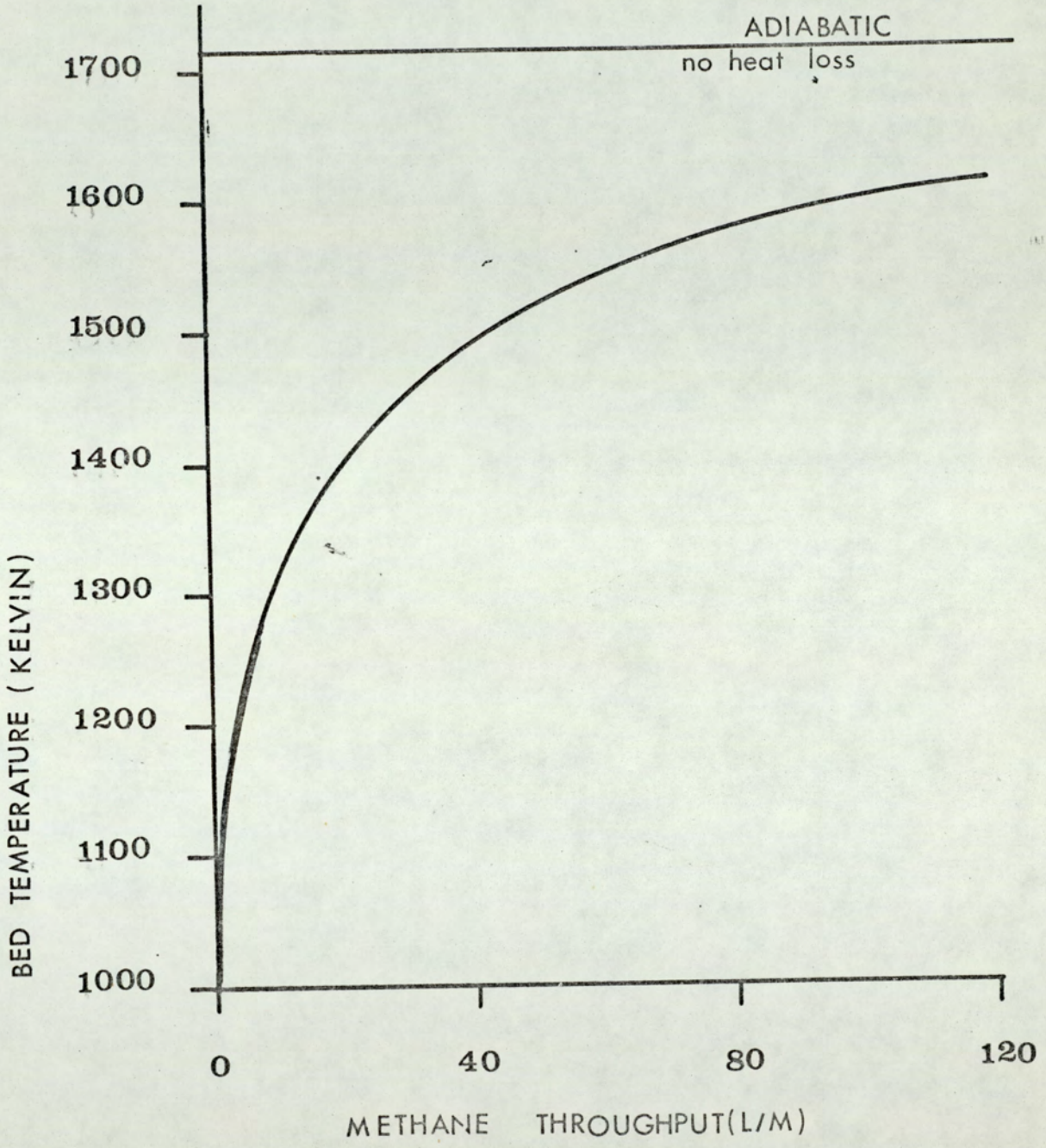

FIG .14

POSSIBL SOLUTIONS OF ONE-DIMENSIONAL FLAME EQUATION

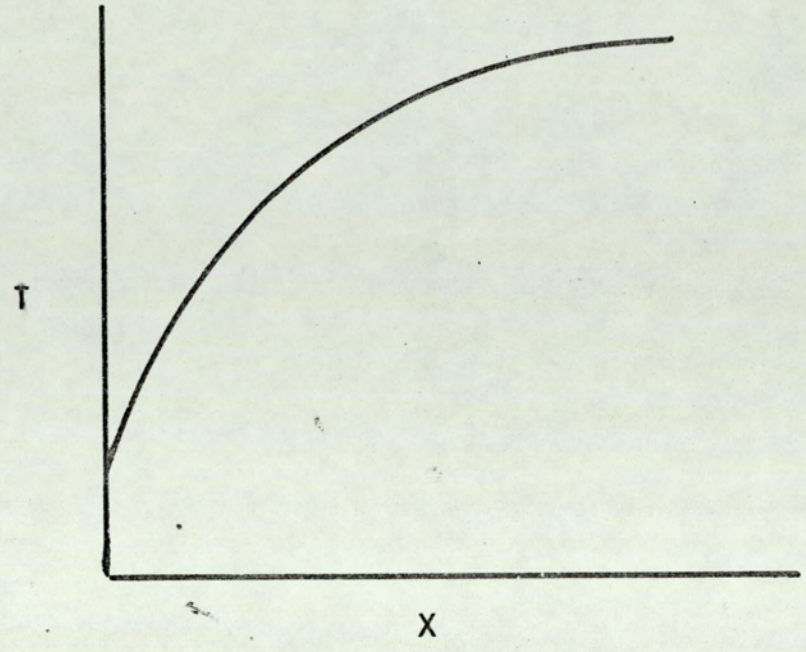

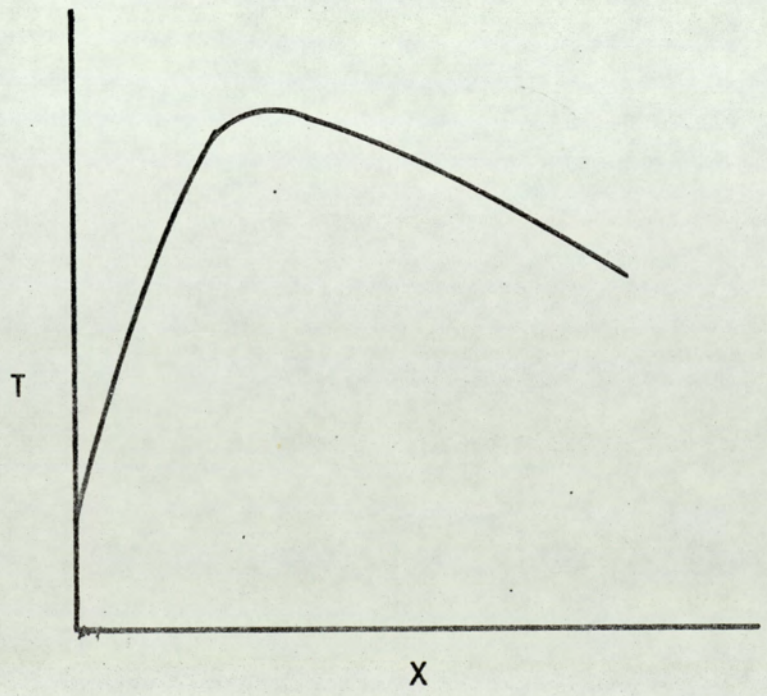

FIG. 15

HEAT TRANSFER DUE TO PARTICLE MOVEMENT

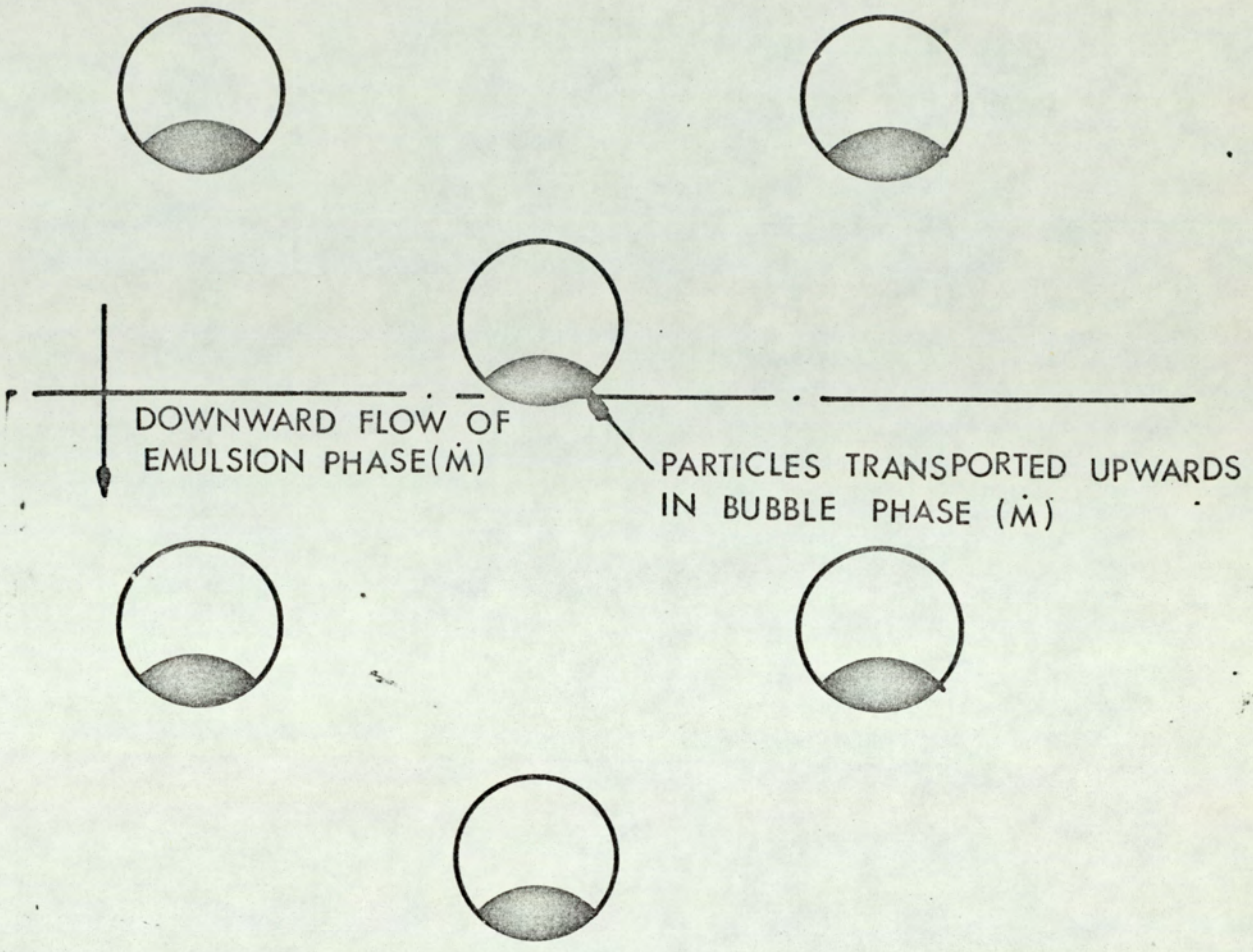

UPWARD CONVECTION $= \dot{M} C (T_b - T_s)$

FIG.16

BED TEMPERATURES & DEGREE OF REACTION FROM SIMPLE MODEL

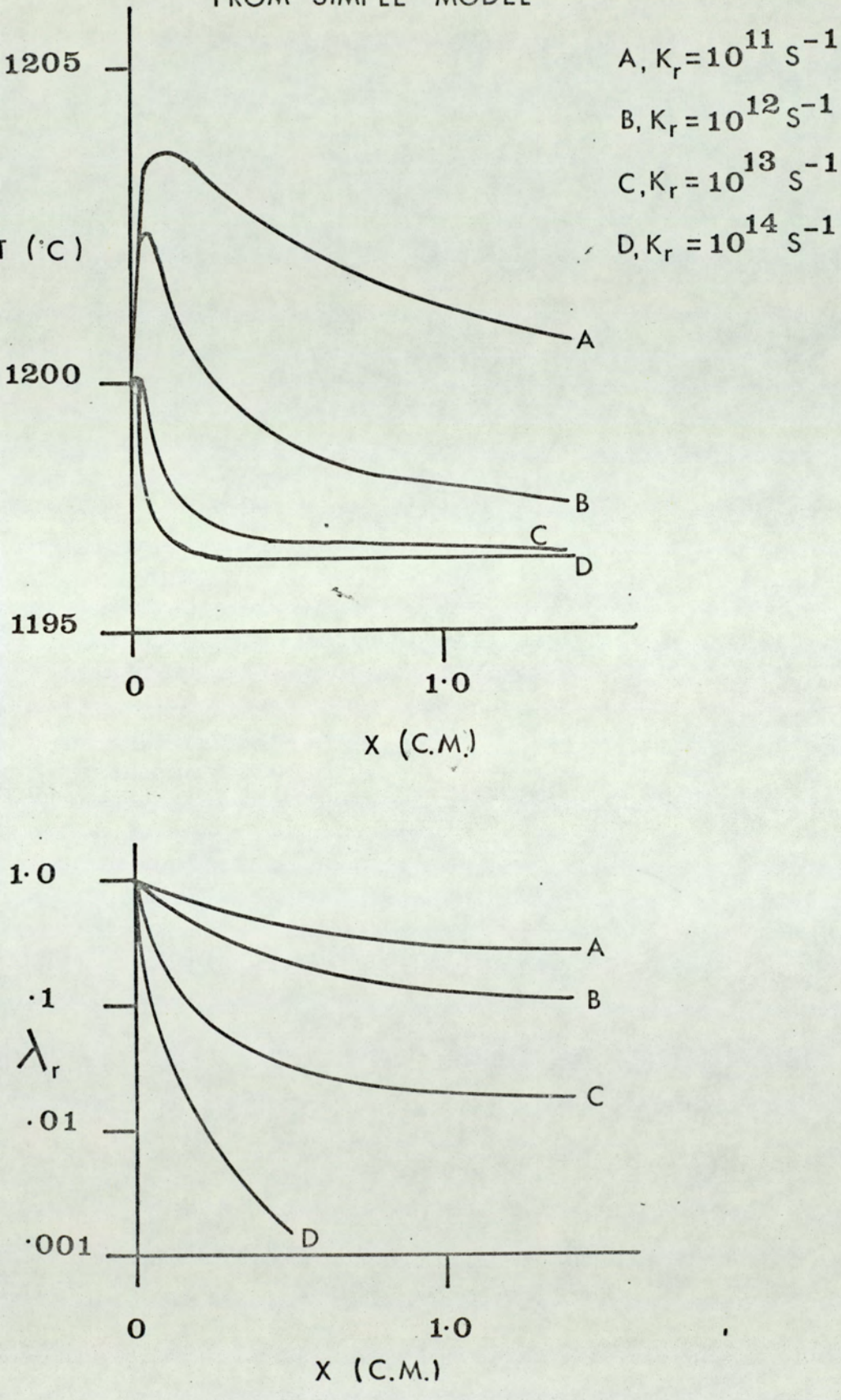

FIG.17

VARIATION OF PROFILE WITH SOLIDS RECIRCULATION

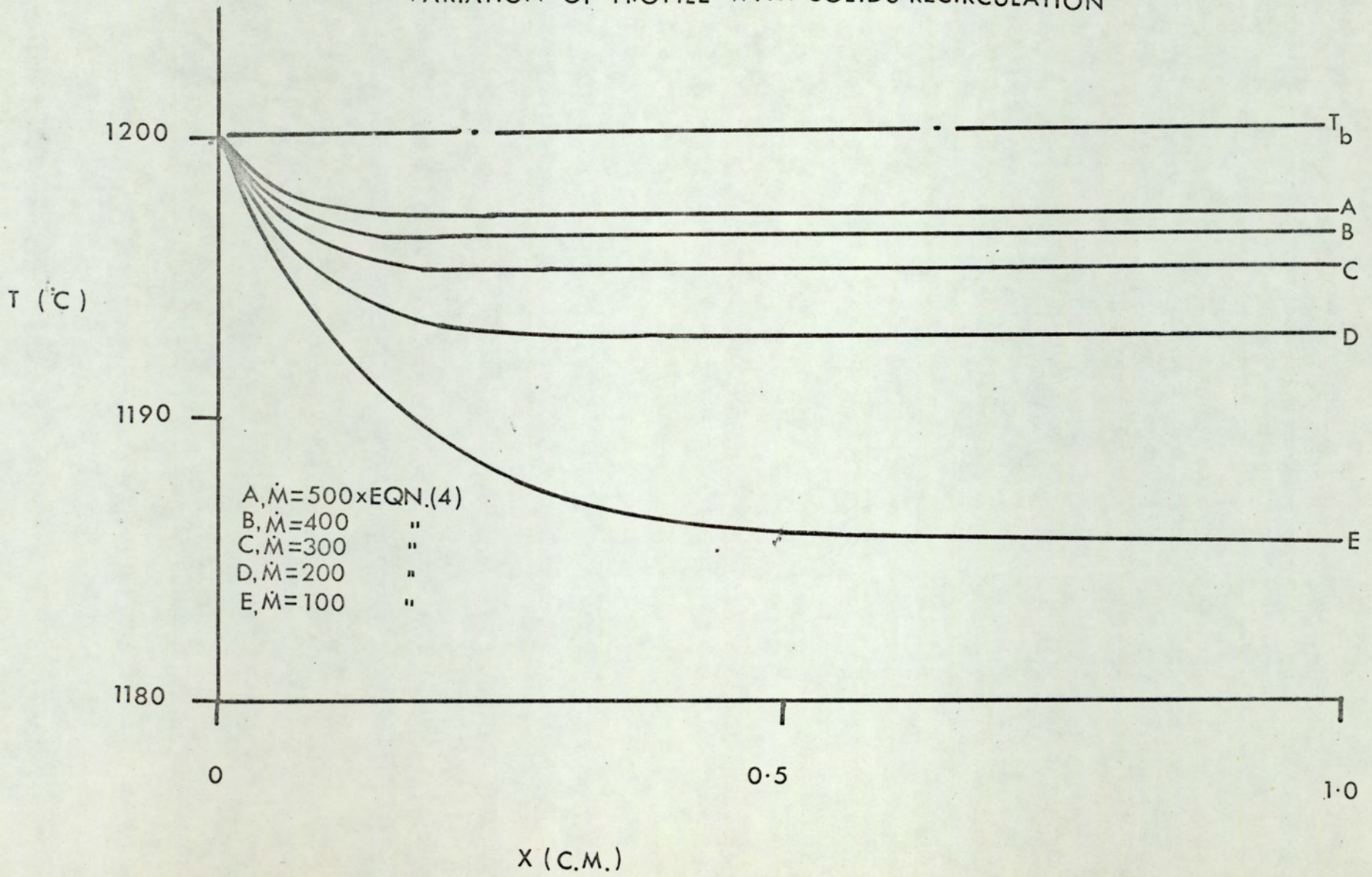

FIG. 18

COMPUTED BED PROFILES

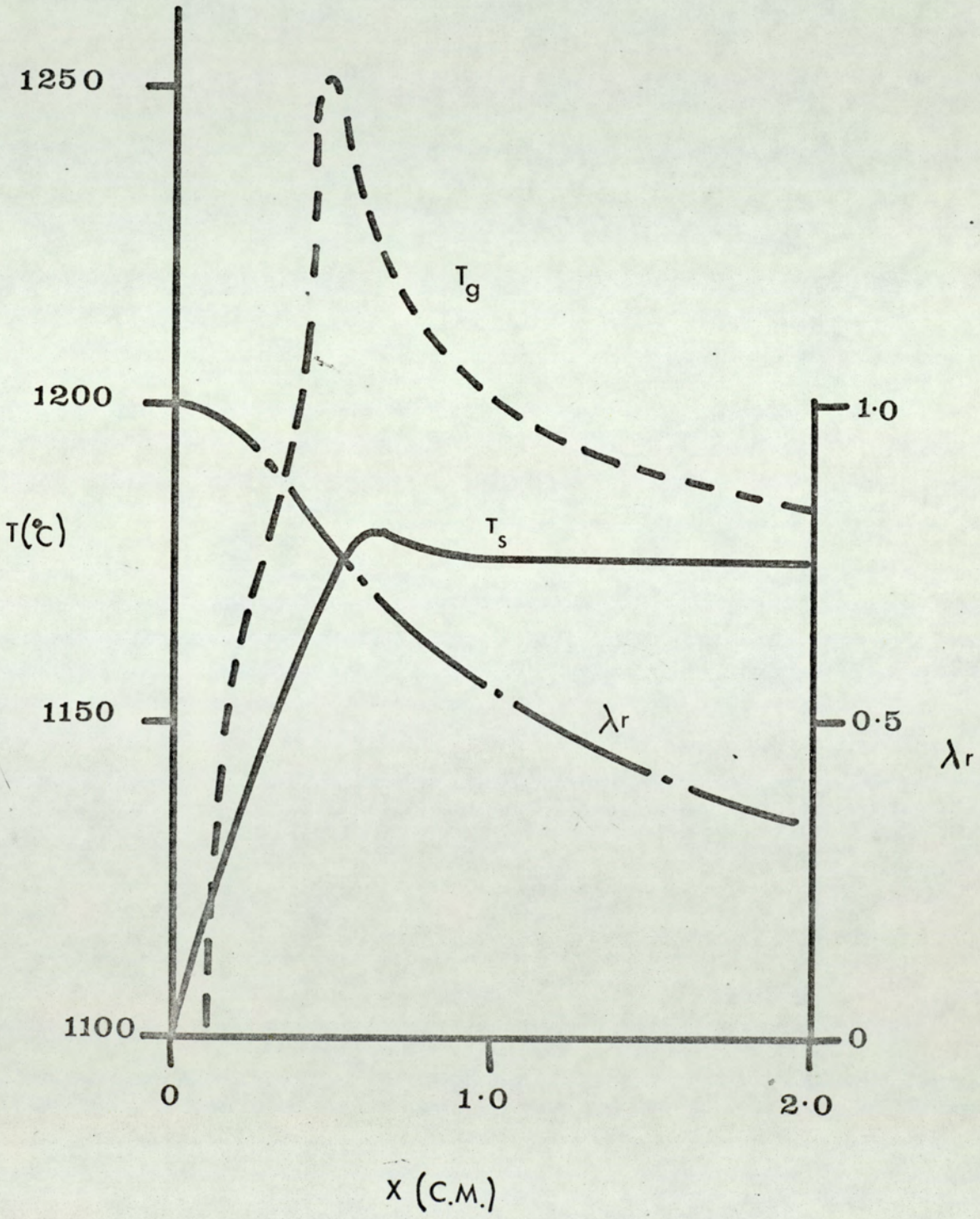

FIG.19

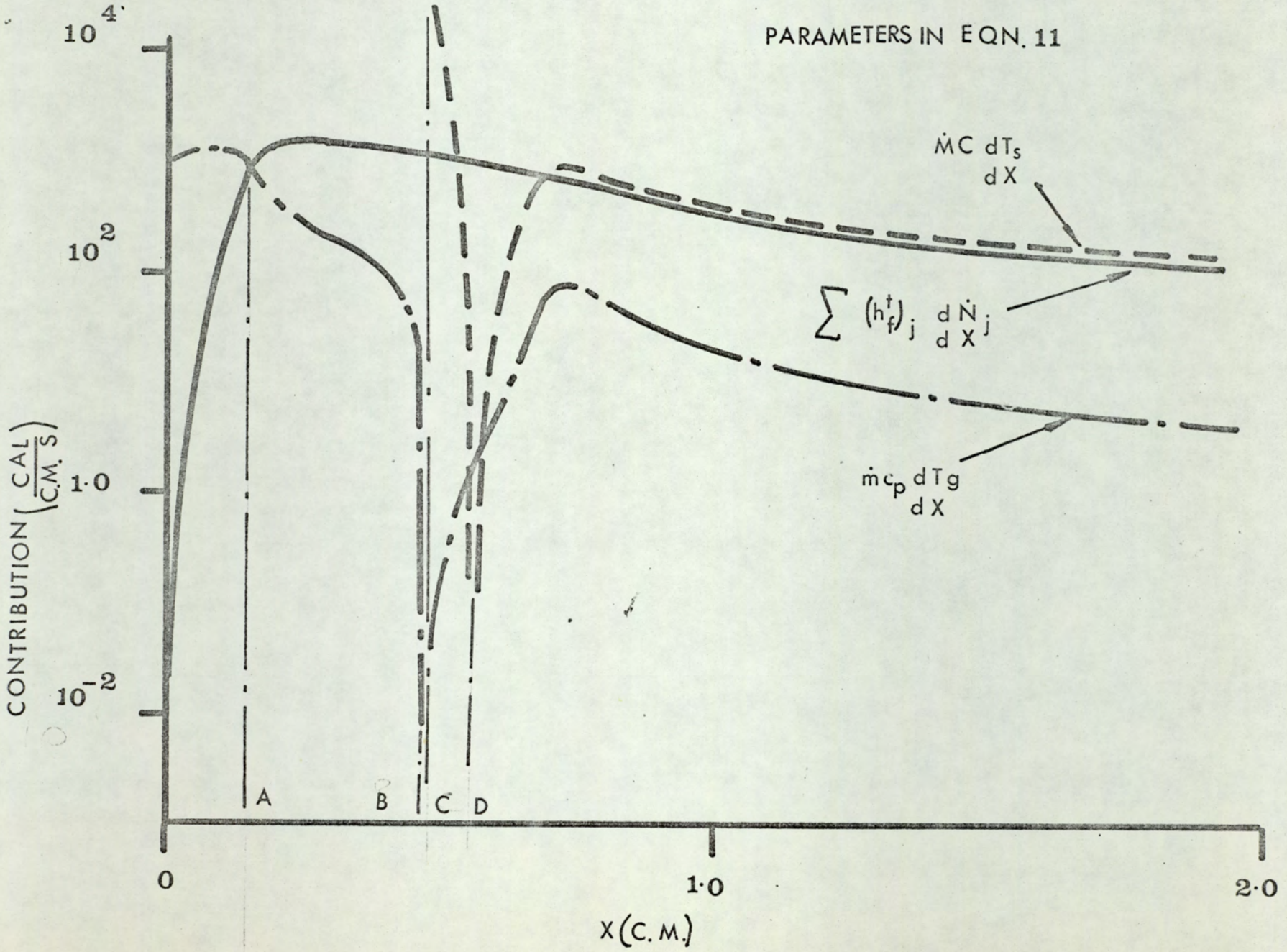
PARAMETERS IN EQN. 11
$\dot{M}C\frac{dT_s}{dX}$
$\sum (h_f^t)_j \frac{d\dot{N}_j}{dX}$
$\dot{m}c_p\frac{dT_g}{dX}$
CONTRIBUTION $\left(\frac{CAL}{C.M.S}\right)$
10^4
10^2
1·0
10^{-2}
A
B
C
D
0
1·0
2·0
X (C.M.)

FIG. 20

EFFECT OF BED CONDUCTIVITY

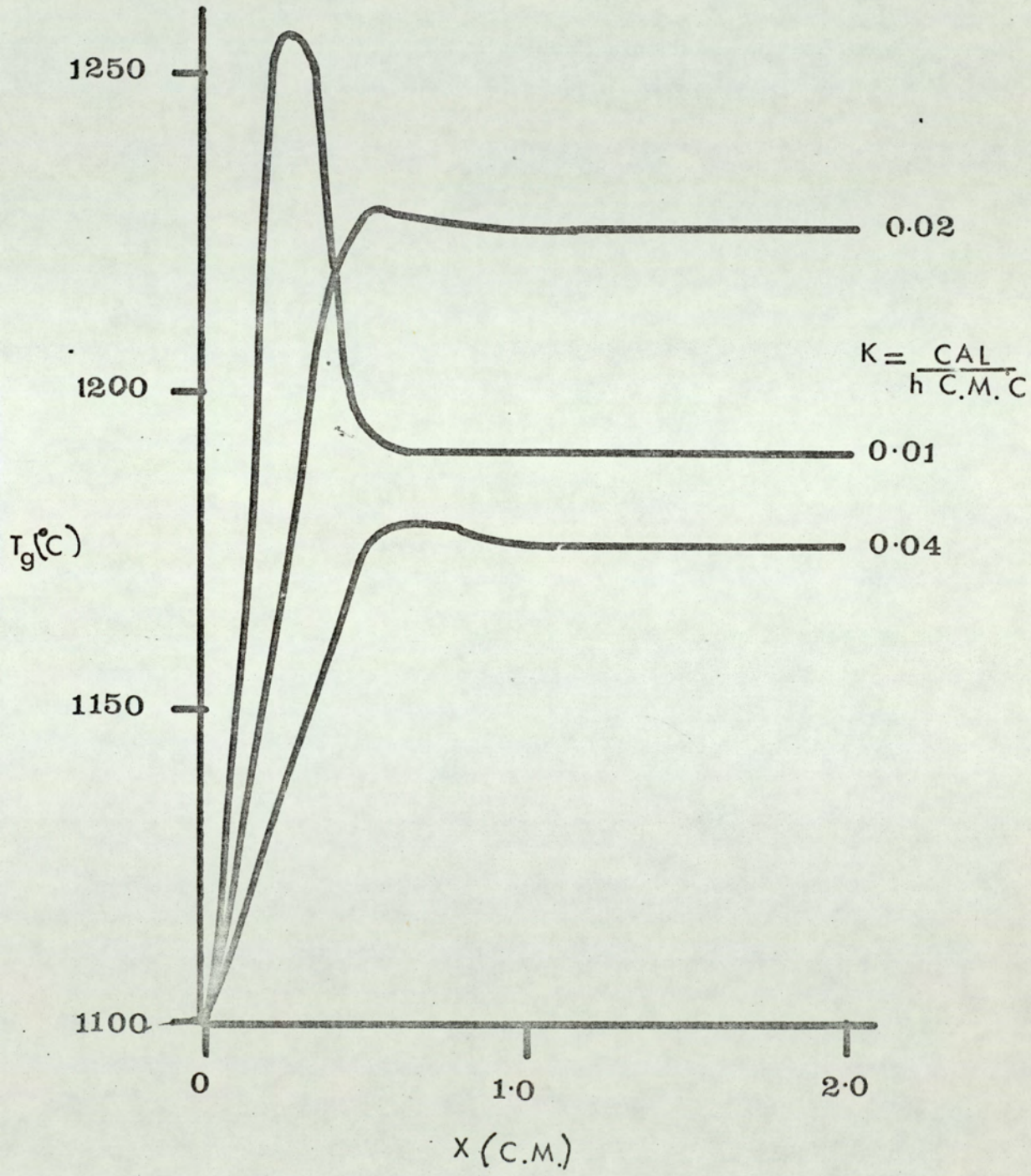

FIG. 21

EFFECT OF PARTICLE TRANSPORTATION

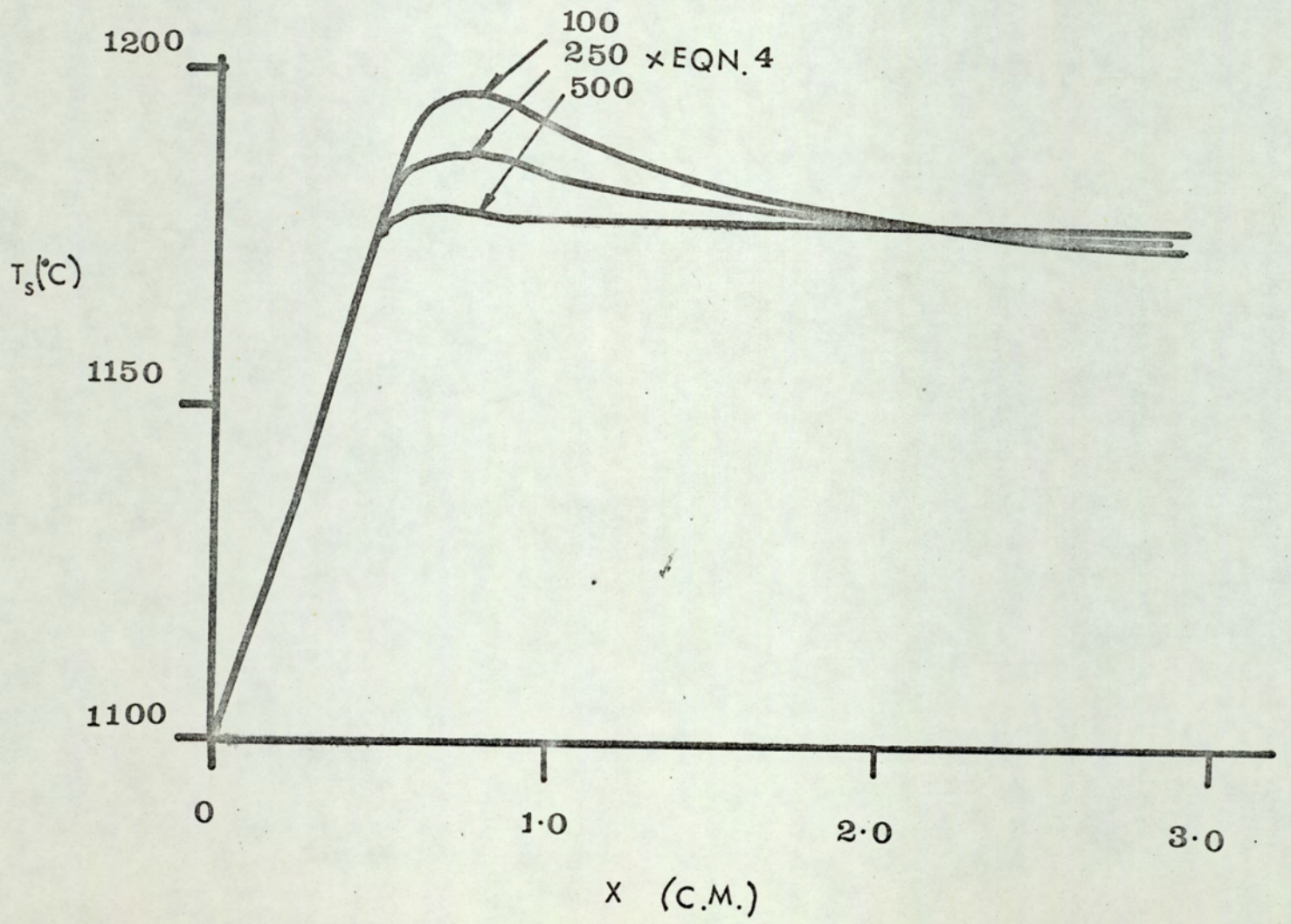

FIG. 22

EFFECT OF GAS-PARTICLE
HEAT TRANSFER (H)

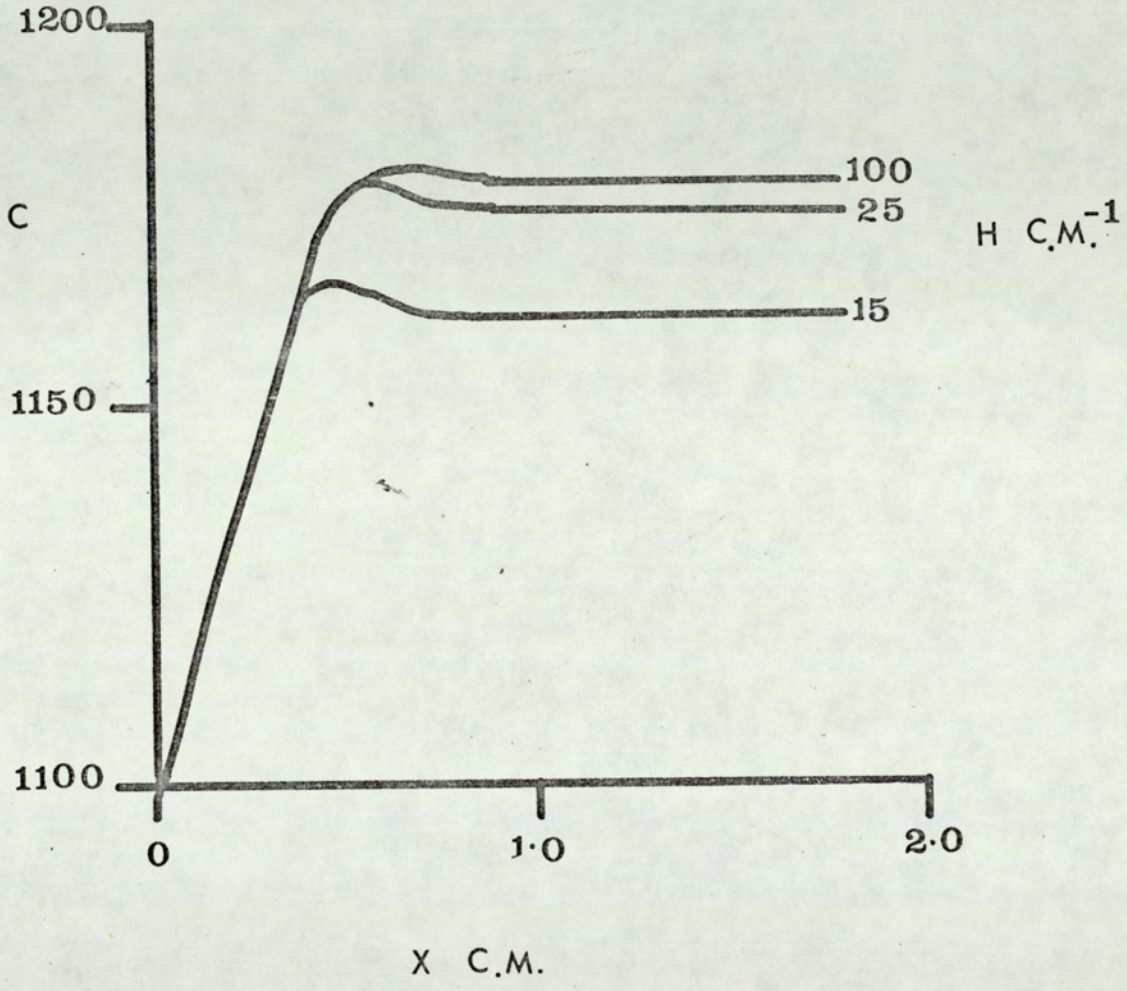

FIG. 23

EFFECT OF H

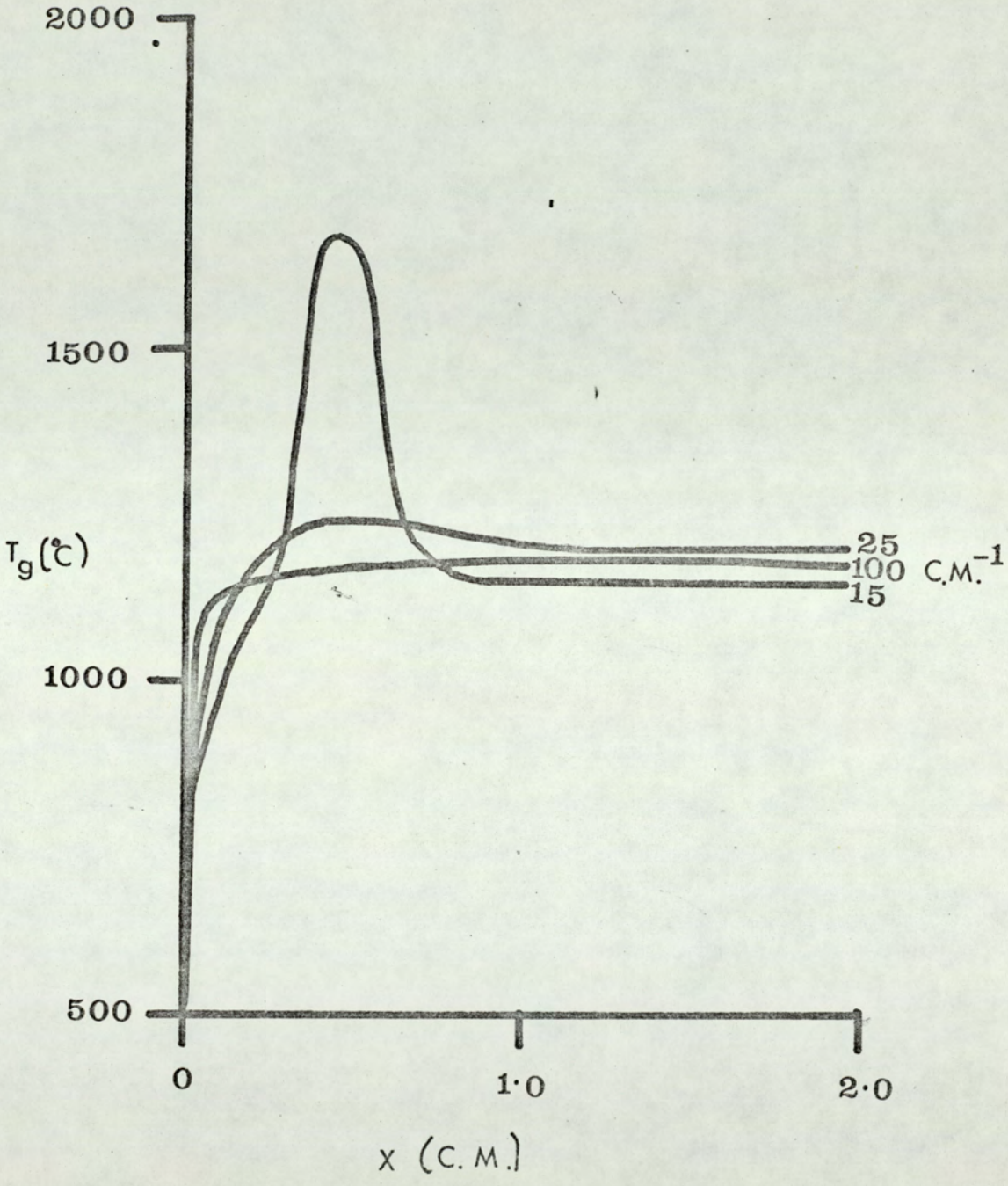

FIG. 24

EFFECT OF CHEMICAL KINETICS

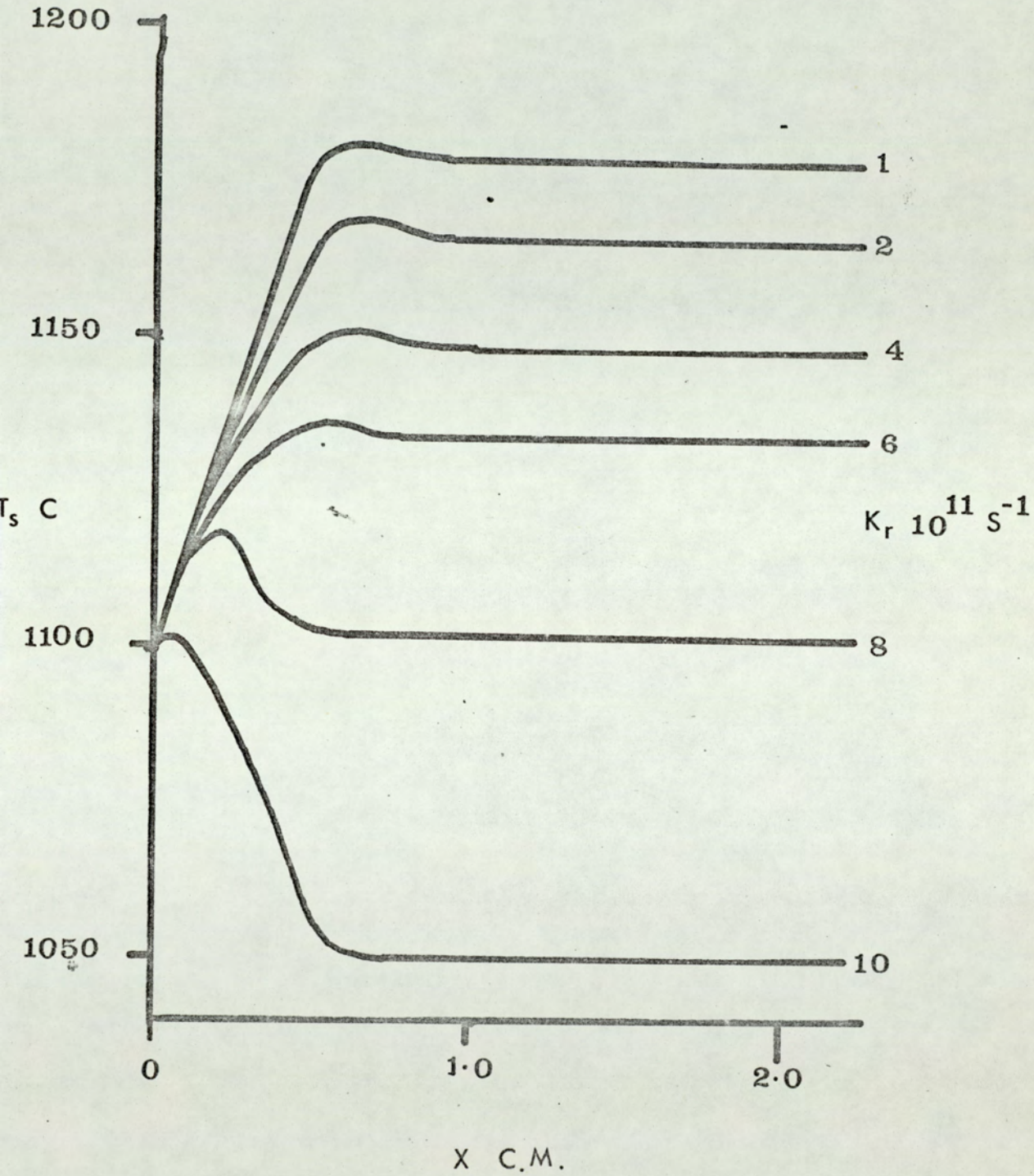

-FIG.25

MIXING WITH VERY HIGH PARTICLE TRANSPORTATION RATES

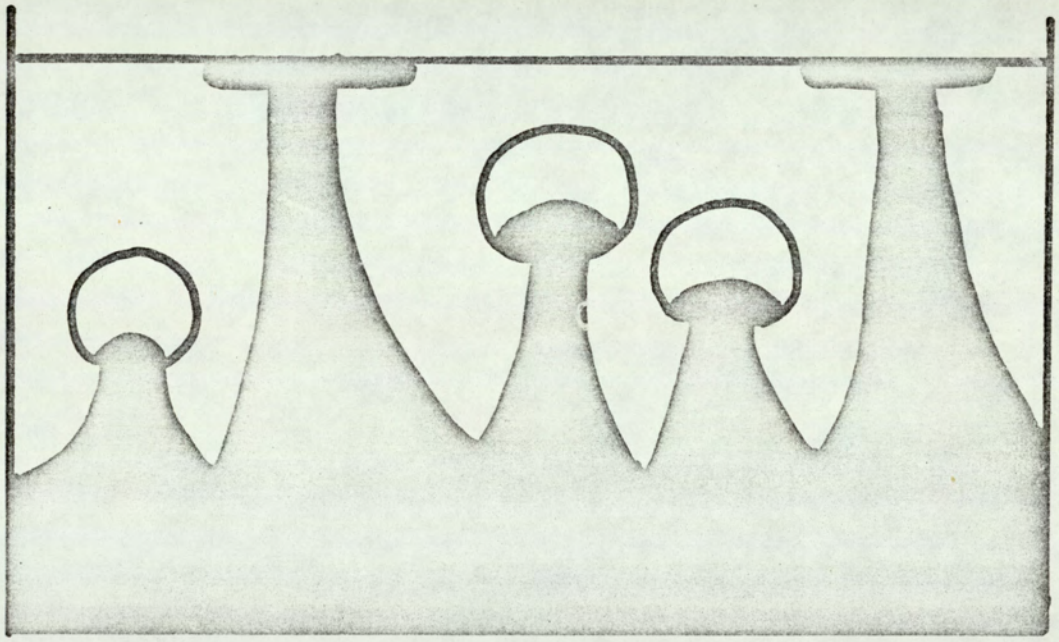

FIG. 26

COMBUSTION BED WITH STEEL DISTRIBUTOR PLATE

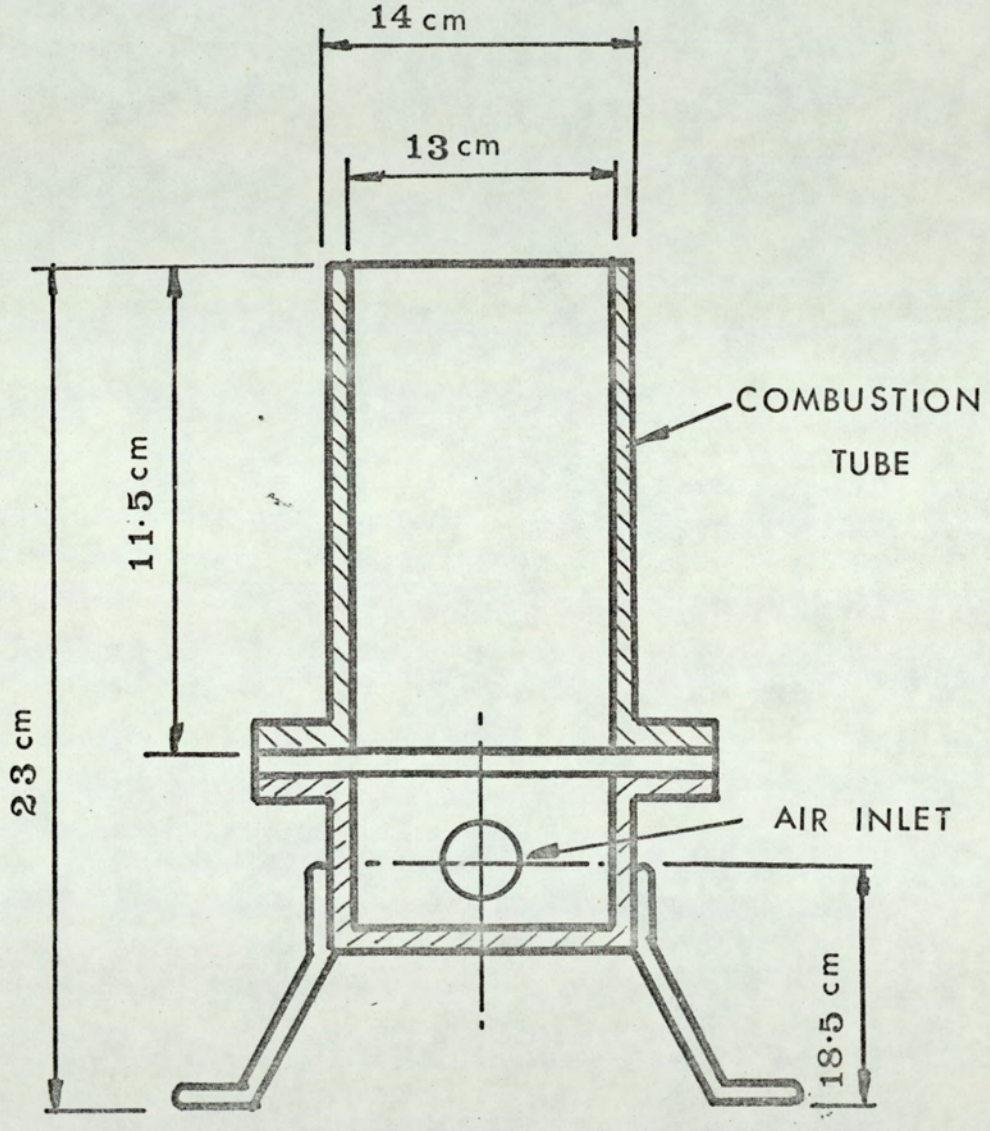

FIG. 27

COMBUSTION TUBE WITH REFRACTORY DISTRIBUTOR PLATE

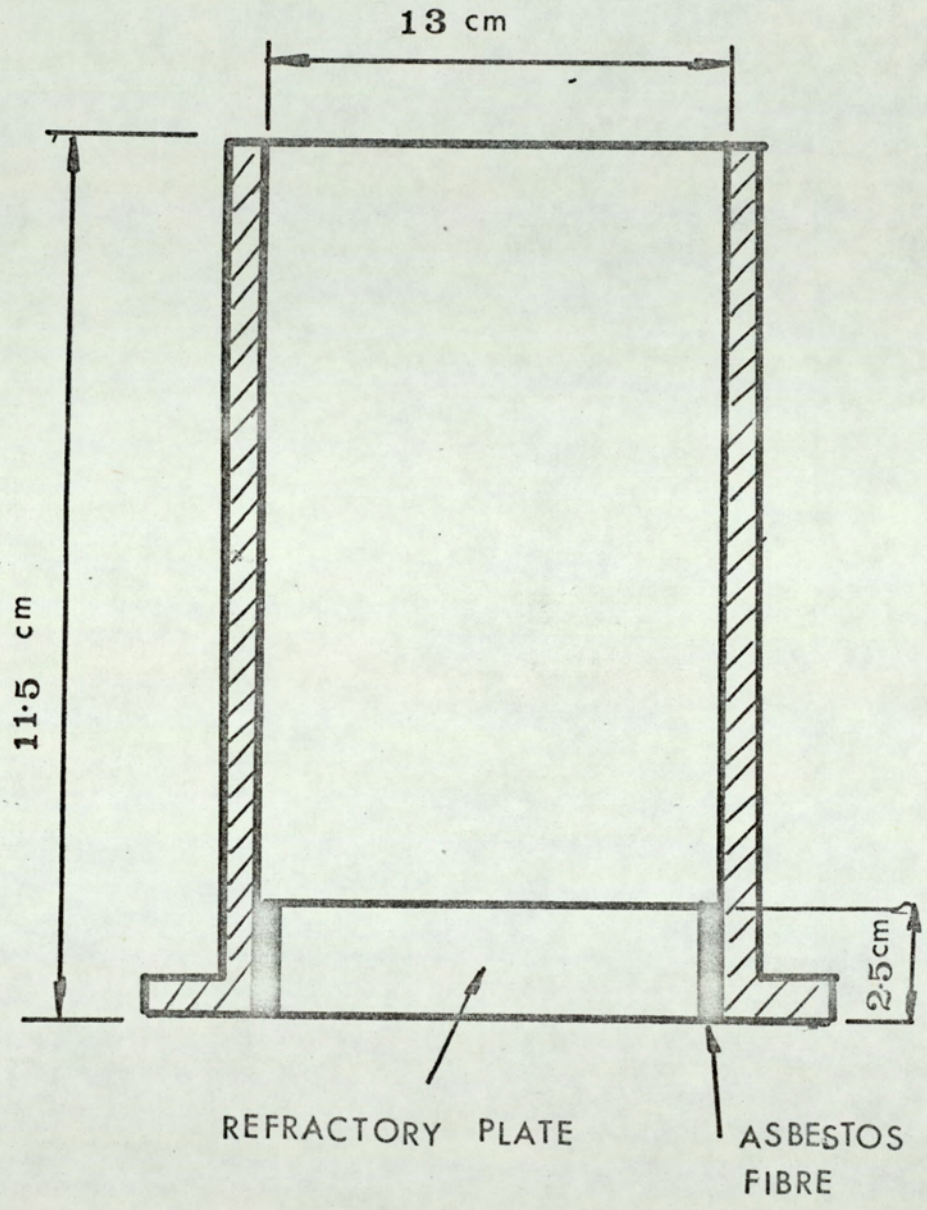

PARTICLE TRAP FIG. 28

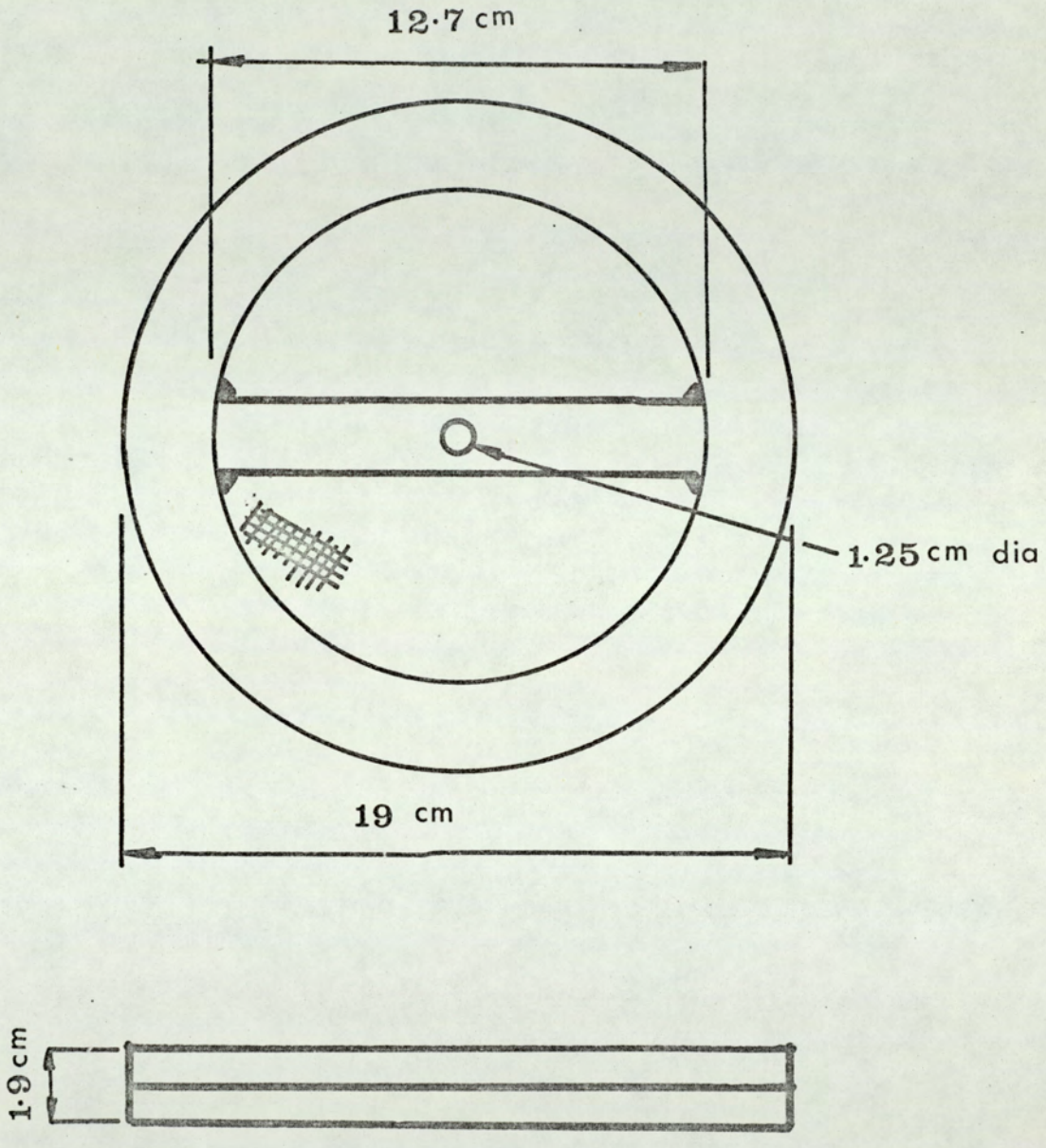

FIG. 29

PARTICLE TRAP

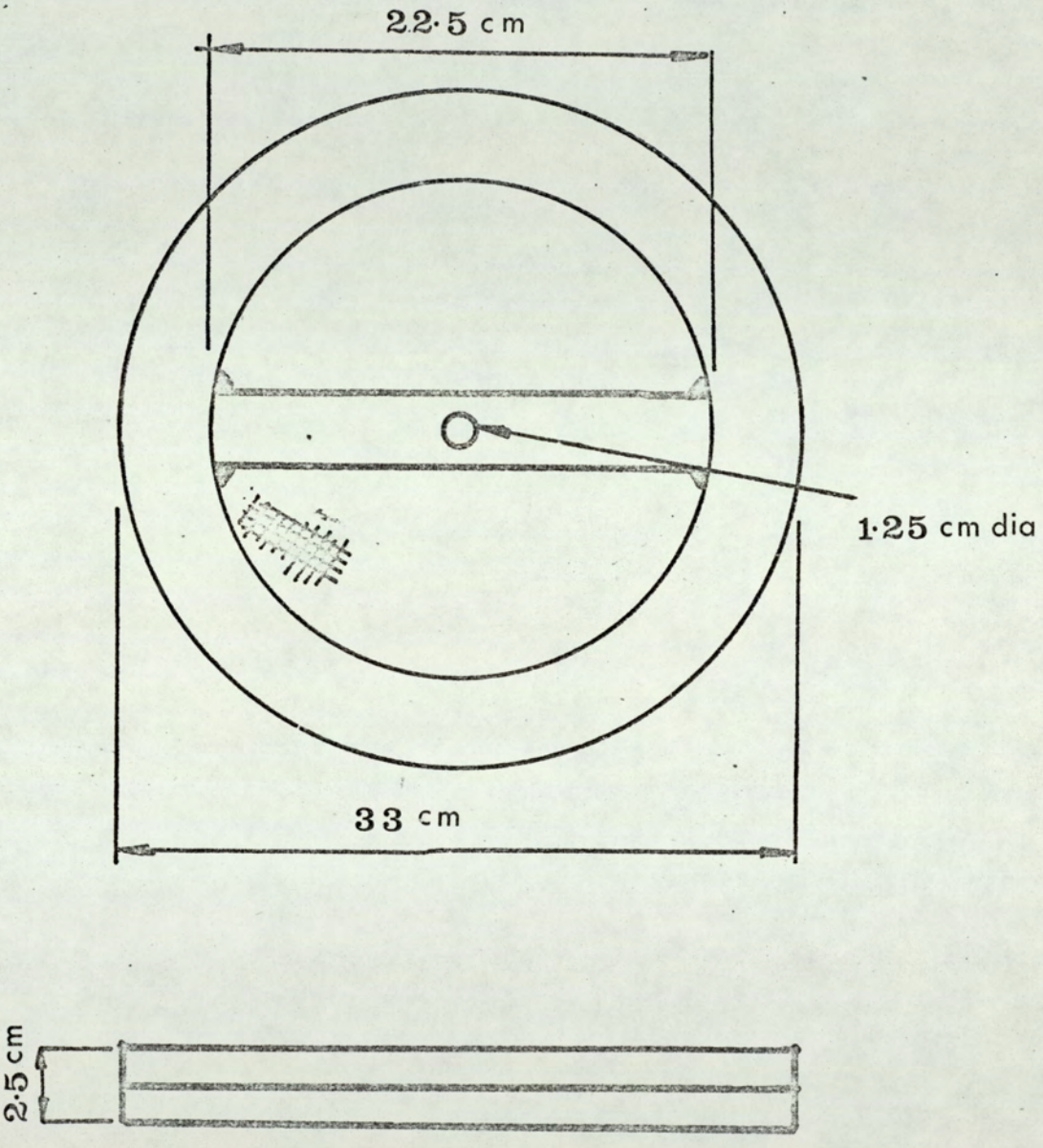

FIG. 30

BED FUNNEL

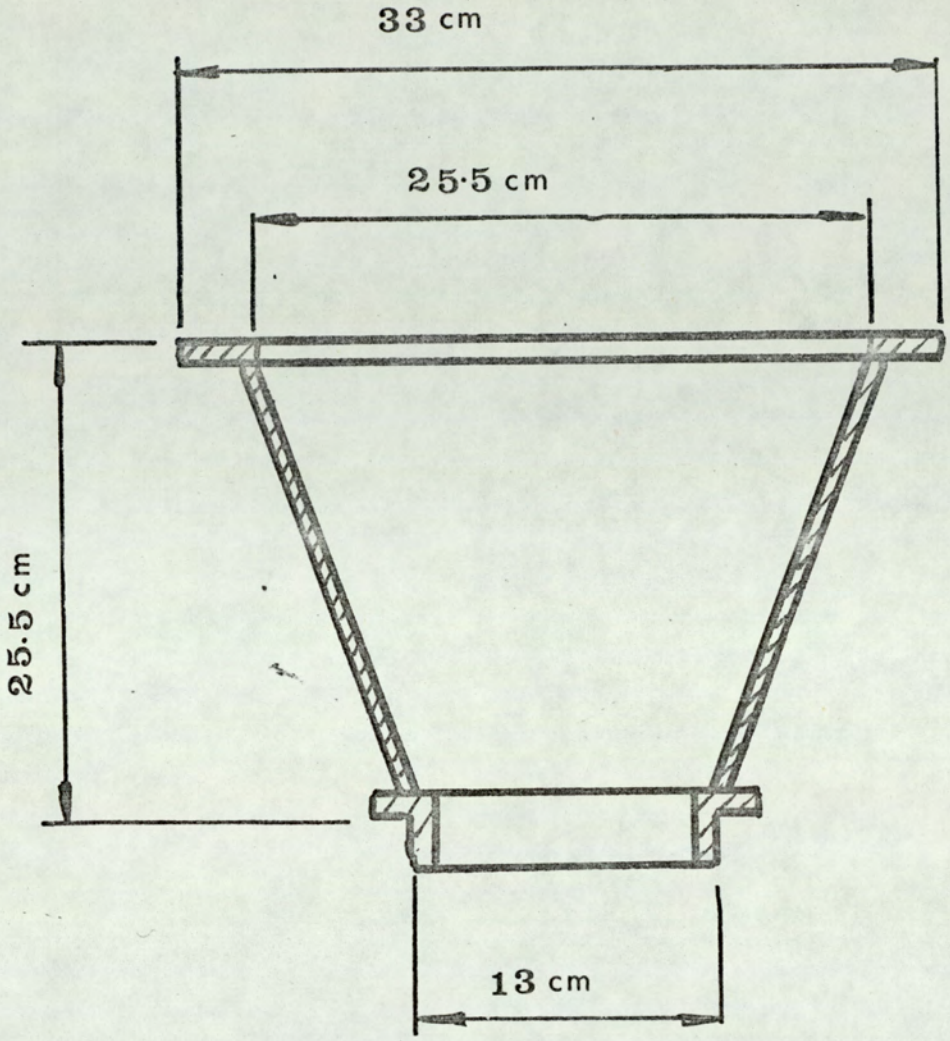

FIG.31

EQUIPMENT LAYOUT

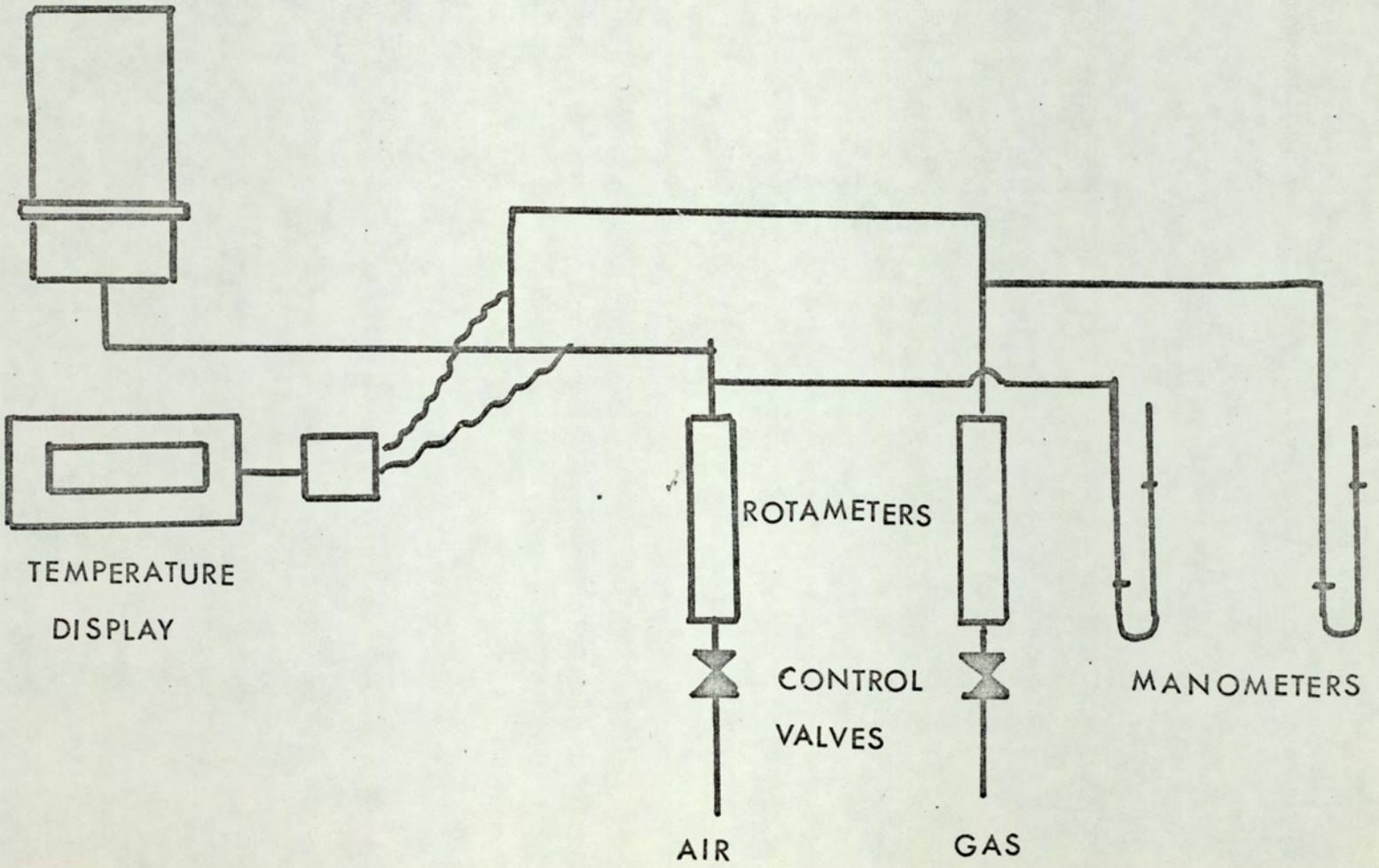

FIG. 32

METHOD OF EVALUATING U_{mf}

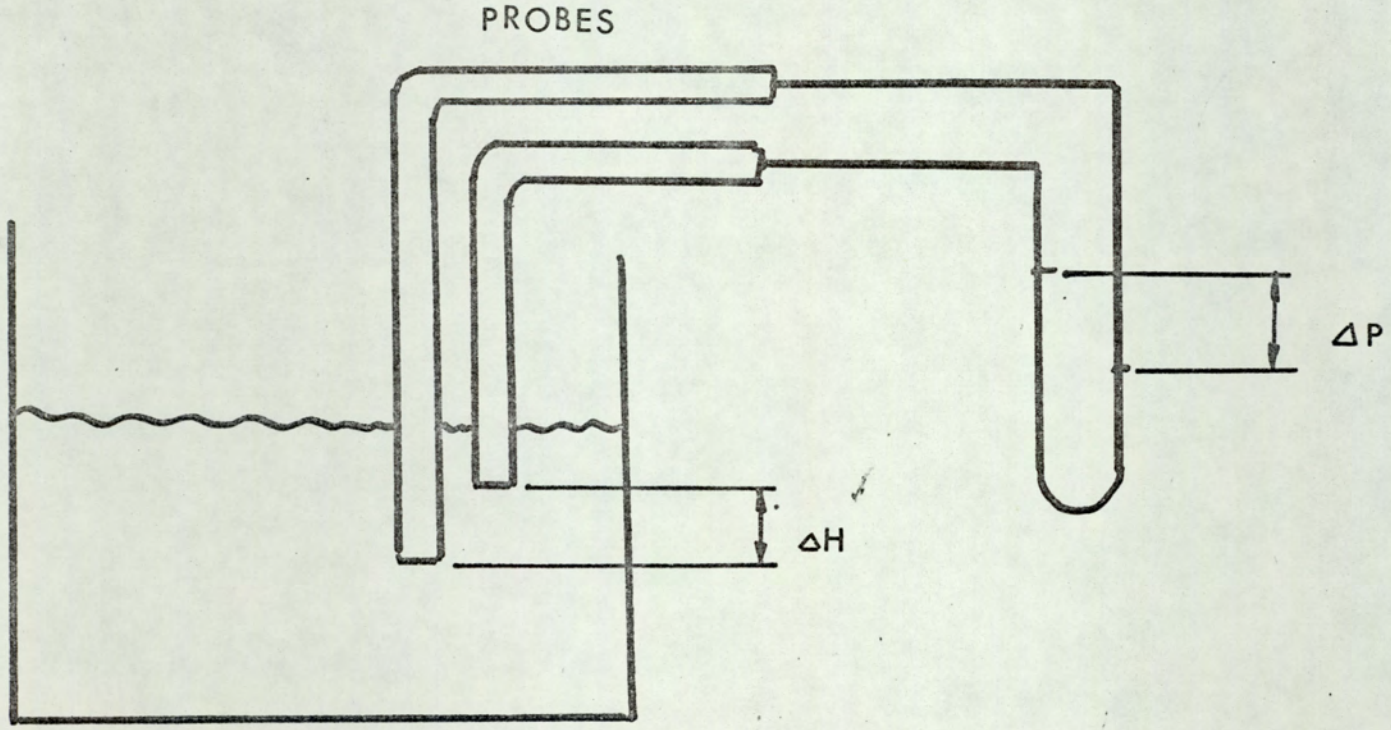

FIG. 33

FLUIDISING VELOCITIES

ZIRCONIUM SILICATE

(0·6 – 0·71) mm dia

U_{mf} = 54·5 $\frac{cm}{s}$

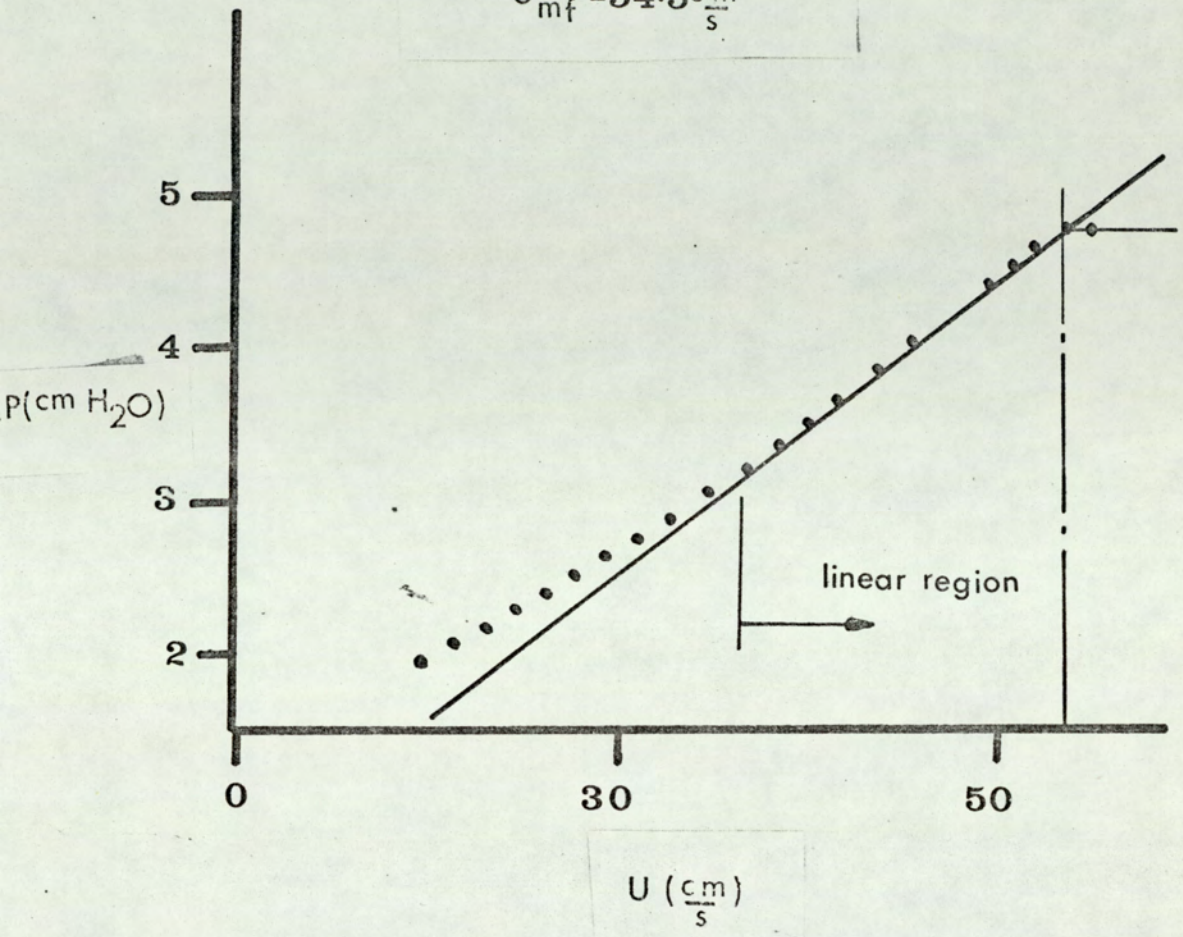

FIG. 34

FLUIDISING VELOCITIES

SILICA DIOXIDE

(0·6 - 0·71) mm dia

U_{mf} = 24·75 $\frac{cm}{s}$

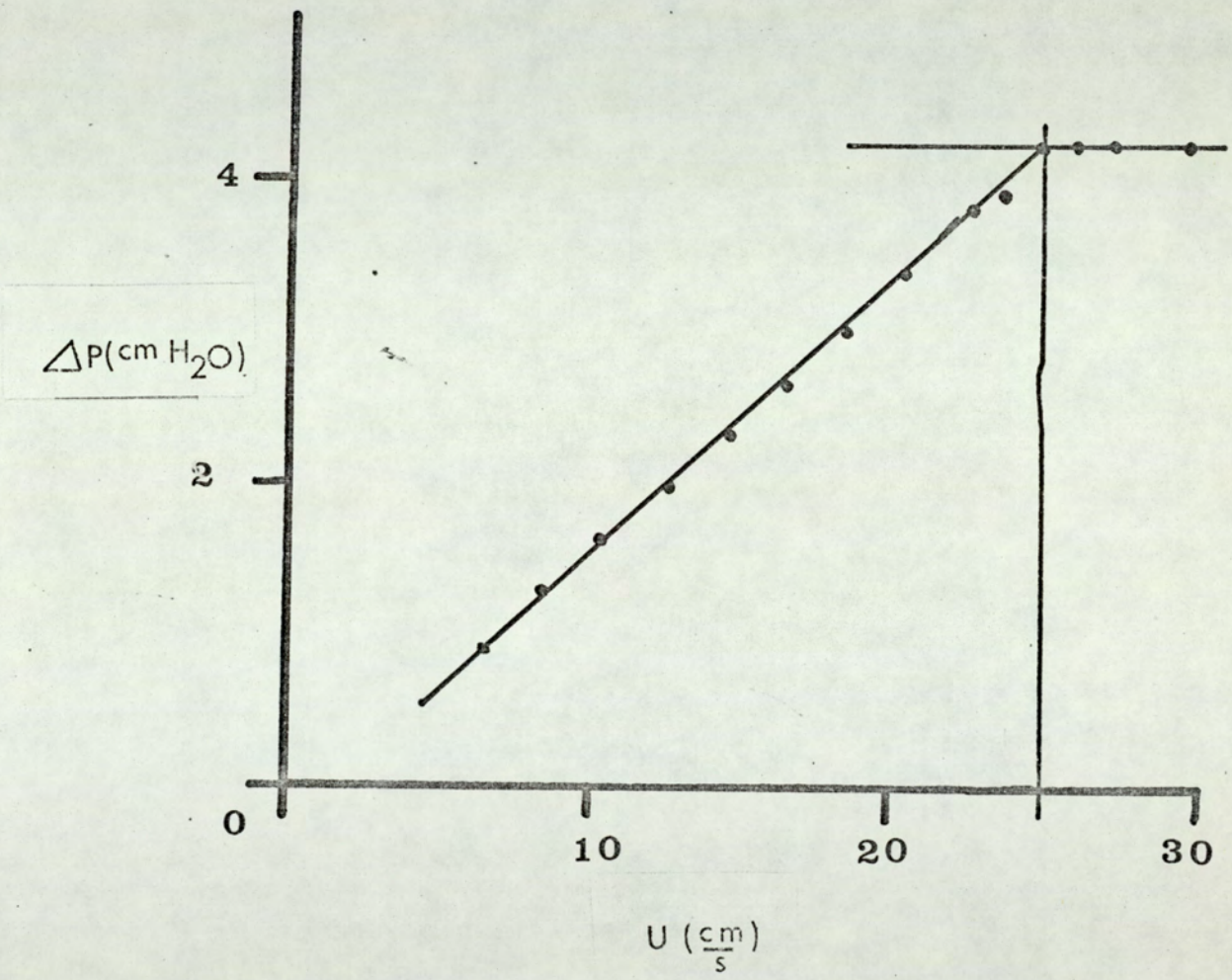

FLUIDISING VELOCITIES

FIG. 35

SILICA DIOXIDE

(·71-·85) mm dia

U_{mf} = 27·2 $\frac{cm}{s}$

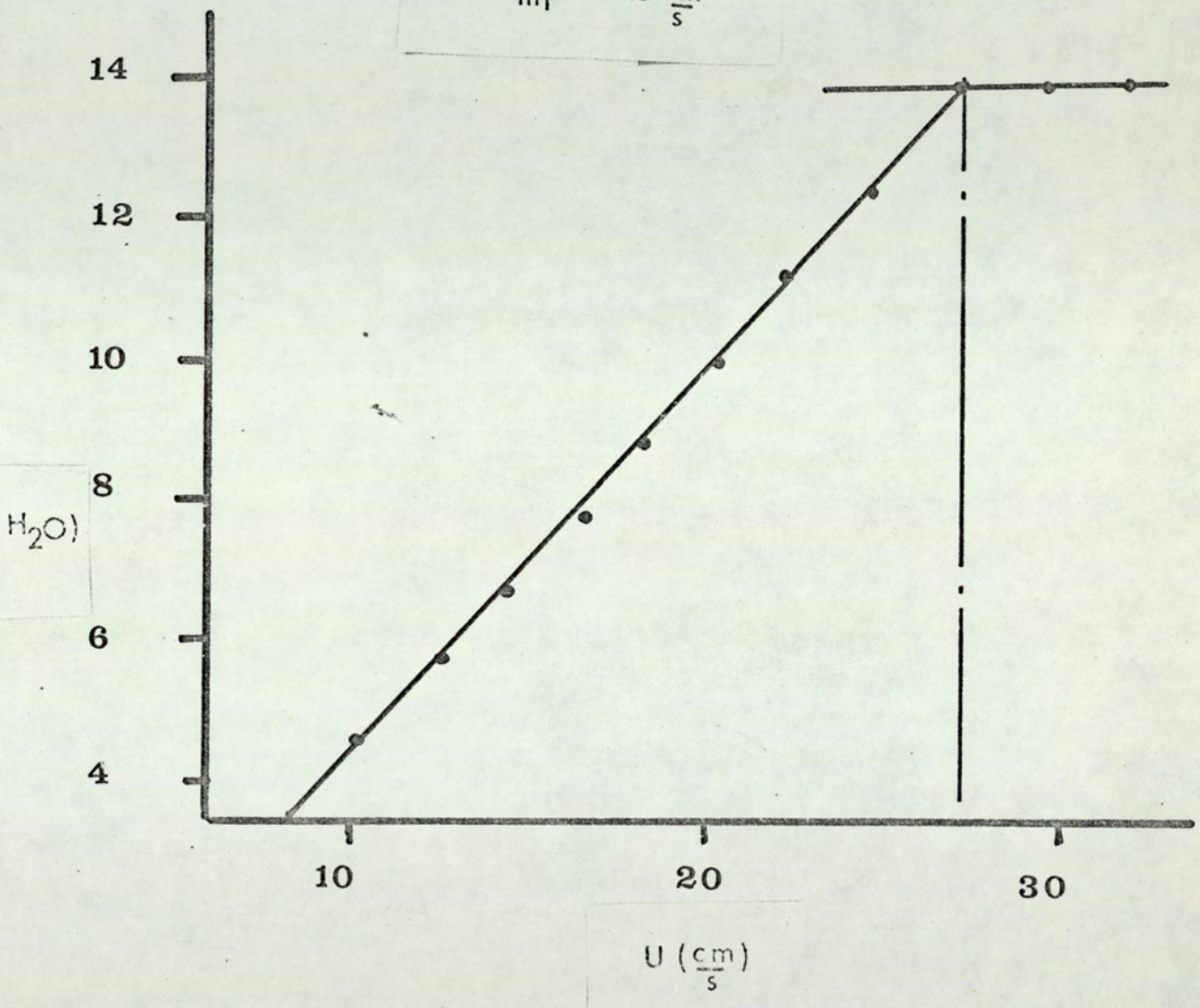

FIG.36

FLUIDISING VELOCITIES

ZIRCONIUM SILICATE

(0·71-0·85) mm dia

$U_{mf} = 67{\cdot}5 \frac{cm}{s}$

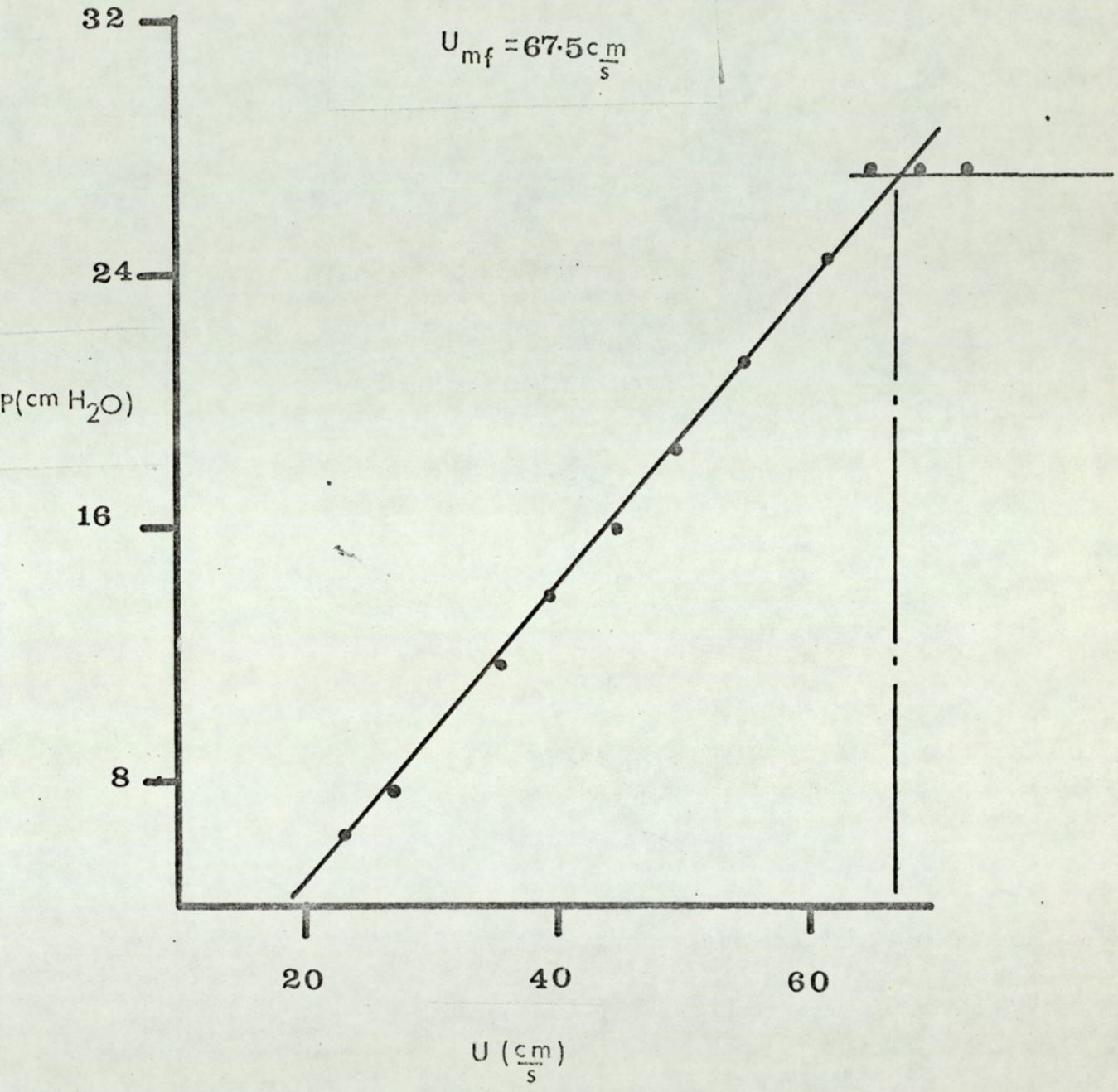

FIG.37

FLUIDISING VELOCITIES

ZIRCONIUM SILICATE

(1·0 –1·4) mm dia

U_{mf} =113 $\frac{cm}{s}$

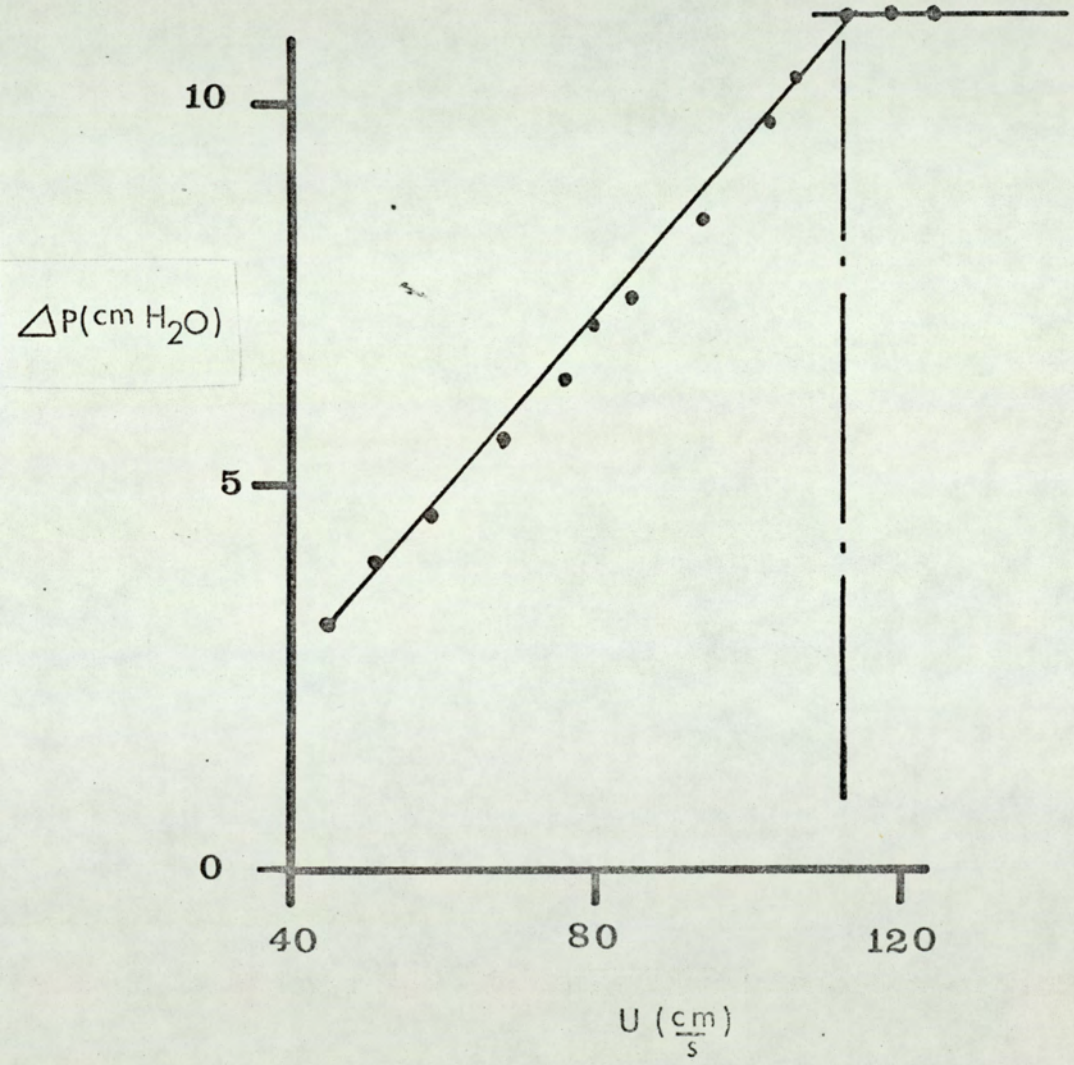

FIG.38

VARIATION OF U_{mf} WITH TEMPERATURE

ZIRCONIUM SILICATE

(1·0 −1·4) mm dia

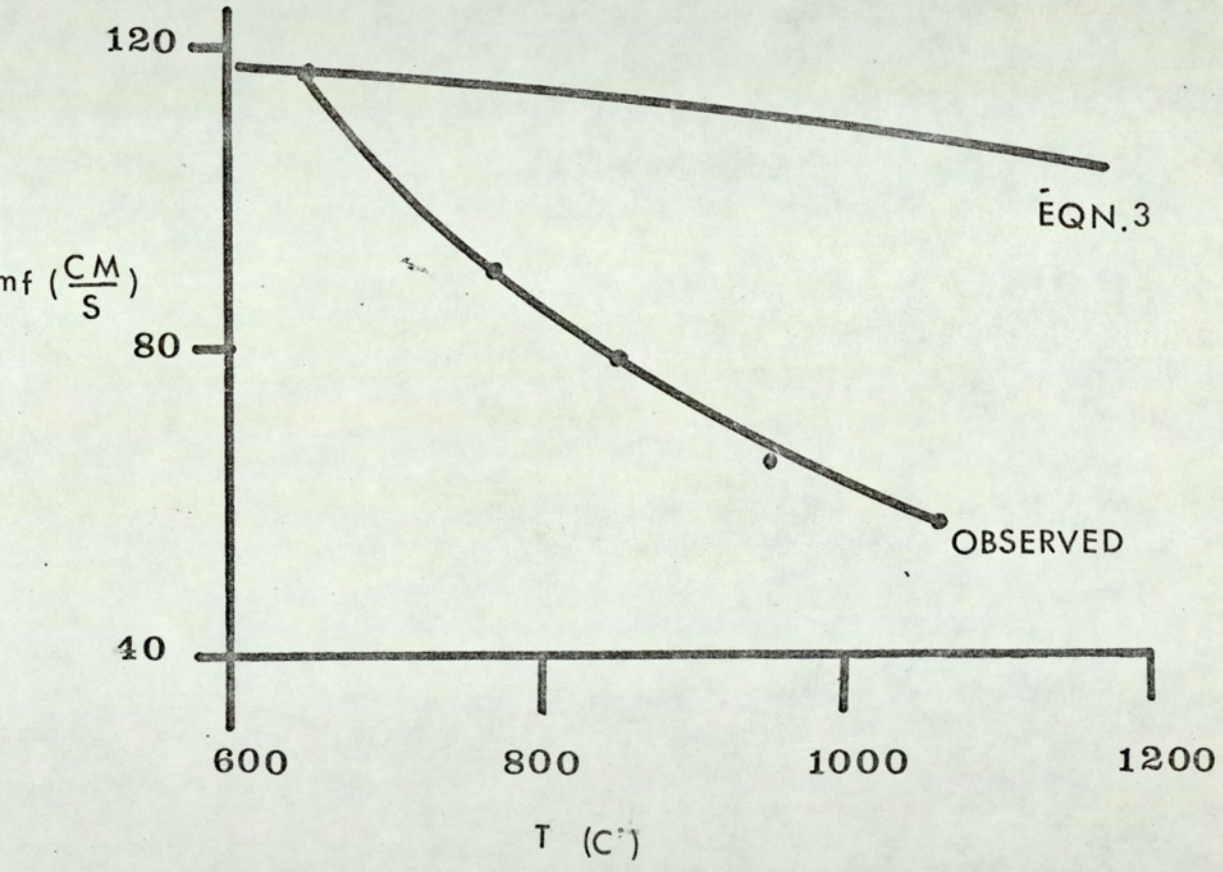

FIG. 39

COPPER TUBE SAMPLING PROBE

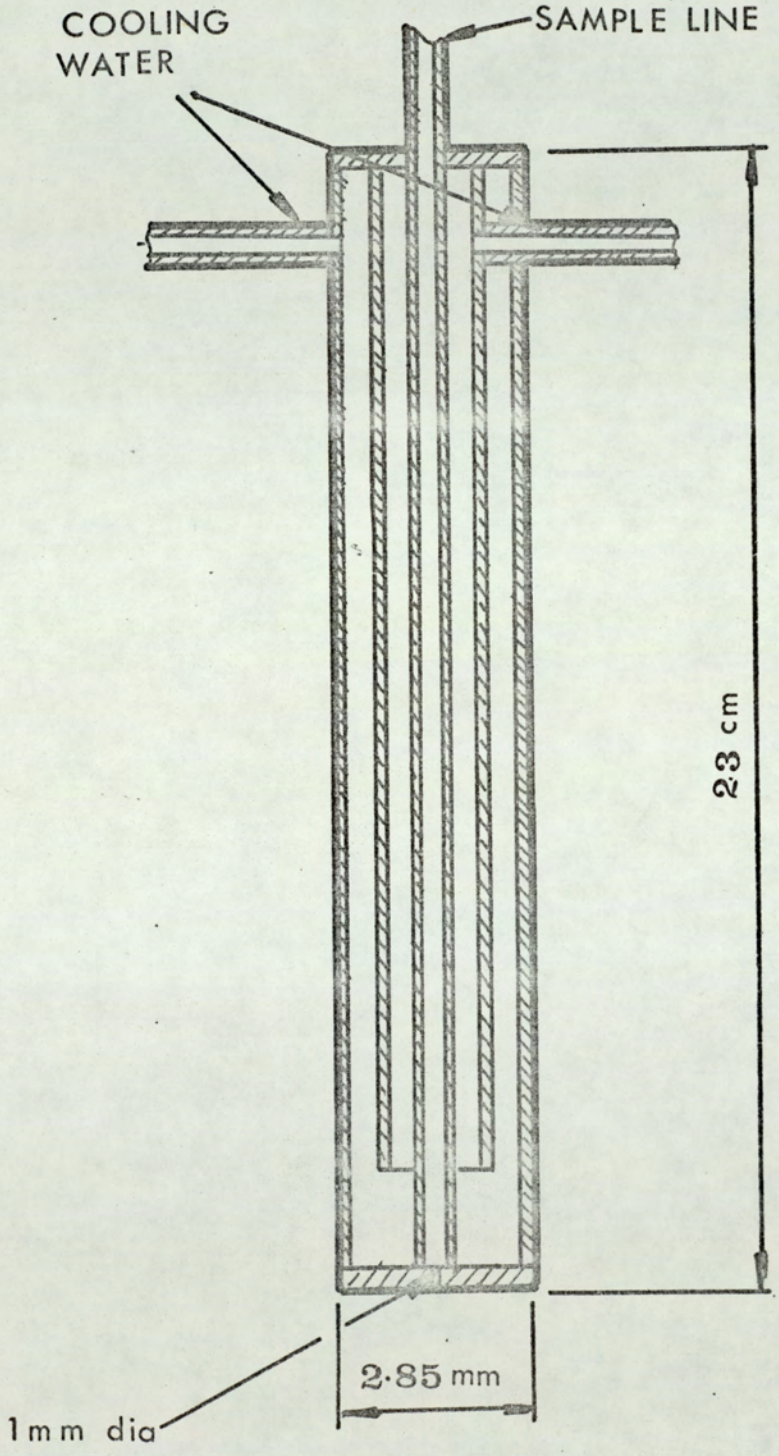

ADIBATIC COMBUSTION TEMPERATURES

METHANE – AIR MIXTURES

(dissociation neglected)

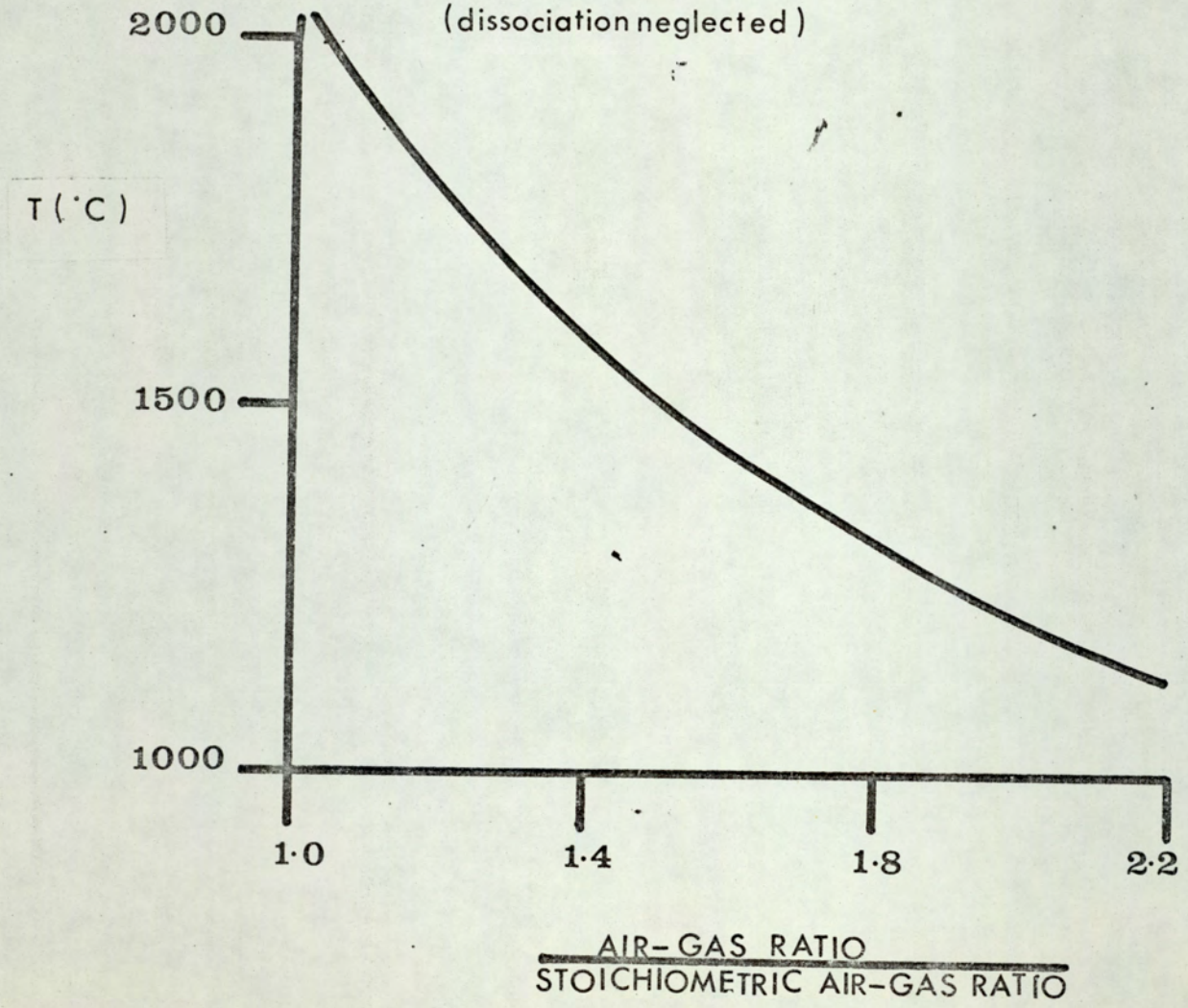

FIG.41

BED TEMPERATURES

ZIRCONIUM SILICATE

(1·0 — 1·4) m.m.

1·5 x STOICHIOMETRIC AIR

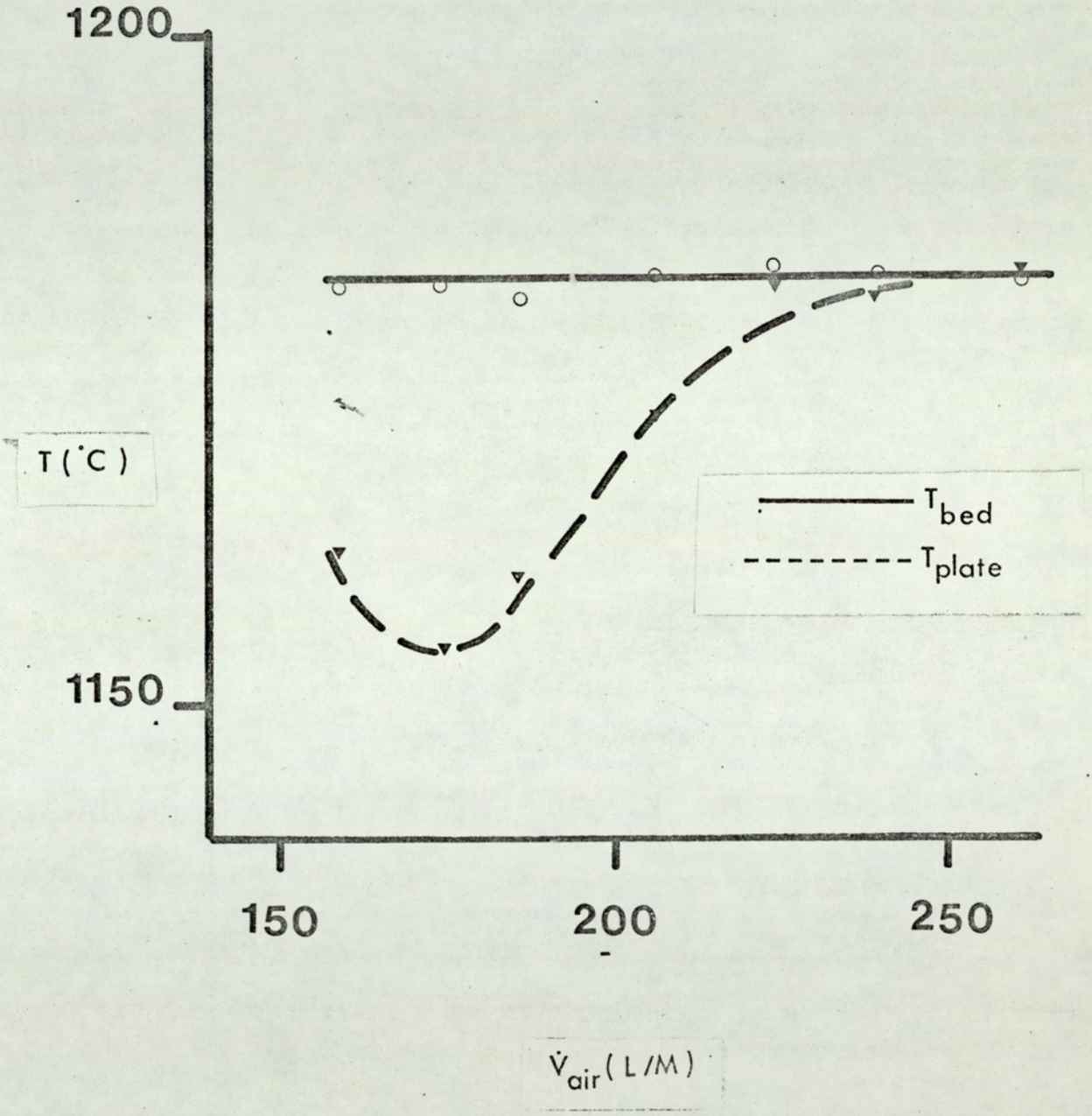

FIG. 42

BED TEMPERATURES

ZIRCONIUM SILICATE

(1·0 — 1·4) m.m. dia

1·6 x STOICHIOMETRIC AIR

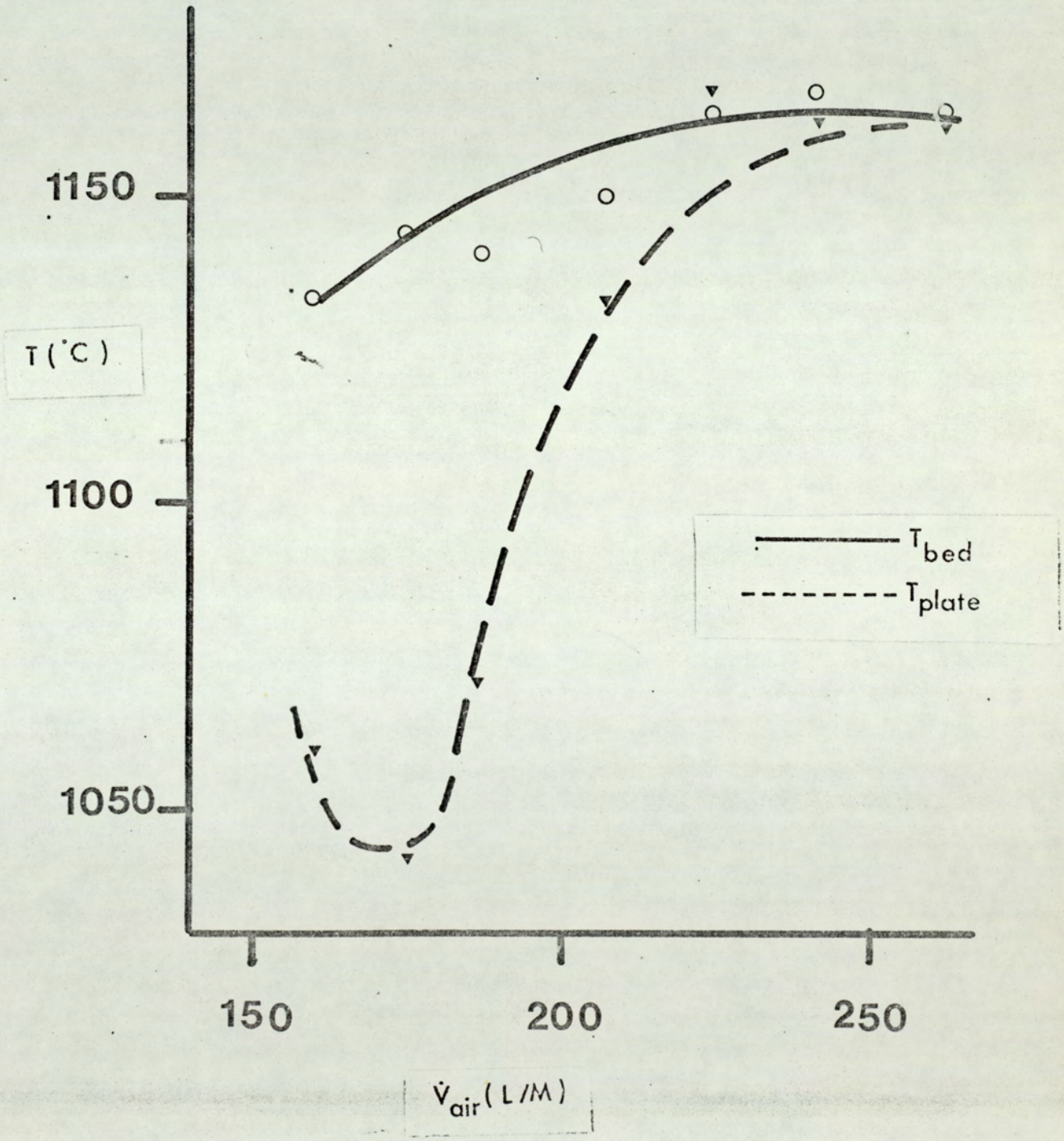

FIG. 43

BED TEMPERATURES

ZIRCONIUM SILICATE

(1·0 — 1·4) m.m.

1·7 x STOICHIOMETRIC AIR

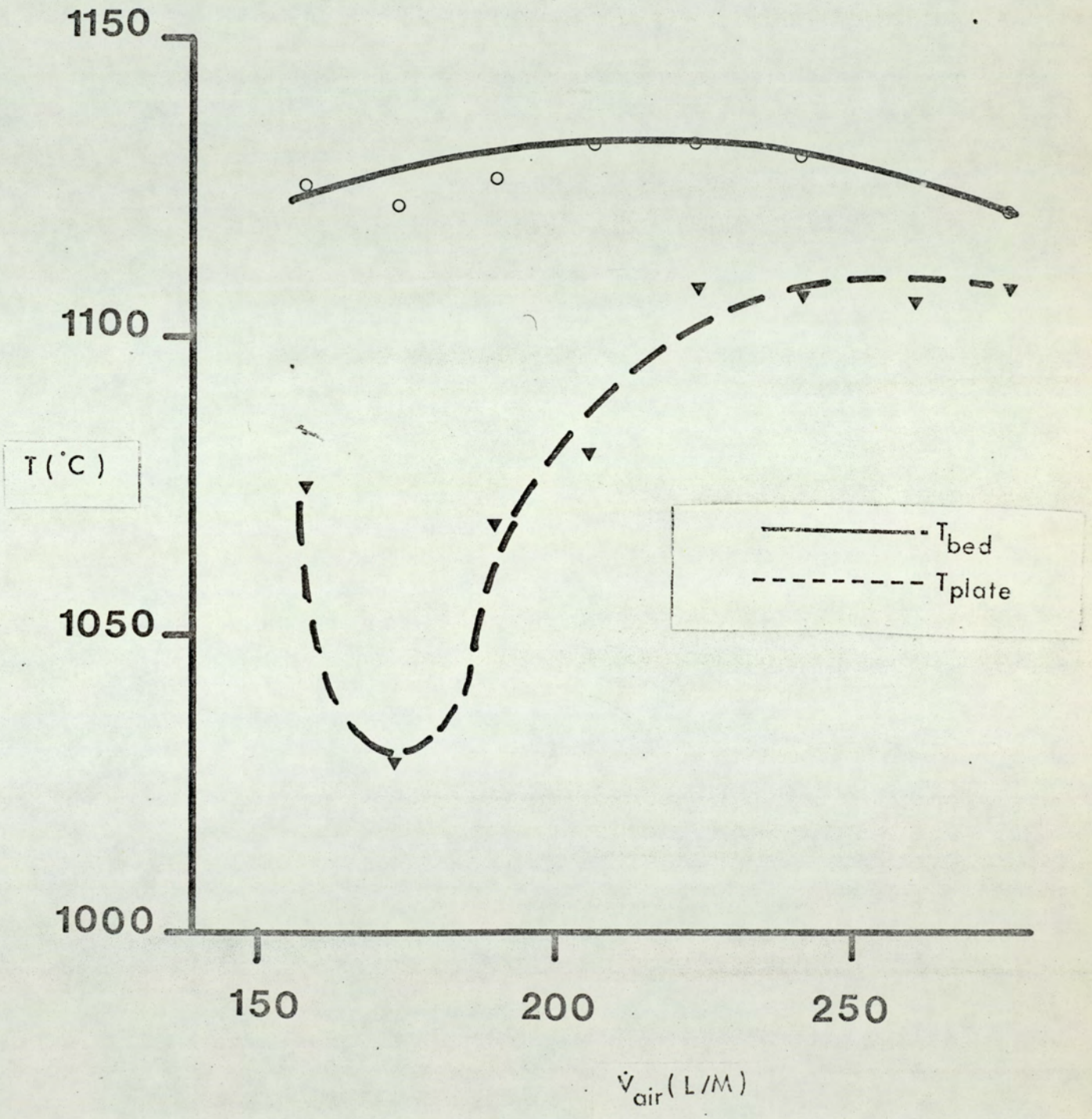

FIG. 44

BED TEMPERATURES

ZIRCONIUM SILICATE

(1·0 —— 1·4) m.m.

1·8 x STOICHIOMETRIC AIR

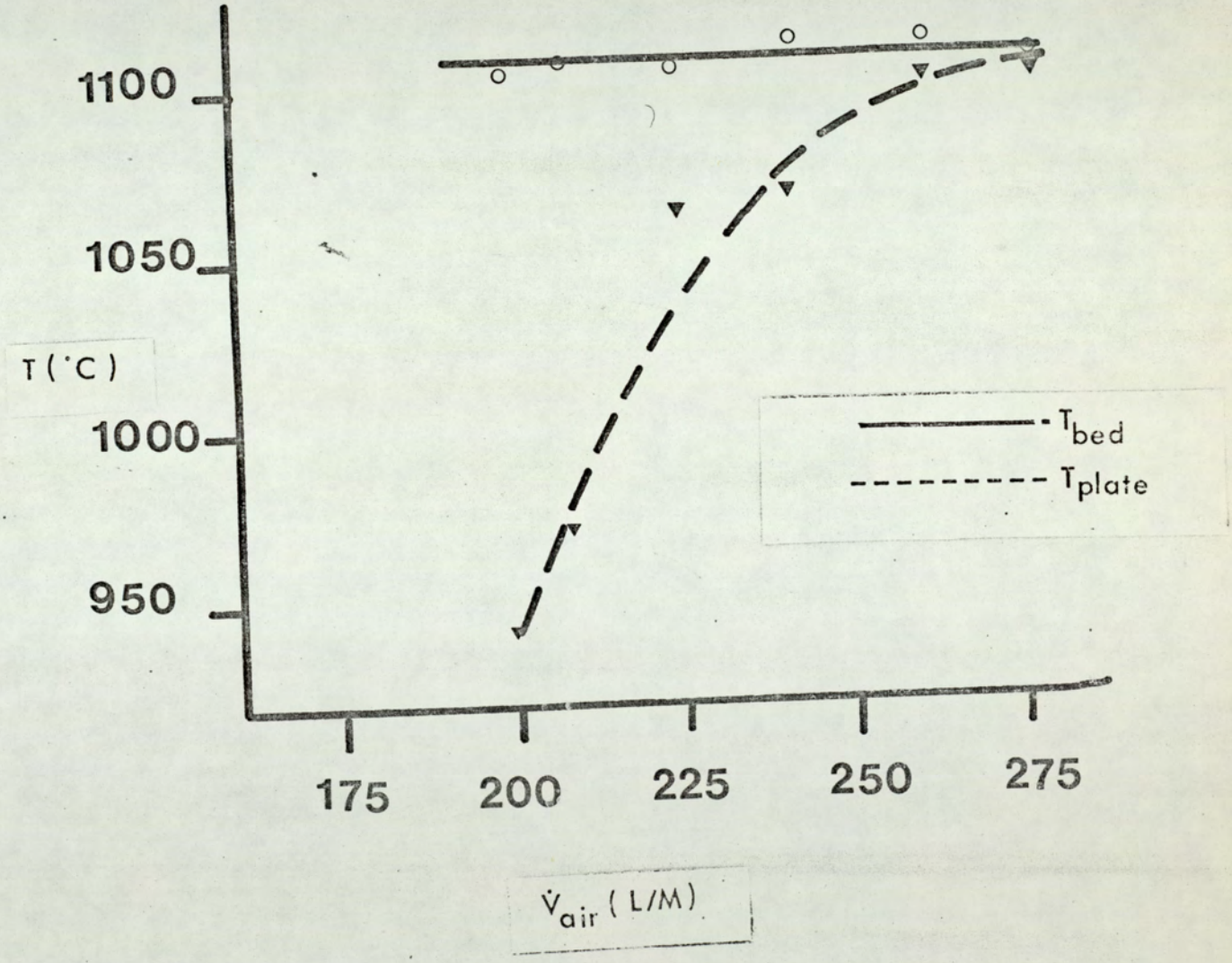

FIG. 45

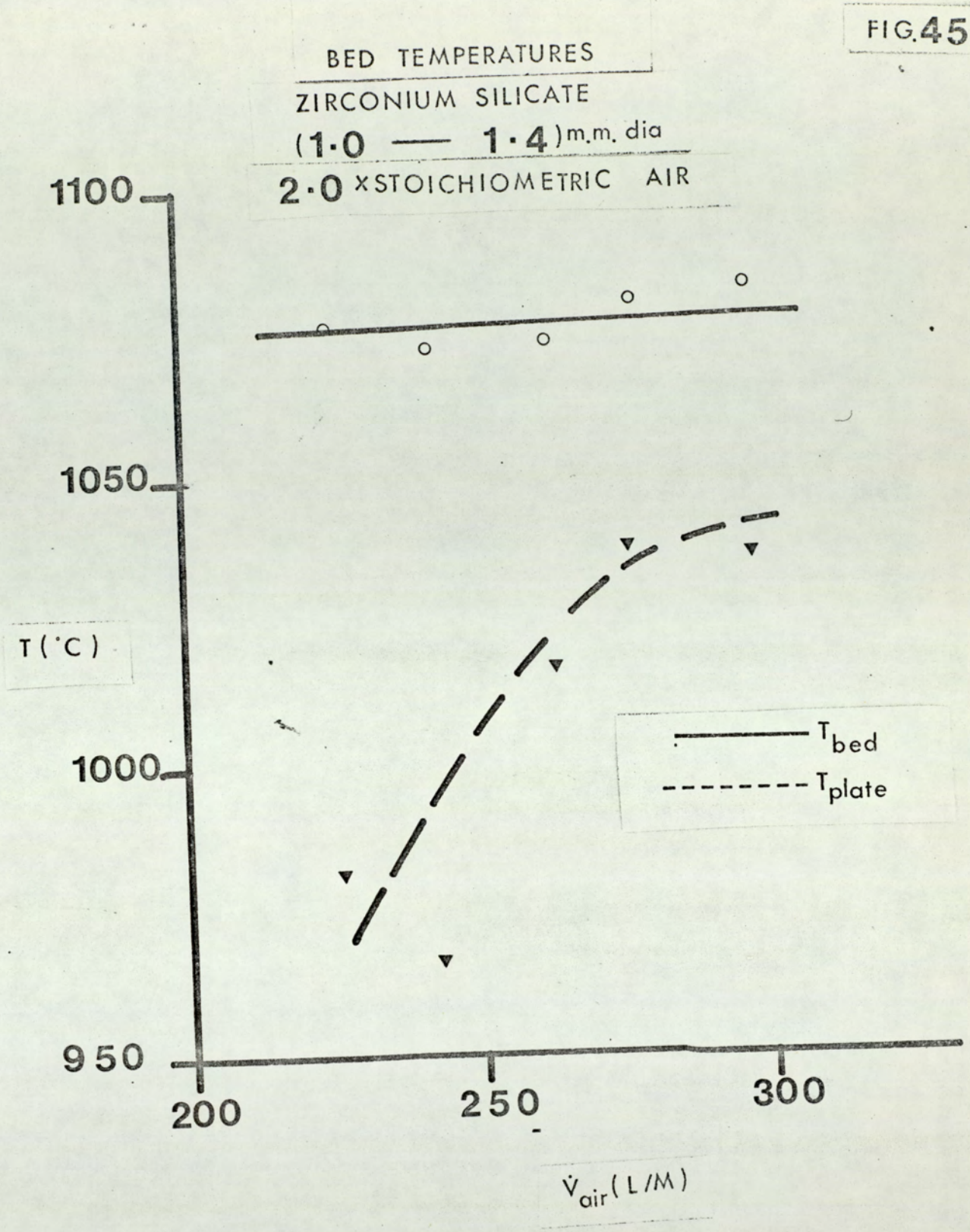
BED TEMPERATURES
ZIRCONIUM SILICATE
(1·0 — 1·4) m.m. dia
2·0 X STOICHIOMETRIC AIR
1100
1050
1000
950
T (°C)
200
250
300
$\dot{V}_{air}$ (L/M)
T_{bed}
T_{plate}

FIG.46

BED TEMPERATURES
ZIRCONIUM SILICATE
(0·71 — 0·85) m.m.
1·6 x STOICHIOMETRIC AIR

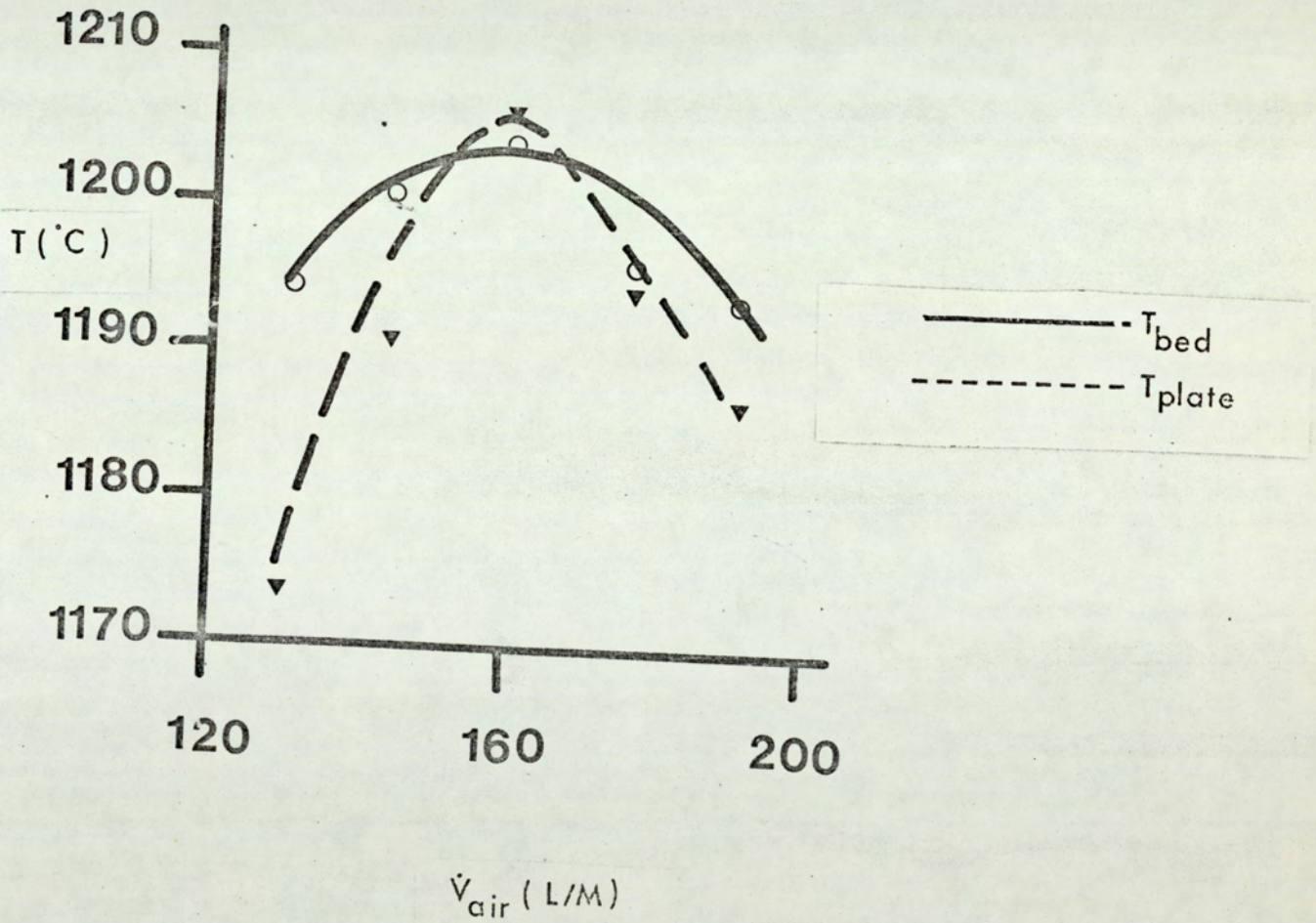

FIG. 47

BED TEMPERATURES

ZIRCONIUM SILICATE

(0·71 — 0·85) m.m. dia

1·8 X STOICHIOMETRIC AIR

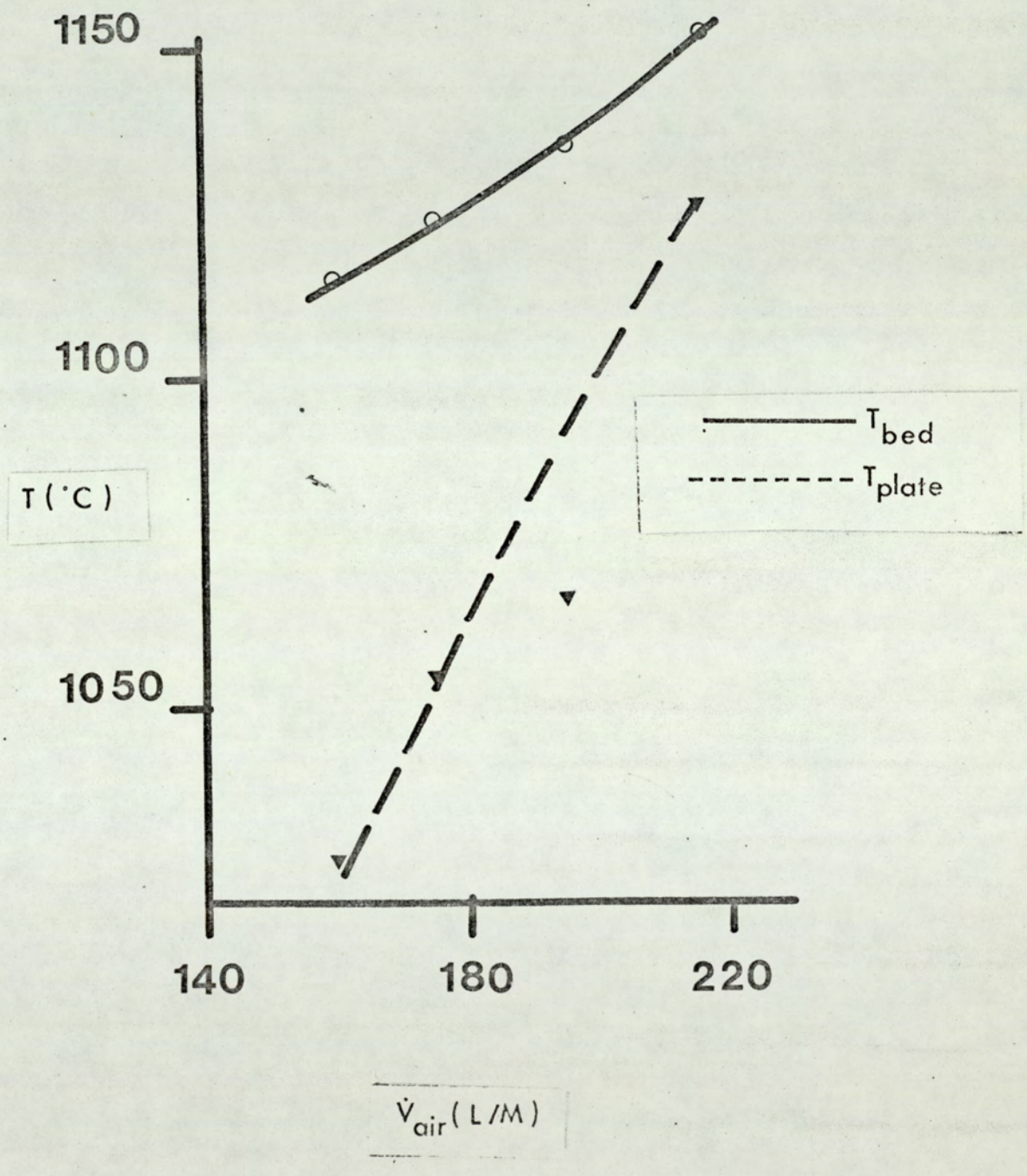

FIG. 48

BED TEMPERATURES

ZIRCONIUM SILICATE

(0·71 — 0·85) m.m. dia

2·0 x STOICHIOMETRIC AIR

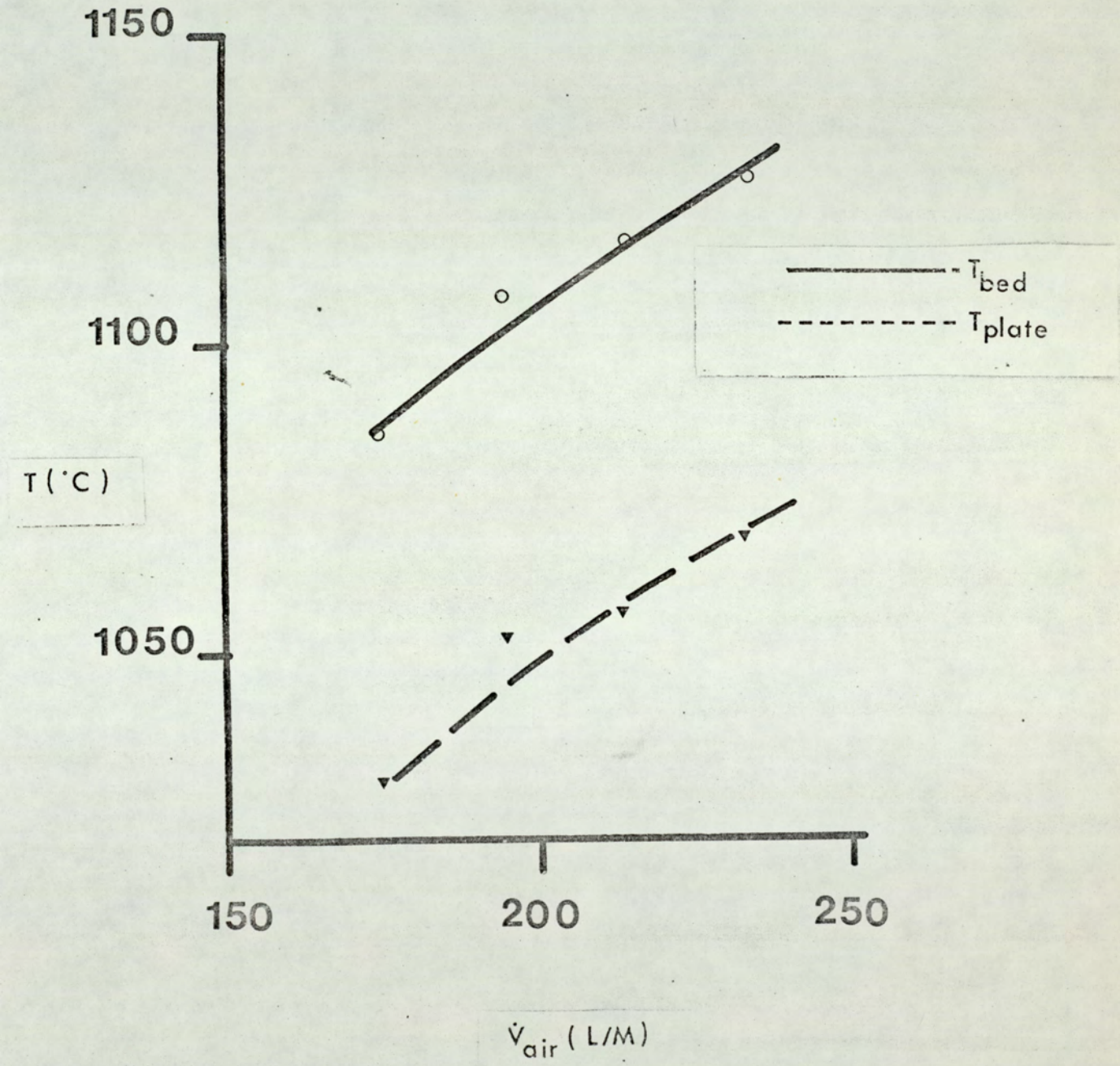

FIG. 49

BED TEMPERATURES

ZIRCONIUM SILICATE

(0·6 — 0·71) m.m.

1·4 x STOICHIOMETRIC AIR

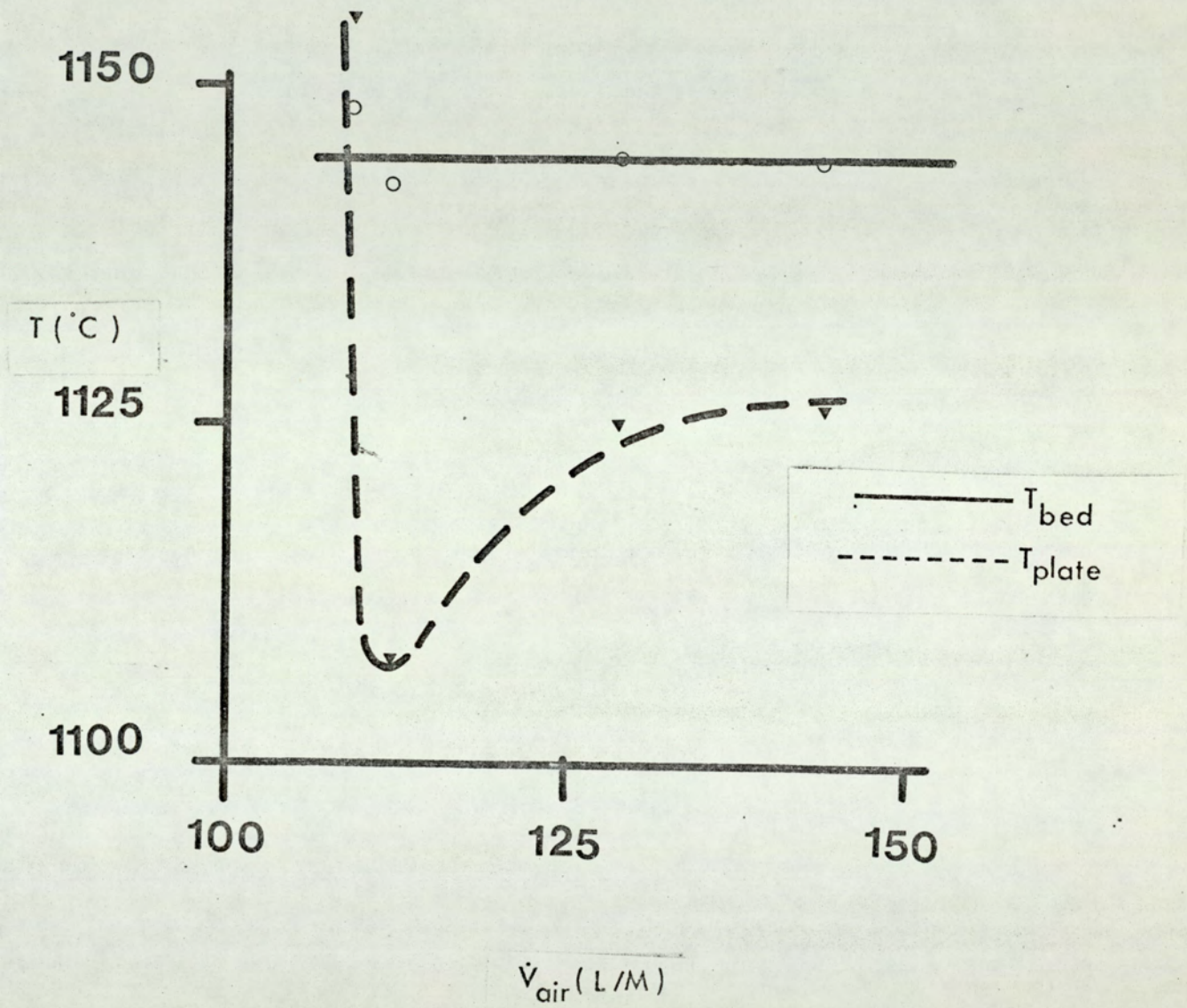

FIG.50

BED TEMPERATURES

ZIRCONIUM SILICATE

(0·6 — 0·71) m.m.

1·6 x STOICHIOMETRIC AIR

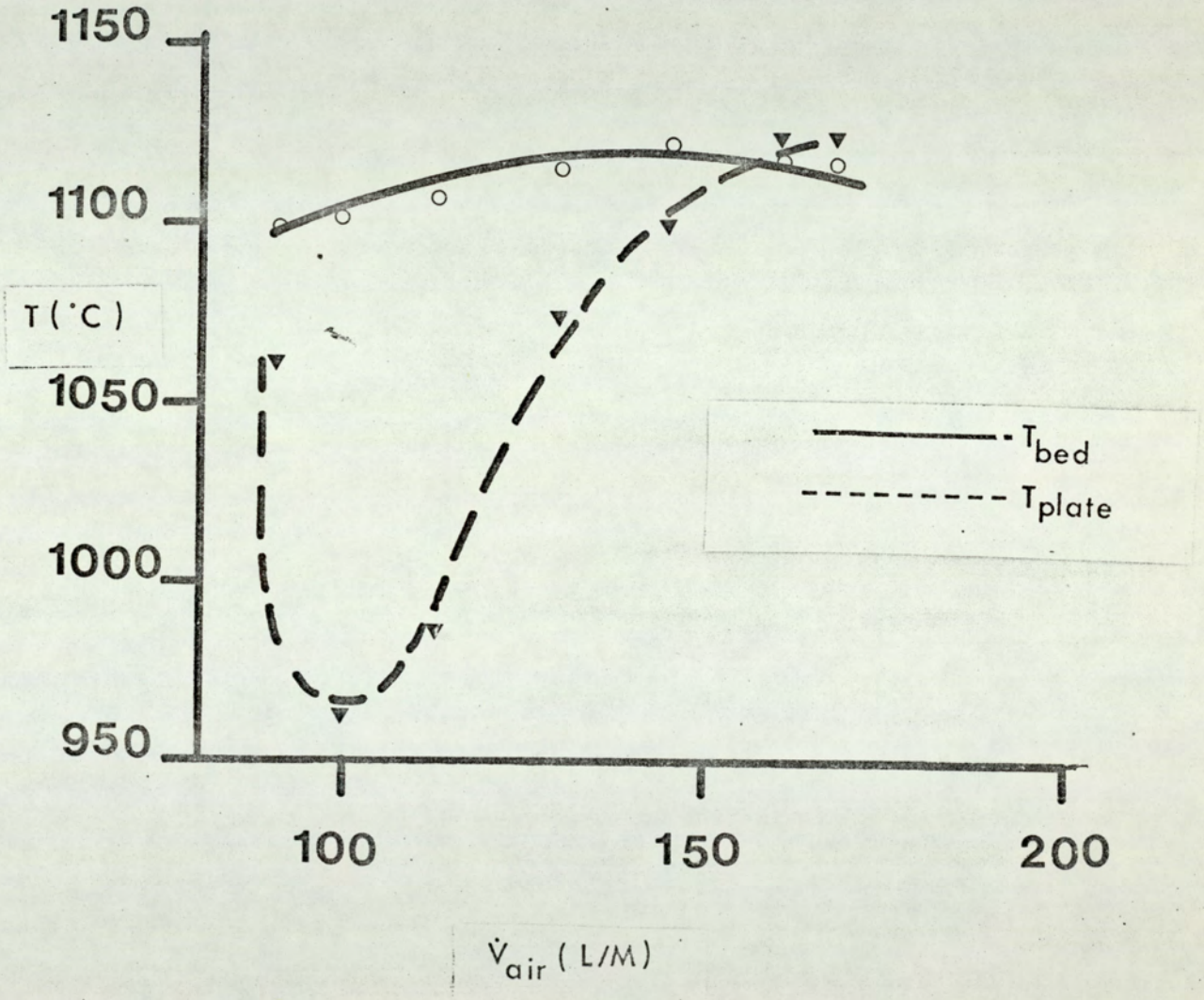

FIG. 51

BED TEMPERATURES

ZIRCONIUM SILICATE

(0·6 — 0·71) m.m.

1·8 x STOICHIOMETRIC AIR

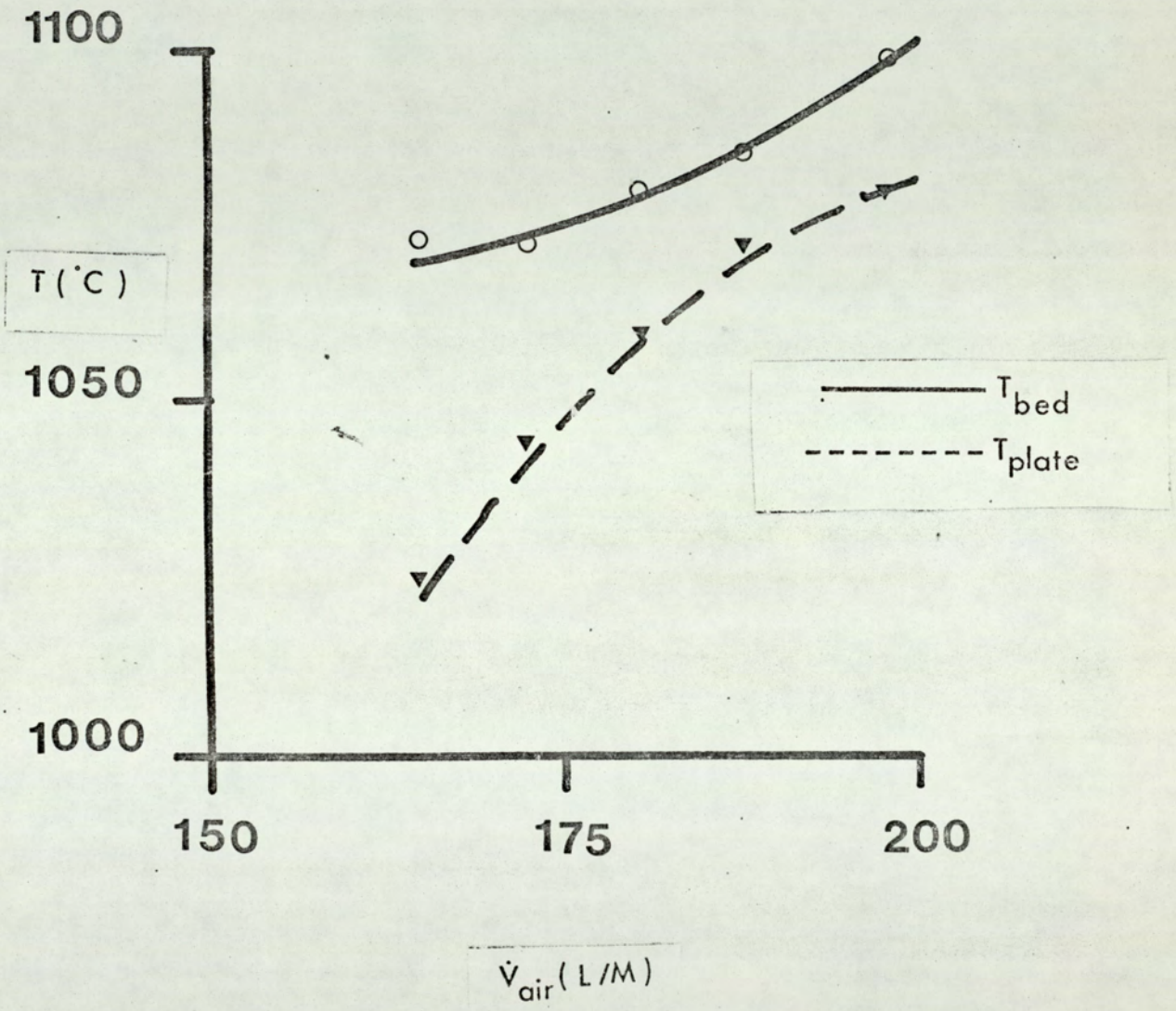

FIG.52

BED TEMPERATURES

ZIRCONIUM SILICATE

(0·6 — 0·71)m.m. dia

2·0 x STOICHIOMETRIC AIR

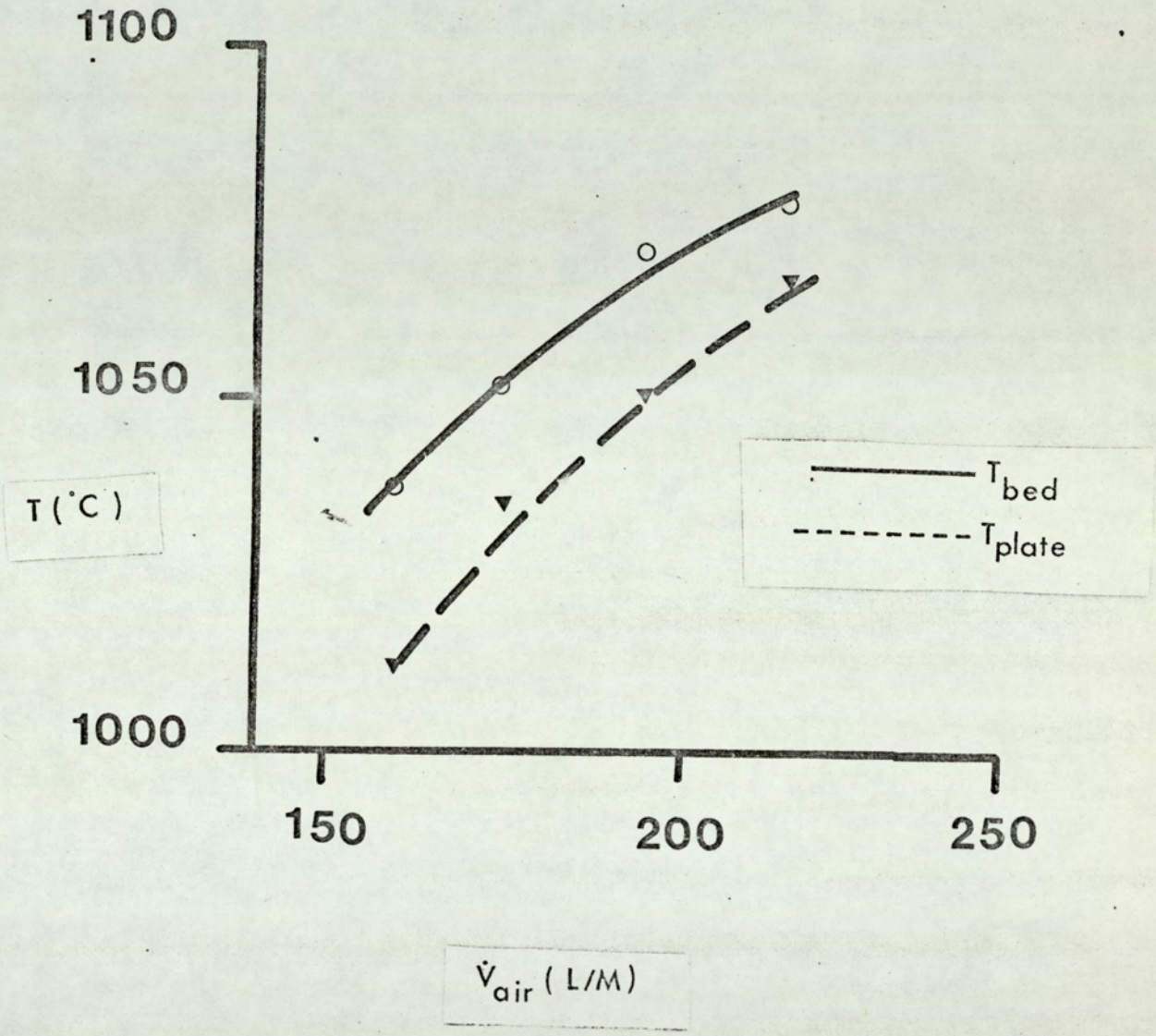

FIG. 53

BED TEMPERATURES

SILICA DIOXIDE

(0·71 — 0·85) m.m. dia

1·0 x STOICHIOMETRIC AIR

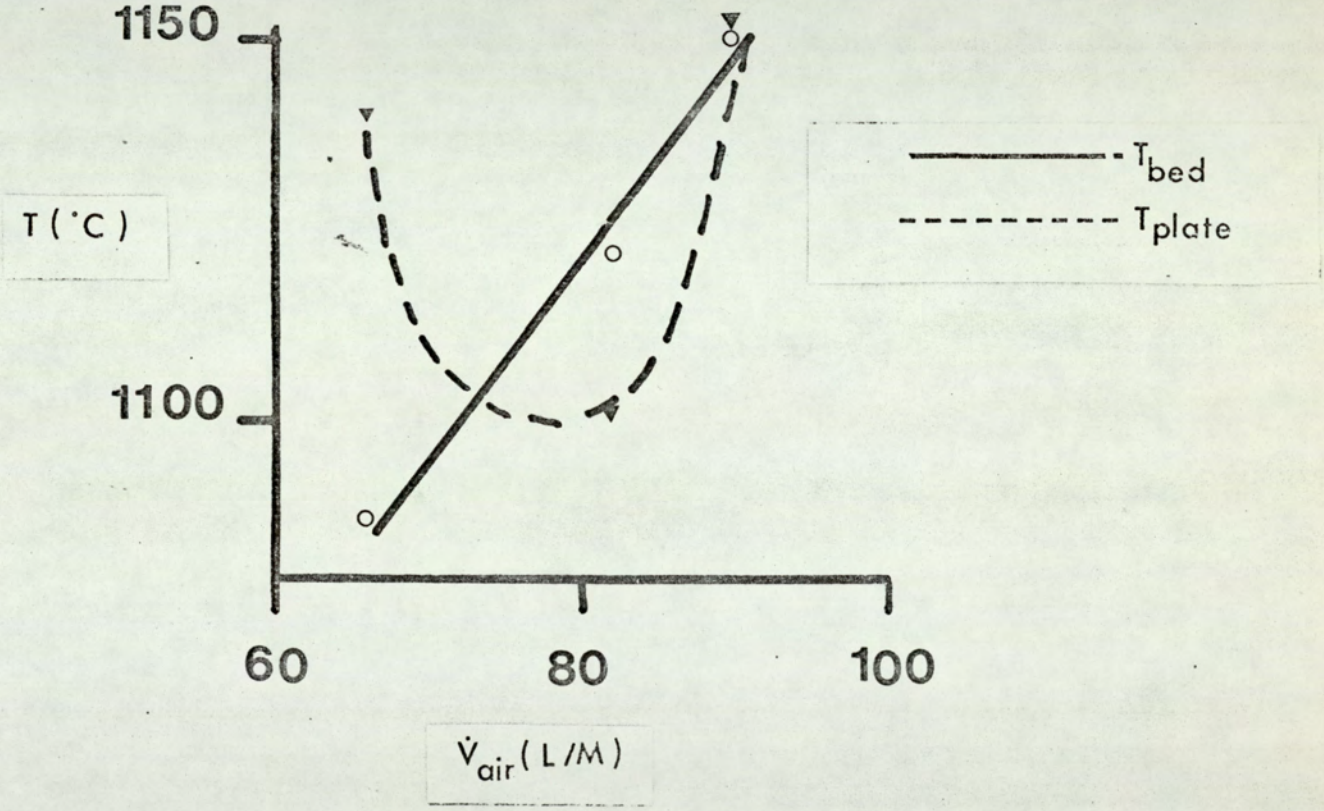

FIG. 54

BED TEMPERATURES

SILICA DIOXIDE

(0·71— 0·85)m.m. dia

1·2 x STOICHIOMETRIC AIR

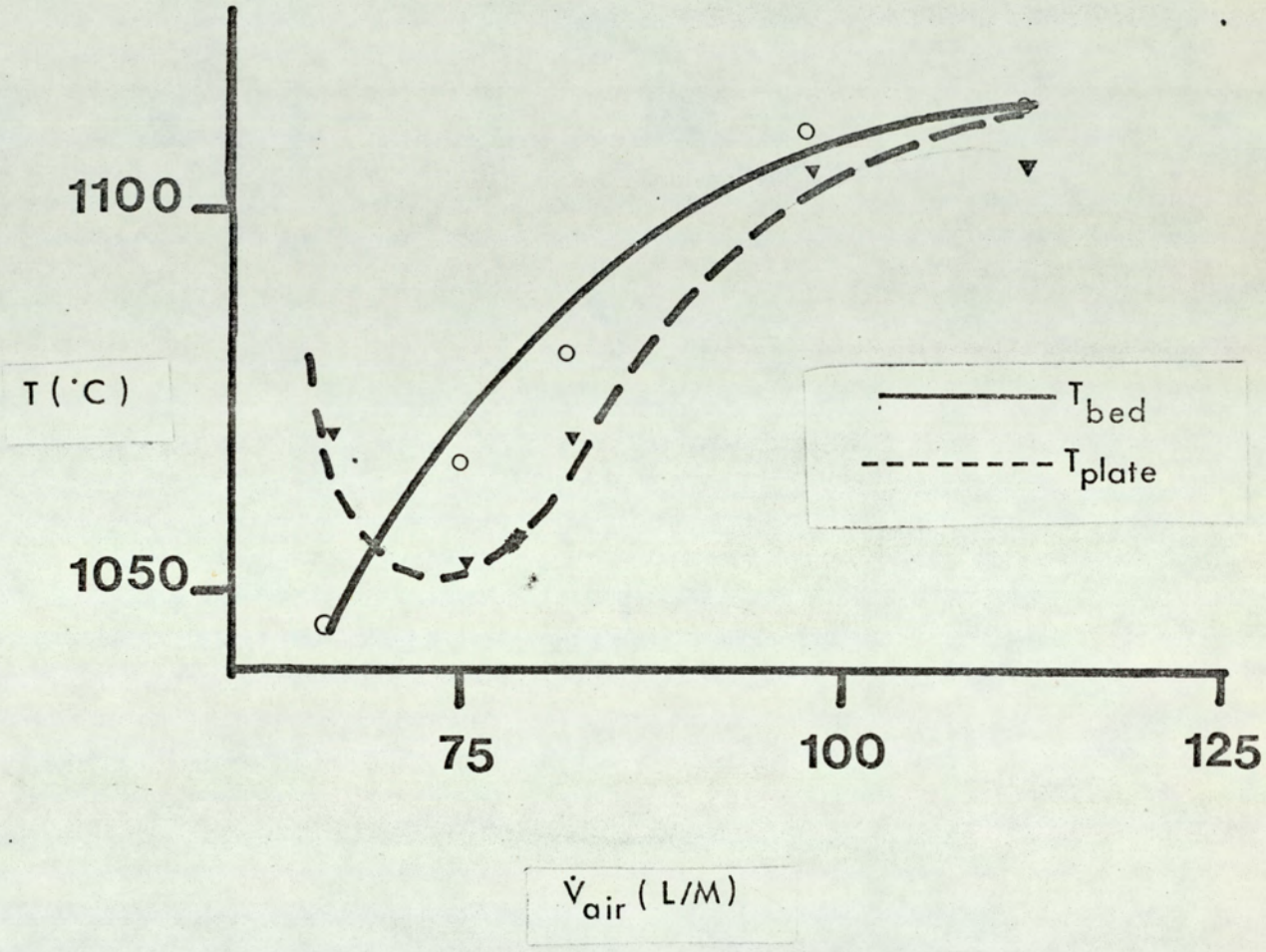

FIG.55

BED TEMPERATURES

SILICA DIOXIDE

(0·71— 0·85) m.m. dia

1·4 X STOICHIOMETRIC AIR

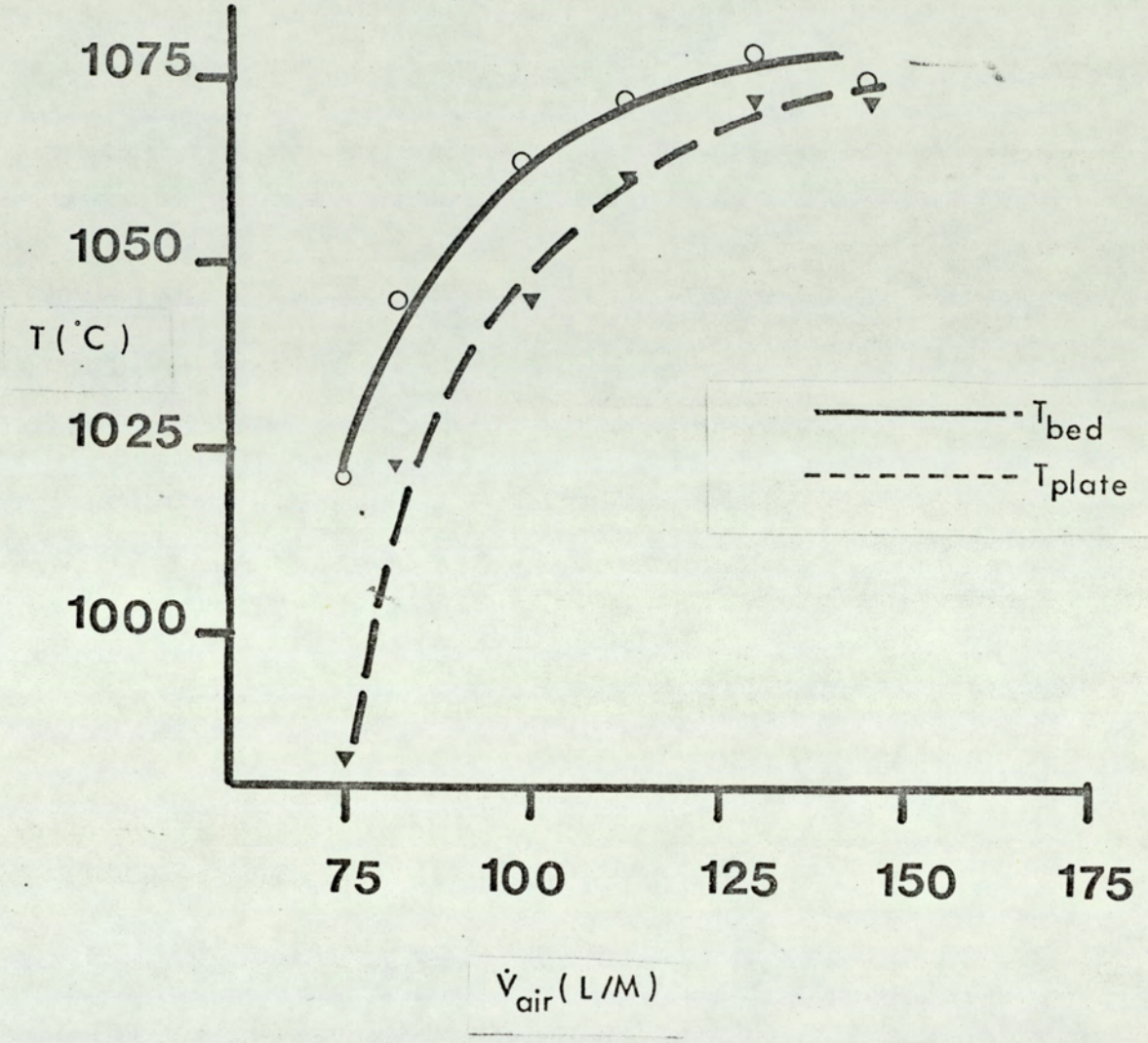

FIG. 56

BED TEMPERATURES

SILICA DIOXIDE

(0·71 — 0·85) m.m. dia

1·6 x STOICHIOMETRIC AIR

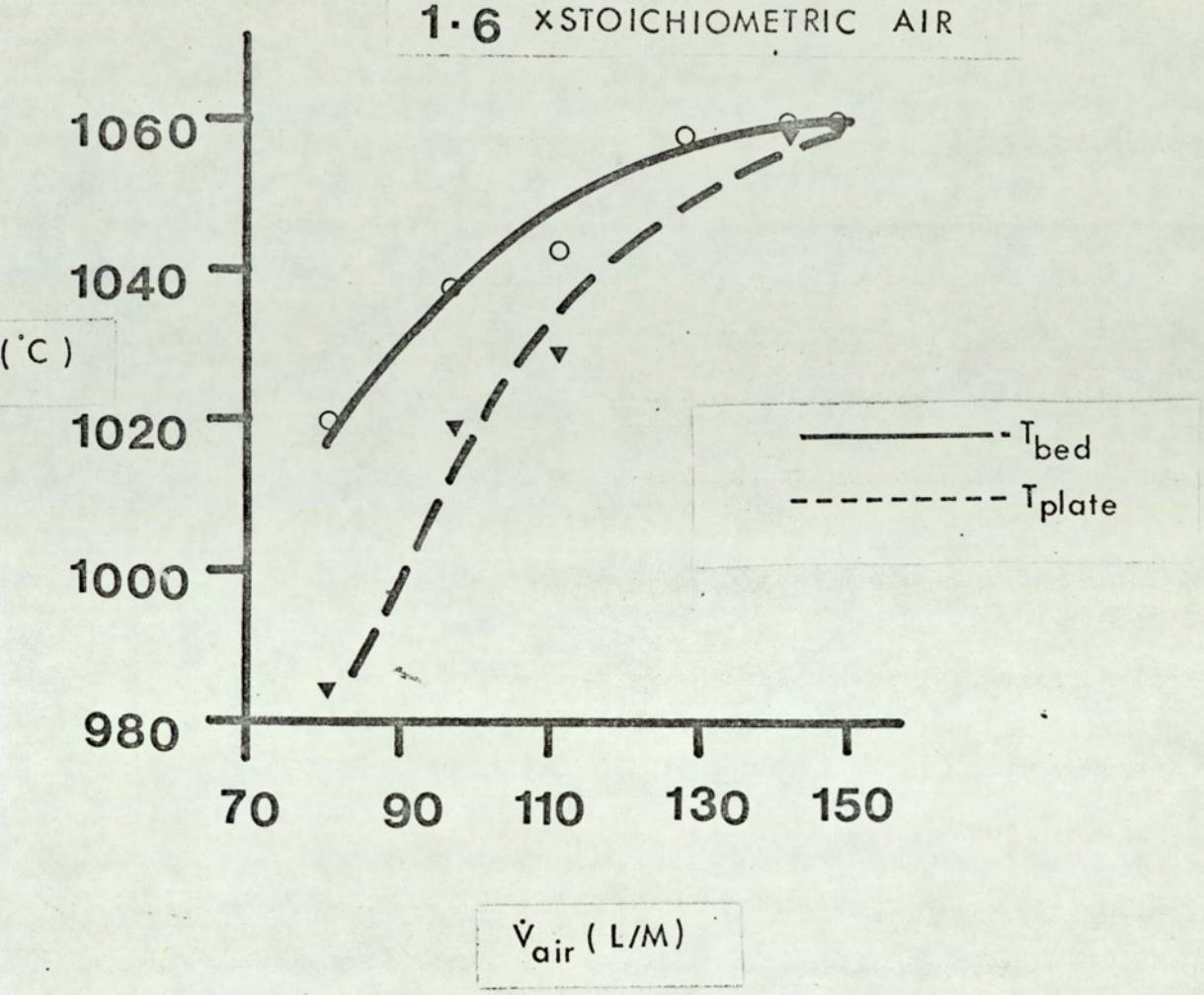

FIG.57

BED TEMPERATURES

SILICA DIOXIDE

(0·71 — 0·85) m.m. dia

1·8 x STOICHIOMETRIC AIR

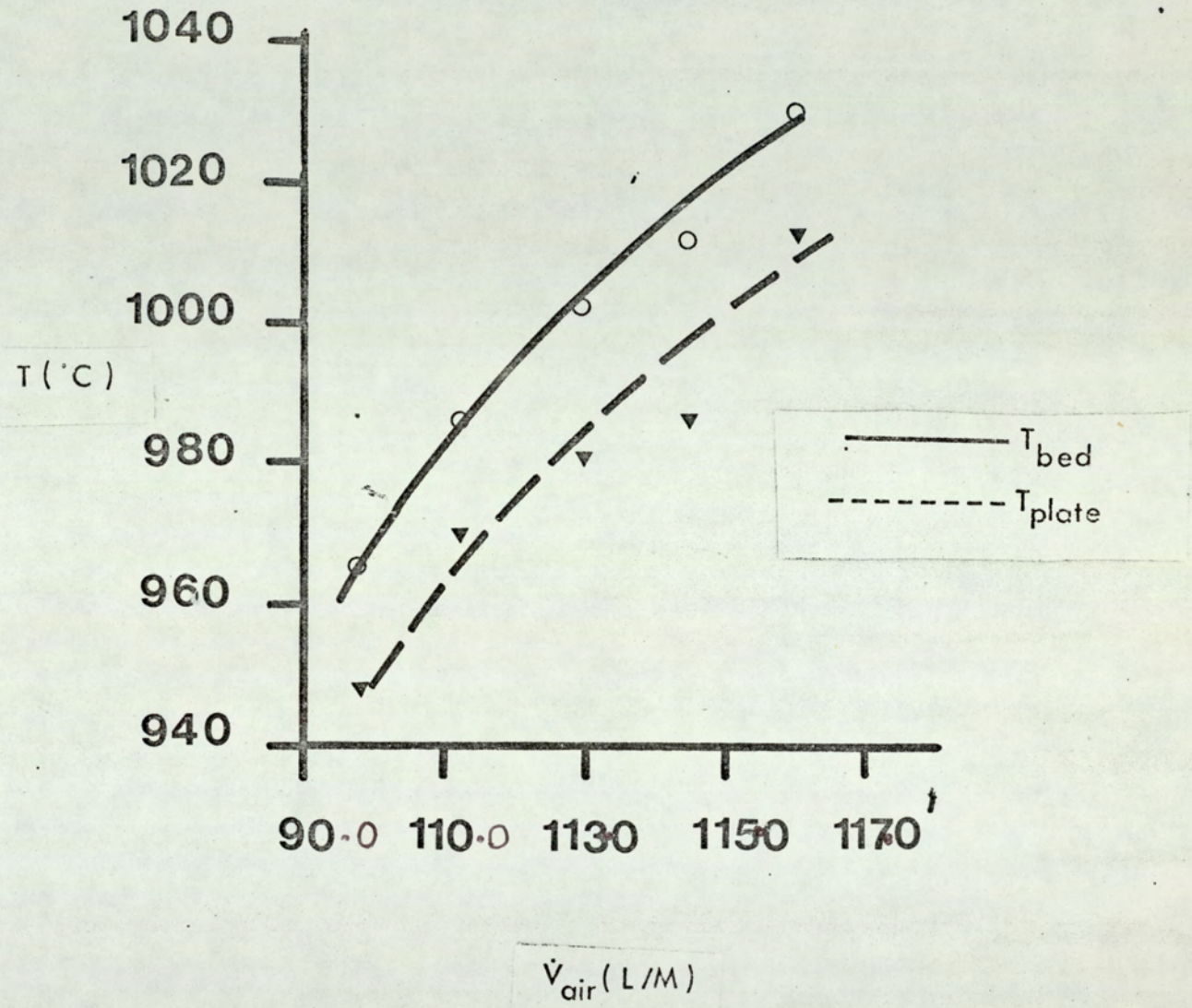

FIG. 58

BED TEMPERATURES

SILICA DIOXIDE

(0·71 — 0·85) m.m. dia

2·0 x STOICHIOMETRIC AIR

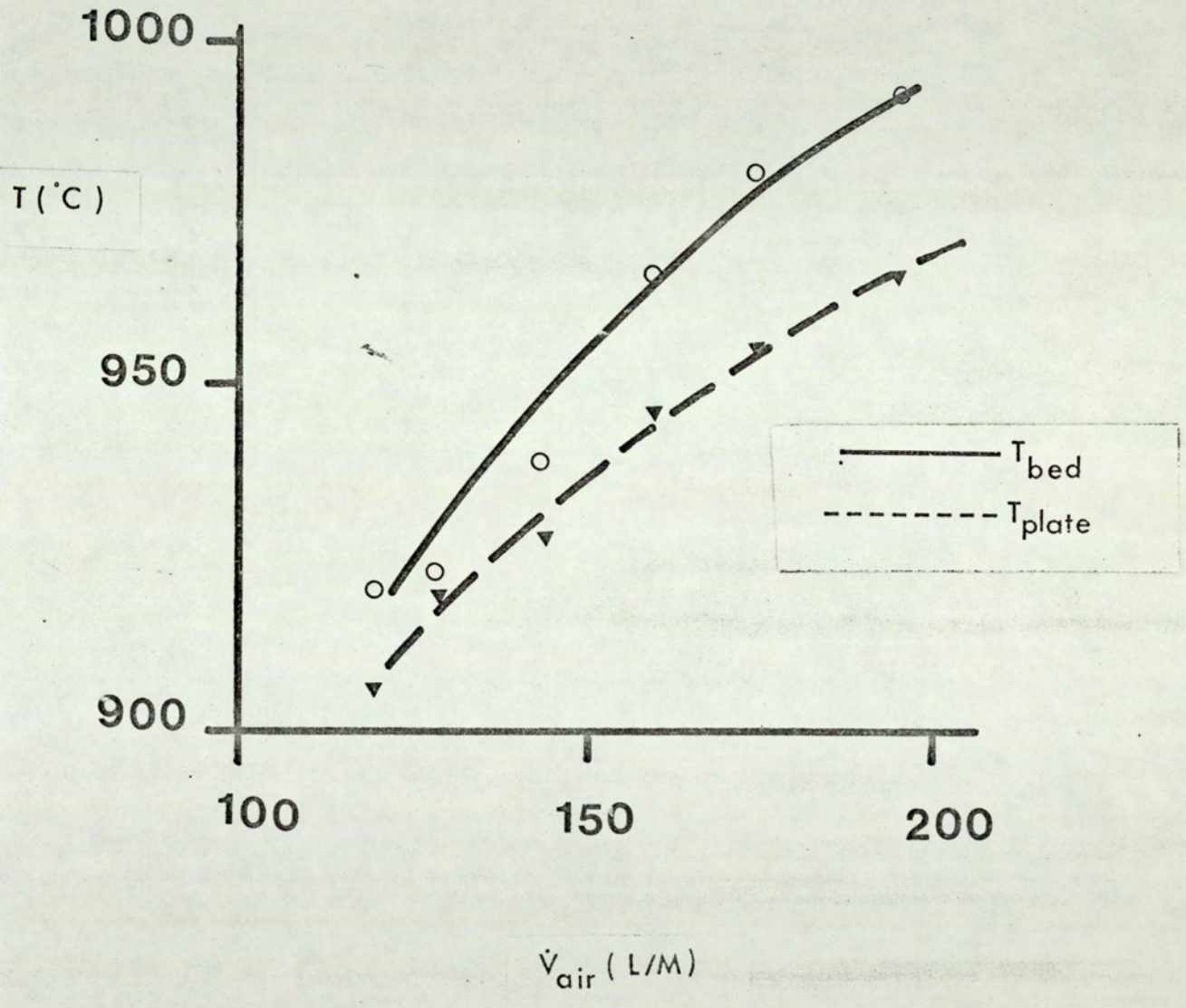

BED TEMPERATURES

FIG. 59

SILICA DIOXIDE

(0·71— 0·85)m.m. dia

2·1 x STOICHIOMETRIC AIR

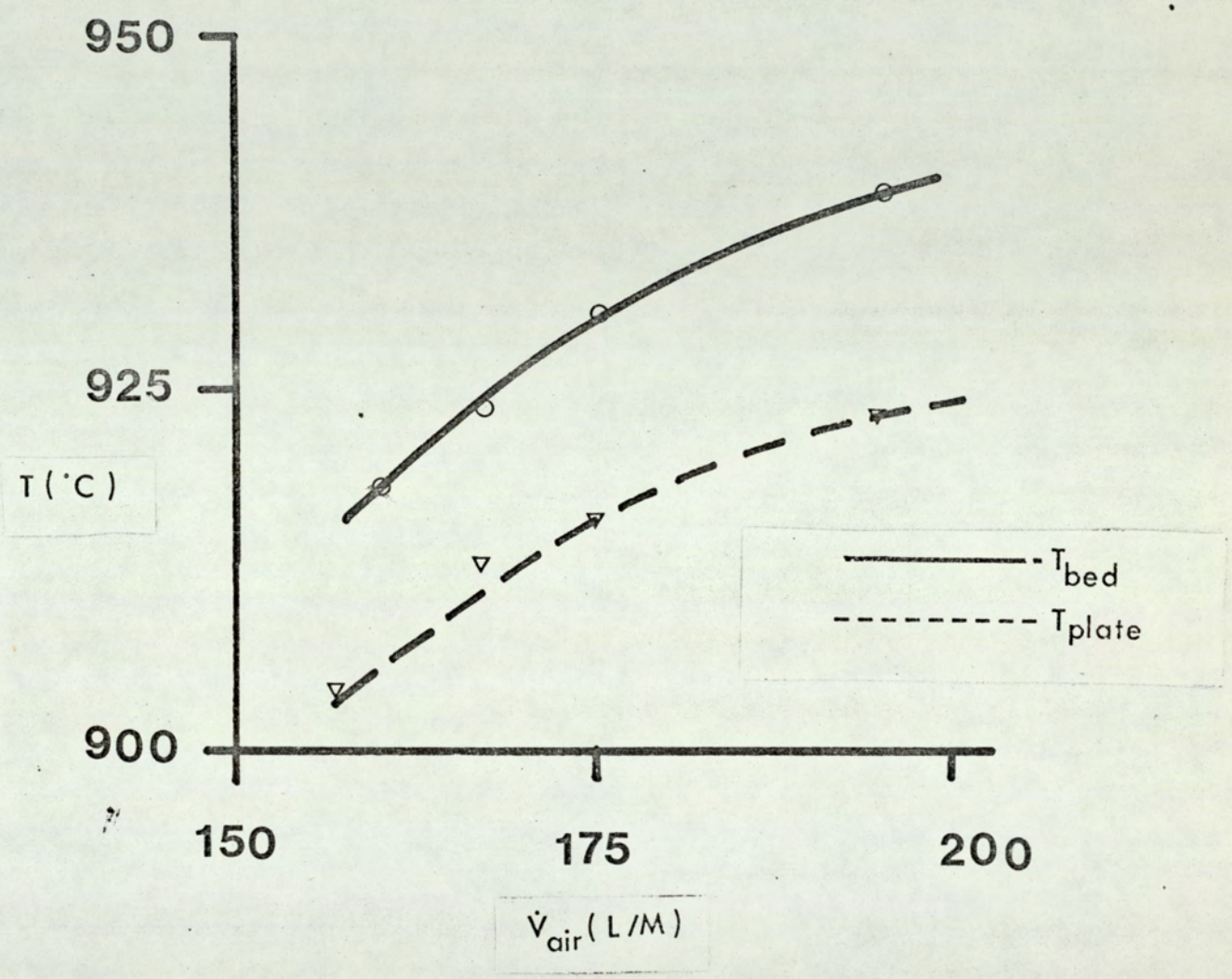

FIG.60

BED TEMPERATURES

SILICA DIOXIDE

(0·6 — 0·71)m.m. dia

1·0 x STOICHIOMETRIC AIR

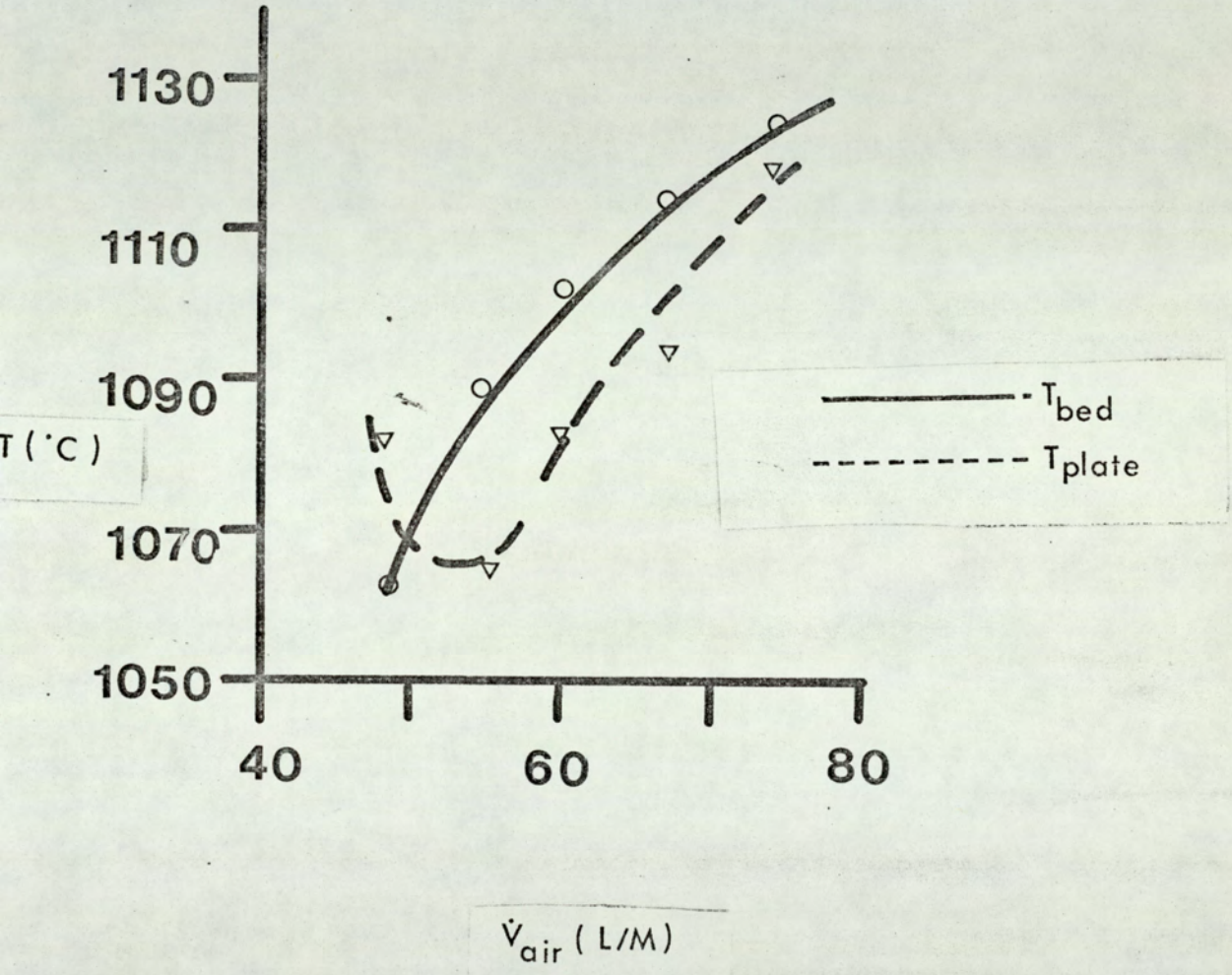

FIG. 61

BED TEMPERATURES

SILICA DIOXIDE

(0·6 – 0·71) m.m. dia

1·2 x STOICHIOMETRIC AIR

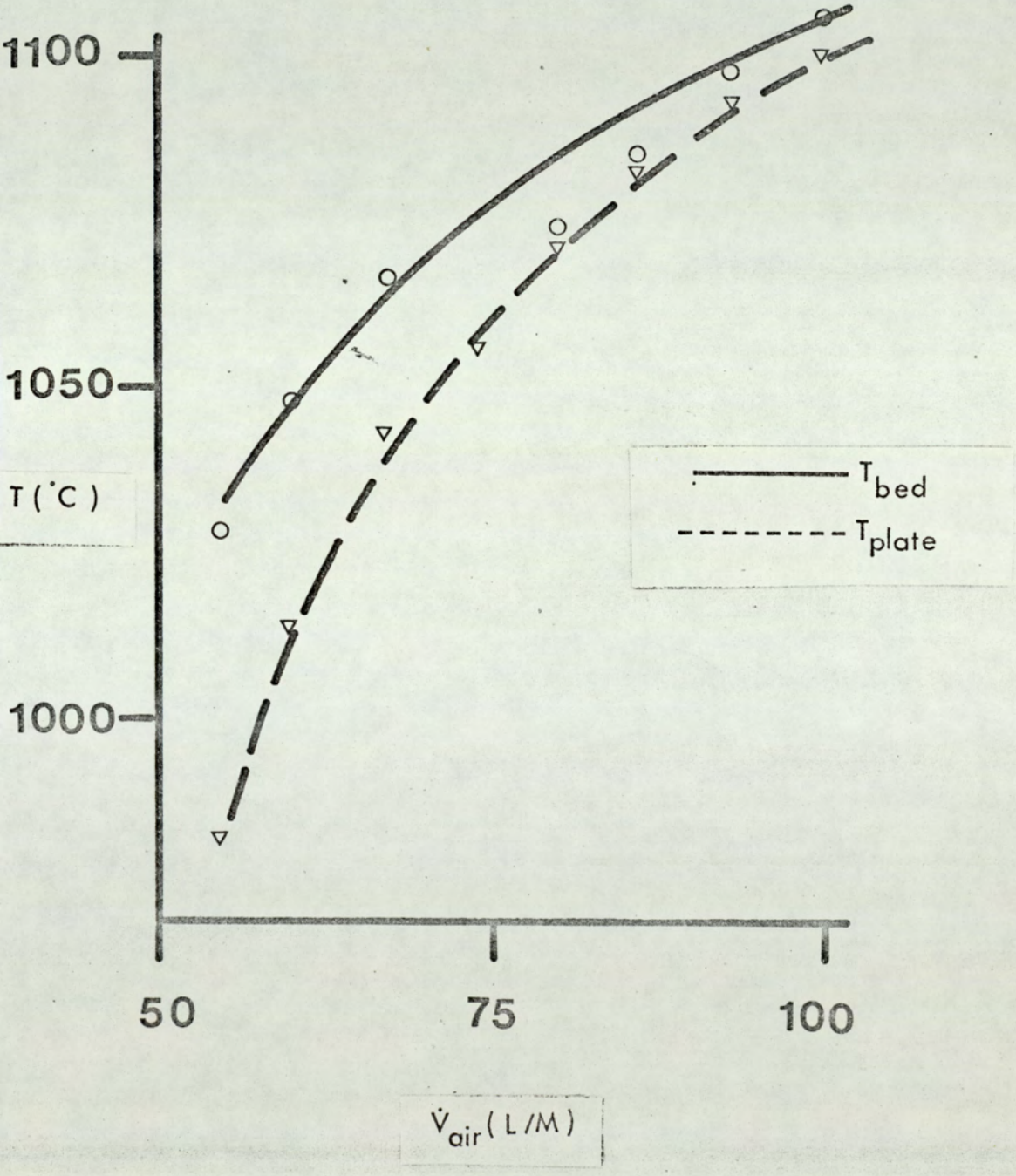

FIG. 62

BED TEMPERATURES

SILICA DIOXIDE

(0·6 — 0·71)m.m. dia

1·4 x STOICHIOMETRIC AIR

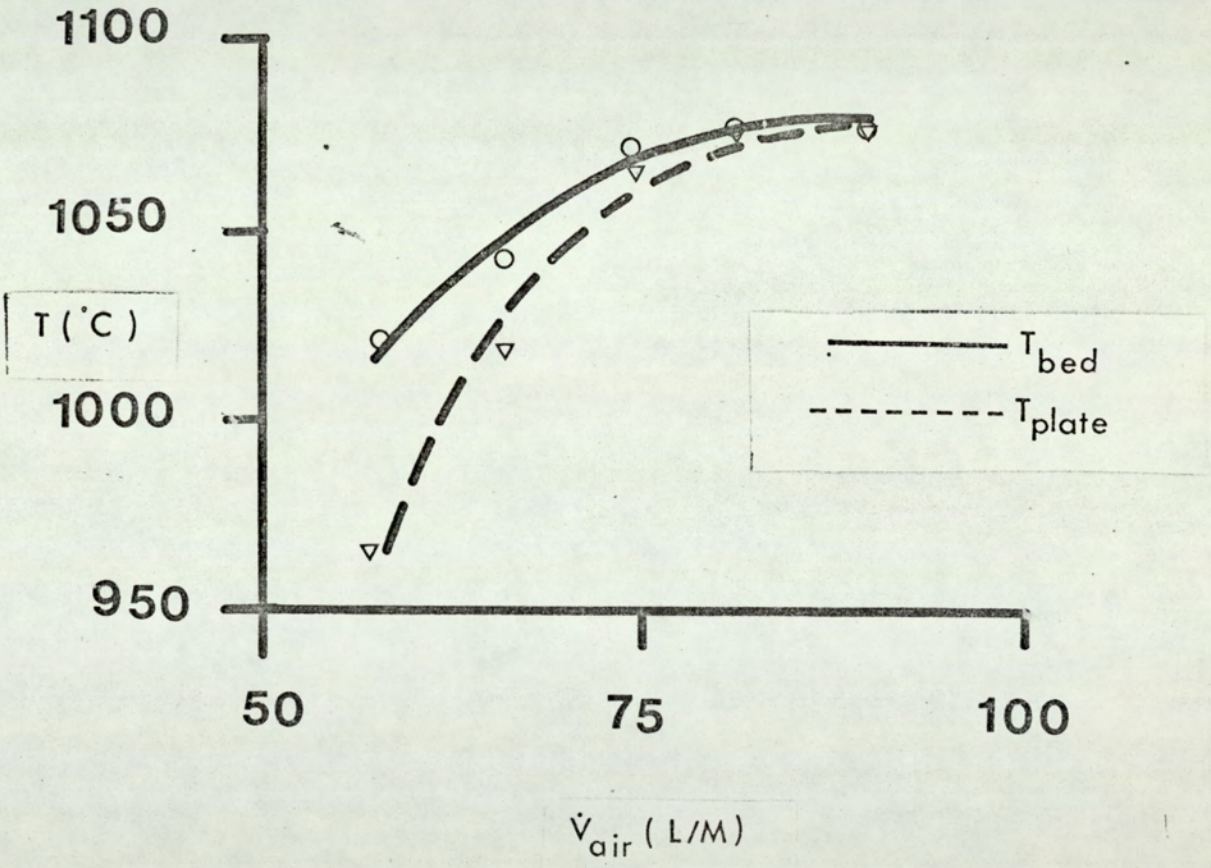

FIG. 63

BED TEMPERATURES

SILICA DIOXIDE

(0·6 — 0·71) m.m. dia

1·6 x STOICHIOMETRIC AIR

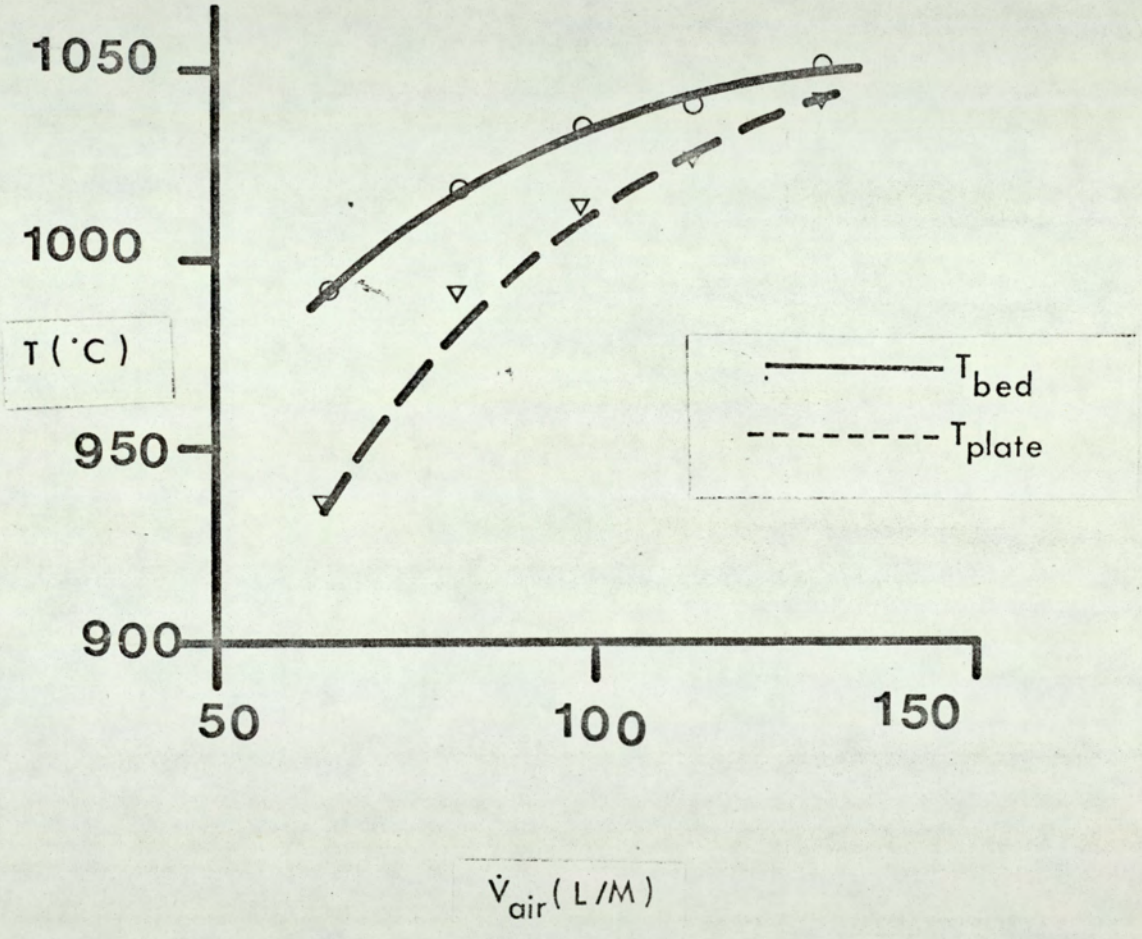

FIG.64

BED TEMPERATURES

SILICA DIOXIDE

(0·6 — 0·71) m.m. dia

1·8 x STOICHIOMETRIC AIR

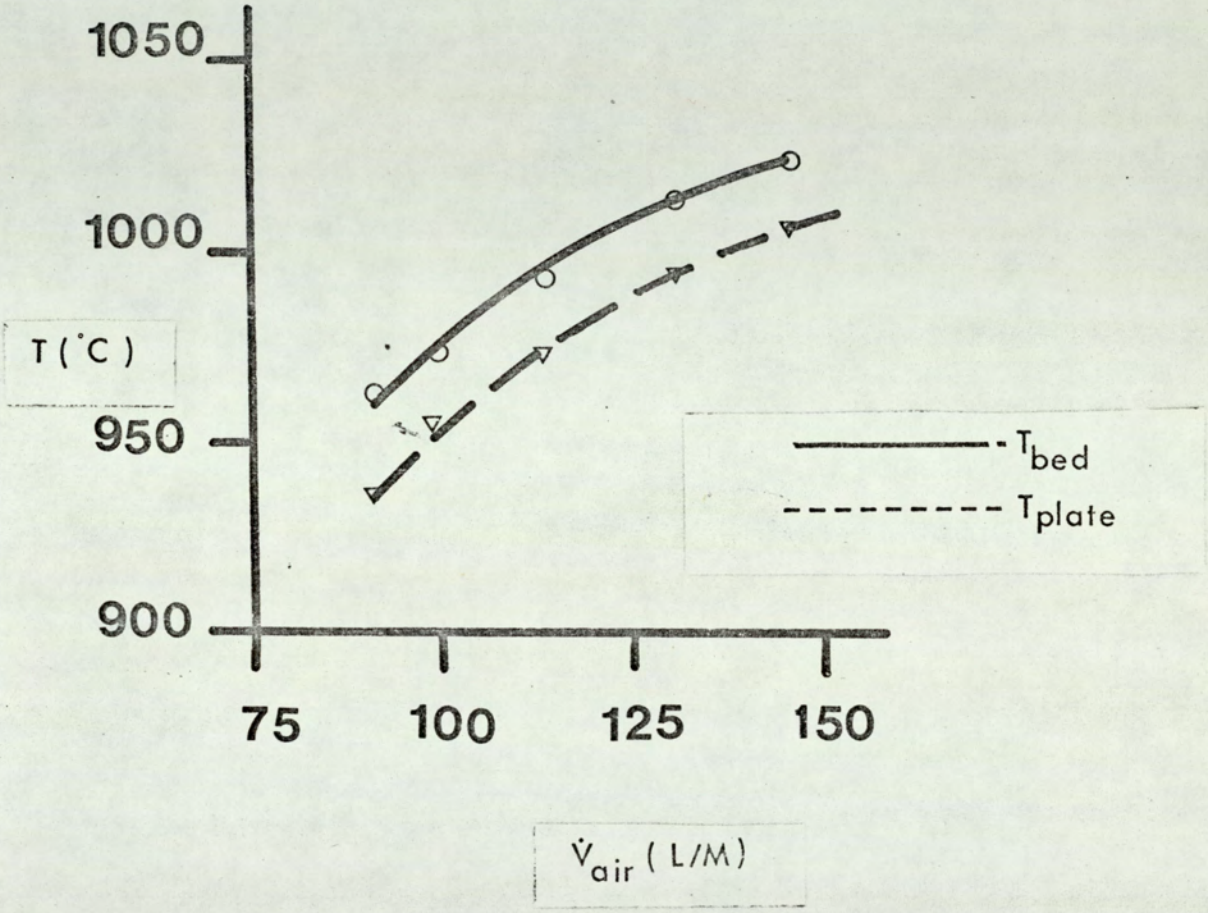

BED TEMPERATURES

SILICA DIOXIDE

(0·6 — 0·71) m.m. dia

2·0 x STOICHIOMETRIC AIR

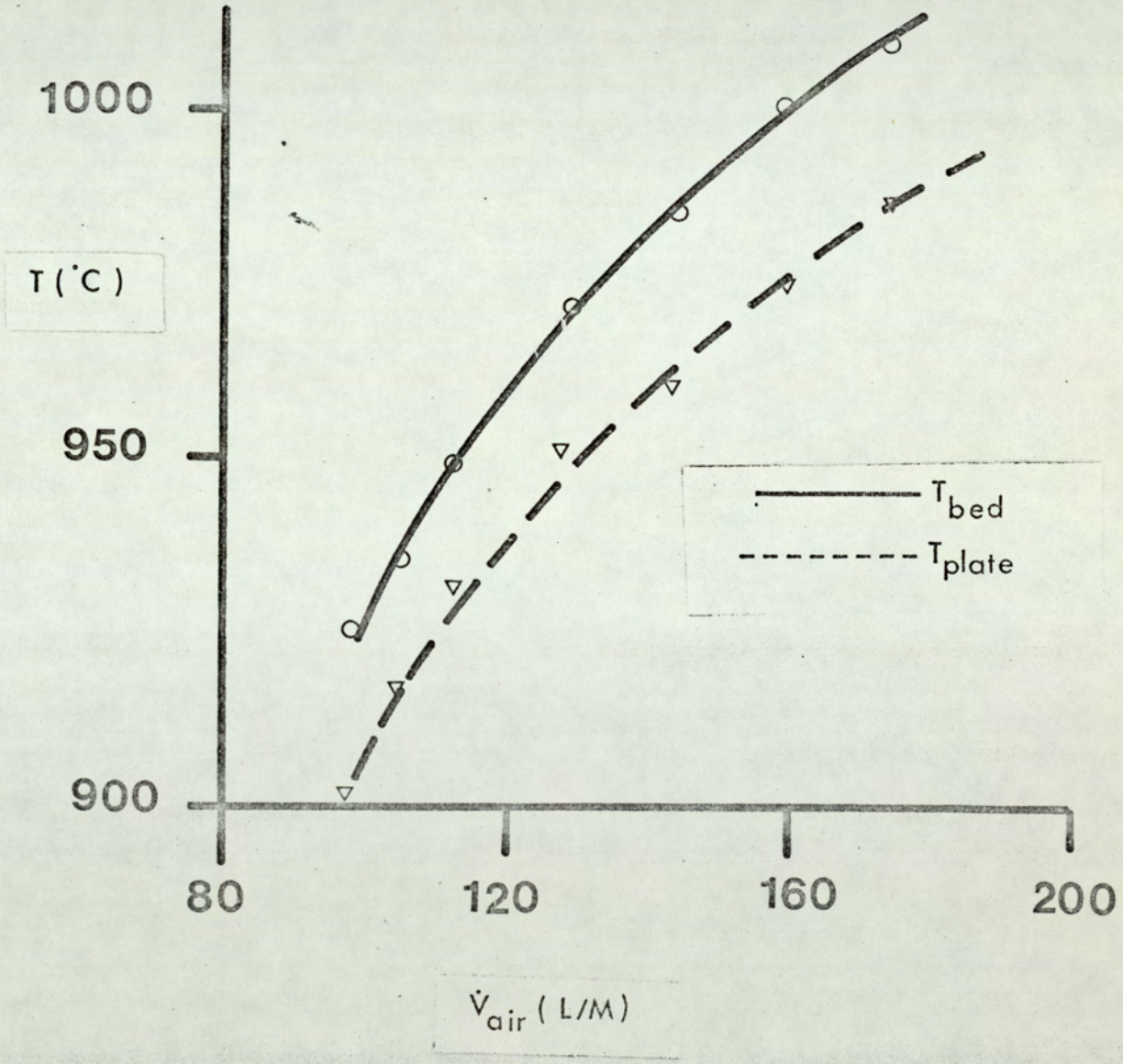

FIG. 66

BED TEMPERATURES
SILICA DIOXIDE
(0·6 – 0·71) m.m. dia
2·1 x STOICHIOMETRIC AIR

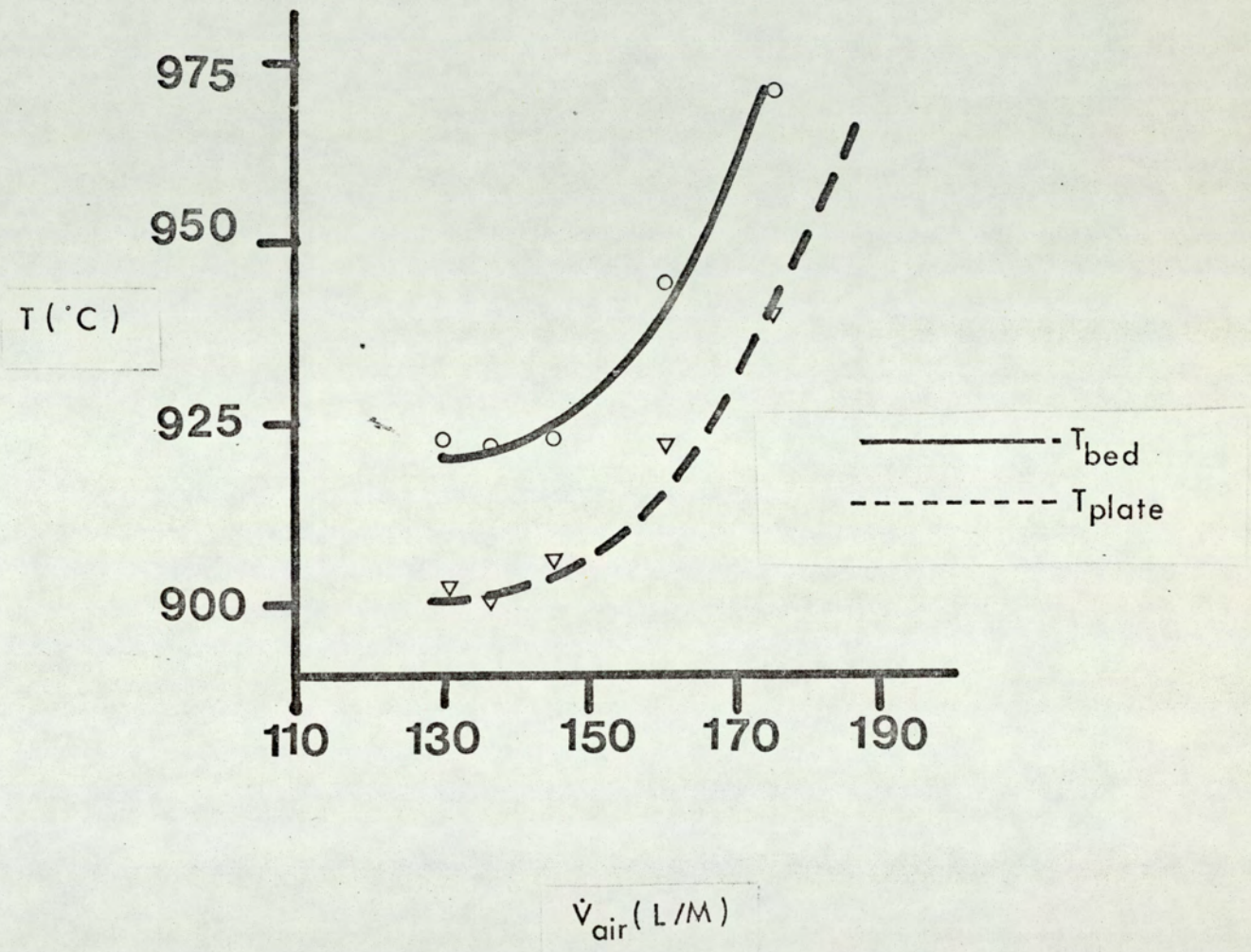

FIG.67

COMARISON OF BED HEIGHTS

ZIRCONIUM SILICATE

(0·6 — 0·71)m.m. dia

1·8 XSTOICHIOMETRIC AIR

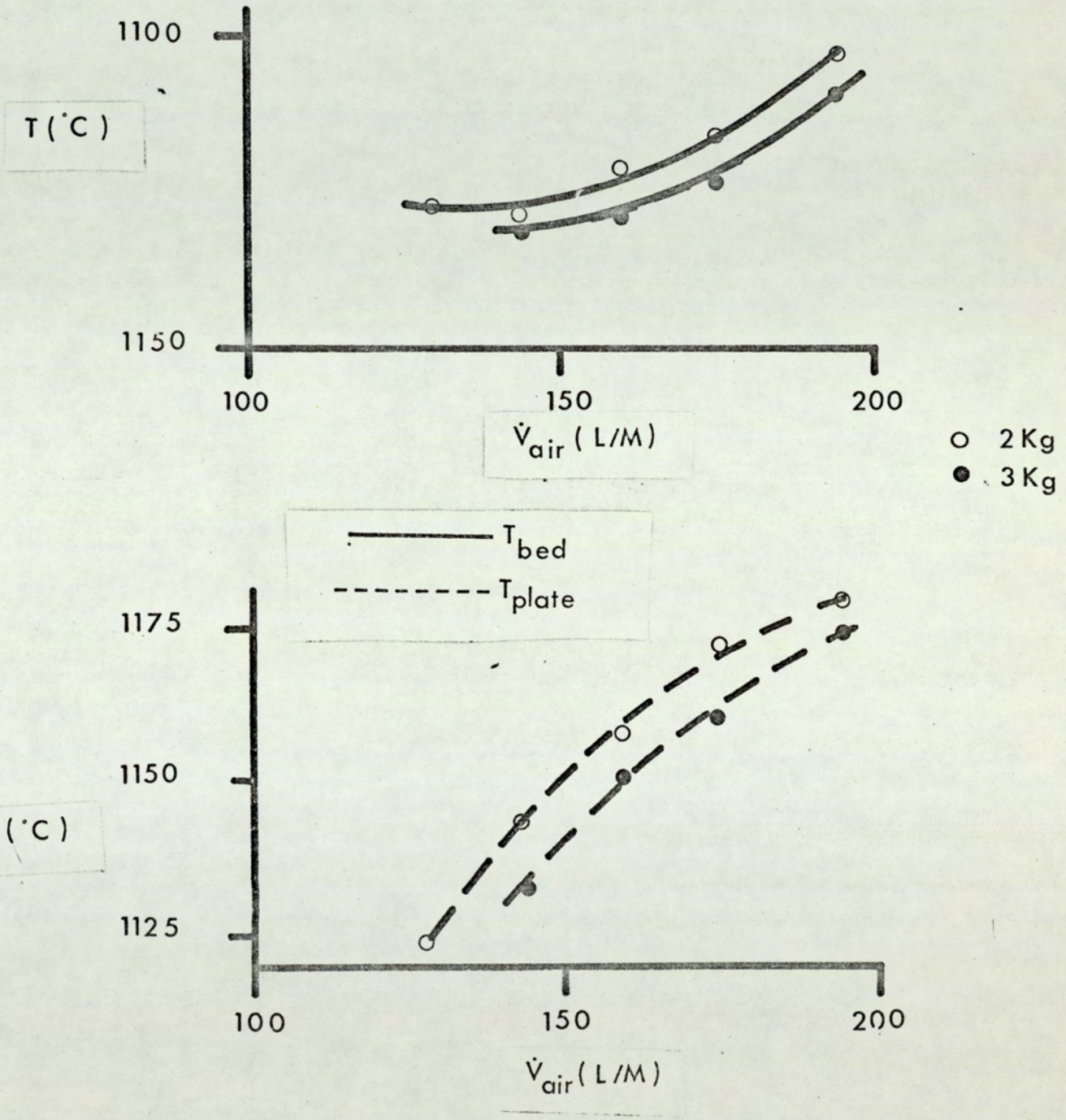

FIG. 68

COMPARISON OF DISTRIBUTOR PLATES

ZIRCONIUM SILICATE

(1·0 — 1·4) m.m.

1·8 x STOICHIOMETRIC AIR

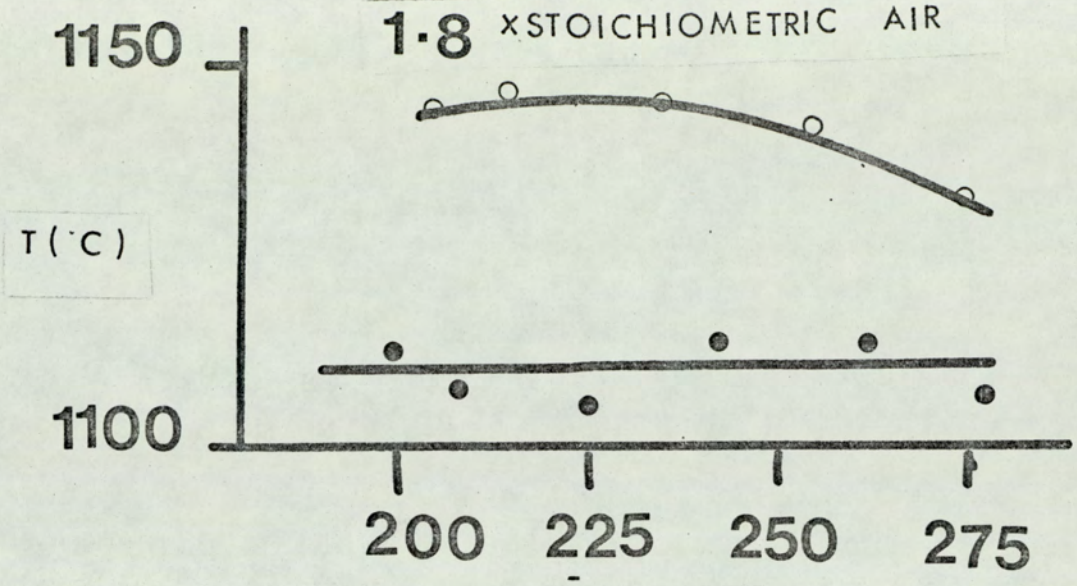

○ REFRACTORY
● MILD STEEL

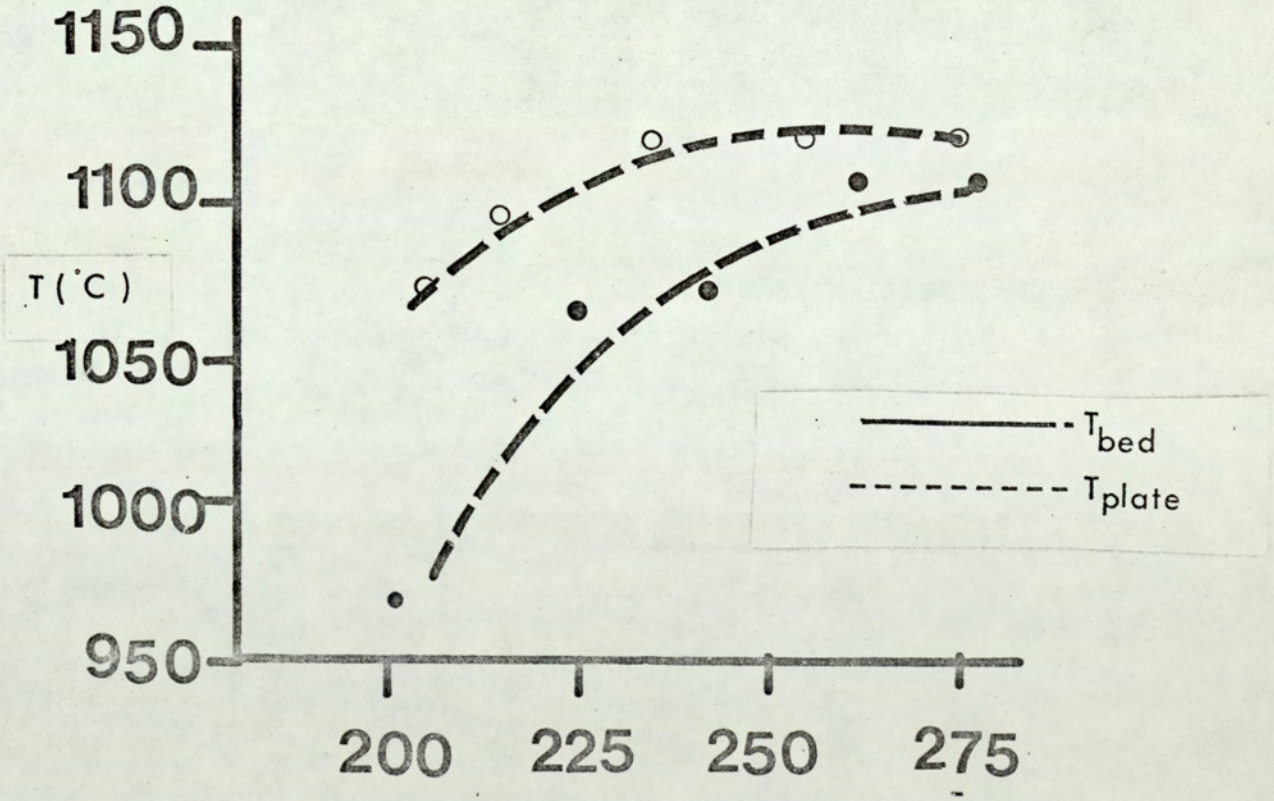

FIG. 69

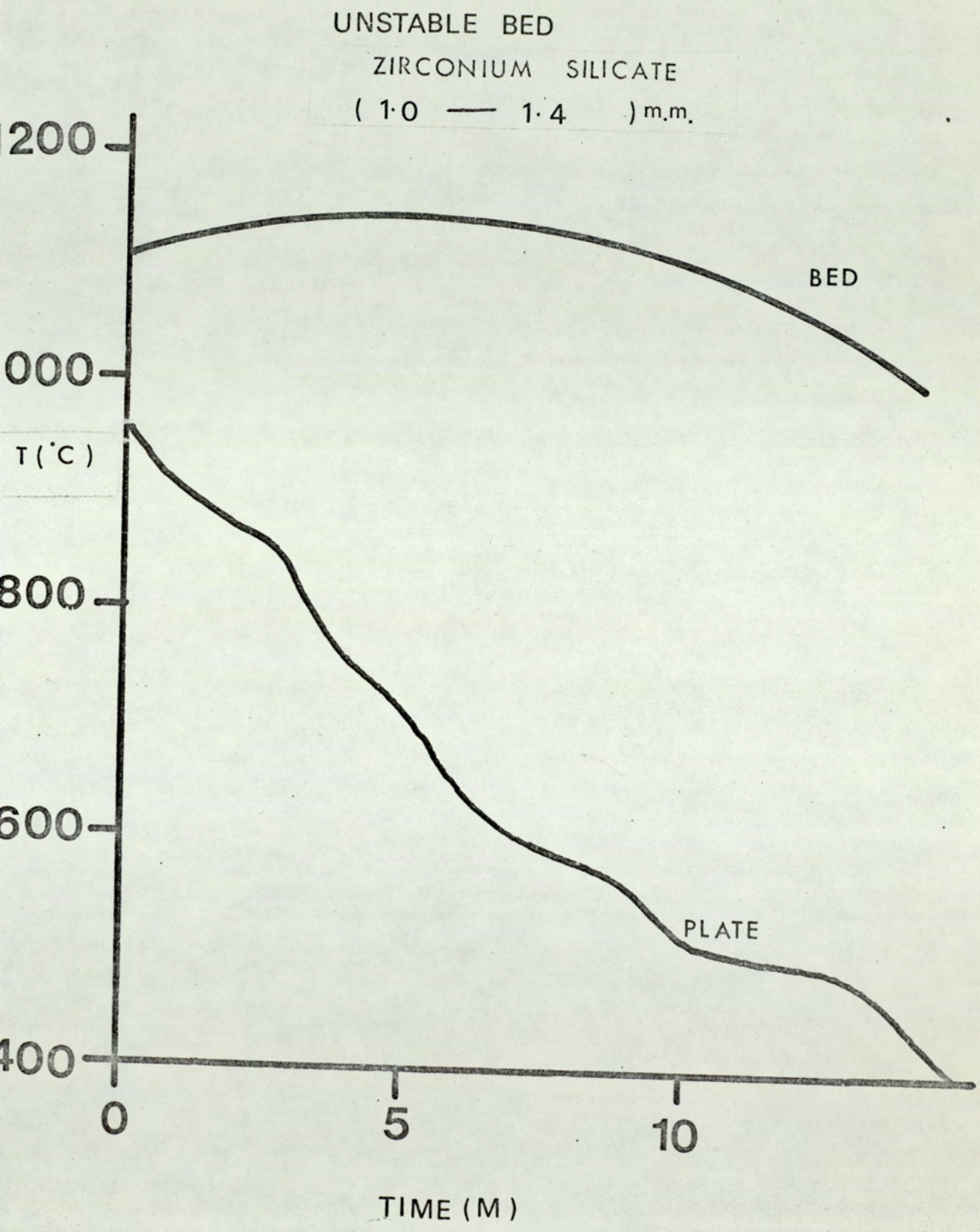
UNSTABLE BED
ZIRCONIUM SILICATE
(1·0 — 1·4) m.m.
1200
000
T(°C)
800
600
400
BED
PLATE
0
5
10
TIME (M)

FIG. 70

STABILITY LIMITS
SILICA DIOXIDE
(0·71 — 0·85)m.m. dia

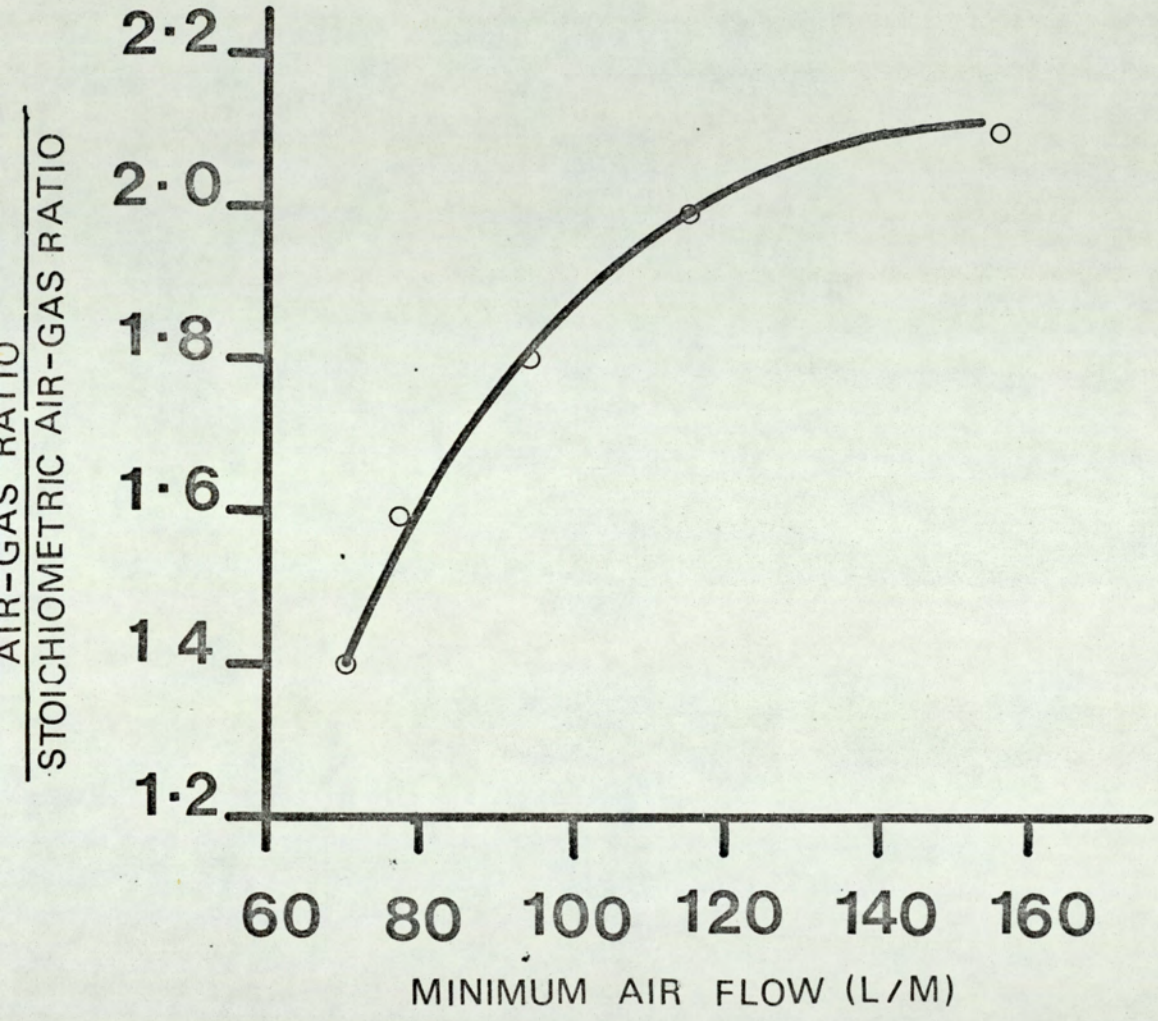

FIG. 71

STABILITY LIMITS
SILICA DIOXIDE
(0·6 — 0·71)m.m. dia

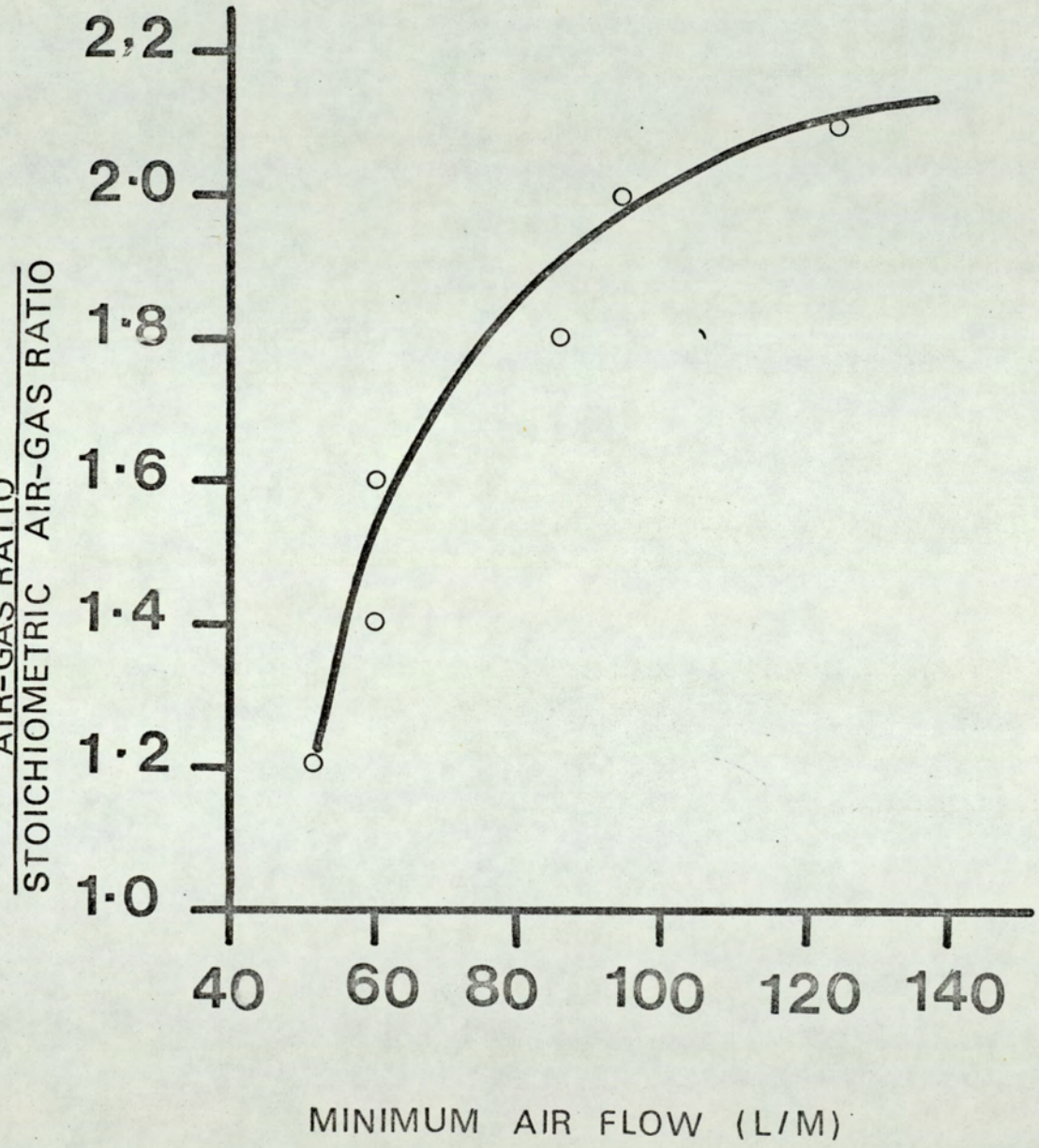

FIG. 72

COMPARISON OF STABILITY LIMITS

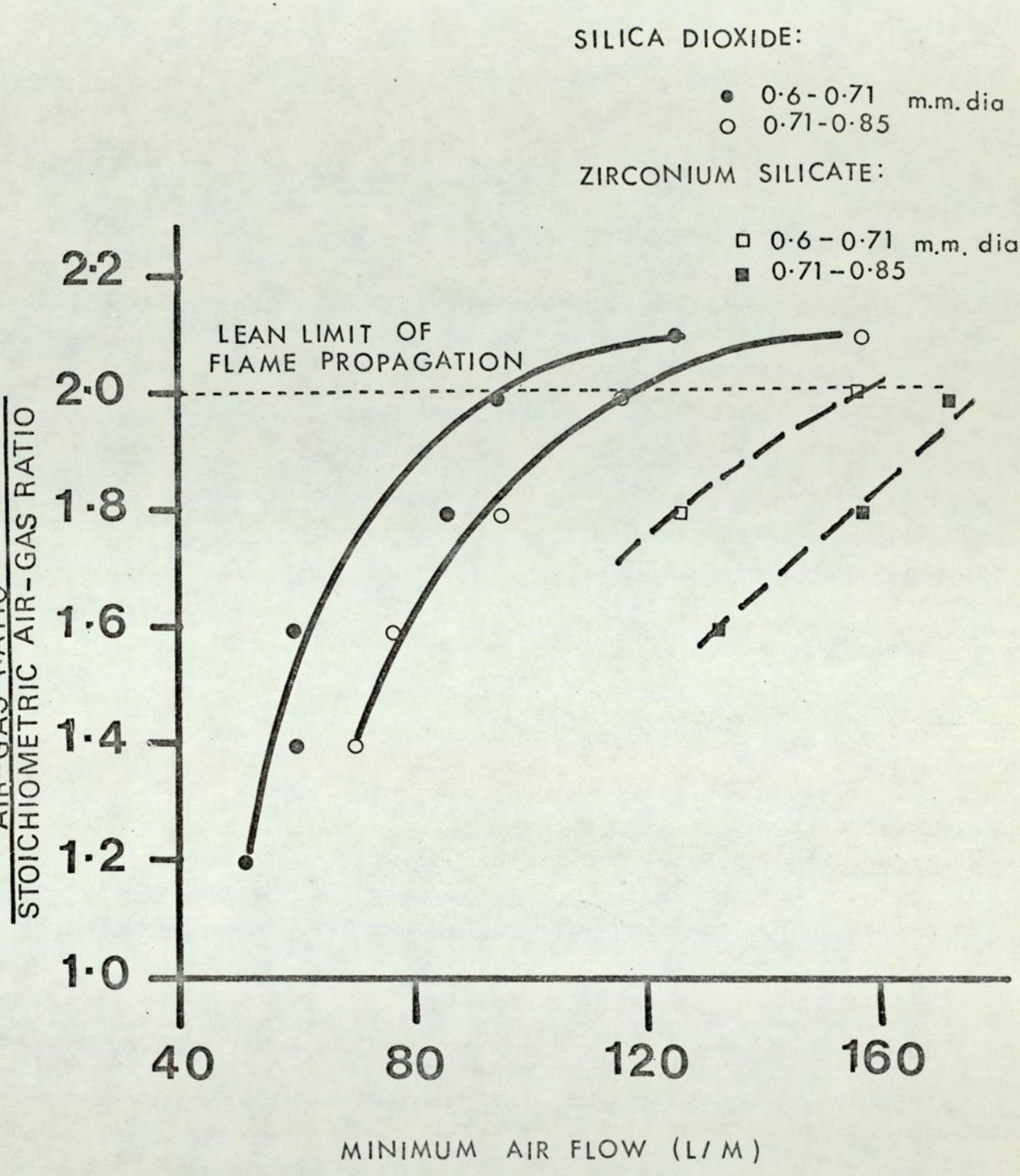

TEMPERATURE PROFILE

FIG. 73

ZIRCONIA SILICATE
(1·0 – 1·4) m.m. dia
$\dot{V}_{air}$ = 150 L/M
$\dot{V}_{gas}$ = 12

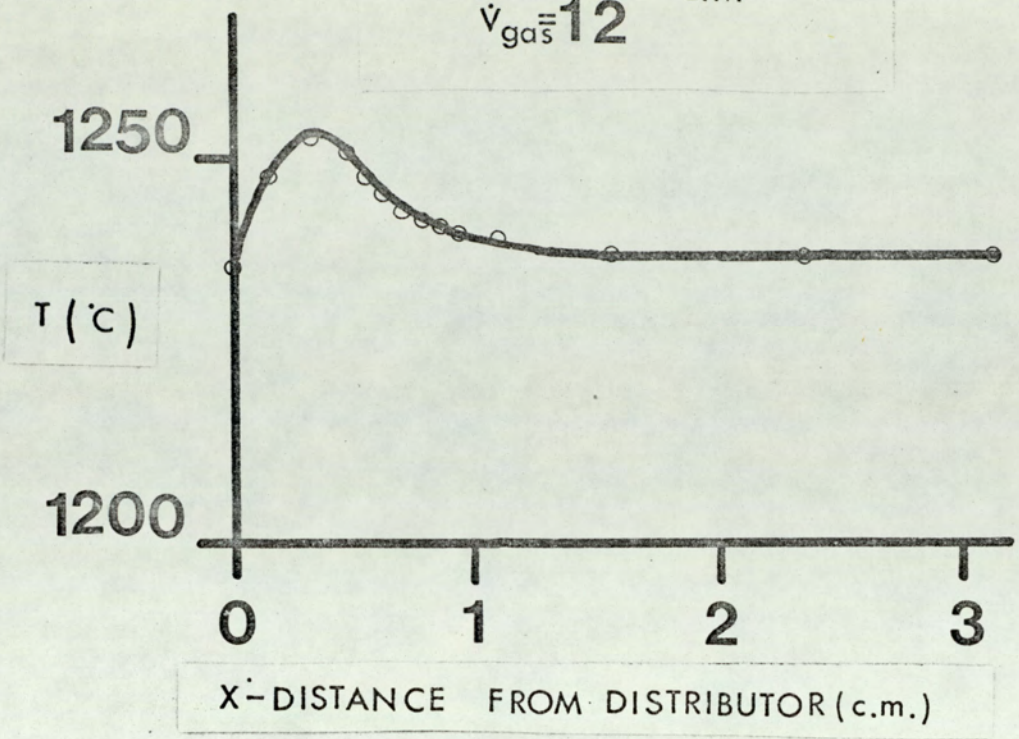

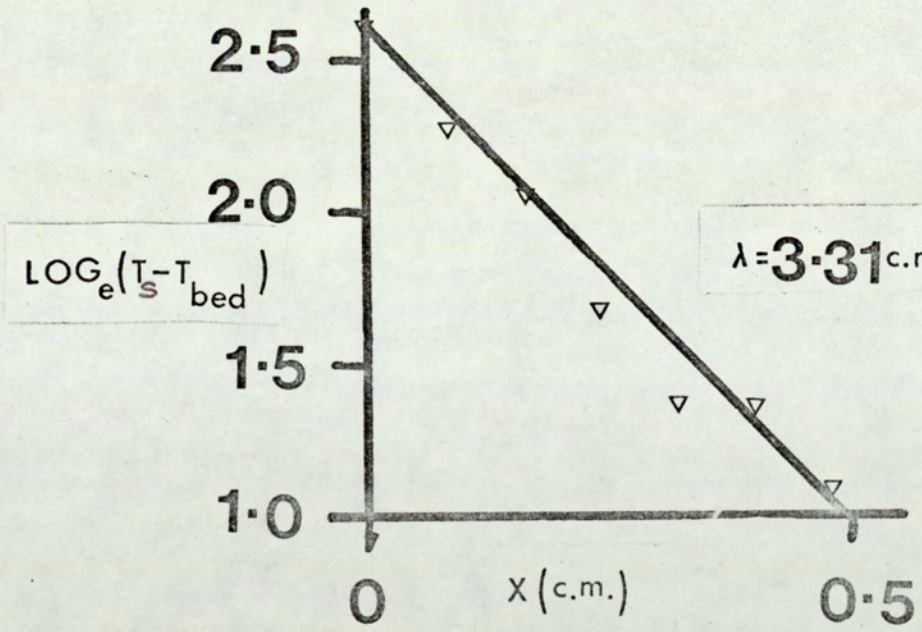

FIG. 74

TEMPERATURE PROFILE

ZIRCONIA SILICATE

(1·0 – 1·4) m.m. dia

$\dot{V}_{air}$ = 185 L/M

$\dot{V}_{gas}$ = 11·25

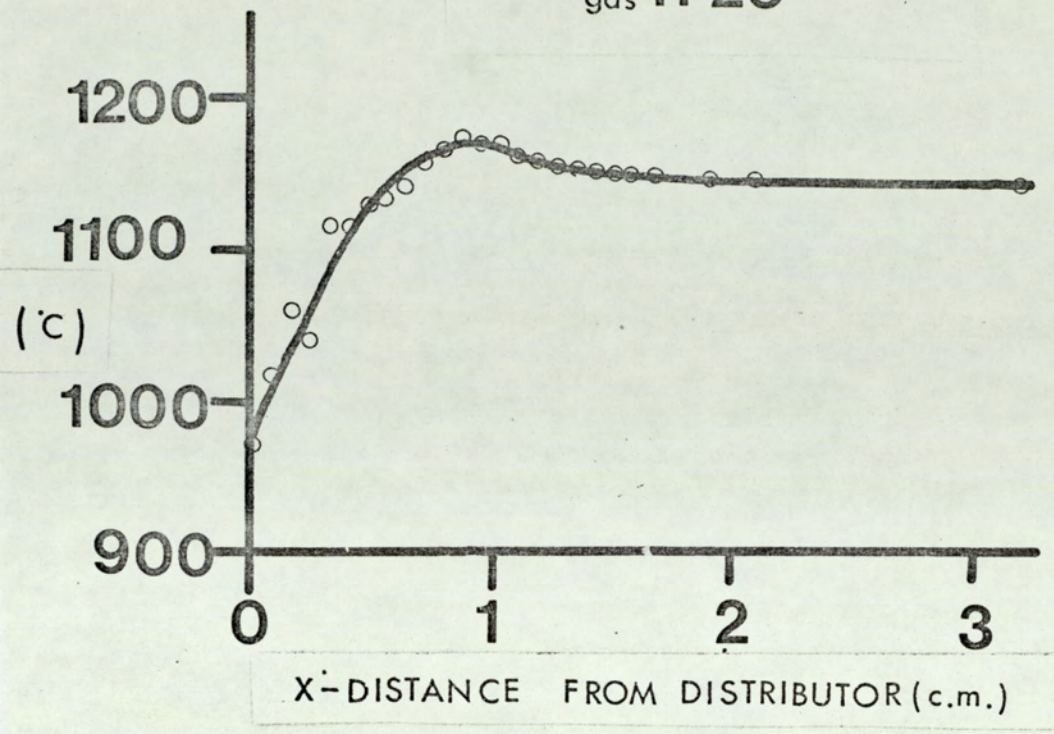

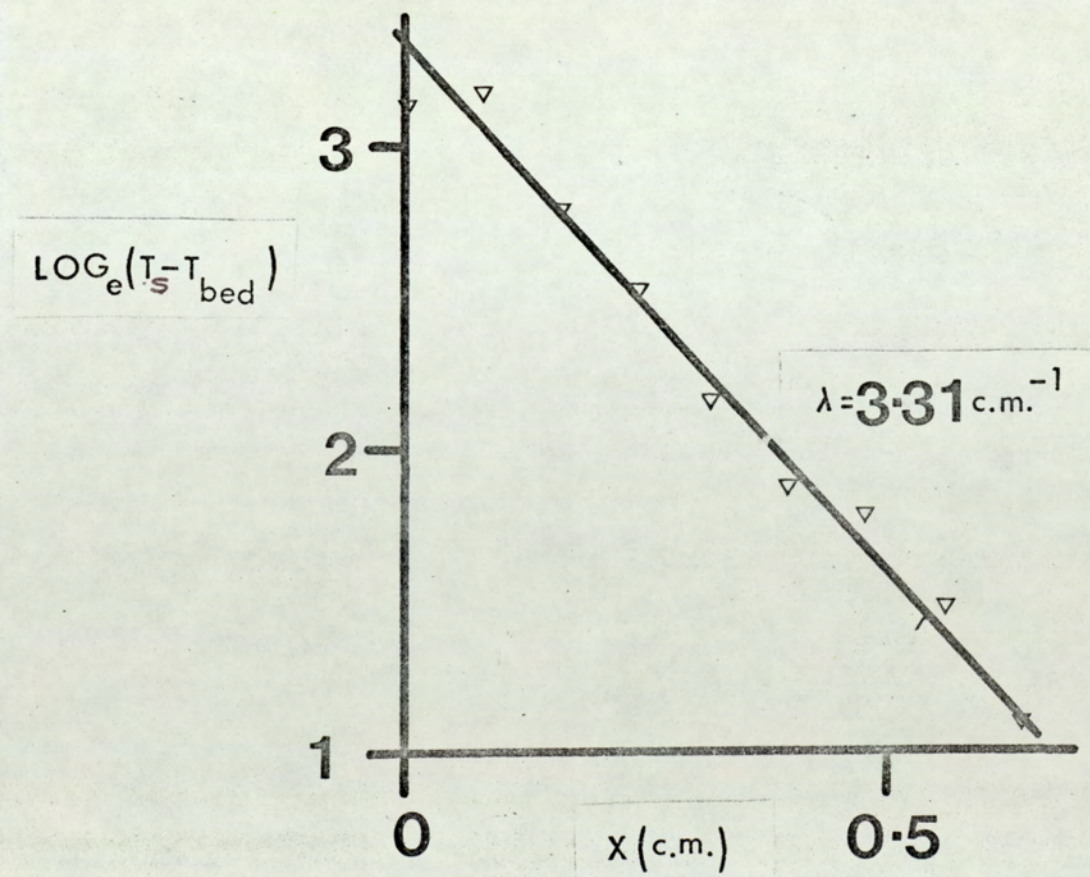

FIG.75

TEMPERATURE PROFILE

ZIRCONIA SILICATE
(1·0 – 1·4) m.m. dia

$\dot{V}_{air}$ = 193 L/M

$\dot{V}_{gas}$ = 12·5

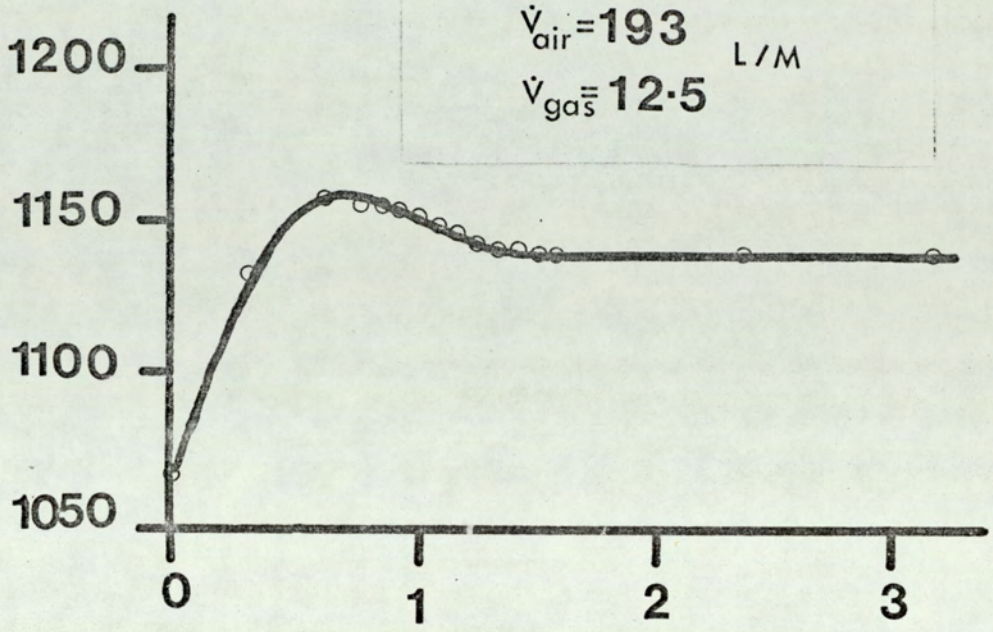

(°C)

X – DISTANCE FROM DISTRIBUTOR (c.m.)

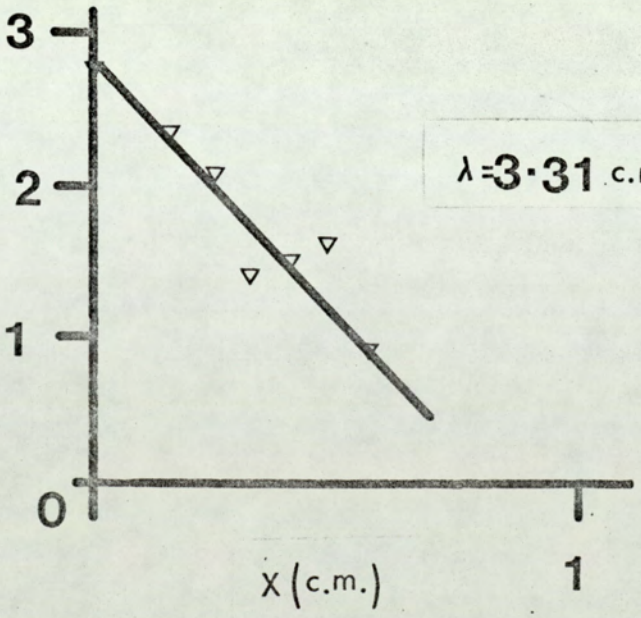

$\lambda = 3·31$ c.m.$^{-1}$

$G_e(T_s - T_{bed})$

FIG. 76

TEMPERATURE PROFILE

ZIRCONIA SILICATE
(1·0 – 1·4) m.m. dia

$\dot{V}_{air} = 193$ L/M

$\dot{V}_{gas} = 11·7$

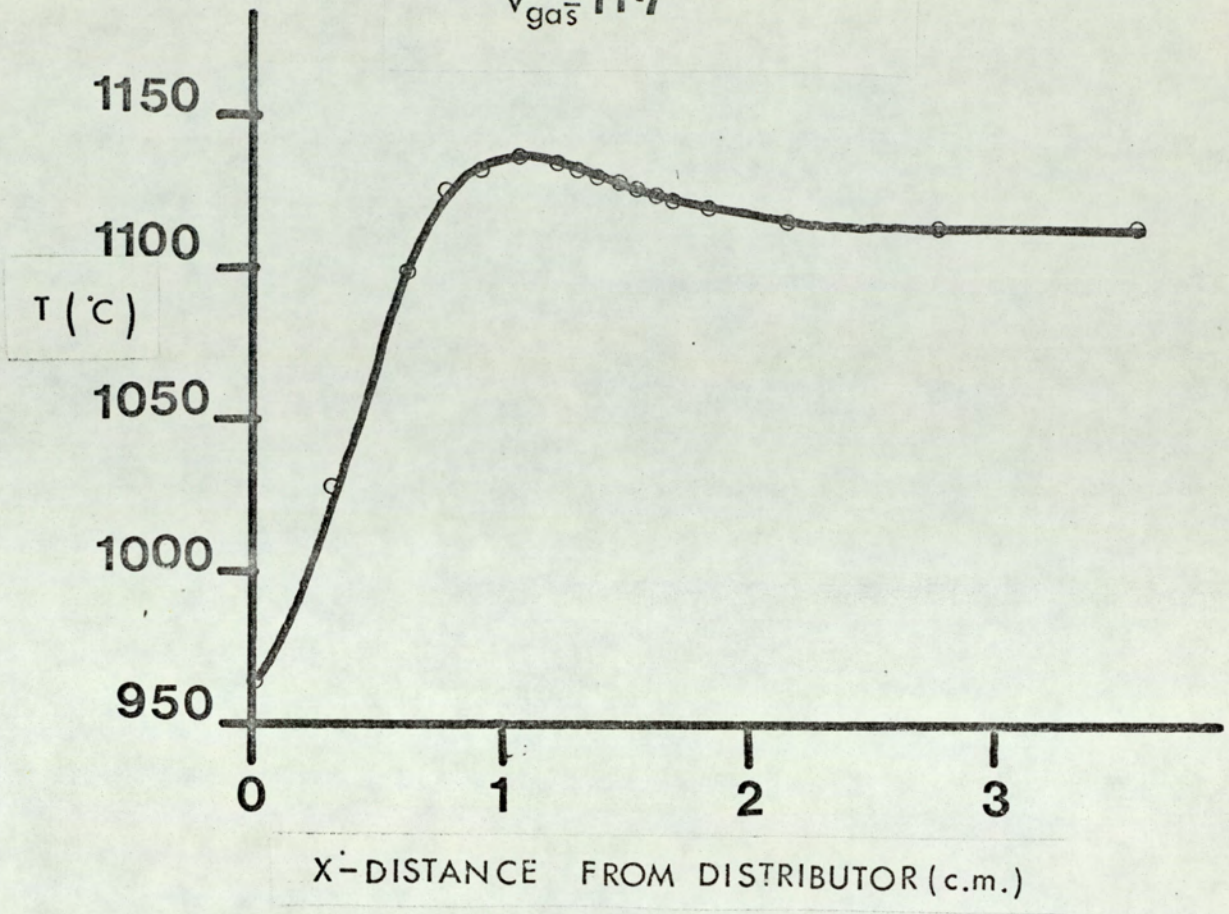

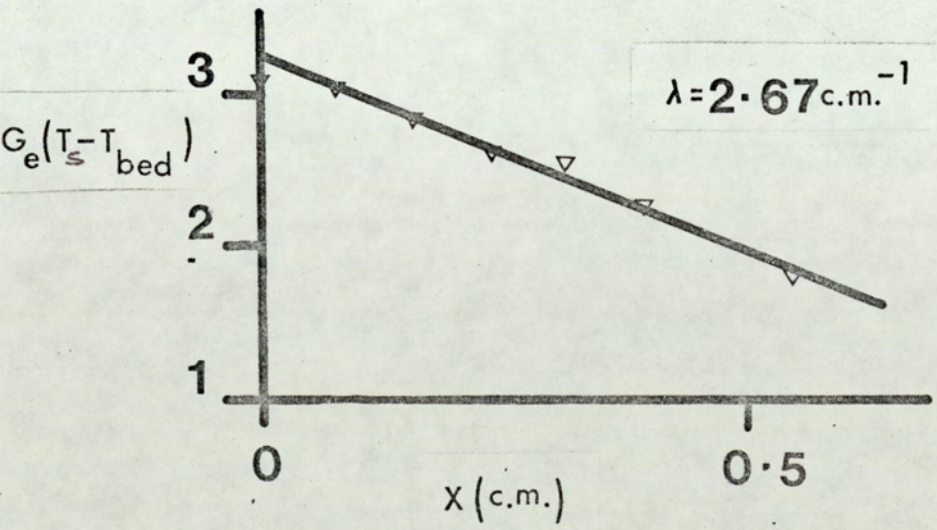

FIG. 77

TEMPERATURE PROFILE

ZIRCONIA SILICATE
(1·0 – 1·4) m.m. dia

$\dot{V}_{air}$ = 168 L/M

$\dot{V}_{gas}$ = 9·75

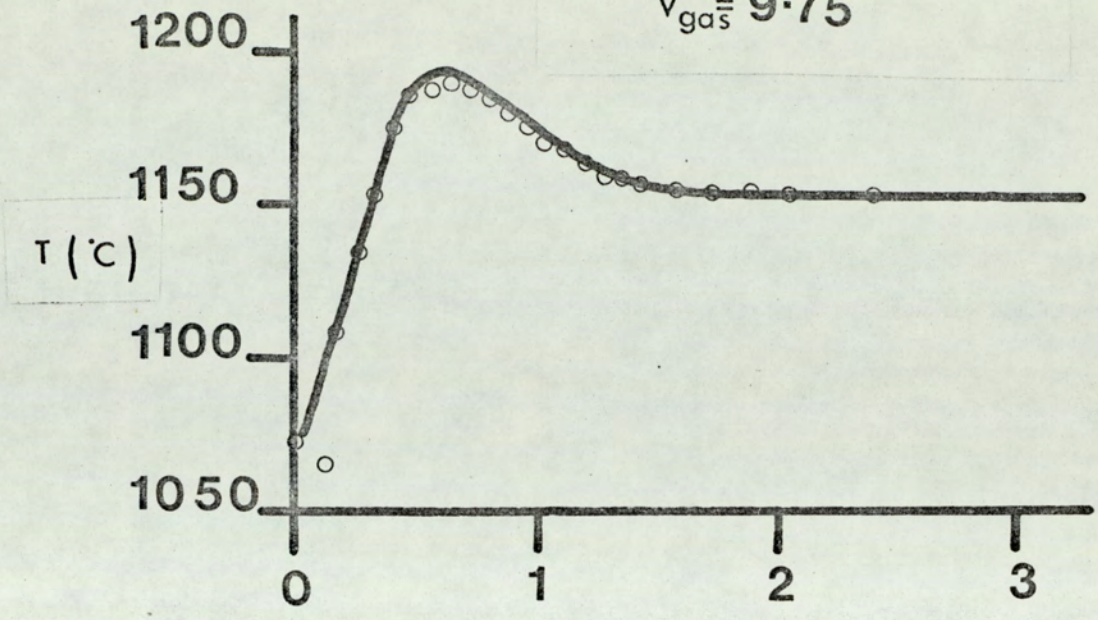

X – DISTANCE FROM DISTRIBUTOR (c.m.)

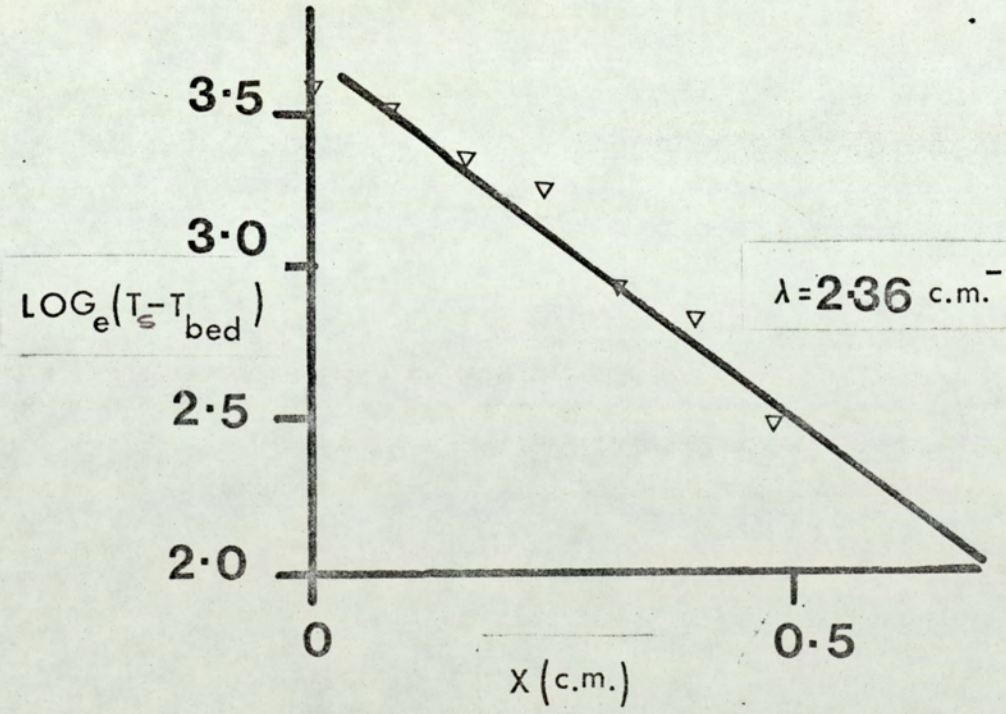

λ = 2·36 c.m.$^{-1}$

FIG. 78

TEMPERATURE PROFILE

ZIRCONIA SILICATE
(1·0 – 1·4) m.m. dia

$\dot{V}_{air} = 181$ L/M

$\dot{V}_{gas} = 11·1$

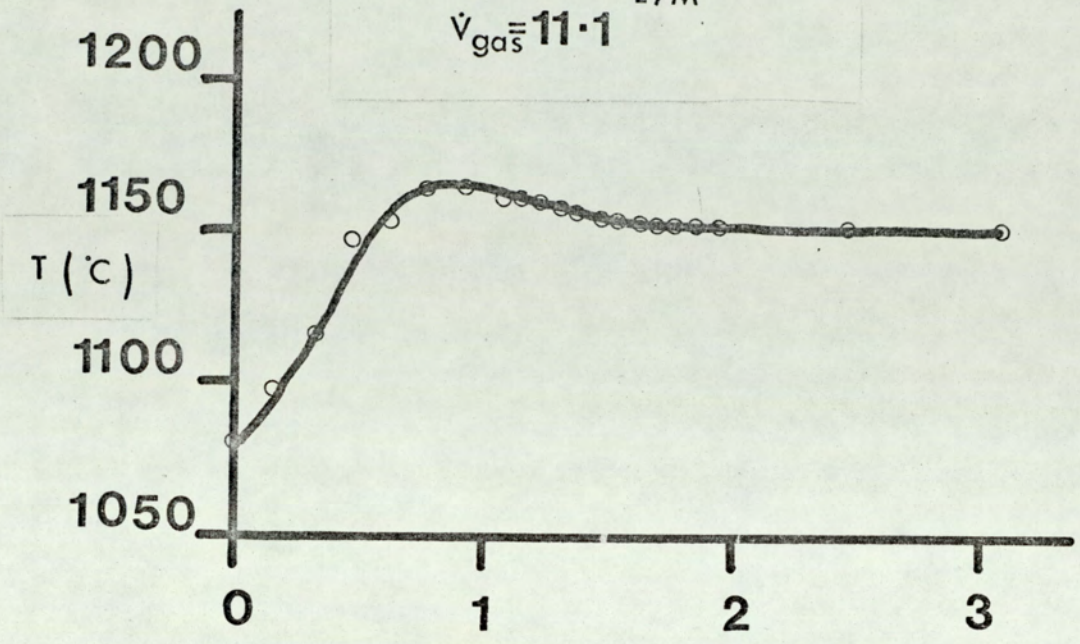

X – DISTANCE FROM DISTRIBUTOR (c.m.)

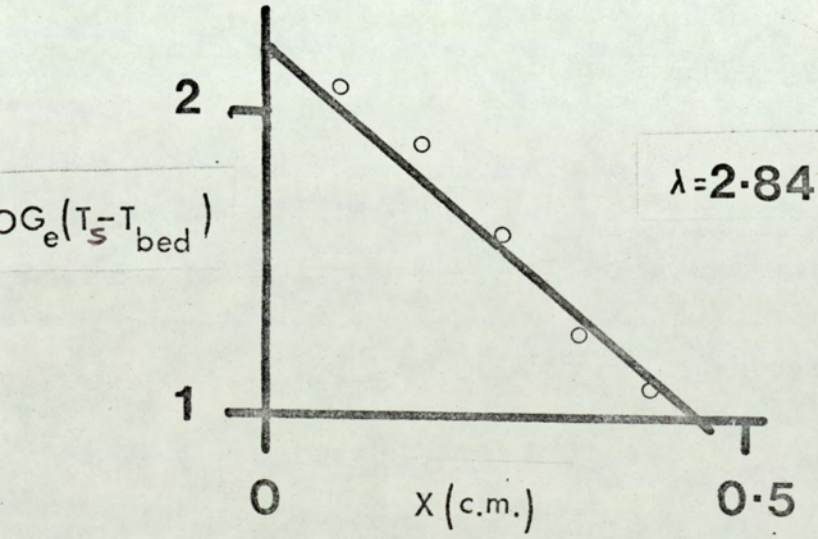

$\lambda = 2·84$ c.m.$^{-1}$

TEMPERATURE PROFILE

FIG.79

ZIRCONIA SILICATE
(1·0 – 1·4) m.m. dia
$\dot{V}_{air}$ = 185 L/M
$\dot{V}_{gas}$ = 11·1

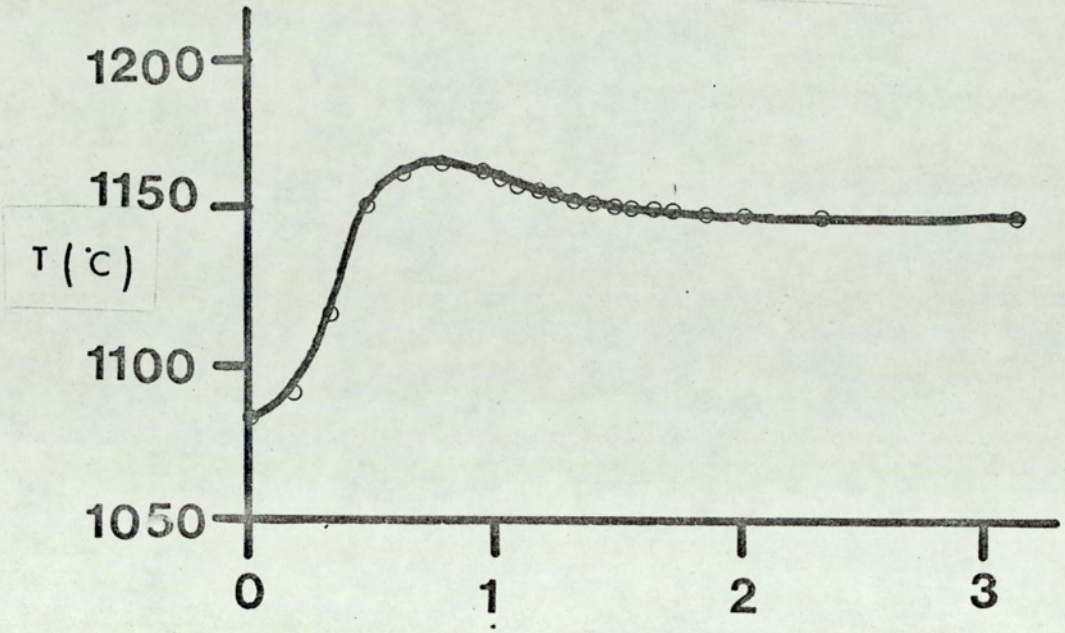

X – DISTANCE FROM DISTRIBUTOR (c.m.)

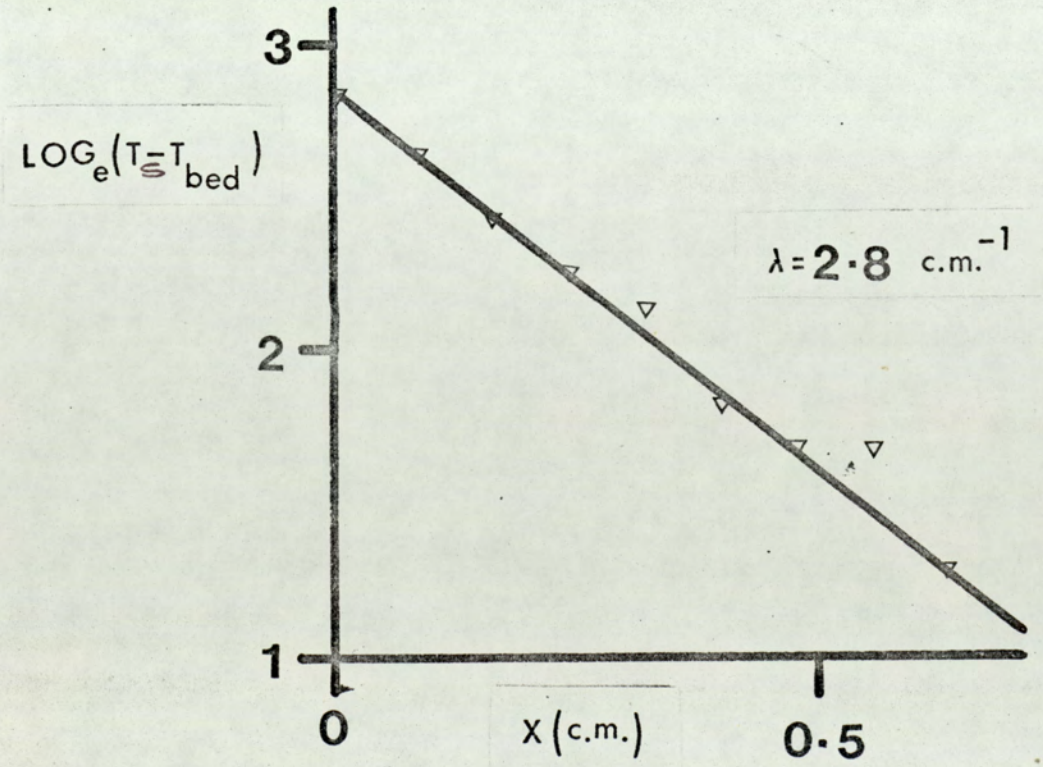

TEMPERATURE PROFILE

FIG.80

ZIRCONIA SILICATE

(1·0 – 1·4) m.m. dia

$\dot{V}_{air}$ = 235 L/M

$\dot{V}_{gas}$ = 14·25

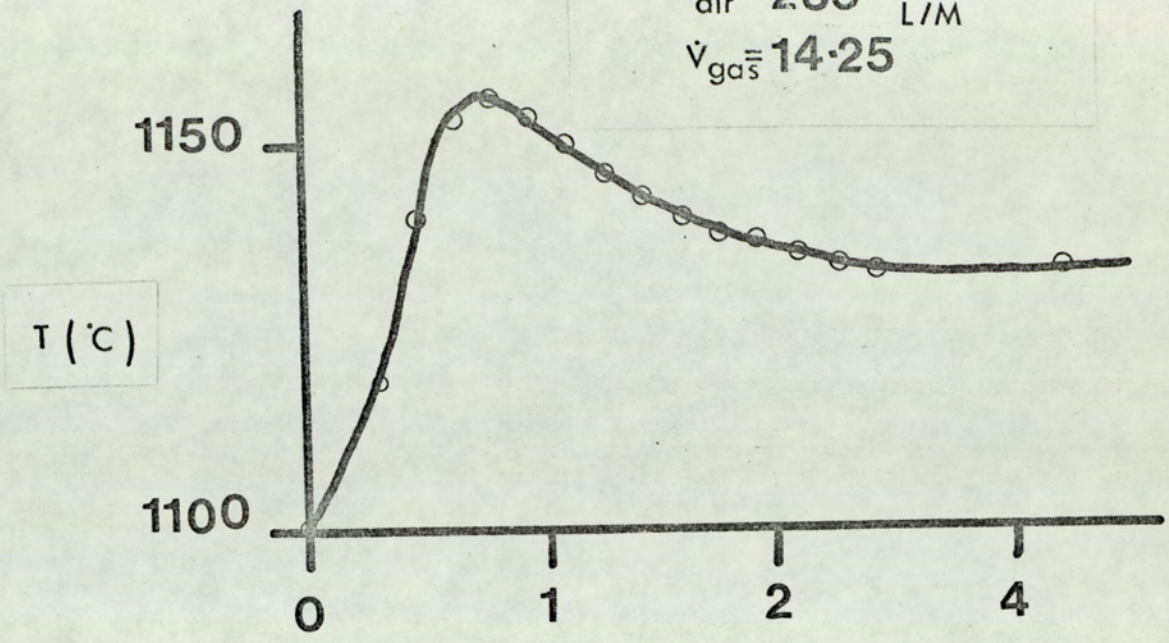

X – DISTANCE FROM DISTRIBUTOR (c.m.)

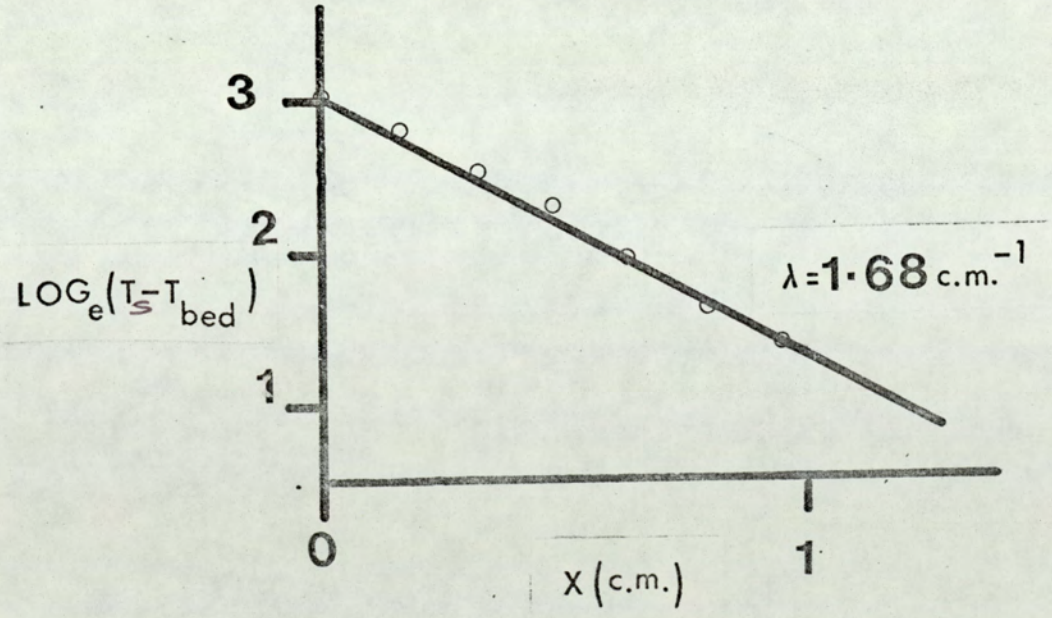

FIG.81

TEMPERATURE PROFILE

ZIRCONIA SILICATE
(1·0 – 1·4) m.m. dia
$\dot{V}_{air}$ = 150
$\dot{V}_{gas}$ = 9·75 L/M

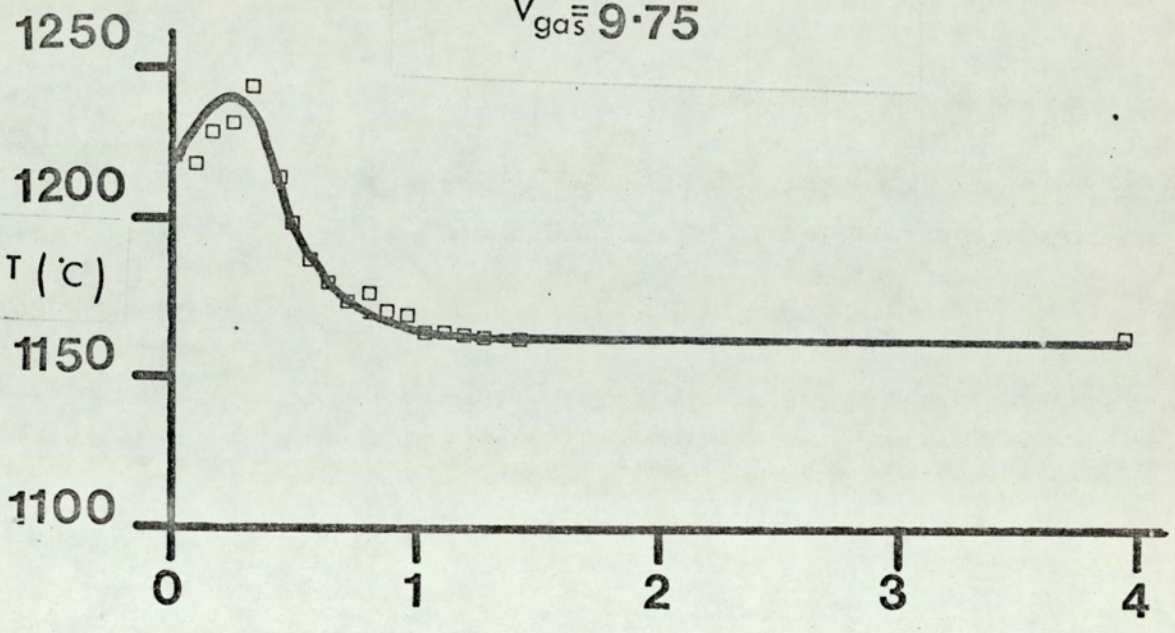

X – DISTANCE FROM DISTRIBUTOR (c.m.)

TEMPERATURE PROFILE

ZIRCONIA SILICATE
(1·0 – 1·4) m.m. dia
$\dot{V}_{air}$ = 144
$\dot{V}_{gas}$ = 10·5

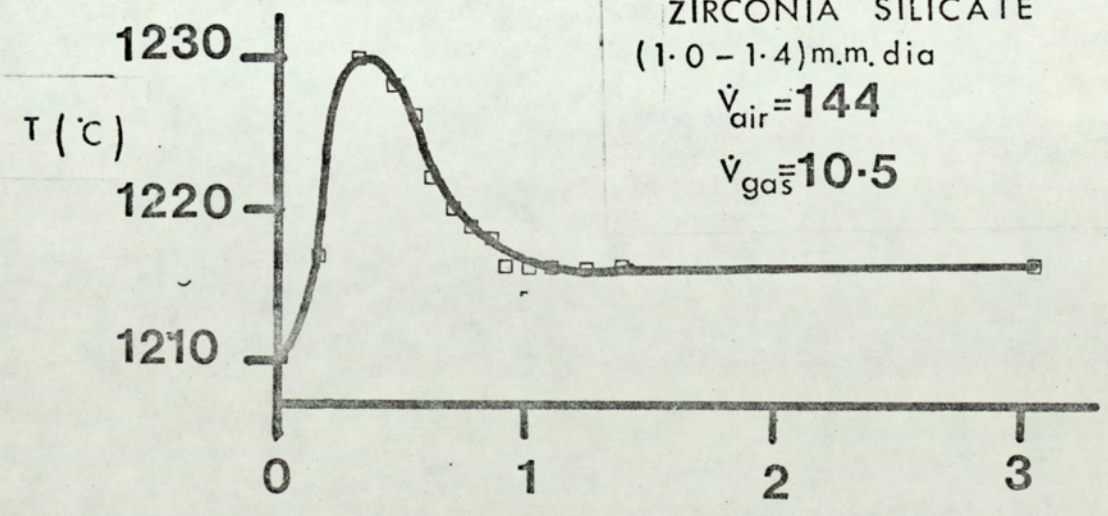

X – DISTANCE FROM DISTRIBUTOR (c.m.)

FIG. 82

CONCENTRATIONS FOR STOICHIOMETRIC EQUILIBRIUM MIXTURES

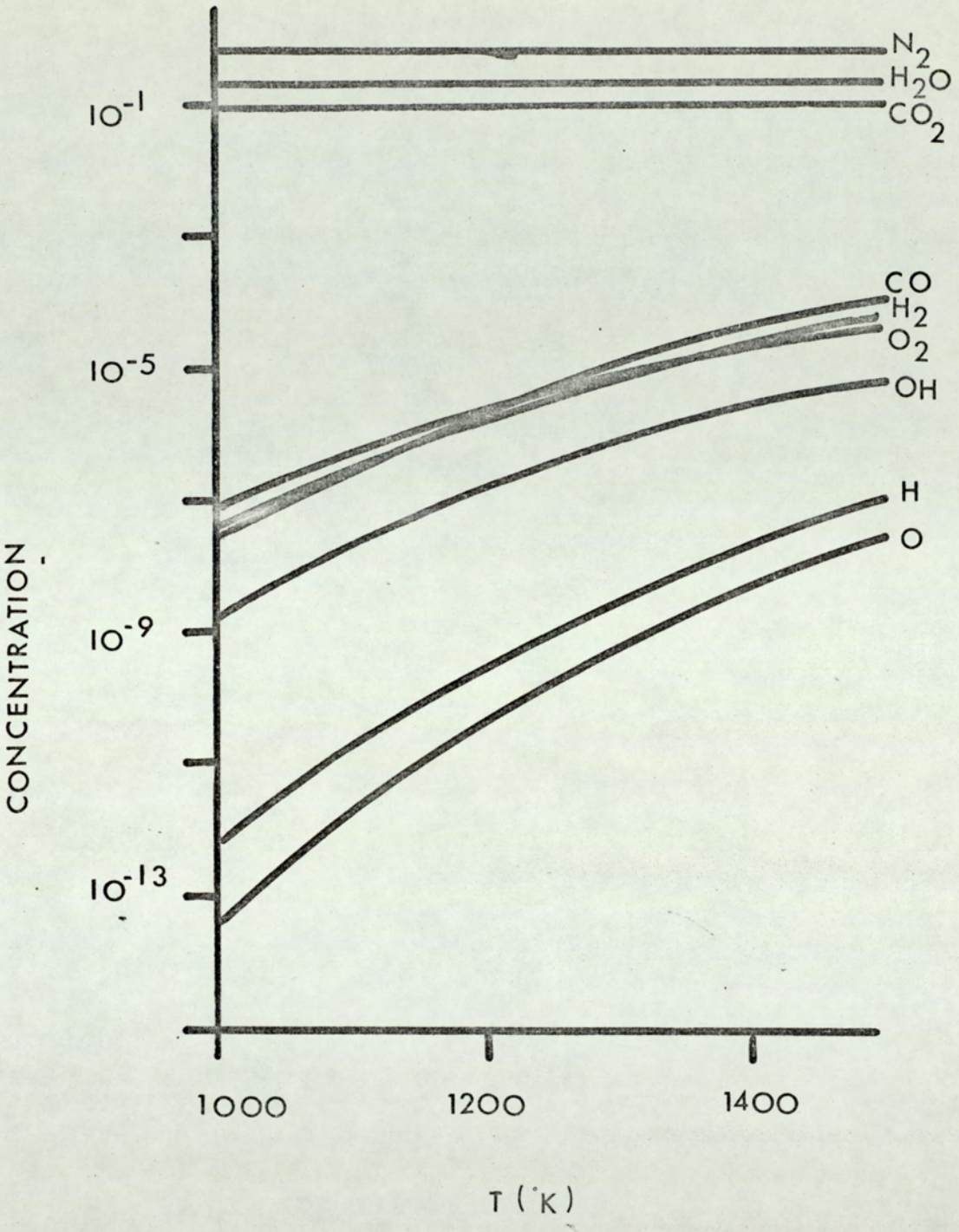

FIG.83

VARIATION OF CO EQUILIBRIUM

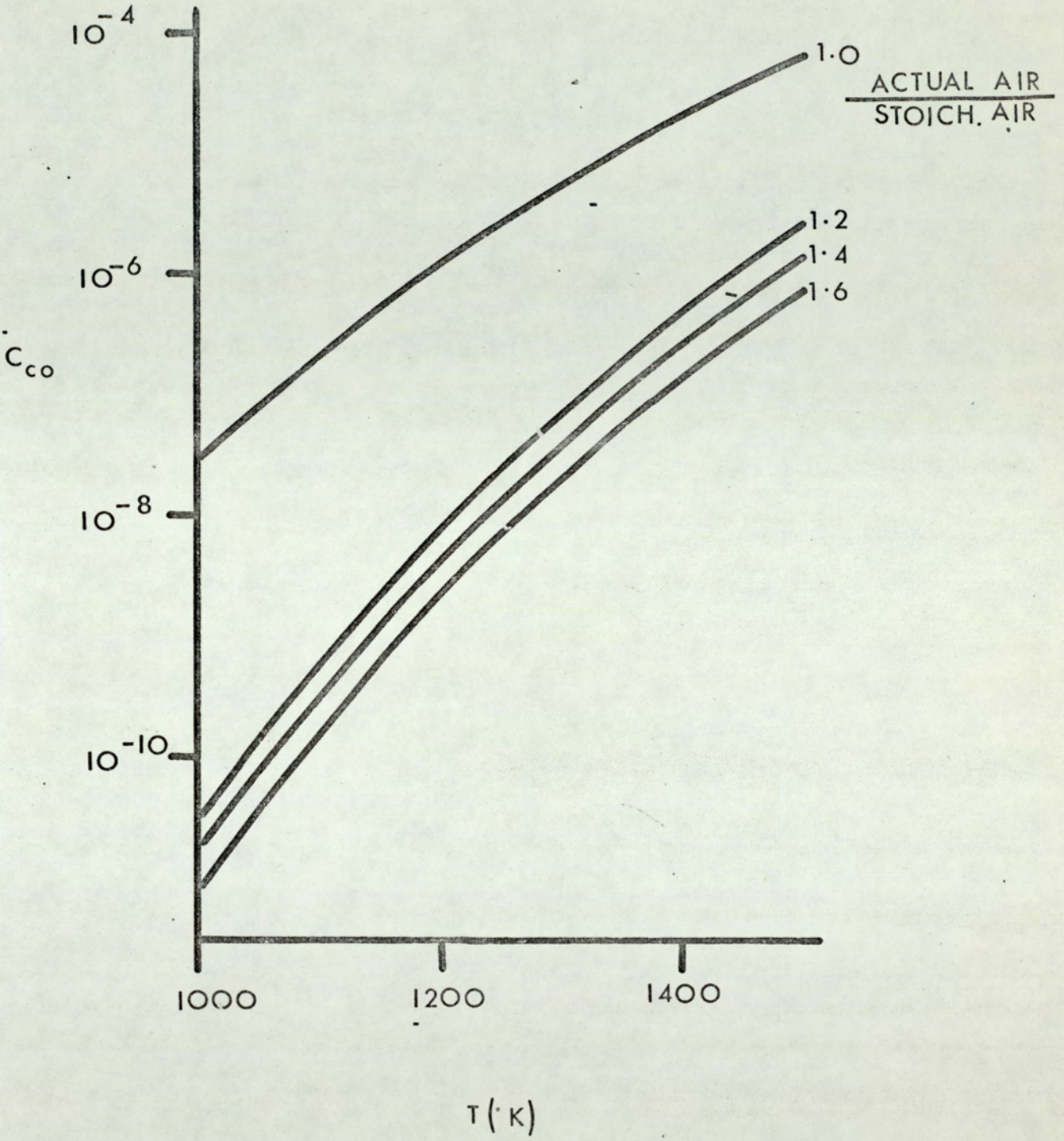

VARIATION OF CO EQUILIBRIUM AT 1400°K

FIG. 84

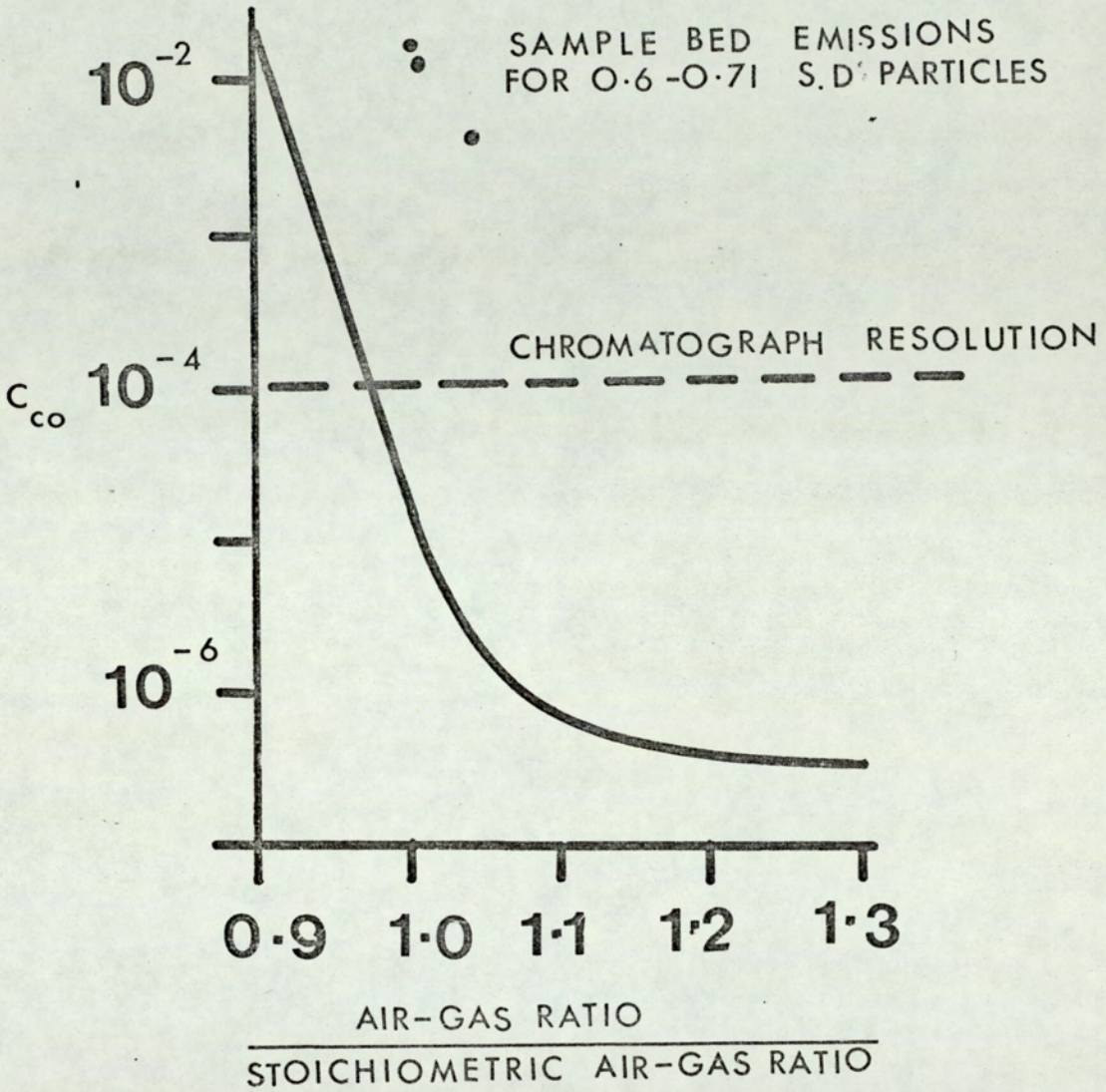

FIG. 85

H_2 EQUILIBRIUM CONCENTRATIONS

AT 1400° K

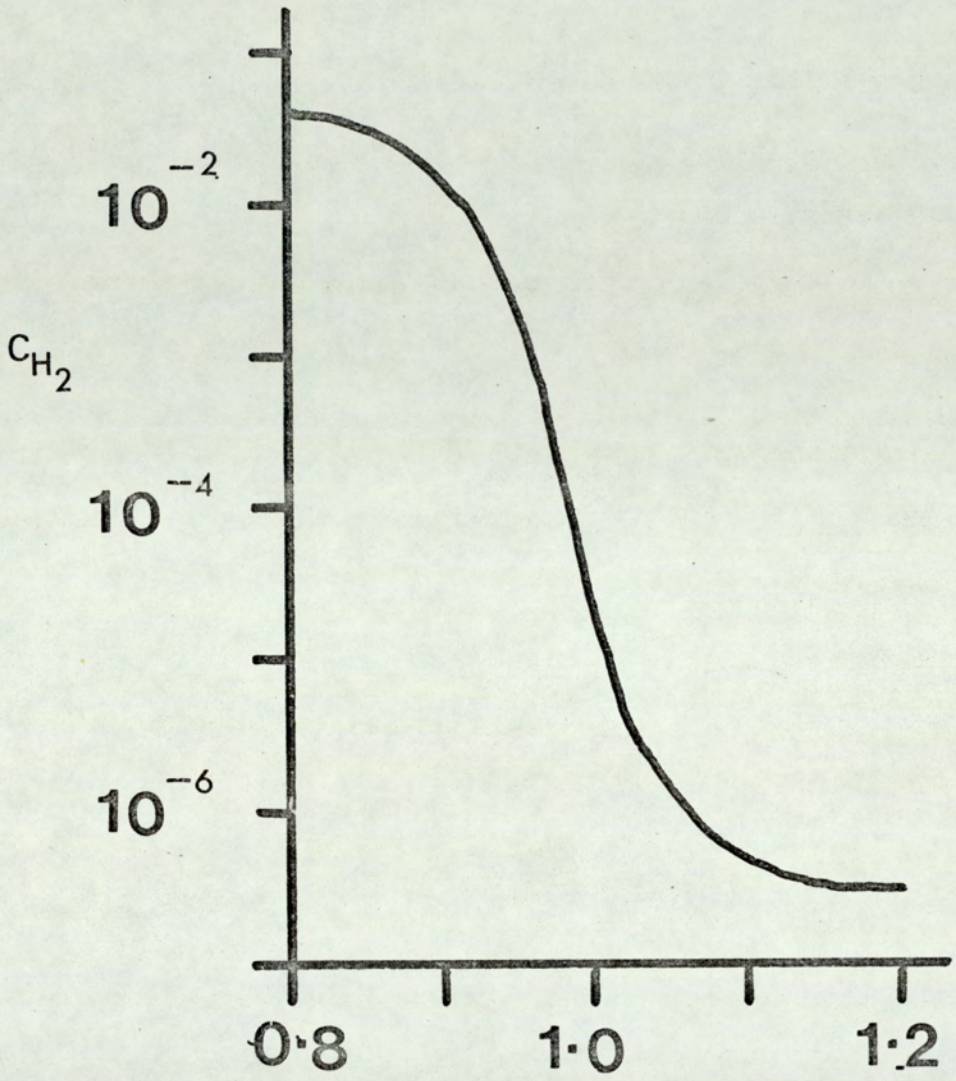

REFERENCES

REFERENCES

[1] JOHNSON, M L M (1970). PhD Thesis, Penn.State University

[2] ELLIOTT, D E and PILLAI, K K (1974). IChemE Symp Series No.38

[3] ELLIOTT, D E. Private communication

[4] DAVIDSON, J F and HARRISON, D (1971). "Fluidization", Academic Press, London

[5] KUNII, D and LEVENSPEIL, O (1969). "Fluidization Engineering" Wiley, New York, USA

[6] ERGUN, S (1952). Chem.Eng.Prog. 48, No.2, 89.

[7] CRANFIELD, R R (1972). PhD Thesis, C.N.A.A.

[8] CRANFIELD, R R and GELDART, D (1972). Chem.Eng.Jnl. 3, 211

[9] DAVIDSON, J F and HARRISON, D (1963). "Fluidized Particles" Cambridge University Press

[10] TALMOR, E and BENENATI, R F (1963). AIChemE Jnl. 9, 536

[11] ROWE, P N and PARTRIDGE, B A (1962). "Symposium on the Interaction between Fluids and Particles" IChemE, London

[12] ROWE, P N and PARTRIDGE (1965). Trans IChemE, 43, T157.

[13] WOOLARD, N M and POTTER, O E (1968). AIChemE Jnl, 14, 388

[14] PYLE, D L and ROSE, P L (1965). Chem.Eng.Sc. 20, 25

[15] DAVIDSON, J F (1961). Trans. IChemE, 39, 230

[16] ROWE, P N and PARTRIDGE, A (1963). Chem.Eng.Sci. 18, 511

[17] ROWE, P N and PARTRIDGE, A (1966). Trans.I.Chem.E. 44, T335

[18] SHRIKHANDE, K Y (1955). Jnl.Sci and Ind.Res, 14b, 457

[19] LEWIS, W K, GILLIAND, E R and GIROUARD, H (1962). Chem.Eng. Prog. 58, 87

[20] JAIN, S C and CHEN, B H (1971). AIChemE Symp Series, 67, 97

[21] GABOR, J D (March 1965). ANL-6859

[22] ZABRODSKY, S S (1966). "Hydrodynamics and Heat Transfer in Fluidized Beds, M I T Press

[23] BASKAKOV, A P, KUNOS, I V and SVETLAKOV, V I (1968). Gasov.Prom, 13, 25

[24] BASKAKOV, A P and ANTIFEEV, V A (1966). 7,52 'Metalloved - Term Obrabothea Metal'

[25] TAMALET, M (1968). Symp.Chem.Eng. in Iron & Steel Ind. IChemE, Swansea

[26] JARRY, R L, ANASTASIA, L J, CARLS, E L, JONKE, A A and VOGEL, G J (1970). Second Int.Conf. on Fluidized Bed Combustion, Hueston Woods, Ohio, USA

[27] BROUGHTON, J (1972). PhD Thesis, University of Newcastle

[28] COLE, W E and ESSENHIGH, R H (1972). Third Int.Conf. on Fluidized Bed Combustion, Hueston Woods, Ohio, USA

[29] ELLIOTT, D E and VIRR, M J (1972). Third Int.Conf. on Fluidized Bed Combustion, Hueston Woods, Ohio, USA

[30] DEISSLER, R G and ELAN, C S (1952). National Advisory Committee Aeronaut, RME 52C05

[31] SCHOTTE, W (1960). AIChemE Jnl, 6, 63

[32] SEMENOFF, N (1935). "Chemical Kinetics and Chain Reactions" Clarendon Press, Oxford

[33] KARMILOVA, L V, ENIKOLOPYAN, N S, NALBANDYAN, A B (1960). Russn.Jnl.Phys.Chem. 34, 261

[34] SPIERS, H M (1962). "Technical Data on Fuel" London

[35] RITTENHOUSE, G (1944). Jnl.Sed.Petr. 13, 79.

[36] MII, T, YOSHIDA, K and KUNII, D (1973). Jnl.Chem.Eng.Japan, 6, 100

[37] FRISTROM, R M and WESTENBERG, A A (1965). "Flame Structure" McGraw-Hill, USA

[38] Van ZEGGEREN, F and STOREY, S H (1970). "The Calculation of Chemical Equilibria", Cambridge

[39] WHITE, W B, JOHNSON, S M and DANTZIG, G B (1958). J.Chem.Phys. 28, 751

APPENDIX 1

NUMERICAL SOLUTION OF DIFFERENTIAL EQUATIONS

The following differential equation has to be solved:

$$\dot{m}\, c_p\, T_g - \dot{M}\, C\, T_s - K.A. \frac{dT_s}{dx} + \sum_{j=1}^{N} \int_{\phi=N_j^{\circ}}^{\phi=\dot{N}_j} (h_f^T)_j \, d\Phi = \text{constant}$$

A simple predictor-corrector method as described below is used, starting at the distributor plate and progressing along the axis.

Predict

$$(1)\quad P(T_s) = T_s + \frac{dT_s}{dx}.\delta x$$

$$(2)\quad P(T_g) = T_g + \left[H(T_s - T_g) - \frac{1}{\dot{m} c_p} \sum_{j=1}^{N} (h_f^T) \frac{d\dot{N}_j}{dx}\right]. \delta x$$

$$(3)\quad P(\dot{N}_j) = \dot{N}_j + \frac{d\dot{N}_j}{dx} + \delta x$$

$$(4)\quad P\left[\frac{dT_s}{dx}\right] = \frac{1}{K.A}\left[\dot{m} c_p P(T_g) - \dot{M} C P(T_s) + \sum_{j=1}^{N} \left[P(\dot{N}_j) - \dot{N}_j\right] (h_f^T)_j - \text{constant}\right]$$

From these predicted values, more accurate estimates are made as follows:

Correct

$$(1)\quad C(T_s) = T_s + \left[\frac{dT_s}{dx} + P\left[\frac{dT_s}{dx}\right]\right] \times \frac{\delta x}{2}$$

$$(2)\quad C(T_g) = T_g + H[T_s - T_g + P(T_s) - P(T_g)] \times \frac{\delta x}{2} - \frac{1}{\dot{m}c_p}\left[\sum_{j=1}^{N}(h_f^T)_j \frac{d\dot{N}_j}{dx} + P\left[(h_f^T)_j \frac{d\dot{N}_j}{dx}\right]\right] \times \frac{\delta x}{2}$$

$$(3)\quad C(\dot{N}_j) = \dot{N}_j + \left[\frac{d\dot{N}_j}{dx} + P\left[\frac{d\dot{N}_j}{dx}\right]\right] \times \frac{\delta x}{2}$$

$$(4)\quad C\left[\frac{dT_s}{dx}\right] = \frac{1}{KA}\left[\dot{m}c_p C(T_g) - \dot{M}C\, C(T_s) + \sum_{j=1}^{N}[(C(N_j) - N_j](h_f^T)_j - \text{constant}\right]$$

In this scheme, the integral term in the differential equation is satisfied by adding the summation term in this last equation to the constant value as the solution advances each incriment. Values of δx are chosen to satisfy convergence requirements. A simple artifice is used to ensure that no value of $\dot{N}_j$ becomes negative in an exponential form as shown below:

$$\dot{N}_{CH_4} = \exp(\psi)$$

From this

$$\frac{d\psi}{dx} = \frac{1}{\dot{N}_{CH_4}} \frac{d\dot{N}_{CH_4}}{dx}$$

and for each incriment values of $\delta\psi$ can be found. From the stoichiometry of the reaction values of ψ can be found for all of the other components.

The programme is given at the end of this Appendix.

Two types of solution were made:

(1) The simple solution where $T_g = T_s$ and the drift particles left at the plate

(2) The more realistic solution where $T_g \neq T_s$

The programme is given for the latter but is easily ammended for the former. The exponential form is only used in the last stages of the programme since initially some values of $\dot{N}_j$ are zero, and in this respect the programme is in two parts: one using the exponential notation and one the ordinary.

The programme nomenclature is given below in the order used:

HP = H the gas-particle heat transfer coefficient

C = thermal conductivity

CN(I) = reaction stoichiometric coefficients

[e.g. $CH_4 + 2O_2 = 2O_2 + 2H_2O$ and in this scheme

CN(1) = 1, CN(2) = 2, CN(3) = -1, CN(4) = -2]

N = number of chemical components

TG = gas temperature (T_g)

T = solids temperature (T_s)

A = bed area

QG = $\dot{V}_{gas}$

QA = $\dot{V}_{air}$

GN(I) = $\dot{N}_i$

DlT = dT_s/dx

DEL = δx

D = particle diameter

CS = C(specific heat of particles)

WG = $\dot{m}$

WSC = $\dot{MC}$

WGC = $\dot{mc}_p$

HFl(I) = $(h_f^T)_i$

DNl(I) = dc_i/dt

UMF(T) = U_{mf}

DDN(I) = $\dot{dN}_i/dx \times \delta x$

PT = $P(T_s)$

PTG = $P(T_g)$

PGN(I) = $P(\dot{N}_i)$

PDlT = $P(dT_s/dx)$

CTG = $C(T_g)$

CG(I) = C_i

EN(I) = exponential form of N_i

PEN(I) = predictor for above

Identifiers such as CONST, HSUM, FSUM, SUM, Fl, F2 etc are constants in the differential equation and identifiers used for counting and comparison.

MHF is a subroutine for evaluating thermodynamic data at different temperatures, VEL evaluates the chemical kinetics at different temperatures and compositions, and UMF evaluates U_{mf} at different temperatures.

```
TRACE 1
READ FROM (CR)
TRACE 2
MASTER MJW
DIMENSION GN(10),EN(10),PN(10),CG(10),CN(10),HF1(10),
1HF2(10),DDN(10),PGN(10),PEN(10)
C=0.04
HF=25.0
CN(1)=1.0
CN(2)=2.0
CN(3)=-2.0
CN(4)=-1.0
N=5
TG=500.0
T=1100.0
M=132.75
QG=15.0E 03/60.0
QA=200.0E 03/60.0
GN(1)=QG/293.0/0.087/1.0E 03
GN(2)=QA*0.21/293.0/0.087/1.0E 03
GN(3)=0
GN(4)=0
```

```
      GN(5)=QA*0.79/293.0/0.087/1.0E 03
      D1T=5861.0*(GN(1)+GN(2)+GN(5))/A/C
      WRITE(2,2)D1T
    2 FORMAT(E15.7)
      DEL=0.005
      D=0.118
      CS=0.2
      WG=GN(1)*16.0+GN(2)*32.0+GN(5)*14.0
      WSC=CS*0.785*EXP(-66.3*D)*((QA+QG)*(T+273.0)/288.0-UMF(T)*A)
      WSC=WSC*500.0
      WGC=WG*0.265
      COUNT=0
      WRITE(2,600)WSC,WGC
  600 FORMAT(2E15.7)
      WRITE(2,160)(GN(I),I=1,N)
  160 FORMAT(5E15.7)
      CONST=-D1T*C*A*WGC*TG
      HSUM=-CONST
      DO150KKM=1,100
      COUNT=COUNT+DEL
      CALL VEL (GN,TG,DN1)
      CALL MHF (TG,HF1)
      FSUM=0
      DO989I=1,N
  989 FSUM=FSUM+DN1*CN(I)*HF1(I)/UMF(TG)*0.435
      F2=FSUM
      F1=WGC*HP*(T-TG)-F2
      WRITE(2,987)F1,F2
  987 FORMAT(2E15.7)
      DDN(1)=DN1/UMF(TG)*0.435*DEL
      PT=T+D1T*DEL
      PTG=TG+HP*(T-TG)*DEL-F2/WGC*DEL
      DO100I=1,N
      DDN(I)=DDN(1)*CN(I)
  100 PGN(I)=GN(I)+DDN(I)
      SUM=HSUM
      DO110I=1,N
  110 SUM=SUM+HF1(I)*DDN(I)
```

```
      PD1T=(SUM+WGC*TG)/C/A
      CALLMHF (PTG,HF2)
      CALL VEL (PGN,PTG,DN2)
      FSUM=0
      DO460I=1,N
  460 FSUM=FSUM+DN2*CN(I)*HF2(I)/UMF(TG)*0.435
      CTG=TG+(T-TG+PT-PTG)*HP*DEL/2.0-(F2+FSUM)/2.0*DEL/WGC
      CT=T+(PD1T+D1T)*0.5*DEL
      CALL VEL (PGN,CTG,DN2)
      DDN(1)=(DN1+DN2)*0.5/UMF(TG)*0.435*DEL
      DO120I=1,N
      DDN(I)=DDN(1)*CN(I)
  120 GN(I)=GN(I)+DDN(I)
      CALL MHF (CTG,HF2)
      DO130I=1,N
  130 HSUM=HSUM+(HF1(I)+HF2(I))*0.5*DDN(I)
      T=CT
      TG=CTG
      D1T=(HSUM+WGC*TG)/C/A
      WRITE(2,25)T,TG,COUNT
   25 FORMAT(3E15.7)
      WRITE(2,26)(GN(J),J=1,N)
      SUM=0
      DO70KM=1,N
   70 SUM=SUM+GN(KM)
```

```
      DO71KM=1,N
   71 CG(KM)=GN(KM)/SUM
      WRITE(2,72)(CG(K),K=1,N)
   72 FORMAT(5E15.7)
   26 FORMAT(5E15.7)
  150 CONTINUE
      CONST=-D1T*C*A+WGC*TG-WSC*T
      HSUM=-CONST
      SUM=HSUM
      DO20I=1,N
   20 EN(I)=ALOG(GN(I))
      DO350MM=1,500
      COUNT=COUNT+DEL
      IF(GN(1))850,850,851
  850 SUM=HSUM
      GOTO852
  851 CONTINUE
      CALL VEL (GN,TG,DN1)
      CALL MHF (TG,HF1)
      FSUM=0
      DO985I=1,N
  985 FSUM=FSUM+DN1*CN(I)*HF1(I)/UMF(TG)*0.455
      F2=FSUM
      F3=WSC*D1T
      F1=WGC*HP*(T-TG)-F2
      WRITE(2,984)F1,F2,F3
  984 FORMAT(3E15.7)
      PEN(1)=EN(1)+DN1/GN(1)/UMF(TG)*0.435*DEL
      DDN(1)=EXP(PEN(1))-GN(1)
      DO300I=1,N
      DDN(I)=DDN(1)*CN(I)
  300 PGN(I)=GN(I)+DDN(I)
      SUM=HSUM
```

```
      DO310I=1,N
  310 SUM=SUM+HF1(I)*DDN(I)
  852 PT=T+D1T*DEL
      PTG=TG+HP*(T-TG)*DEL-F2/WGC*DEL
      PD1T=(SUM-WSC*PT+WGC*PTG)/C/A
      CT=T+(PD1T+D1T)*0.5*DEL
      CALL MHF (PTG,HF2)
      CALL VEL (PGN,PTG,DN2)
      FSUM=0
      DO490I=1,N
  490 FSUM=FSUM+DN2*CN(I)*HF2(I)/UMF(TG)*0.435
      CTG=TG+(T-TG*PT-PTG)*HP*DEL/2.0-(F2+FSUM)/2.0*DEL/WGC
      IF(GN(1))860,860,861
  861 CONTINUE
      CALL VEL (PGN,CTG,DN2)
      EN(1)=EN(1)+(DN1/GN(1)*DN2/PGN(1))/UMF(TG)*0.435*DEL*0.5
      DDN(1)=EXP(EN(1))-GN(1)
      DO320I=1,N
      DDN(I)=DDN(1)*CN(I)
  320 GN(I)=GN(I)+DDN(I)
      CALL MHF (CTG,HF2)
      DO330I=1,N
  330 HSUM=HSUM+(HF1(I)+HF2(I))*0.5*DDN(I)
  860 T=CT
      TG=CTG
      D1T=(HSUM+WGC*TG-WSC*T)/C/A
      WRITE(2,250)T,TG,COUNT
  250 FORMAT(3E15.7)
      WRITE(2,260)(GN(J),J=1,N)
  260 FORMAT(5E15.7)
```

```
      SUM=0
      DO75KM=1,N
   75 SUM=SUM+GN(KM)
      DO76KM=1,N
   76 CG(KM)=GN(KM)/SUM
      WRITE(2,77)(CG(K),K=1,N)
   77 FORMAT(5E15.7)
  350 CONTINUE
  999 CONTINUE
      STOP
      END
```

SEGMENT, LENGTH 1425, NAME MJW

```
      FUNCTION UMF(T)
      A=0.1778E 03
      B=0.4324E 00
      C=-0.1808E-03
      D=0.4975E-07
      V=(A+B*T+C*T**2+D*T**3)*1.0E-06
      DP=5.18
      DG=0.00129*273.0/(273.0+T)
      D=0.118
      S=0.81
      VD=0.44
      A=1.75/D/S/VD**3*(DG/V)**2
      C=DG*(DP-DG)*980.0/V**2
      B1=150.0*(1.0-VD)/(D*S)**2/VD**3*(DG/V)
      UMF=(SQRT(B1**2+4*A*C)-B1)/2.0/A
      RETURN
      END
```

END OF SEGMENT, LENGTH 151, NAME UMF

```
      SUBROUTINE VEL (GN,T,DNCH4)
      DIMENSION GN(10)
      SUM=0
      DO11I=1,5
    1 SUM=SUM+GN(I)
      CCH4=GN(1)/SUM
      CO2=GN(2)/SUM
      DNCH4=-1.0E 11*EXP(-46.0E 03/1.9859/(T+273.0))*SUM*CCH4**2*CO2
      RETURN
      END
```

END OF SEGMENT, LENGTH 92, NAME VEL

```
      SUBROUTINE MHF (T,HF)
      DIMENSION HF(10)
      TT=T+273.0
      A=-0.1436E 05
      B=-0.1341E 02
      C=0.7974E-02
      D=-0.1637E-05
      HF(1)=A+B*TT+C*TT**2+D*TT**3
      HF(2)=0
      A=-0.5605E 05
```

```
B=-0.3116E 01
C=0.9705E-03
D=-0.1187E-06
HF(3)=A+B*TT+C*TT**2+D*TT*3
A=-0.9370E 05
B=-0.8507E 00
C=0.3282E-03
D=-0.9427E-07
HF(4)=A+B*TT+C*TT**2+D*TT*3
RETURN
END

END OF SEGMENT, LENGTH   156, NAME  MHF
```

APPENDIX 2

CHEMICAL EQUILIBRIUM CONSIDERATIONS

Given a number (N) of chemical species it is required to find a set of concentrations (C_1, C_2, ... C_N) such that the mixture of these chemical species is in a state of chemical equilibrium. This condition is attained when the free energy of the mixture, at the required temperature and pressure, is at a minimum.

If an ideal gas mixture is assumed then the molar free energy of a chemical species, i, is given by

$$f_i = (f_{f_1}^T) + R\,T\,\log_e P_i$$

where $(f_f^T)_i$ is the free energy of formation of the species

R is the gas constant

T is the temperature

P_i is the partial pressure

If (Y_1, Y_2, ... Y_N) are the mole numbers of the components in the gas mixture, then the free energy of the gas mixture is given by:

$$F = \sum_{j=1}^{N} Y_i\, f_i$$

The values of (Y_1, Y_2, ... Y_N) are required such that F is a minimum. The values of (Y_1, Y_2, ... Y_N) cannot vary arbitrarily. In specifying the gas mixture under consideration there will be given quantities of atoms from which the molecular species are made, and only variations of (Y_1, Y_2, ... Y_N) that do not violate

the conservation of atomic species are permitted. This consideration is written as:

$$\sum_{j=1}^{N} a_{ji} Y_i = b_j \quad (j = 1, M)$$

where a_{ji} represents the number of atoms of species j that are in chemical species i, and the values of b_j are those which specify the mixture. M is the number of atomic species.

In this study, a methane-air mixture is under consideration. Possible chemical species to be considered in the equilibrium mixture are:

CO_2, CO, CH_4, H_2, H_2O, H, N_2, NO, O, OH, O_2

The emission of any one component will effect the calculated equilibrium concentration of the others, and how great will be its effect depends upon the contribution of that component to the total free energy of the mixture.

Several methods have been proposed for calculating complex chemical equilibria problems, and these are collated in a small but useful volume by van Zeggerean and Storey[38]. Each method has its own merits and conditions under which it is eminently suitable. Of those tried during this work, the method of White, Johnson and Dantzig[39] was found to be the most suitable.

With this method an initial set of mole numbers (Y_1°, Y_2°, ... Y_N°) is assumed satisfying the atomic constraints for this mixture.

With the initial values, an approximation is made with a Taylors expansion to give a new value of free energy with the condition that this shall be a minimum value for any variation around the starting point. The atomic balance constraints are used with Lagrangian multipliers to ensure that the new mole numbers do not violate the conservation of atomic species.

The calculation procedure is given below and equation numbers are those in the paper by White *et al.*

Start with values of T, P, $[(f_f^T)_1, (f_f^T)_2 \ldots (f_f^T)_N]$, $(Y_1^\circ, Y_2^\circ, \ldots Y_N^\circ)$, $(a)_{ij}$, $(b \ , b \ \ldots \ b_M)$

(1) Evaluate for all i

$$f_i = (f_f^T)_i + RT \log_e P_L^\bullet = (f_f^T)_i + RT\left[\log_e P + \log_e \frac{Y_i}{Y}\right]$$

(2) Formulate the matrice $(C)_{kj}$ given by

$$C_{jk} = C_{kj} = \sum_{j=1}^{N} a_{ij} \, a_{ik} \, Y_i \qquad (17)$$

(3) Solve the (M+1) linear simultaneous equations for λ_i and υ

$$C_{11}\lambda_1 + C_{12}\lambda_2 + \ldots\ldots C_{IM}\lambda_M + b_1\upsilon = \sum_{j=1}^{N} a_{i1} \, f_i$$

$$C_{21}\lambda_1 + C_{22}\lambda_2 + \ldots\ldots C_{2M}\lambda_M + b_2\upsilon = \sum_{j=1}^{N} a_{i2} \, f_i$$

$$\vdots$$

$$C_{M1}\lambda_1 + C_{M2}\lambda_2 + \ldots\ldots C_{MM}\lambda_M + b_M\upsilon = \sum_{j=1}^{N} a_{iM} \, f_i$$

$$b_1\lambda_1 + b_2\lambda_2 + \ldots\ldots b_M\lambda_M + 0 = \sum_{j=1}^{N} f_i$$

These are equations (18) in White's paper.

(4) Solve $\bar{X} = (\upsilon + 1)\bar{Y}$ - equation (19)

where:

$$\bar{X} = \sum_{j=1}^{N} X_i \quad \text{(new mole numbers)}$$

$$\bar{Y} = \sum_{j=1}^{N} Y_i \quad \text{(old mole numbers)}$$

(5) Solve for the new mole numbers from:

$$x_i = -f_i + \left[\frac{Y_i}{\bar{Y}}\right]\bar{x} + \sum_{j=1}^{M} \lambda_j a_{ij})Y_i \quad \text{- equation (14)}$$

With these new estimates the cycle is repeated.

To ensure that all of the new estimates converge upon the point of minimum energy and do not overshoot, the estimates of mole numbers are modified to ensure that the function:

$$f(X_i) = \sum_{i=1}^{N} \Delta_i\left[(f_f^T)_i + R.T.\log_e P + \log_e \frac{Y_i + \lambda\Delta_i}{\bar{Y} + \lambda\bar{\Delta}}\right]$$

where $\Delta_i = X_i - Y_i$ does not become positive. Values of λ in the domain $0 < \lambda < 1$ are chosen to meet this requirement.

The computer programme and the results are given at the end of this Appendix. As a guide, the computer programme nomenclature is given below in the order used:

N = number of chemical species

M = number of atomic species

A(I,J), B(J), Y(I) = as used in atomic constraints with Y(I) as mole numbers etc

G(I) = $(f_f^T)_i/T$

AP = $\log_e P$

TY = $\bar{Y}$

F(I) = f_i/RT

C(K,J) = C_{kj}

FP(I) = $\sum_{j=1}^{N} a_{ji} f_j$

RI(I) = solutions of equation (18)

TX = $\bar{X}$

X(I) = new mole numbers

D(I) = Δ_i

DD(I) = variation of Δ_i as check for -ve mole numbers made

DX(I) = variation of X_i as check is made for -ve mole numbers. Also used as concentration

T & TT = values of X used in search

TF = free energy of mixture

Besides integer variables used in DO LOOPS, the following identifiers were used for counting etc and have no physical or chemical significance:

ASUM, BSUM, SUM, T, V, E, W, S

The tables of computed results are for a mixture of CO, CO_2, O_2, N_2, H_2O, H_2, NO, OH, O, H. It was found that including CH_4 greatly increased the computing time and its omission did not appear to affect the results. Its value was smaller than the others, being just less than the oxygen atom concentrations. All chemical constants used were taken from reference 34.

```
C*************************************************************************
C     SOLUTION OF COMPLEX CHEMICAL EQUILIBRIA BY THE RAND METHOD        *
C     ALL REFERENCECES ARE TO WHITES PAPER ( J.CHEM.PHYS.28,751-5,(1958))*
C*************************************************************************
      DIMENSION D(20),DD(20),DX(20),X(20)
      DIMENSION F(20),FP(20),RI(20),Y(20),G(20),B(20),C(20,20),A(20,20)
      N=8
      M=4
      READ(1,81)((A(I,J),J=1,4),I=1,N)
   81 FORMAT(4E0.0)
      READ(1,82)(B(J),J=1,4)
   82 FORMAT(4E0.0)
      READ(1,83)(Y(I),I=1,N)



   83 FORMAT(E0.0)
      READ(1,80)(G(I),I=1,N)
   80 FORMAT(E0.0)
      AP=0
      DO1K=1,N
    1 G(K)=G(K)/1.9859
  305 TY=0
      DO65I=1,N
   65 TY=TY+Y(I)
      DO66I=1,N
   66 F(I)=Y(I)*(G(I)+AP+ALOG(Y(I)/TY))
      DO67J=1,M
      DO67K=1,M
      SUM=0
      DO67I=1,N
      SUM=SUM+(A(I,J)*A(I,K)*Y(I))
   67 C(K,J)=SUM
C*************************************************************************
C     ELEMENT R(K,J) IN EQN. 17                                         *
C*************************************************************************
      DO68I=1,M
      ASUM=0
```

```
      DO68J=1,N
      ASUM=ASUM+(F(J)*A(J,I))
   68 FP(I)=ASUM
C*****************************************************************************
C     R.H. ELEMENT FOUND IN EQN. 18                                           *
C*****************************************************************************
      BSUM=0
      DO69I=1,N
   69 BSUM=BSUM+F(I)
      IX=M+1
      IY=M+2
      DO70I=1,M
      C(I,IX)=B(I)
      C(IX,I)=B(I)
   70 C(I,IY)=FP(I)
      C(IX,IX)=0
      C(IX,IY)=BSUM
C*****************************************************************************
C     BOTTOM ROW AND LAST COLUMN IN DET (EQN. 18) FOUND                       *
C     SOLUTION OF S.L.E. COMMENCES                                            *
C*****************************************************************************
      DO30I=1,M
      IP=I+1
      DO10J=IP,IX
      IF(ABS(C(I,I))-ABS(C(J,I)))5,10,10
    5 DO7K=1,IY
      T=C(I,K)
      C(I,K)=C(J,K)
    7 C(J,K)=T
   10 CONTINUE
      V=C(I,I)
      DO29K=I,IY
   29 C(I,K)=C(I,K)/V
      DO 30 J=IP,IX
      T=C(J,I)
      DO 30 K=I,IY
   30 C(J,K)=C(J,K)-(C(I,K)*T)
      E=C(IX,IX)
```

```
      C(IX,IX)=C(IX,IX)/E
      C(IX,IY)=C(IX,IY)/E
      DO40I=1,IX



   40 RI(I)=C(I,IY)
C*****************************************************************
C     S.L.E. IS SOLVED FOR RI(K)                                  *
C*****************************************************************
      DO50I=1,M
      K=IX-I
      IP=K+1
      DO50J=IP,IX
   50 RI(K)=RI(K)-(C(K,J)*RI(J))
      TX=TY*(1+RI(IX))
      DO200I=1,N
      SUM=0
      DO150J=1,M
  150 SUM=SUM+(RI(J)*A(I,J))
      X(I)=-F(I)+((Y(I)/TY)*TX)+(SUM+Y(I))
C*****************************************************************
C     NEW MOLE NUMBERS FOUND FROM EQN. 14                         *
C*****************************************************************
  200 D(I)=X(I)-Y(I)
C*****************************************************************
C     CHECK FOR +VE MOLE NUMBERS FOLLOWS                          *
C*****************************************************************
      W=0
      S=0
      DO220I=1,100
      S=S+1
      IF(W)220,205,220
  205 DO220J=1,N
      DD(J)=(S*D(J))/100
      DX(J)=Y(J)+DD(J)
      IF(DX(J))201,201,220
  201 W=1
```

```
      T=(S-1)/100
      NN=I-1
  220 CONTINUE
      IF(W)265,265,270
  265 T=1
      NN=100
C*****************************************************************************
C     CHECK FOR +VE MOLE NUMBERS MADE                                         *
C     CHECK FOR +VE GRADIENTS TO FOLLOW                                       *
C*****************************************************************************
  270 W=0
      S=0
      DO231I=1,NN
      S=S+1
      IF(W)231,221,231
  221 SUM=0
      DO230J=1,N
      DD(J)=D(J)*(S/100)
  230 SUM=SUM+(D(J)*(G(J)+AP+ALOG((Y(J)+DD(J))/(TY+((S/100)*(TX-TY))))))
      IF(SUM)231,231,250
  250 W=1
      TT=(S-1)/100
  231 CONTINUE
C*****************************************************************************
C     CHECK FOR +VE GRADIENTS MADE                                            *
C*****************************************************************************
      IF(W)271,271,253
  271 TT=T
  253 DO260J=1,N
  260 DX(J)=Y(J)+(TT*D(J))
      W=0


      DO300J=1,N
      DD(J)=TT*D(J)
      IF((DD(J)/Y(J))-0.000001)300,300,301
```

```
C*************************************************************************
C     CHECK FOR END OF COMPUTATION                                       *
C*************************************************************************
  501 W=1
  300 CONTINUE
      IF(W)302,302,303
  303 DO304J=1,N
  304 Y(J)=DX(J)
      GO TO 305
      TY=0
      DO400I=1,N
  400 TY=TY+Y(I)
  302 DO999J=1,N
      Y(J)=DX(J)
  999 DX(J)=DX(J)/TY
      WRITE(2,306)(DX(J),J=1,N)
  306 FORMAT(E15.7)
      TF=0
      DO800J=1,N
      F(J)=Y(J)*(G(J)+AP*ALOG(DX(J)))
  800 TF=TF+F(J)
      WRITE(2,306)TF
      STOP
      END
```

CHEMICAL EQUILIBRIUM FOR METHANE-AIR MIXTURE

MOLE FRACTIONS AT A PRESSURE OF ONE ATMOSPHERE

FRACTION OF STOICHIOMETRIC AIR=0.700E 00

COMPONENT	TEMPERATURE(KELVIN)				
	0.1000E 04	0.1200E 04	0.1400E 04	0.1750E 04	0.2000E 04
CARBON MONOXIDE	0.4228E-01	0.5535E-01	0.6424E-01	0.7367E-01	0.7769E-01
CARBON DIOXIDE	0.7876E-01	0.6568E-01	0.5679E-01	0.4736E-01	0.4330E-01
OXYGEN	0.1345E-19	0.4512E-15	0.7976E-12	0.6393E-08	0.5759E-06
HYDROGEN	0.1030E 00	0.8989E-01	0.8100E-01	0.7153E-01	0.6736E-01
WATER VAPOUR	0.1391E 00	0.1522E 00	0.1611E 00	0.1705E 00	0.1744E 00
NITROGEN	0.6369E 00	0.6369E 00	0.6369E 00	0.6369E 00	0.6367E 00
O	0.2177E-19	0.6171E-15	0.9581E-12	0.6616E-08	0.5539E-06
H	0.7189E-09	0.5851E-07	0.1372E-05	0.6176E-04	0.4194E-03
OH	0.1534E-11	0.6001E-09	0.4289E-07	0.7226E-05	0.9383E-04
NO	0.7865E-14	0.8871E-11	0.1361E-08	0.5790E-06	0.1197E-04

CHEMICAL EQUILIBRIUM FOR METHANE-AIR MIXTURE

MOLE FRACTIONS AT A PRESSURE OF ONE ATMOSPHERE

FRACTION OF STOICHIOMETRIC AIR=0.800E 00

COMPONENT	TEMPERATURE(KELVIN)				
	0.1000E 04	0.1200E 04	0.1400E 04	0.1750E 04	0.2000E 04
CARBON MONOXIDE	0.2507E-01	0.3484E-01	0.4178E-01	0.4933E-01	0.5261E-01
CARBON DIOXIDE	0.8586E-01	0.7609E-01	0.6915E-01	0.6160E-01	0.5829E-01
OXYGEN	0.4547E-19	0.1528E-14	0.2797E-11	0.2413E-07	0.2275E-05
HYDROGEN	0.6368E-01	0.5390E-01	0.4697E-01	0.3940E-01	0.3605E-01
WATER VAPOUR	0.1582E 00	0.1680E 00	0.1749E 00	0.1824E 00	0.1855E 00
NITROGEN	0.6672E 00	0.6672E 00	0.6672E 00	0.6672E 00	0.6670E 00
O	0.4003E-19	0.1136E-14	0.1794E-11	0.1285E-07	0.1101E-05
H	0.5654E-09	0.4531E-07	0.1044E-05	0.4584E-04	0.3069E-03
OH	0.2218E-11	0.8553E-09	0.6116E-07	0.1042E-04	0.1364E-03
NO	0.1480E-13	0.1671E-10	0.2609E-08	0.1151E-05	0.2435E-04

CHEMICAL EQUILIBRIUM FOR METHANE-AIR MIXTURE

MOLE FRACTIONS AT A PRESSURE OF ONE ATMOSPHERE

FRACTION OF STOICHIOMETRIC AIR=0.900E 00

COMPONENT	TEMPERATURE(KELVIN)				
	0.1000E 04	0.1200E 04	0.1400E 04	0.1750E 04	0.2000E 04
CARBON MONOXIDE	0.1123E-01	0.1656E-01	0.2047E-01	0.2474E-01	0.2665E-01
CARBON DIOXIDE	0.9116E-01	0.8582E-01	0.8191E-01	0.7764E-01	0.7571E-01
OXYGEN	0.2555E-18	0.8608E-14	0.1634E-10	0.1523E-06	0.1496E-04
HYDROGEN	0.2973E-01	0.2439E-01	0.2048E-01	0.1621E-01	0.1440E-01
WATER VAPOUR	0.1750E 00	0.1804E 00	0.1843E 00	0.1885E 00	0.1901E 00
NITROGEN	0.6928E 00	0.6928E 00	0.6928E 00	0.6928E 00	0.6926E 00
O	0.9490E-19	0.2696E-14	0.4336E-11	0.3230E-07	0.2824E-05
H	0.3863E-09	0.3048E-07	0.6897E-06	0.2940E-04	0.1940E-03
OH	0.3592E-11	0.1365E-08	0.9760E-07	0.1679E-04	0.2212E-03
NO	0.3576E-13	0.4041E-10	0.6426E-08	0.2948E-05	0.6363E-04

CHEMICAL EQUILIBRIUM FOR METHANE-AIR MIXTURE

MOLE FRACTIONS AT A PRESSURE OF ONE ATMOSPHERE

FRACTION OF STOICHIOMETRIC AIR=0.100E 01

COMPONENT	TEMPERATURE(KELVIN)				
	0.1000E 04	0.1200E 04	0.1400E 04	0.1750E 04	0.2000E 04
CARBON MONOXIDE	0.2885E-07	0.1432E-05	0.2295E-04	0.6116E-03	0.3051E-02
CARBON DIOXIDE	0.9506E-01	0.9506E-01	0.9503E-01	0.9440E-01	0.9178E-01
OXYGEN	0.4208E-07	0.1412E-05	0.1750E-04	0.3686E-03	0.1677E-02
HYDROGEN	0.7956E-07	0.2008E-05	0.2041E-04	0.3314E-03	0.1345E-02
WATER VAPOUR	0.1901E 00	0.1901E 00	0.1901E 00	0.1896E 00	0.1879E 00
NITROGEN	0.7148E 00	0.7148E 00	0.7148E 00	0.7144E 00	0.7127E 00
O	0.3851E-13	0.3452E-10	0.4488E-08	0.1539E-05	0.2990E-04
H	0.6320E-12	0.2765E-09	0.2177E-07	0.4204E-05	0.5927E-04
OH	0.2385E-08	0.1586E-06	0.3189E-05	0.1181E-03	0.7156E-03
NO	0.1474E-07	0.5257E-06	0.6756E-05	0.1473E-03	0.6834E-03

CHEMICAL EQUILIBRIUM FOR METHANE-AIR MIXTURE

MOLE FRACTIONS AT A PRESSURE OF ONE ATMOSPHERE

FRACTION OF STOICHIOMETRIC AIR=0.110E 01

COMPONENT	TEMPERATURE(KELVIN)				
	0.1000E 04	0.1200E 04	0.1400E 04	0.1750E 04	0.2000E 04
CARBON MONOXIDE	0.4111E-10	0.1183E-07	0.6691E-06	0.8328E-04	0.9095E-03
CARBON DIOXIDE	0.8717E-01	0.8717E-01	0.8717E-01	0.8707E-01	0.8617E-01
OXYGEN	0.1743E-01	0.1740E-01	0.1732E-01	0.1692E-01	0.1664E-01
HYDROGEN	0.1134E-09	0.1658E-07	0.5949E-06	0.4492E-04	0.3934E-03
WATER VAPOUR	0.1743E 00	0.1743E 00	0.1743E 00	0.1741E 00	0.1731E 00
NITROGEN	0.7211E 00	0.7210E 00	0.7209E 00	0.7205E 00	0.7192E 00
O	0.2479E-10	0.3833E-08	0.1412E-06	0.1076E-04	0.9417E-04
H	0.2386E-13	0.2513E-10	0.3717E-08	0.1548E-05	0.3206E-04
OH	0.5793E-07	0.1601E-05	0.1713E-04	0.2945E-03	0.1219E-02
NO	0.9527E-05	0.5862E-04	0.2135E-03	0.1002E-02	0.2162E-02

CHEMICAL EQUILIBRIUM FOR METHANE-AIR MIXTURE

MOLE FRACTIONS AT A PRESSURE OF ONE ATMOSPHERE

FRACTION OF STOICHIOMETRIC AIR=0.120E 01

COMPONENT	TEMPERATURE(KELVIN)				
	0.1000E 04	0.1200E 04	0.1400E 04	0.1750E 04	0.2000E 04
CARBON MONOXIDE	0.2793E-10	0.8036E-08	0.4543E-06	0.5640E-04	0.6197E-03
CARBON DIOXIDE	0.8049E-01	0.8049E-01	0.8049E-01	0.8042E-01	0.7980E-01
OXYGEN	0.3219E-01	0.3215E-01	0.3204E-01	0.3146E-01	0.3074E-01
HYDROGEN	0.7702E-10	0.1126E-07	0.4039E-06	0.3041E-04	0.2673E-03
WATER VAPOUR	0.1610E 00	0.1610E 00	0.1610E 00	0.1608E 00	0.1599E 00
NITROGEN	0.7263E 00	0.7263E 00	0.7262E 00	0.7256E 00	0.7242E 00
O	0.3368E-10	0.5210E-08	0.1921E-06	0.1468E-04	0.1280E-03
H	0.1967E-13	0.2071E-10	0.3063E-08	0.1274E-05	0.2643E-04
OH	0.6489E-07	0.1793E-05	0.1920E-04	0.3305E-03	0.1366E-02
NO	0.1299E-04	0.7997E-04	0.2914E-03	0.1371E-02	0.2949E-02

CHEMICAL EQUILIBRIUM FOR METHANE-AIR MIXTURE

MOLE FRACTIONS AT A PRESSURE OF ONE ATMOSPHERE

FRACTION OF STOICHIOMETRIC AIR=0.130E 01

COMPONENT	TEMPERATURE(KELVIN)				
	0.1000E 04	0.1200E 04	0.1400E 04	0.1750E 04	0.2000E 04
CARBON MONOXIDE	0.2198E-10	0.6323E-08	0.3573E-06	0.4432E-04	0.4873E-03
CARBON DIOXIDE	0.7476E-01	0.7476E-01	0.7476E-01	0.7470E-01	0.7421E-01
OXYGEN	0.4485E-01	0.4481E-01	0.4468E-01	0.4397E-01	0.4299E-01
HYDROGEN	0.6061E-10	0.8863E-08	0.3177E-06	0.2389E-04	0.2099E-03
WATER VAPOUR	0.1495E 00	0.1495E 00	0.1495E 00	0.1493E 00	0.1485E 00
NITROGEN	0.7309E 00	0.7308E 00	0.7307E 00	0.7300E 00	0.7285E 00
O	0.3976E-10	0.6150E-08	0.2268E-06	0.1735E-04	0.1514E-03
H	0.1744E-13	0.1837E-10	0.2717E-08	0.1129E-05	0.2342E-04
OH	0.6795E-07	0.1878E-05	0.2010E-04	0.3463E-03	0.1431E-02
NO	0.1539E-04	0.9470E-04	0.3451E-03	0.1626E-02	0.3498E-02

CHEMICAL EQUILIBRIUM FOR METHANE-AIR MIXTURE

MOLE FRACTIONS AT A PRESSURE OF ONE ATMOSPHERE

FRACTION OF STOICHIOMETRIC AIR=0.140E 01

COMPONENT	TEMPERATURE(KELVIN)				
	0.1000E 04	0.1200E 04	0.1400E 04	0.1750E 04	0.2000E 04
CARBON MONOXIDE	0.1839E-10	0.5290E-08	0.2989E-06	0.3705E-04	0.4075E-03
CARBON DIOXIDE	0.6979E-01	0.6979E-01	0.6979E-01	0.6974E-01	0.6933E-01
OXYGEN	0.5582E-01	0.5578E-01	0.5563E-01	0.5484E-01	0.5368E-01
HYDROGEN	0.5071E-10	0.7416E-08	0.2658E-06	0.1997E-04	0.1753E-03
WATER VAPOUR	0.1396E 00	0.1396E 00	0.1396E 00	0.1394E 00	0.1386E 00
NITROGEN	0.7348E 00	0.7348E 00	0.7346E 00	0.7338E 00	0.7323E 00
O	0.4436E-10	0.6862E-08	0.2531E-06	0.1938E-04	0.1691E-03
H	0.1596E-13	0.1681E-10	0.2485E-08	0.1032E-05	0.2140E-04
OH	0.6934E-07	0.1916E-05	0.2052E-04	0.3536E-03	0.1461E-02
NO	0.1721E-04	0.1059E-03	0.3862E-03	0.1820E-02	0.3918E-02

CHEMICAL EQUILIBRIUM FOR METHANE-AIR MIXTURE

MOLE FRACTIONS AT A PRESSURE OF ONE ATMOSPHERE

FRACTION OF STOICHIOMETRIC AIR=0.150E 01

COMPONENT	TEMPERATURE(KELVIN)				
	0.1000E 04	0.1200E 04	0.1400E 04	0.1750E 04	0.2000E 04
CARBON MONOXIDE	0.1593E-10	0.4582E-08	0.2589E-06	0.3207E-04	0.3527E-03
CARBON DIOXIDE	0.6544E-01	0.6544E-01	0.6544E-01	0.6540E-01	0.6504E-01
OXYGEN	0.6543E-01	0.6538E-01	0.6522E-01	0.6437E-01	0.6304E-01
HYDROGEN	0.4392E-10	0.6422E-08	0.2301E-06	0.1728E-04	0.1516E-03
WATER VAPOUR	0.1309E 00	0.1309E 00	0.1309E 00	0.1307E 00	0.1299E 00
NITROGEN	0.7382E 00	0.7382E 00	0.7380E 00	0.7372E 00	0.7356E 00
O	0.4802E-10	0.7429E-08	0.2740E-06	0.2099E-04	0.1833E-03
H	0.1485E-13	0.1564E-10	0.2312E-08	0.9600E-06	0.1990E-04
OH	0.6987E-07	0.1931E-05	0.2068E-04	0.3563E-03	0.1473E-02
NO	0.1868E-04	0.1150E-03	0.4191E-03	0.1977E-02	0.4257E-02

CHEMICAL EQUILIBRIUM FOR METHANE-AIR MIXTURE

MOLE FRACTIONS AT A PRESSURE OF ONE ATMOSPHERE

FRACTION OF STOICHIOMETRIC AIR=0.160E 01

COMPONENT	TEMPERATURE(KELVIN)				
	0.1000E 04	0.1200E 04	0.1400E 04	0.1750E 04	0.2000E 04
CARBON MONOXIDE	0.1411E-10	0.4058E-08	0.2293E-06	0.2839E-04	0.3122E-03
CARBON DIOXIDE	0.6160E-01	0.6160E-01	0.6160E-01	0.6156E-01	0.6124E-01
OXYGEN	0.7391E-01	0.7386E-01	0.7369E-01	0.7278E-01	0.7136E-01
HYDROGEN	0.3890E-10	0.5688E-08	0.2038E-06	0.1530E-04	0.1341E-03
WATER VAPOUR	0.1232E 00	0.1232E 00	0.1232E 00	0.1230E 00	0.1222E 00
NITROGEN	0.7413E 00	0.7412E 00	0.7411E 00	0.7401E 00	0.7385E 00
O	0.5104E-10	0.7896E-08	0.2912E-06	0.2232E-04	0.1950E-03
H	0.1398E-13	0.1472E-10	0.2176E-08	0.9032E-06	0.1872E-04
OH	0.6989E-07	0.1931E-05	0.2068E-04	0.3565E-03	0.1474E-02
NO	0.1989E-04	0.1224E-03	0.4464E-03	0.2106E-02	0.4537E-02

CHEMICAL EQUILIBRIUM FOR METHANE-AIR MIXTURE

MOLE FRACTIONS AT A PRESSURE OF ONE ATMOSPHERE

FRACTION OF STOICHIOMETRIC AIR=0.170E 01

COMPONENT	TEMPERATURE(KELVIN)				
	0.1000E 04	0.1200E 04	0.1400E 04	0.1750E 04	0.2000E 04
CARBON MONOXIDE	0.1269E-10	0.3651E-08	0.2063E-06	0.2554E-04	0.2808E-03
CARBON DIOXIDE	0.5819E-01	0.5819E-01	0.5819E-01	0.5815E-01	0.5787E-01
OXYGEN	0.8145E-01	0.8140E-01	0.8122E-01	0.8026E-01	0.7875E-01
HYDROGEN	0.3501E-10	0.5118E-08	0.1834E-06	0.1376E-04	0.1206E-03
WATER VAPOUR	0.1164E 00	0.1164E 00	0.1164E 00	0.1162E 00	0.1154E 00
NITROGEN	0.7440E 00	0.7439E 00	0.7437E 00	0.7428E 00	0.7411E 00
O	0.5358E-10	0.8290E-08	0.3058E-06	0.2344E-04	0.2049E-03
H	0.1326E-13	0.1396E-10	0.2064E-08	0.8566E-06	0.1775E-04
OH	0.6959E-07	0.1923E-05	0.2059E-04	0.3551E-03	0.1468E-02
NO	0.2092E-04	0.1288E-03	0.4695E-03	0.2216E-02	0.4775E-02

CHEMICAL EQUILIBRIUM FOR METHANE-AIR MIXTURE

MOLE FRACTIONS AT A PRESSURE OF ONE ATMOSPHERE

FRACTION OF STOICHIOMETRIC AIR=0.180E 01

COMPONENT	TEMPERATURE(KELVIN)				
	0.1000E 04	0.1200E 04	0.1400E 04	0.1750E 04	0.2000E 04
CARBON MONOXIDE	0.1156E-10	0.3325E-08	0.1878E-06	0.2324E-04	0.2556E-03
CARBON DIOXIDE	0.5513E-01	0.5513E-01	0.5513E-01	0.5510E-01	0.5484E-01
OXYGEN	0.8820E-01	0.8814E-01	0.8796E-01	0.8696E-01	0.8538E-01
HYDROGEN	0.3187E-10	0.4660E-08	0.1670E-06	0.1252E-04	0.1097E-03
WATER VAPOUR	0.1103E 00	0.1103E 00	0.1103E 00	0.1101E 00	0.1093E 00
NITROGEN	0.7464E 00	0.7463E 00	0.7461E 00	0.7452E 00	0.7434E 00
O	0.5576E-10	0.8626E-08	0.3182E-06	0.2440E-04	0.2133E-03
H	0.1265E-13	0.1332E-10	0.1969E-08	0.8172E-06	0.1693E-04
OH	0.6910E-07	0.1910E-05	0.2045E-04	0.3526E-03	0.1458E-02
NO	0.2180E-04	0.1342E-03	0.4894E-03	0.2310E-02	0.4979E-02

CHEMICAL EQUILIBRIUM FOR METHANE-AIR MIXTURE

MOLE FRACTIONS AT A PRESSURE OF ONE ATMOSPHERE

FRACTION OF STOICHIOMETRIC AIR=0.190E 01

COMPONENT	TEMPERATURE(KELVIN)				
	0.1000E 04	0.1200E 04	0.1400E 04	0.1750E 04	0.2000E 04
CARBON MONOXIDE	0.1062E-10	0.3055E-08	0.1726E-06	0.2136E-04	0.2348E-03
CARBON DIOXIDE	0.5238E-01	0.5238E-01	0.5238E-01	0.5235E-01	0.5211E-01
OXYGEN	0.9427E-01	0.9422E-01	0.9403E-01	0.9299E-01	0.9135E-01
HYDROGEN	0.2929E-10	0.4283E-08	0.1534E-06	0.1150E-04	0.1007E-03
WATER VAPOUR	0.1048E 00	0.1048E 00	0.1048E 00	0.1046E 00	0.1039E 00
NITROGEN	0.7486E 00	0.7485E 00	0.7483E 00	0.7473E 00	0.7455E 00
O	0.5765E-10	0.8919E-08	0.3290E-06	0.2523E-04	0.2206E-03
H	0.1213E-13	0.1277E-10	0.1888E-08	0.7833E-06	0.1622E-04
OH	0.6849E-07	0.1893E-05	0.2027E-04	0.3495E-03	0.1445E-02
NO	0.2258E-04	0.1390E-03	0.5067E-03	0.2392E-02	0.5157E-02

CHEMICAL EQUILIBRIUM FOR METHANE-AIR MIXTURE

MOLE FRACTIONS AT A PRESSURE OF ONE ATMOSPHERE

FRACTION OF STOICHIOMETRIC AIR=0.200E 01

COMPONENT	TEMPERATURE(KELVIN)				
	0.1000E 04	0.1200E 04	0.1400E 04	0.1750E 04	0.2000E 04
CARBON MONOXIDE	0.9834E-11	0.2829E-08	0.1598E-06	0.1977E-04	0.2173E-03
CARBON DIOXIDE	0.4989E-01	0.4989E-01	0.4989E-01	0.4987E-01	0.4964E-01
OXYGEN	0.9977E-01	0.9971E-01	0.9952E-01	0.9846E-01	0.9675E-01
HYDROGEN	0.2712E-10	0.3965E-08	0.1421E-06	0.1065E-04	0.9321E-04
WATER VAPOUR	0.9978E-01	0.9978E-01	0.9977E-01	0.9959E-01	0.9890E-01
NITROGEN	0.7505E 00	0.7505E 00	0.7503E 00	0.7492E 00	0.7474E 00
O	0.5930E-10	0.9175E-08	0.3385E-06	0.2596E-04	0.2271E-03
H	0.1167E-13	0.1229E-10	0.1817E-08	0.7536E-06	0.1560E-04
OH	0.6779E-07	0.1874E-05	0.2006E-04	0.3460E-03	0.1431E-02
NO	0.2325E-04	0.1432E-03	0.5220E-03	0.2465E-02	0.5515E-02